EUROPEAN
JOURNAL OF
BIOLOGY

OFFICIAL JOURNAL OF ISTANBUL UNIVERSITY'S SCIENCE FACULTY

https://iupress.istanbul.edu.tr/en/journal/ejb/home

ISTANBUL
UNIVERSITY
PRESS

Indexing and Abstracting

Zoological Record - Clarivate Analytics
CAB Abstracts
CABI
- AgBiotechNet Database
- Animalscience Database
- VetMed Resource
- Environmental Impact Database
- Horticultural Science Database
- Nutrition and Food Sciences Database .
Chemical Abstracts Service (CAS)
ULAKBIM TR Index
Scopus
DOAJ
EBSCO Central & Eastern European Academic Source
SOBİAD
Cabells Journalytics
Gale Cengage

Authors bear responsibility for the content of their published articles.

The publication language of the journal is English.

This is a scholarly, international, peer-reviewed and open-access journal published biannually in June and December.

Publication Type: Periodical

EDITORIAL MANAGEMENT BOARD

EDITORIAL BOARD

AIMS AND SCOPE

European Journal of Biology (Eur J Biol) is an international, scientific, open access periodical published in accordance with independent, unbiased, and double-blinded peer-review principles. The journal is the official publication of Istanbul University Faculty of Science and it is published biannually on June and December. The publication language of the journal is English. European Journal of Biology has been previously published as IUFS Journal of Biology. It has been published in continuous publication since 1940.

European Journal of Biology aims to contribute to the literature by publishing manuscripts at the highest scientific level on all fields of biology. The journal publishes original research and review articles, and short communications that are prepared in accordance with the ethical guidelines in all fields of biology and life sciences.

The scope of the journal includes but not limited to; animal biology and systematics, plant biology and systematics, hydrobiology, ecology and environmental biology, microbiology, cell and molecular biology, biochemistry, biotechnology and genetics, physiology, toxicology, cancer biology, developmental and stem cell biology.

The target audience of the journal includes specialists and professionals working and interested in all disciplines of biology.

The editorial and publication processes of the journal are shaped in accordance with the guidelines of the International Committee of Medical Journal Editors (ICMJE), World Association of Medical Editors (WAME), Council of Science Editors (CSE), Committee on Publication Ethics (COPE), European Association of Science Editors (EASE), and National Information Standards Organization (NISO). The journal is in conformity with the Principles of Transparency and Best Practice in Scholarly Publishing (doaj.org/bestpractice).

European Journal of Biology is currently indexed SCOPUS, TUBITAK ULAKBIM TR Index, Zoological Record - Clarivate Analytics, CAB Abstracts, DOAJ, CABI, Chemical Abstracts Service (CAS), EBSCO Central & Eastern European Academic Source, SOBIAD, Cabells Journalytics.

Processing and publication are free of charge with the journal. No fees are requested from the authors at any point throughout the evaluation and publication process. All manuscripts must be submitted via the online submission system, which is available at dergipark. gov.tr/iufsjb. The journal guidelines, technical information, and the required forms are available on the journal's web page.

All expenses of the journal are covered by the Istanbul University.

Statements or opinions expressed in the manuscripts published in the journal reflect the views of the author(s) and not the opinions of the Istanbul University Faculty of Science, editors, editorial board, and/or publisher; the editors, editorial board, and publisher disclaim any responsibility or liability for such materials.

All published content is available online, free of charge at https://dergipark.org.tr/tr/pub/iufsjb. Printed copies of the journal are distributed free of charge.

OPEN ACCESS

INSTRUCTIONS TO AUTHORS

European Journal of Biology (Eur J Biol) is an international, scientific, open access periodical published in accordance with independent, unbiased, and double-blinded peer-review principles. The journal is the official publication of Istanbul University Faculty of Science and it is published biannually on June and December. The publication language of the journal is English. European Journal of Biology has been previously published as IUFS Journal of Biology. It has been published in continuous publication since 1940.

European Journal of Biology aims to contribute to the literature by publishing manuscripts at the highest scientific level on all fields of biology. The journal publishes original research and review articles, and short communications that are prepared in accordance with the ethical guidelines in all fields of biology and life sciences.

The scope of the journal includes but not limited to; animal biology and systematics, plant biology and systematics, hydrobiology, ecology and environmental biology, microbiology, cell and molecular biology, biochemistry, biotechnology and genetics, physiology, toxicology, cancer biology, developmental and stem cell biology.

The editorial and publication processes of the journal are shaped in accordance with the guidelines of the International Council of Medical Journal Editors (ICMJE), the World Association of Medical Editors (WAME), the Council of Science Editors (CSE), the Committee on Publication Ethics (COPE), the European Association of Science Editors (EASE), and National Information Standards Organization (NISO). The journal conforms to the Principles of Transparency and Best Practice in Scholarly Publishing (doaj.org/bestpractice).

Originality, high scientific quality, and citation potential are the most important criteria for a manuscript to be accepted for publication. Manuscripts submitted for evaluation should not have been previously presented or already published in an electronic or printed medium. Manuscripts that have been presented in a meeting should be submitted with detailed information on the organization, including the name, date, and location of the organization.

Manuscripts submitted to European Journal of Biology will go through a double-blind peer-review process. Each submission will be reviewed by at least three external, independent peer reviewers who are experts in their fields in order to ensure an unbiased evaluation process. The editorial board will invite an external and independent editor to manage the evaluation processes of manuscripts submitted by editors or by the editorial board members of the journal. The Editor in Chief is the final authority in the decision-making process for all submissions.

An approval of research protocols by the Ethics Committee in accordance with international agreements (World Medical Association Declaration of Helsinki "Ethical Principles for Medical Research Involving Human Subjects," amended in October 2013, www.wma.net) is required for experimental, clinical, and drug studies. If required, ethics committee reports or an equivalent official document will be requested from the authors.

The Journal takes as principle to comply with the ethical standards of Basel Declaration and WMA Statement on Animal Use in Biomedical Research and World Medical Association (WMA) Declaration of Helsinki – Ethical Principles for Medical Research Involving Human Subjects.

The journal requires experimental research studies on vertebrates or any regulated invertebrates to comply with relevant institutional, national and/or international guidelines, and authors are advised to clearly state their compliance with relevant guidelines. For studies involving animals, it is required to obtain approval of research protocols from an ethics committee. The committee reviews protocols to ensure compliance with applicable regulations and guidelines, including the Guide for the Care and Use of Laboratory Animals (8th Edition, 2011), International Council for Laboratory Animal Science (ICLAS), and the International Guiding Principles for Biomedical Research Involving Animals (2012). These guidelines offer comprehensive instructions on how to carry out animal research ethically and humanely and are widely acknowledged as the benchmark for such research. Authors should provide detailed explanation of the ethical treatment of animals in their manuscripts, including measures taken to avoid pain and distress. This is crucial to ensure the humane conduct of the study and enable verification that it conforms to the relevant ethical criteria. The ARRIVE checklist is a useful tool authors can use to present this information clearly and thoroughly.

European Journal of Biology advises authors to comply with IUCN Policy Statement on research Involving Species at Risk of Extinction and the Convention on the Trade in Endangered Species of Wild IUCN Policy Statement on Research Involving Species at Risk of Extinction and the Convention on the Trade in Endangered Species of Wild Fauna and Flora.

An approval of research protocols by the Ethics Committee in accordance with international standards mentioned above is required for experimental, clinical, and

drug studies and for some case reports. If required, ethics committee reports or an equivalent official document will be requested from the authors. For manuscripts concerning experimental research on humans, a statement should be included that shows that written informed consent of patients and volunteers was obtained following a detailed explanation of the procedures that they may undergo. Information on patient consent, the name of the ethics committee, and the ethics committee approval number should also be stated in the Materials and Methods section of the manuscript. It is the authors' responsibility to carefully protect the patients' anonymity. For photographs that may reveal the identity of the patients, signed releases of the patient or of their legal representative should be enclosed.

All submissions are screened by a similarity detection software (iThenticate by CrossCheck).

In the event of alleged or suspected research misconduct, e.g., plagiarism, citation manipulation, and data falsification/fabrication, the Editorial Board will follow and act in accordance with COPE guidelines.

Each individual listed as an author should fulfil the authorship criteria recommended by the International Committee of Medical Journal Editors (ICMJE - www.icmje.org). The ICMJE recommends that authorship be based on the following 4 criteria:

1. Substantial contributions to the conception or design of the work; or the acquisition, analysis, or interpretation of data for the work; AND

2. Drafting the work or revising it critically for important intellectual content; AND

3. Final approval of the version to be published; AND

4. Agreement to be accountable for all aspects of the work in ensuring that questions related to the accuracy or integrity of any part of the work are appropriately investigated and resolved.

In addition to being accountable for the parts of the work he/she has done, an author should be able to identify which co-authors are responsible for specific other parts of the work. In addition, authors should have confidence in the integrity of the contributions of their co-authors.

All those designated as authors should meet all four criteria for authorship, and all who meet the four criteria should be identified as authors. Those who do not meet all four criteria should be acknowledged in the title page of the manuscript.

European Journal of Biology requires corresponding authors to submit a signed and scanned version of the authorship contribution form (available for download through the journal's web page) during the initial submission process in order to act appropriately on authorship rights and to prevent ghost or honorary authorship. If the editorial board suspects a case of "gift authorship," the submission will be rejected without further review. As part of the submission of the manuscript, the corresponding author should also send a short statement declaring that he/she accepts to undertake all the responsibility for authorship during the submission and review stages of the manuscript.

European Journal of Biology requires and encourages the authors and the individuals involved in the evaluation process of submitted manuscripts to disclose any existing or potential conflicts of interests, including financial, consultant, and institutional, that might lead to potential bias or a conflict of interest. Any financial grants or other supports received for a submitted study from individuals or institutions should be disclosed to the Editorial Board. To disclose a potential conflict of interest, the ICMJE Potential Conflict of Interest Disclosure Form should be filled and submitted by all contributing authors. Cases of a potential conflict of interest of the editors, authors, or reviewers are resolved by the journal's Editorial Board within the scope of COPE and ICMJE guidelines.

The Editorial Board of the journal handles all appeal and complaint cases within the scope of COPE guidelines. In such cases, authors should get in direct contact with the editorial office regarding their appeals and complaints. When needed, an ombudsperson may be assigned to resolve cases that cannot be resolved internally. The Editor in Chief is the final authority in the decision-making process for all appeals and complaints.

When submitting a manuscript to European Journal of Biology, authors accept to assign the copyright of their manuscript to Istanbul University Faculty of Science. If rejected for publication, the copyright of the manuscript will be assigned back to the authors. European Journal of Biology requires each submission to be accompanied by a Copyright Transfer Form (available for download at the journal's web page). When using previously published content, including figures, tables, or any other material in both print and electronic formats, authors must obtain permission from the copyright holder. Legal, financial and criminal liabilities in this regard belong to the author(s).

Statements or opinions expressed in the manuscripts published in European Journal of Biology reflect the views of the author(s) and not the opinions of the editors, the editorial board, or the publisher; the editors, the editorial board, and the publisher disclaim any responsibility

European Journal of Biology
DECEMBER 2024,
VOLUME 83, NUMBER 2

İSTANBUL
UNIVERSITY
— P R E S S —

or liability for such materials. The final responsibility in regard to the published content rests with the authors.

MANUSCRIPT SUBMISSION

European Journal of Biology endorses ICMJE-Recommendations for the Conduct, Reporting, Editing, and Publication of Scholarly Work in Medical Journals (updated in December 2015 - http:/ / www.icmje.org/ icmje-recommendations.pdf). Authors are required to prepare manuscripts in accordance with the CONSORT guidelines for randomized research studies, STROBE guidelines for observational original research studies, STARD guidelines for studies on diagnostic accuracy, PRISMA guidelines for systematic reviews and meta-analysis, ARRIVE guidelines for experimental animal studies, TREND guidelines for non-randomized public behaviour, and COREQ guidelines for qualitative research.

Manuscripts can only be submitted through the journal's online manuscript submission and evaluation system, available at the journal's web page. Manuscripts submitted via any other medium will not be evaluated.

Manuscripts submitted to the journal will first go through a technical evaluation process where the editorial office staff will ensure that the manuscript has been prepared and submitted in accordance with the journal's guidelines. Submissions that do not conform to the journal's guidelines will be returned to the submitting author with technical correction requests.

During the initial submission, authors are required to submit the following:

- Copyright Agreement Form,
- Author Contributions Form, and

ICMJE Potential Conflict of Interest Disclosure Form (should be filled in by all contributing authors). These forms are available for download at the journal's web page.

Preparation of the Manuscript

Title page: A separate title page should be submitted with all submissions and this page should include:

- The full title of the manuscript as well as a short title (running head) of no more than 50 characters,
- Name(s), affiliations, and highest academic degree(s) of the author(s),
- Grant information and detailed information on the other sources of support,

- Name, address, telephone (including the mobile phone number) and fax numbers, and email address of the corresponding author,
- Acknowledgment of the individuals who contributed to the preparation of the manuscript but who do not fulfil the authorship criteria.

Abstract: Abstract with subheadings should be written as structured abstract in submitted papers except for Review Articles and Letters to the Editor. Please check Table 1 below for word count specifications (250 words).

Keywords: Each submission must be accompanied by a minimum of three to a maximum of six keywords for subject indexing at the end of the abstract. The keywords should be listed in full without abbreviations.

Manuscript Types

Original Articles: This is the most important type of article since it provides new information based on original research. A structured abstract is required with original articles and it should include the following subheadings: Objective, Materials and Methods, Results and Conclusion. The main text of original articles should be structured with Introduction, Materials and Methods, Results, Discussion, and Conclusion subheadings. Please check Table 1 for the limitations of Original Articles. Statistical analysis to support conclusions is usually necessary. Statistical analyses must be conducted in accordance with international statistical reporting standards. Information on statistical analyses should be provided with a separate subheading under the Materials and Methods section and the statistical software that was used during the process must be specified. Units should be prepared in accordance with the International System of Units (SI).

Short Communications: Short communication is for a concise, but independent report representing a significant contribution to Biology. Short communication is not intended to publish preliminary results. But if these results are of exceptional interest and are particularly topical and relevant will be considered for publication. Short Communications should include an abstract and should be structed with the following subheadings: "Introduction", "Materials and Methods", "Results and Discussion".

Editorial Comments: Editorial comments aim to provide a brief critical commentary by reviewers with expertise or with high reputation in the topic of the research article published in the journal. Authors are selected and invited by the journal to provide such comments. Abstract, Keywords, and Tables, Figures, Images, and other media are not included.

Review Articles: Reviews prepared by authors who have extensive knowledge on a particular field and whose scientific background has been translated into a high volume of publications with a high citation potential are welcomed. These authors may even be invited by the journal. Reviews should describe, discuss, and evaluate the current level of knowledge of a topic in clinical practice and should guide future studies. The main text should contain Introduction, Experimental and Clinical Research Consequences, and Conclusion sections. Please check Table 1 for the limitations for Review Articles.

Letters to the Editor: This type of manuscript discusses important parts, overlooked aspects, or lacking parts of a previously published article. Articles on subjects within the scope of the journal that might attract the readers' attention, particularly educative cases, may also be submitted in the form of a "Letter to the Editor." Readers can also present their comments on the published manuscripts in the form of a "Letter to the Editor." Abstract, Keywords, and Tables, Figures, Images, and other media should not be included. The text should be unstructured. The manuscript that is being commented on must be properly cited within this manuscript.

Tables

Tables should be included in the main document, presented after the reference list, and they should be numbered consecutively in the order they are referred to within the main text. A descriptive title must be placed above the tables. Abbreviations used in the tables should be defined below the tables by footnotes (even if they are defined within the main text). Tables should be created using the "insert table" command of the word processing software and they should be arranged clearly to provide easy reading. Data presented in the tables should not be a repetition of the data presented within the main text but should be supporting the main text.

Figures and Figure Legends

Figures, graphics, and photographs should be submitted as separate files (in TIFF or JPEG format with 1200 dpi for graphic and 600 dpi for colour images) through the submission system. The files should not be embedded in a Word document or the main document. When there are figure subunits, the subunits should be labeled merged to form a single image. Each subunit should be submitted separately through the submission system. Images should be labeled (a, b, c, etc.) to indicate figure subunits.

Thick and thin arrows, arrowheads, stars, asterisks, and similar marks can be used on the images to support fig-

ure legends. Like the rest of the submission, the figures too should be blind. Any information within the images that may indicate an individual or institution should be blinded. The minimum resolution of each submitted figure should be 300 DPI. To prevent delays in the evaluation process, all submitted figures should be clear in resolution and large in size (minimum dimensions: 100 × 100 mm). Figure legends should be listed at the end of the main document.

All acronyms and abbreviations used in the manuscript should be defined at first use, both in the abstract and in the main text. The abbreviation should be provided in parentheses following the definition.

When a drug, chemical, product, hardware, or software program is mentioned within the main text, product information, including the name of the product, the producer of the product, and city and the country of the company (including the state if in USA), should be provided in parentheses in the following format: "Discovery St PET/CT scanner (General Electric, Milwaukee, WI, USA)"

All references, tables, and figures should be referred to within the main text, and they should be numbered consecutively in the order they are referred to within the main text.

Limitations, drawbacks, and the shortcomings of original articles should be mentioned in the Discussion section before the conclusion paragraph.

References

European Journal of Biology uses the **AMA citation style.** In the paper, you are writing, materials are cited using superscript numerals. The first reference used in a written document is listed as 1 in the reference list, and a 1 is inserted into the document immediately next to the fact, concept, or quotation being cited. If the same reference is used multiple times in one document, use the same number to refer to it throughout the document.

Example:

Finding treatments for breast cancer is a major goal for scientists.[1,2] Some classes of drugs show more promise than others. Gradishar evaluated taxanes as a class.[3] Other scientists have investigated individual drugs within this class, including Andre and Zielinski[2] and Joensuu and Gligorov.[4] Mita et al's investigation of cabazitaxel 5 seems to indicate a new role for this class of drugs.

While citing publications, preference should be given to the latest, most up to date publications. If an ahead of print publication is cited, the DOI number should be pro-

Table 1. Limitations for each manuscript type

Type of manuscript	Word limit	Abstract word limit	Reference limit	Table limit	Figure limit
Original Article	4500	250 (Structured)	No limit	6	Maximum 8
Short Communication	2500	200	30	3	4
Review Article	5500	250	No limit	5	6
Letter to the Editor	500	No abstract	5	No tables	No media

vided. Authors are responsible for the accuracy of references. Journal titles should be abbreviated in accordance with the journal abbreviations in Index Medicus/ MEDLINE/PubMed. When there are six or fewer authors, all authors should be listed. If there are seven or more authors, the first six authors should be listed followed by "et al."

At the end of the document, include a reference list with full citations to each item. The reference styles for different types of publications are presented in the following examples.

Print journal article with six or fewer authors:

Kayalar O, Oztay F, Ongen HG. Gastrin-releasing peptide induces fibrotic response in MRC5s and proliferation in A549s. *Cell Commun Signal.* 2020;18(1):96-107.

Kazerouni NN, Currier RJ, Hodgkinson C, Goldman S, Lorey F, Roberson M. Ancillary benefits of prenatal maternal serum screening achieved in the California program. *Prenat Diagn.* 2010;30 (10):981-987.

Print journal article with more than six authors:

Baba Y, Yoshida N, Kinoshita K, et al. Clinical and prognostic features of patients with esophageal cancer and multiple primary cancers: A retrospective single-institution study. *Ann Surg.* 2018;267(3):478-483.

Online journal article:

Florez H, Martinez R, Chakra W, Strickman-Stein M, Levis S. Outdoor exercise reduces the risk of hypovitaminosis D in the obese. *J Steroid Biochem Mol Bio.* 2007;103(3-5):679-681. doi:10.1016/j.jsbmb.2006.12.032.

Journal article with no named author or group name:

Centers for Disease Control and Prevention (CDC). Licensure of a meningococcal conjugate vaccine (Menveo) and guidance for use-Advisory Committee on Immunization Practices (ACIP), 2010. *MMWR Morb Mortal Wkly Rep.* 2010;59(9):273

Book:

Brownson RC. *Evidence-based Public Health.* 2nd ed. New York, N.Y.: Oxford University Press; 2011.

Book Chapter:

Guyton JL, Crockarell JR. Fractures of acetabulum and pelvis. In: Canale ST, ed. *Campbell's Operative Orthopaedics.* 10th ed. Philadelphia, PA: Mosby, Inc; 2003:2939-2984.

Webpage:

Fast facts. National Osteoporosis Foundation website. http://www.nof.org/osteoporosis/diseasefacts.htm. Accessed August 27, 2007.

Official organization report published on a webpage:

Office of Women's Health, California Department of Public Health. California Adolescent Health 2009. http://www.cdph.ca.gov/pubsforms/Pubs/OWH-AdolHealthReport09.pdf. Accessed January 5, 2011.

Conference Proceedings:

Fritz TC, Soni MG. Use of dietary supplements in sports drinks: Consumption and safety determinations for regulatory compliance. Poster presented at: *Annual International Society of Sports Nutrition Conference and Expo*; June 16-18, 2005; New Orleans, LA.

Thesis

Yildirim M. The determination of effective long non-coding RNA on human pulmonary fibrosis in an in vitro model. Istanbul University, Science Institute, Master Thesis, 2018.

REVISIONS

When submitting a revised version of a paper, the author must submit a detailed "Response to the reviewers" that states point by point how each issue raised by the reviewers has been covered and where it can be found

(each reviewer's comment, followed by the author's re-ply and line numbers where the changes have been made) as well as an annotated copy of the main document. Re-vised manuscripts must be submitted within 30 days from the date of the decision letter. If the revised version of the manuscript is not submitted within the allocated time, the revision option may be cancelled. If the submitting au-thor(s) believe that additional time is required, they should request this extension before the initial 30-day period is over. Accepted manuscripts are copy-edited for grammar, punctuation, and format. Once the publication process of a manuscript is completed, it is published online on the journal's webpage as an ahead-of-print publication before it is included in its scheduled issue. A PDF proof of the accepted manuscript is sent to the corresponding author and their publication approval is requested within 2 days of their receipt of the proof.

Editor in Chief: Prof. Dr. Fusun OZTAY
Address: Istanbul University, Faculty of Science, Depart-ment of Biology,
34134 Vezneciler, Fatih, Istanbul, Türkiye
Phone: +90 212 4555700 (Ext. 20319)
Fax: +90 212 5280527
E-mail: fusoztay@istanbul.edu.tr

CONTENTS

İSTANBUL UNIVERSITY PRESS

CONTENTS

İSTANBUL
UNIVERSITY
― P R E S S ―

RESEARCH ARTICLE

Membrane Damaging and Protective Effects of *Gypsophila bicolor*'s Grossh. (Caryophyllaceae) Root Extract on H1299, A549, and A431 Cells

Zeynep Demir[1] (iD), Aysun Ozkan[2] (iD), Esin Ari[3] (iD)

[1]Akdeniz University, Institute of Natural and Applied Sciences, Department of Biology, Antalya, Türkiye
[2]Akdeniz University, Faculty of Science, Department of Biology, Antalya, Tü rkiye
[3]Akdeniz University, Faculty of Agriculture, Department of Agricultural Biotechnology, Antalya, Türkiye

ABSTRACT

Objective: This study aims to determine the effects of the *Gypsophila bicolor* Grossh. root extract on cell viability and to investigate its protective (antioxidant) effects against hydrogen peroxide (H_2O_2)-induced cytotoxicity and membrane damage in A431, A549, and H1299 cells.

Materials and Methods: The study uses the Cell Titer-BlueR Cell Viability assay to determine the cytotoxic effects of catechol on cells and the fluorometric method to determine cellular malondialdehyde (MDA) levels. The study uses DPPH free radical scavenging, superoxide anion scavenging, hydroxyl radical scavenging, and reducing power assays to determine the antioxidant capacity of the *G. bicolor* root extract.

Results: The IC_{50} values were respectively calculated as 60, 200, and 70 µg/mL in the H1299, A549, and A431 cells incubated with the root extract for 24 h. The IC_{50} values of H_2O_2, a strong oxidizing agent, were found to be 50, 400, and 295 µM, respectively. The most effective cytoprotective concentrations against H_2O_2 cytotoxicity in the cells pre-incubated with low concentrations of root extract were found to be 5 µg/mL for the A549 and A431 cells and 10 µg/mL for the H1299 cells. MDA levels increased in cells exposed to H_2O_2 and the root extract (IC_{50} and IC_{70}) but decreased in the cells pre-incubated with low doses of root extract prior to H_2O_2 exposure. The root extract's antioxidant capacity has also been supported by other tests.

Conclusion: While the root extract caused membrane damage in cells due to high concentrations, it showed a protective effect against H_2O_2 at low concentrations.

Keywords: *Gypsophila bicolor*, Anticancer, Antioxidant, Oxidant, Malondialdehyde

INTRODUCTION

Lung cancer is one of the most common cancers in both men and women worldwide. Because of the cancer's systemic nature with a high rate of recurrence and clinically nonspecific symptoms, most patients are diagnosed at an advanced stage, with the standard treatment still being anticancer drugs.[1] However, the majority of current anticancer drugs have significant side effects with poor prognoses. Therefore, a great need exists to develop a novel anti-cancer drug with low toxicity and high potency. In recent years, the fact that most anticancer drugs are obtained from natural extracts has made plants the focus of drug research.[2] Thus, a popular approach among scientists has been to focus on phytotherapy in cancer treatment. However, extracts obtained from plants for phytotherapy contain many bioactive components, and living things cannot safely use these components without knowing their therapeutic concentrations.

The current study uses this approach to investigate the dose-dependent anticancer and antioxidant effects of *Gypsophila bicolor* root extract on different cancer cell lines. Members of this genus are known as *çöven* in Turkish and soapwort in English. One study demonstrated *Gypsophila oldhamiana gypsogenin* (GOG) to be able to stimulate apoptosis and suppress the proliferation of the NCI-N87 (human gastric cancer cell line), observing GOG be able to decrease the vascular endothelial growth factor (VEGF) and matrix metalloprotein (MMP-9) expression in a dose-dependent manner while increasing the expression of Bax proteins and caspase-3.[3] Another study revealed the effects of *Gypsophila oldhamiana* root extract, which is rich in triterpenoid saponins,

on SMMC-7721 (human hepatoma) and L02 (normal human liver) cells to vary in a concentration-dependent manner. As a result of the cytotoxic assay, that study calculated the IC$_{50}$ value of TGOE in SMMC-7721 cells as 19.50 ± 3.63 µg/mL and 40.48 ± 3.74 µg/mL in L02 cells, thus concluding the root extract to show selective toxicity against cancer cells. Those results suggested that *G. oldhamiana* root extract may have potentially beneficial effects against hepatocellular carcinoma.[4] Studies in the literature have shown many plant extracts with high saponin and phenolic content similar to *G. bicolor* to have concentration-dependent antioxidant and anticancer properties.[4-7] The concentration of an antioxidant substance plays an important role in its effect on oxidation reactions. Factors such as the structure of the antioxidant in question, the conditions in which oxidation takes place, and the change in the structure of the oxidized substance are effective in this case. High concentrations of antioxidants are known to gain pro-oxidant properties. As a result, antioxidants can act as prooxidants by causing damage at increasing concentrations while protecting the membrane against oxidants at low concentrations. Recent studies have shown the toxic and anti-prooxidant properties of molecules with this feature to change in a dose-dependent manner and to be unsafe for humans when used without proper awareness.

Therefore, the current study investigates the concentration-dependent cytoprotective and membrane protective effects of *G. bicolor* root extract against hydrogen peroxide (H$_2$O$_2$), a strong oxidant, on H1299, A549, and A431 cells. The study also evaluates the cytotoxic and membrane-damaging effects of the root extract at higher concentrations on cell lines. The study uses four different complementary *in vitro* tests to evaluate the antioxidant properties of the *G. bicolor* root extract.

MATERIALS AND METHODS

Obtaining the *G. bicolor* Root Extract

G. bicolor root extract was obtained from Akdeniz University, Faculty of Engineering, Department of Food Engineering, and prepared using 80% methanol and modifying Güçlü-Üstündağ and Mazza's method.[8,9]

DPPH (2,2'-diphenyl-1-picrylhydrazyl) Assay

DPPH is a stable radical molecule used to measure the free radical scavenging effect of natural compounds. A hydrogen donor antioxidant compound is used to reduce it to yellow diphenyl picryl hydrazine. The absorbance of the generated yellow compound is measured colorimetrically. This spectrophotometric experiment utilizes the stable DPPH radical as a reagent.[10] Using this method, 50 µl was taken from samples of the various concentrations that had been prepared by dissolving the *G. bicolor* root extract in methanol and put into tubes. 5 mL of the DPPH solution prepared in 0.004% (w/v) methanol was

added to each tube. The absorbance of the samples was measured at 517 nm after 30 min of incubation at room temperature. Five replicate measurements were made. The absorbance value of the root extract at different concentrations was assessed against the blank control (50 µl methanol). The DPPH radical's percentage of inhibition (%I) value was computed as follows:

$$\%I = ((A_{control} - A_{sample}/A_{control}) \times 100) \qquad (1)$$

The obtained % I value was plotted against concentrations, with the concentration value that ensures 50% color lightening being computed as the 50% inhibition (EC$_{50}$) value. Butyl-hydroxytoluene (BHT), ascorbic acid, and α-tocopherol were utilized as positive controls for comparison. The selected concentration range was determined as a result of preliminary trials.

Hydroxyl Radical Scavenging Activity

The study uses the 2-deoxyribose oxidation method to test *G. bicolor*'s ability to scavenge hydroxyl radicals.[11] The method is based on measuring the absorbance of the generated reactive products through the degradation of deoxyribose by the hydroxyl radical that is released by the Fe/Ascorbate/EDTA/H$_2$O$_2$ system at a wavelength of 532 nm. 100 µl of deoxyribose (60 mM), 100 µl of FeCl$_3$ (1 mM), 100 µl of EDTA (1 mM), and 100 µl of ascorbic acid, as well as 100 µl of H$_2$O$_2$ (12 mM) were added to the root extract samples at different concentrations. The mixture was left for one hour at a temperature of 3°C. Afterward, the reaction was stopped by adding 1% thiobarbituric acid (TBA) and 2.8% trichloroacetic acid (TCA) to the reaction mixture. The reaction mixture was boiled for 15 min, then cooled on ice and extracted with *n*-butanol. The color intensity of the resulting-colored complex was measured at 532 nm against *n*-butanol (blank control). BHT is a synthetic antioxidant and additive and was employed as a positive control. The selected concentration range was determined as a result of preliminary trials. The percentages of inhibition of the plant extract and the standard were calculated using Equation 1.

Reduction Potential Method

The reduction potential was determined by Oyaizu.[12] As another method based on free radical seizure activity, the reduction potential method shows high absorbance to imply a high reduction potential. 1 mL of different concentrations of root extract samples was combined with 2.5 mL of phosphate buffer (0.2 M) and 2.5 mL of potassium ferricyanide [K$_3$Fe(CN)$_6$] solution (%1 w/v). The mixture was incubated at 50 °C for 20 min. The mixture was then centrifuged at 1000 x g for 10 min with 2.5 mL (10% w/v) of TCA added. 2.5 mL of this mixture was then taken from the top and mixed with 2.5 mL of deionized water and 0.5 mL (0.1 percent) FeCl$_3$, after which the absorbance at 700 nm was measured against the blank control. Ascorbic acid was employed as a positive control. The selected concentration range was determined based on the preliminary trials.

Superoxide Anion Scavenging Activity

The superoxide anion scavenging activity of the *G. bicolor* root extract was measured using the method described by Liu.[13] This method is based on reducing the yellow NBT to its blue-violet-colored formazan derivative through the superoxide radical produced by the NADH/PMS/O_2 system. Low absorbance levels are obtained when the reaction environment includes compounds with superoxide anion scavenging activity. The production of superoxide anions occurred in a 3 mL Tris-HCl buffer (16 mM, pH 8.0) that contained 1 mL of NADH (78 µM) solution, 1 mL of NBT (50 µM) solution, and sample solutions. A 1 mL phenazine methosulfate (PMS) solution (10 µM) was added to the mixture to start the reaction. The mixture was then incubated for 5 min at 25 °C, and the absorbance was measured against a blank sample at 560 nm. Ascorbic acid was utilized as the positive control. The selected concentration range was determined based on the preliminary trials. Superoxide radical scavenging activity (%) was calculated by Equation 1. Values in all *in vitro* antioxidant assays are presented as the mean of five replicate measurements.

Cancer Cell Culture

Human lung cancer (H1299 and A549) and epidermoid carcinoma (A431) cell lines were acquired from the American Type Culture Collection in Rockville, Maryland. The cells were cultured in an RPMI 1640 medium containing 10% fetal bovine serum and 1% antibiotic - antimycotic solution at 37 °C within a humid atmosphere containing 5% CO_2.

Cytotoxicity Analysis

The H1299, A549, and A431 cells (10,000 cells/well, monolayer) were trypsinized to remove them from the surface of the flask to which they were adhered. The trypan blue (1:1 ratio) assay was used to count cells while transferring them to well plates (96 well plates). The method is based on the principle that live cells do not take up the dye, but dead cells do, with the number of cells per mL being calculated using the live and dead cells on a hemocytometer slide. 200 µl of cell suspension was dispensed into 96 well plates at 1×10^4 cells per well. The medium used in the wells was removed and replaced after a 24 h incubation at 37 °C. The *G. bicolor* root extract was diluted with a medium and administered to the wells containing cells at doses ranging from 20 to 400 µg/mL. The control group consists of cells that had received no treatment. The cells were incubated for 24 h in an incubator at 37 °C. The viability of the cells was determined using the Cell Titer-Blue® Cell viability assay kit after incubation. This method is based on the ability of live cells to convert resazurin into the fluorescent substance resorufin, whereas dead cells cannot make fluorescent-signaling products because their metabolic capacity is rapidly depleted. After 5 sets of 24-hour incubations, 20 µl of the Cell TiterBlue®

Cell viability assay kit was added to each well and incubated at 37 °C for 1 h. The reduction of cells from resazurin to resorufin was calculated by measuring the excitation at 560 nm and emission values at 590 nm in a fluorescent spectrophotometer (PerkinElmer LS55).[14] The percentage of live cells was calculated by comparing the mean absorbance value of the cell-only control group with the mean absorbance values of cells incubated with different concentrations of the *G. bicolor* root extract. The results are expressed as a percentage of live cells. H_2O_2 cytotoxicity on the H1299, A549, and A431 cells was measured in the same way. Cells were pre-incubated with different concentrations of the root extract (2.5-20 g/mL) for 1 h before 24 h of the H_2O_2 treatment to measure the root extract's antioxidant effect against H_2O_2 cytotoxicity (IC_{50} and IC_{70}). Each concentration and control were replicated five times. The IC_{50} values were calculated based on Equation 1. The root extract was dissolved in 0.5% dimethyl sulfoxide (DMSO).

Determining the Malondialdehyde Levels

The malondialdehyde (MDA) levels were measured using Wasowicz, Neve, and Peretz's method,[15] whose basic principle is that MDA is a product of lipid peroxidation resulting from membrane damage and reacts with TBA. The resulting compound is extracted in the butanol phase, and fluorescence spectrophotometry (PerkinElmer LS 55) is used to read the excitation at 525 nm and emission values at 547 nm. The MDA levels in the H1299, A549, and A431 cells were measured after 24 h of exposure to various root extract concentrations (IC_{50}, IC_{70}). To measure the root extract's membrane protective effect against H_2O_2, the cells were pre-incubated for 1 h at various concentrations (2.5-20 µg/mL) of the root extract before being exposed to the IC_{50} and IC_{70} concentrations of H_2O_2 and then treated with H_2O_2 (IC_{50} and IC_{70}) for 24 h. The root extract is dissolved in a 0.5% DMSO solution. The cells were centrifuged for 10 min at 600 x g after being taken from the culture environment. The cells were washed with a phosphate buffer, sonicated for 3 sets of 15 sec with 50 mM potassium phosphate (pH 7.2) containing 1 µg/ mL leupeptin and 1 mM PMSF, and centrifuged for 45 min at 15,000 x g. The MDA levels were determined in the supernatant. Protein was determined according to the Bradford method using bovine serum albumin as a standard.[16]

Statistical Analysis

The program Minitab Release 13.0 was used to analyze the data statistically.[17] The ANOVA GLM (General Linear Model) procedure was used to compare between groups.

RESULTS

The study has conducted four *in vitro* assays (i.e., the DPPH radical scavenging, superoxide anion scavenging, hydroxyl radical scavenging, and reduction potential assays) to investigate

the potential *in vitro* antioxidant properties of the methanol extract from *G. bicolor* roots. The results have been compared to positive controls (i.e., BHT and ascorbic acid).

The study utilized the DPPH assay to measure the antiradical capacity of the *G. bicolor* root extract relative to the activities of synthetic antioxidants such as ascorbic acid, α-tocopherol, and BHT. While the root extract showed a 35.2% radical scavenging activity at 3 μg/mL, the radical scavenging activities of α-tocopherol, ascorbic acid, and BHT were found to be 34.8%, 34.8%, and 25.8%, respectively. This study's extract also showed radical scavenging activity close to the positive controls (Table 1).

The hydroxyl radical scavenging efficacy of the *G. bicolor* root extract increases depending on dosage, as shown in Figure 1. The scavenging activities of 250 μg/mL root extract, α-tocopherol, and BHT were 64.27%, 83.64%, and 87.64%, respectively, with the respective EC_{50} values of 108.51, 53.33, and 24.17 μg/mL being found. The root extract's hydroxyl radical scavenging activity was about 25% lower than that of the positive controls.

The reducing power assay was performed to measure *G. bicolor*'s ability to reduce Fe^{3+} to Fe^{2+}. The reduction potential was found to be 3.06 in the 1,000 μg/mL of the root extract and 3.62 in the 1,000 μg/mL of ascorbic acid (Figure 1). Here the root extract acted as an antioxidant through electron donation.

G. bicolor showed lower superoxide anion scavenging activity than the positive control of ascorbic acid, as shown in Figure 1. At a concentration of 100 μg/mL, the root extract and ascorbic acid exhibited superoxide anion scavenging activity of 57.24% and 65.04%, respectively. While the root extract's EC_{50} value was found 87.35 μg/mL, the EC_{50} of ascorbic acid was found 76.88 μg/mL, at the same concentration.

Many studies have stated antioxidants to act as pro-oxidants as well as antioxidants on cells depending on the concentration and to exert a biphasic effect. The prooxidant or antioxidant effect of an antioxidant is based on the structure of the antioxidant, the conditions in which the oxidation takes place, and the structure of the oxidized substance that makes it unsafe for living things. Therefore, knowing at what concentrations an antioxidant acts as a prooxidant or an antioxidant is important. This study has shown the *G. bicolor* root extract to act as a prooxidant and to have an anti-cancer effect when applied to cancer cells at increasing concentrations.

The viability of H1299, A549, and A431 cancer cells exposed for 24 h to increasing concentrations of the root extract (20, 40, 80, 100, 150, 200, 250, 300, 350, 400 μg/mL) was significantly and increasingly reduced up to 150 μg/mL, with no significant change in viability being observed at concentrations higher than 150 μg/mL ($p \leq 0.05$; Figure 2A).

After 24 h of incubation, the root extract IC_{50} values were
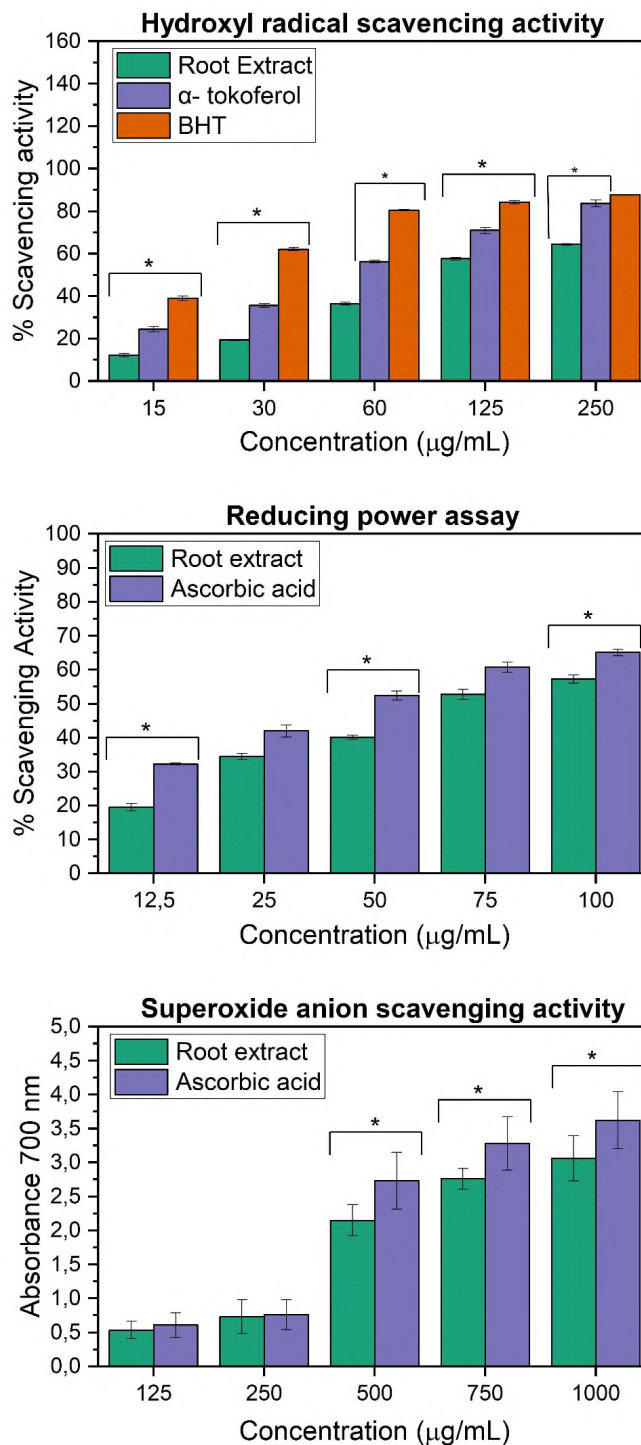
Figure 1. Hydroxyl radical scavenging activity, reducing power, and superoxide anion scavenging activity of root extract and positive controls, respectively. Data were expressed as the mean ± SD for 5 separate experiments. *: p<0.05

calculated as 60, 200, and 70 μg/mL for the H1299, A549, and A431 cell lines, respectively (Figure 2A). The toxic effect of the root extract was found to be three times more sensitive in the H1299 and A431 cells than in the A549 cells. The IC_{50} and IC_{70} values of H_2O_2, a powerful oxidizing agent, were computed for

Table 1. Scavenging capacity of *G. bicolor* root extract to DPPH radical (%).

Sample	0.1 µg/mL	0.2 µg/mL	0.4 µg/mL	0.6 µg/mL	0.8 µg/mL	1 µg/mL	3 µg/mL
G.bicolor	16.9 ± 0.1*	18.4 ± 0.4*	19.7 ± 0.4*	24.5 ± 0.7*	28.6 ± 0.4*	32.7 ± 0.4*	35,2 ± 0.8*
α-tocopherol	17.4 ± 0.5*	19.5 ± 0.1*	23.7 ± 0.3*	24.2 ± 0.1*	27.8 ± 0.8*	29.9 ± 0.3*	34,8 ± 0.3*
Ascorbic acid	17.8 ± 0.2*	20.3 ± 0.5*	22.7 ± 0.6*	26.1 ± 0.4*	28.0 ± 0.1*	33.2 ± 0.1*	34,8 ± 0.1*
BHT (Butyl hydroxytoluene)	12.8 ± 0.5*	15.1 ± 0.4*	15.3 ± 0.1*	17.7 ± 0.4*	22.9 ± 0.2*	23.3 ± 0.9*	25,8 ± 0.4*

*Denotes a statistically significant difference when compared to control values ($p < 0.05$) ± standard deviation (SD). Each datum in the table is an average of five repetitions.
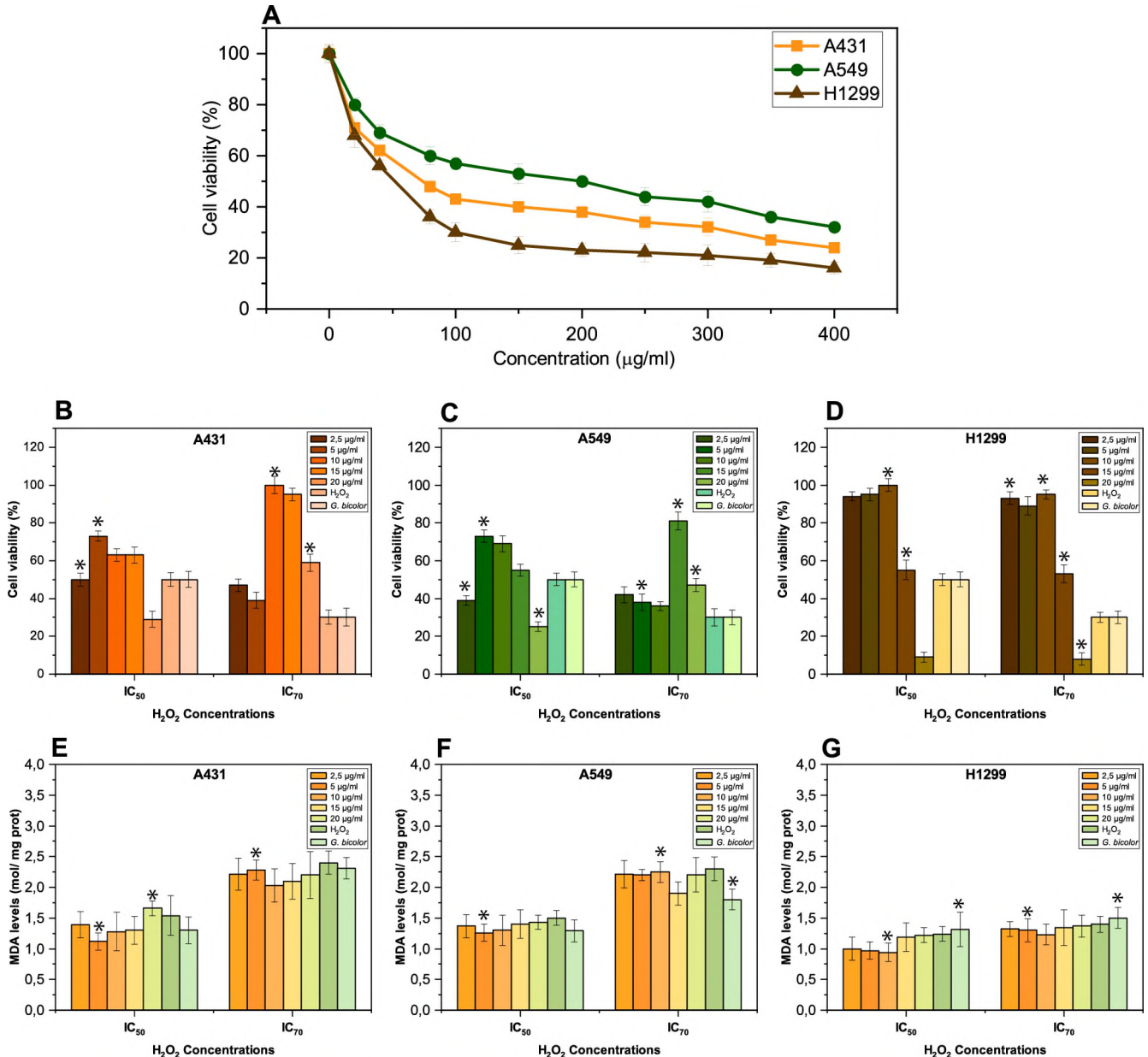
Figure 2. The dose-dependent cytotoxic effect of *G. bicolor* root extract in A549, H1299, and A431 cells (A). The protective (antioxidant) effect of *G. bicolor* root extract concentrations ($<IC_{50}$) on A431 (B), A549 (C), and H1299 (D) against H_2O_2 cytotoxicity. Dose-dependent membrane damaging effects of the root extract from *G. bicolor* on A431 (E), A459 (F), and H1299 (G). Results are presented as viability ratio compared with the control group (treated with only the medium-untreated cells). Values are expressed as the mean of three separate trials with three replications (ANOVA with Tukey test, p<0.05)

Table 2. IC values of root extract and H_2O_2 on the cells.

Cells	Root extract /IC$_{50}$	Root extract /IC$_{70}$	H$_2$O$_2$/IC$_{50}$	H$_2$O$_2$/IC$_{70}$
H1299	70 ± 0.09*	300 ± 0.23*	295 ± 0.16*	450 ± 0.51*
A549	200 ± 0.49*	400 ± 0.32*	400 ± 0.96*	547 ± 0.81*
A431	60 ± 0.78*	100 ± 0.1*	50 ± 0.32*	180 ± 0.46*

*Denotes a statistically significant difference when compared to control values ($p < 0.05$) ± standard deviation (SD). Each datum in the table is an average of five repetitions.

the H1299 cells (50 µM and 400 µM), A549 cells (400 µM and 547 µM), and A431 cells (295 µM and 354 µM; see Table 2).

The cytotoxicity results for the *G. bicolor* root extract applied to the cells in high concentrations showed the extract to reduce cell viability by acting as a strong oxidant similar to H_2O_2. Table 2 shows the IC values for the root extract and H_2O_2 on cells. The *G. bicolor* root extract has a dose-dependent antiproliferative effect, indicating it to perhaps be a potential agent for cancer treatments.

However, pre-incubating the cells with low concentrations of the root extract attenuated the cytotoxic effect induced by H_2O_2, a powerful oxidizing agent. The maximum cytoprotective activity of the root extract against the IC$_{50}$ concentration of H_2O_2 cytotoxicity was found to be 5 µg/mL for the A549 and A431 cells and 10 µg/mL for the H1299 cells. In addition, the concentrations at which the root extract showed maximum cytoprotective activity against IC$_{70}$ H_2O_2 cytotoxicity were calculated as 10 µg/mL for the H1299 and A431 cells and 15 µg/mL for the A549 cells (Figures 2B-2D).

As a result, the *G. bicolor* root extract shows cytotoxic effects on the H1299, A549, and A431 cells at high concentrations while significantly reducing the cytotoxic effects caused by H_2O_2 applied after incubating the cells with the root extract at low concentrations. In this case, the root extract shows an antioxidant or prooxidant effect depending on the concentration. The cytotoxic effect from the H_2O_2 application after the pre-incubation with the root extract was found to be lower than the cytotoxic effect of H_2O_2 alone, which reveals the root extract's cytoprotective effect.

At high concentrations, antioxidants can cause membrane damage by acting as prooxidants, while at lower concentrations they can protect the membrane against oxidants by expressing their antioxidant effect. Oxidative stress created by pro-oxidants in a cell leads to membrane damage by lipid peroxidation and increases the MDA level. In the H1299 cells treated with the IC$_{50}$ and IC$_{70}$ root extract, the quantity of MDA respectively increased by around 5 and 5.7 times compared to the control cells. Similarly, MDA levels in the A431 cells treated with the IC$_{50}$ and IC$_{70}$ concentrations of the root extract were respectively found to be 3.9 and 7 times higher than in the control cells. MDA levels respectively increased 4.6- and 6.4-fold in the A549 cells. H_2O_2 is a powerful oxidizing agent well known for causing oxidative stress and cell membrane damage. Compared to the control cells, MDA levels were found to be 4.8 and

5.4 times higher in the H1299 cells treated with IC$_{50}$ and IC$_{70}$ H_2O_2, respectively. Likewise, MDA levels in the A549 cells treated with IC$_{50}$ and IC$_{70}$ H_2O_2 were determined to be 5.4 and 8.2 times higher than in the control cells. This increase was respectively 4.6 and 7.2 times higher in the A431 cells (Figures 2E, 2F, and 2G).

The study's results from the cytoprotective effect test obtained dosage values where the root extract protects against membrane damage caused by H_2O_2 in cells. To demonstrate the membrane protective effect of the study's root extract, the cells were exposed to IC$_{50}$ and IC$_{70}$ concentrations of H_2O_2 for 24 h after being pre-incubated with low concentrations (2.5-20 µg/mL) of root extract.

The IC$_{10}$ (5 µg/mL) root extract concentration showed the highest membrane protective effect against membrane damage caused by IC$_{50}$ H_2O_2 in the A549 and A431 cells (Figures 2E, 2F, and 2G). Meanwhile, the IC$_{15}$ (10 µg/mL) root extract concentration had the greatest membrane protective effect in the H1299 cells against IC$_{50}$ H_2O_2-induced membrane damage (Figure 2).

When examining the root extract's membrane protective effect against IC$_{70}$ concentrations of H_2O_2, the IC$_{15}$ (10 µg/mL) root extract concentration had the highest protective activity in the H1299 and A431 cells, and the IC$_{20}$ (15 µg/mL) concentration in the A549 cells (Figure 2). The membrane-damaging effect from the H_2O_2 application after being pre-incubated with the root extract was found to be lower than the membrane-damaging effect of H_2O_2 alone, thus revealing the root extract's membrane protective effect. The concentration with the highest cytoprotective effect against H_2O_2 in each cell was also observed to be the concentration with the highest membrane protective effect.

DISCUSSION

One study's DPPH test results showed low concentrations (1 and 5 µg/ mL) of the methanol root extract of *Gypsophila pilulifera* Boiss.&Heldr. to have higher free radical scavenging activity than that of the extracts from *Gypsophila arrostii Guss.* and *Gypsophila simonii* Hub.-Mor.[18] Another study found the antiradical activity of the saponin-rich leaf extract (26.3 mmol Trolox/kg.dw) and the fruit extract (26.9 mmol Trolox/kg.dw) of *Asparagus albus* L. to be higher than that of its rhizome extract (20.5 mmol Trolox/kg.dw).[19] Yet an-

other study found the hydroxyl radical scavenging activity of the *Pouteria campechiana* seed polysaccharide (EC_{50}: 98.72 µg/mL) to be lower than ascorbic acid (EC_{50} = 8.92 µg/mL).[20] One other study showed the hydroxyl radical scavenging activity of the polysaccharide extract (92.62%) of *Polygonum cillinerve* (Nakai) Ohwi to be close to the positive control of ascorbic acid (91.83%).[21] The reducing activity of the *Indigofera tinctoria* L. extract, which has high saponin and flavonoid content, has also been found to be lower than the control, similar to *G. bicolor*.[22] One study found the EC_{50} values for *Pouteria campechiana* (Kunth) Baehmi's polysaccharide and ascorbic acid superoxide anion scavenging activity to be 358.22 and 7.74 g/mL, respectively.[20] The superoxide anion scavenging activity of *P. campechiana* polysaccharide was seen to be lower than that of the *G. bicolor* root extract. One study investigated the cytotoxic effect of the fresh extract from the tuber *Romulea tempskyana* Freyn. on H1299 and Hep-G2 cells determined IC_{50} values of 76.15 µg/mL and 94.79 µg/mL, respectively, and also found low concentrations of the fresh extract from *R. tempskyana* tuber (5-25 µg/mL) to significantly protect cancer cells from H_2O_2 cytotoxicity.[23] Other studies have shown various extracted saponins from the genus *Clematis*, including *Clematis lasiandra* Maxim and *Clematis argentilucida* (H.Lév.&Vaniot) W.T.Wang, to have considerable anti-cancer activity.[23,24] For instance, researchers have isolated seven novel cytotoxic triterpenoid saponins from *C. lasiandra.* Of these, five extracts demonstrated IC_{50} values ranging from 1.40-19.50 µmol/L in human tumor cell lines (i.e., HL-60, HepG-2, and SGC-7901).[23] One study comparatively investigated the antihypertensive, anticholinesterase, anturease, anti-tyrosinase, and anti-elastase enzyme inhibition and anticancer activities of *in vivo* (collected male and female root, stem, and leaf parts) and *in vitro* samples (germinated root, stem, and leaf parts) of *Pistacia khinjuk* stocks and found all the samples analyzed for anticancer activity to have cytotoxic effects against MCF-7 (human breast cancer) and HT-29 (colon cancer) cell lines. However, the study stated the in vivo samples had higher biological activity than the *in vitro* samples.[25] Another study investigated the effect of saponins obtained from garlic on the stress created by hypoxic conditions in PC12 cells and showed garlic saponins at concentrations of 0-5 ng/mL to significantly reduce hypoxic stress and to increase cell viability by 73% in 72 h.[26] One study found the methanol extract of the above-ground parts of *G. bicolor* and *Gypsophila ruscifolia* Boiss. to have cytotoxic effects on MCF-7 cells (IC_{50} <100 µg/mL) but failed to observe any cytotoxic effect in the A-549 (non-small cell lung carcinoma) and AGO-1522 cells (human fibroblast cell) at the tested doses of the extracts (0.01-1 mg/mL).[27] Another study analyzed the biological activities; gas chromatography and mass spectrometry (GC-MS) analysis; and antioxidant, antimicrobial, antioxidant, antimicrobial, DNA fragmentation, and anticancer activity of methanol (MeOH) and petroleum ether (PE) extracts of *Symphytum aintabicum* Hub.-Mor.&Wickens regarding MCF-7 cells. The IC_{50} values of the PE and MeOH extracts were 414.73 µg/mL and 443.31 µg/mL, respectively. That study's findings indicated *S. aintabicum* shows interesting pharmacological and biological activities and is a particularly suitable candidate for anticancer drug development.[28] One study examining the effect of saponins extracted from *Panax quinquefolius* L. leaves on acetaminophen (APAP)-)-induced liver toxicity in rats observed saponins to decrease the increased hepatic MDA levels.[29] Another study investigated the protective effect of saponins obtained from *Platycodon grandiflorum* A. DC. on hypoxia/reoxygenation-induced oxidative stress in cardiomyocytes (H9c2), observing *P. grandiflorum* saponins at a concentration of 20 µM to significantly decrease the MDA level and to cause an increase in superoxide dismutase and catalase activity.[30]

CONCLUSION

The results from the current study's four *in vitro* tests have revealed the root extract's antioxidant properties as well as hydroxyl, superoxide, and DPPH radical scavenging activity, and reducing power activity. The root extract shows antioxidant properties by protecting cancer cells against the oxidizing effect of H_2O_2, which supports the results presented above. The study's results also observed the root extract to act as a prooxidant at high concentrations, thus causing cytotoxic and membrane-damaging effects. However, the cytotoxic and membrane damage effects were reduced in cells that had been preincubated with low concentrations of the root extract compared to cells that had been exposed to H_2O_2 alone, thus revealing the extract's antioxidant effect. Due to the root extract showing biphasic effects such as being an antioxidant or prooxidant in cells depending on its dosage, foods containing *G. bicolor* root extract should be consumed carefully. This report showcases the potential the root extract has for decreasing the toxicity of hydrogen peroxide in cancer cells. However, further investigation on pharmacokinetics, pharmacodynamics, and toxicology is required before any clinical recommendations on root extraction supplementation can be made.

ORCID IDs of the authors

Zeynep Demir   0000-0003-4014-8467
Aysun Ozkan   0000-0002-9403-3342
Esin Ari   0000-0003-0239-9935

REFERENCES

1. Liu WJ, Du Y, Wen R, Yang M, Xu J. Drug resistance to targeted therapeutic strategies in non-small cell lung cancer. *Pharmacol Ther*. 2020;206:107438. doi:10.1016/j.pharmthera.2019.107438

2. Zhang L, Man S, Wang Y, et al. Paris Saponin II induced apoptosis via activation of autophagy in human lung cancer cells. *Chem Biol Interact*. 2016;253:125-133.

3. Liu J, Xu Y, Yang J, et al. Discovery, semisynthesis, biological activities, and metabolism of ocotillol-type saponins. *J Ginseng Res*. 2017;41(3):373-378.

4. Zhang W, Luo JG, Zhang C, Kong LY. Different apoptotic effects of triterpenoid saponin-rich *Gypsophila oldhamiana* root extract on human hepatoma SMMC-7721 and normal human hepatic L02 cells. *Biol Pharm Bull*. 2013;36(7):1080-1087.

5. Karakas FP, Turker AU, Karakas A, Mshvildadze V, Pichette A, Legault J. *In vitro* cytotoxic, antibacterial, anti-inflammatory and antioxidant activities and phenolic content in wild-grown flowers of common daisy—A medicinal plant. *J Herbal Med*. 2017;8:31-39.

6. Shin D, Moon HW, Oh Y, Kim K, Kim DD, Lim CJ. Defensive properties of ginsenoside re against UV-B-induced oxidative stress through up-regulating glutathione and superoxide dismutase in HaCaT keratinocytes. *Iran J Pharm Res*. 2018;17(1):249-260.

7. Vukic MD, Vukovic NL, Djelic GT, et al. Phytochemical analysis, antioxidant, antibacterial and cytotoxic activity of different plant organs of *Eryngium serbicum* L. *Ind Crop Prod*. 2018;115:88-97.

8. Güçlü Üstündağ Ö, Mazza G. Effects of pressurized low polarity water extraction parameters on antioxidant properties and composition of cow cockle seed extracts. *Plant Foods Hum Nutr*. 2008;64:32-38.

9. Cam I, Topuz A. Production of soapwort concentrate and soapwort powder and their use in Turkish delight and tahini halvah. *J Food Process Eng*. 2017;41. doi:10.1111/jfpe.12605

10. Burits M, Bucar F. Antioxidant activity of *Nigella sativa* essential oil. *Phytother Res*. 2000;14(5):323-328.

11. Halliwell B, Gutteridge JMC, Aruoma OI. The deoxyribose method: A simple "test-tube" assay for determination of rate constants for reactions of hydroxyl radicals. *Anal Biochem*. 1987;165(1):215-219.

12. Oyaizu M. Studies on products of browning reaction antioxidative activities of products of browning reaction prepared from glucosamine. *Jpn J Nutr Diet*. 1986;44(6):307-315.

13. Liu Q, Zhu G, Huang P. Anti-inflammatory, analgesic and sedative effects of *Leontice kiangnanensis* P.L. Chiu. *Zhongguo Zhong Yao Za Zhi*. 1991;16(1):50-65.

14. Gloeckner H, Jonuleit T, Lemke HD. Monitoring of cell viability and cell growth in a hollow-fiber bioreactor by use of the dye Alamar Blue. *J Immunol Methods*. 2001;252(1-2):131-138.

15. Wasowicz W, Nève J, Peretz A. Optimized steps in fluorometric determination of thiobarbituric acid-reactive substances in serum: Importance of extraction pH and influence of sample preservation and storage. *Clin Chem*. 1993;39(12):2522-2526.

16. Bradford MM. A rapid and sensitive method for the quantitation of microgram quantities of protein utilizing the principle of protein-dye binding. *Anal Biochem*. 1976;72:248-254.

17. Ozdamar K. Statistical Data Analysis with Packaged Programs.

18. Arslan I, Celik A. Saponin rich fractions (SRPs) from soapwort show antioxidant and hemolytic activity. *APCBEE Procedia*. 2013;7:103-108.

19. Hamdi A, Jaramillo-Carmona S, Srairi Beji R, et al. The phytochemical and bioactivity profiles of wild *Asparagus albus* L. plant. *Food Res Int*. 2017;99(Pt1):720-729.

20. Ma JS, Liu H, Han CR, et al. Extraction, characterization and antioxidant activity of polysaccharide from *Pouteria campechiana* seed. *Carbohydr Polym*. 2020;229:115409. doi:10.1016/j.carbpol.2019.115409

21. Zhou Y, Ma W, Wang L, et al. Characterization and antioxidant activity of the oligo-maltose fraction from *Polygonum cillinerve*. *Carbohydrate Polymers*. 2019;226:115307. doi:10.1016/j.carbpol.2019.115307

22. Singh R, Sharma S, Sharma V. Comparative and quantitative analysis of antioxidant and scavenging potential of *Indigofera tinctoria* Linn. extracts. *J Integr Med*. 2015;13(4):269-278.

23. Tian X, Feng J, Tang H, et al. New cytotoxic triterpenoid saponins from the whole plant of *Clematis lasiandra* Maxim. *Fitoterapia*. 2013;90:233-239.

24. Zhao M, Ma N, Qiu F, et al. Triterpenoid saponins from the roots of *Clematis argentilucida* and their cytotoxic activity. *Planta Med*. 2014;80(11):942-948.

25. Tilkat EA, Batibay H, Yener I, et al. Determination of enzyme inhibition potential and anticancer effects of *Pistacia khinjuk* stocks raised in *in vitro* and *in vivo* conditions. *Agronomy*. 2021;11(1):154. doi:10.3390/agronomy11010154

26. Luo H, Huang J, Liao WG, Huang QY, Gao YQ. The antioxidant effects of garlic saponins protect PC12 cells from hypoxia-induced damage. *Br J Nutr*. 2011;105(8):1164-1172.

27. Saeedi Rad A, Esmaeili S, Mohammadi Motamed S, Hamzeloo-Moghadam M. Cytotoxicity of two gypsophila species to human breast adenocarcinoma (MCF-7). *Internl Pharm Acta (IPA)*. 2018;1(1):82-82.

28. Kaplan, A. GC-MS profiling, antioxidant, antimicrobial activities, DNA cleavage effect of *Symphytum aintabicum* Hub.-Mor. & Wickens (Boraginaceae) and its anticancer activityon MCF-7 cell line. *Turkish J Bot*. 2021;45(8):750-764.

29. Xu X-Y, Wang Z, Ren S, et al. Improved protective effects of American ginseng berry against acetaminophen-induced liver toxicity through TNF-α-mediated caspase-3/-8/-9 signaling pathways. *Phytomedicine*. 2018;51:128-138.

30. Wang Y, Che J, Zhao H, Tang J, Shi G. Platycodin D inhibits oxidative stress and apoptosis in H9c2 cardiomyocytes following hypoxia/reoxygenation injury. *Biochem Biophys Res Commun*. 2018;503(4):3219-3224.

Optimization of Extraction Parameters of Phenolic Compounds from Cau Banana (*Musa paradisiaca*) Peel and Evaluation for Antioxidant and Antibacterial Potential

Truong Quoc Tat[1] ⓘ, Nguyen Duy Khanh[2] ⓘ

[1]Dong Thap University, Natural Resources and Environmental, Agriculture, Dong Thap-Vietnam
[2]Ho Chi Minh City Open University, Faculty of Biotechnology, Ho Chi Minh City-Vietnam

ABSTRACT

Objective: This study aims to demonstrate the potential reuse of Cau banana peel (CBP), a fruit by-product in the Mekong Delta, Vietnam, based on its antioxidant and antibacterial activity.

Materials and Methods: The determination of optimal extraction conditions for phenolics using response surface methodology from CBP powder. Then, the CBP extract was evaluated for total phenolic content (TPC), flavonoid content (TFC), phytochemical constituents, and antioxidant activity by the DPPH free radical scavenging assay, whereas antibacterial effects against the pathogens *Staphylococcus aureus* and *Escherichia coli* were determined by the agar diffusion and broth dilution methods.

Results: The highest TPC (38.42 mgGAE/g) and TFC (9.75 mgQE/g) were achieved with 1 g of the CBP powder, 58 mL of 60% ethanol solution, and 76 min of processing time at 56°C. The CBP extract contained tannins, flavonoids, alkaloids, saponins, and glycosides, with TPC and TFC of 543.48 mgGAE/g and 158.96 mgQE/g, respectively. The IC_{50} was 105.85 µg/mL, and the MBC/MIC ratios were ≤2.0 mg/mL. Therefore, it could be a strong antioxidant and bactericidal agent.

Conclusion: These results show that the peel waste of CBP could be helpful in the medical or health food industry for various applications instead of dumping them in landfills.

Keywords: Cau banana peel, Response surface methodology, Antioxidant, Antibacterial activity.

INTRODUCTION

Cau banana (*Musa paradisiaca*) belongs to the *Musaceae* family and is a native crop and a rich source of nutritional fruit in Vietnam. It is classified as a plantain banana and is typically eaten when fully ripened although it can also be cooked. In the production of frozen bananas, the peel is often discarded and comprises 18%-30% of the whole fruit weight,[1] leading to serious waste management challenges. Several recent studies have explored using banana peel waste, including composting,[2] protein,[3] ethanol,[4] alpha-amylase,[5] and dietary fibre production[6] through biotechnological processes.

In addition, there is growing interest in the medicinal properties of banana peels among researchers worldwide.[7,8] In Vietnamese ethnomedicine, banana peels have been traditionally used for various health purposes, such as treating gastric ulceration, persistent diarrhoea, dysentery, acne, and warts.[9] Recent analyses have shown that ripe banana peels contain a variety of phytonutrients and phytochemicals, including high levels of carbohydrates, dietary fibre, crude protein, crude fat, ash, starch, and resistant starch, respectively.[10] They also contain pigments (xanthophyll, beta-carotenoid) and vitamins (vitamins A and C) with antioxidant activity,[11-13] as well as essential minerals, such as potassium, calcium, sodium, manganese, and iron.[14] Banana peels are also rich in phenolics and have been linked to numerous health benefits, including the prevention of cardiovascular diseases, cancer, diabetes, and obesity.[15] They consist mainly of gallocatechin, catechin, and epicatechin.[16] Pereira et al.[17] demonstrated that the phenolic content was high in banana peel, accounting for 244 mgGAE/g. Toxic substances in banana peels, hydrogen cyanide, and oxalates were present at low levels of 1.3 mg/g and 0.5 mg/g, respectively, and within the safety limits Anhwange et al.[18] suggested that they are safe for human consumption.

In light of the growing problem of drug-resistant bacterial pathogens, which render antibiotics ineffective in treatment, there is a pressing need for new antibacterial agents,[19] such as using plant extracts as an effective therapy against resistant

bacterial strains.[20] Banana peels possess natural antibacterial properties and have shown activity against various inflammatory diseases.[21] Previous studies have demonstrated the effectiveness of banana peels against common pathogenic bacteria by biosorption and disruption of cell membrane activity.[22] Moreover, banana peels against *Porphyromonas gingivalis* and *Actinobacillus actinomycetemcomitans*.[23]

To the best of our understanding, while previous research in Vietnam has focussed on utilising banana peels for compost, fertilisers, bio-ethanol, composites, and activated carbon production,[24] less attention has been given to extracting phytochemical compounds from these by-products for medicinal or functional food purposes. In recent years, Vietnamese scientists have optimised the extraction conditions for phytochemical compounds from banana peels for medicinal or functional food purposes.[9,25] It has been found that using aqueous ethanol solution as a solvent is the most efficient method for extracting these compounds. This is due to the low boiling point and safety for human consumption of ethanol and the ability to expand and soften plant material, making it easier to extract the desired compounds.[25] However, it should be noted that there is no universal extraction procedure for all types of materials, and the specific extraction parameters must be determined for each type of material. Therefore, this study was conducted to determine the optimal extraction process for phenolic compounds from CBP collected in Tien Giang province, Mekong Delta, Vietnam, using ethanol as an extraction solvent, as well as to evaluate the antioxidant and antibacterial properties of the obtained crude extract.

MATERIALS AND METHODS

Chemicals

Cemaco (Vietnam) supplied the ethanol solvent for extraction. Sigma-Aldrich (United States) supplied DPPH (2,2-diphenyl-1-picrylhydrazyl), ascorbic acid, gallic acid, and Folin-Ciocalteu reagent which were used for antioxidant tests and determination of phenolic content, DMSO (Dimethyl sulfoxide) dissolved crude extract. Himedia (India) supplied tryptic soy agar (TSA) was used to store organisms, while Mueller-Hinton broth and agar (MHB and MHA) were used to determine antibacterial activity. The purified water and other chemicals used in this work were of analytical reagent grade.

Preparation of Sample, Extraction and Crude Extract

Plant Material

The unripe fruits of Cau banana (*M. paradisiaca*) were harvested from home gardens in Chau Thanh district, Tien Giang province, Mekong Delta, Vietnam. After 5-7 days, the peel of fresh banana fruit at stage 6 of ripening (yellow peel) was thoroughly rinsed, cut into small pieces, and dried at 50°C until the

moisture content was 12%. The dried peel was then blended and sifted through a 1.5-mm sieve to create a fine powder. Finally, the powdered banana peel sample was packed in vacuum-sealed PA bags and stored in refrigeration (4 ± 2°C) until needed for use, as shown in Figure 1.
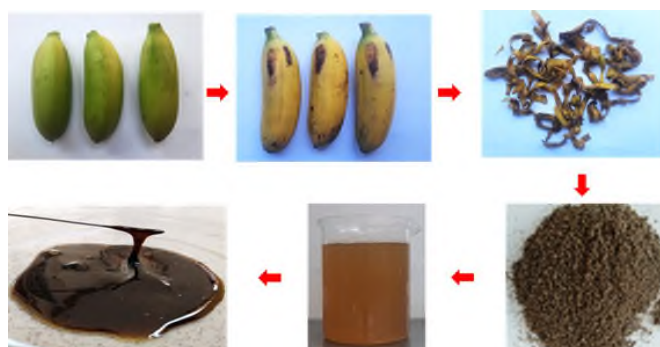
Figure 1. Crude extraction process from the CBP.

Crude Extract Collection

One hundred (100 grammes) of the CBP powder was used for extraction with ethanol (60%). The filtered transparent extract using Whatman number 1 philtre papers. The removed residues were re-extracted twice under the same conditions. The filtrates were combined and concentrated at 50°C using a rotary evaporator and then air-dried to obtain the crude extract. Finally, the extracted sample was kept in a clean brown bottle at 4 ± 2°C, before analysis.

$$Extraction\ yield(\%) = \frac{Weight\ of\ extract}{Weight\ of\ material}.100\% \quad (1)$$

Optimisation of Extraction Conditions of Phenolics from CBP Powder

The extraction process for phenolic compounds from the CBP powder was optimised using response surface methodology (RSM) with Box-Behnken design. This study examined the influence of three factors: the ratio of the CBP powder mass to ethanol volume (A), temperature (B), and time (C) on the total phenolic content-TPC (Y_1) and total flavonoid content-TFC (Y_2) of the transparent extracts (Table 1).

The extraction was performed with 1 g of dried sample in a flask, placed in a water bath, and shaken at a speed of 100 rpm. The transparent extract was then filtered using Whatman Number 1 philtre papers. The TPC and TFC of the extracts were analysed. The experiment was conducted in triplicate, and the data were analysed using multiple regression and analysis of variance (ANOVA) with Statgraphics Centurion XV software. The effect of the independent variables on the response (Y) model is described in the following section.

$$Y = b_0 + b_1 A + b_2 B + b_3 C + b_4 AB + b_5 AC + b_6 BC + b_7 A^2 + b_8 B^2 + b_9 C^2 \quad (2)$$

Table 1. Optimization experience plan using response surface methodology (RSM) and the research results.

No.	A (mL/g)	B (°C)	C (min)	Y_1 (mgGAE/g) Experimental*	Y_1 Predicted	Y_2 (mgQE/g) Experimental*	Y_2 Predicted
1	60 (0)	60 (0)	90 (0)	40.19 ± 0.06	40.18	9.52 ± 0.13	9.48
2	60 (0)	60 (0)	90 (0)	39.77 ± 0.20	40.18	9.44 ± 0.18	9.48
3	60 (0)	50 (-1)	120 (1)	37.33 ± 0.20	37.66	8.71 ± 0.07	8.71
4	60 (0)	60 (0)	90 (0)	40.11 ± 0.28	40.18	9.55 ± 0.14	9.48
5	60 (0)	60 (0)	90 (0)	40.67 ± 0.06	40.18	9.60 ± 0.07	9.48
6	70 (1)	70 (1)	90 (0)	38.34 ± 0.10	38.32	9.34 ± 0.05	9.45
7	60 (0)	60 (0)	90 (0)	40.18 ± 0.15	40.18	9.42 ± 0.08	9.48
8	50 (-1)	60 (0)	120 (1)	38.89 ± 0.33	38.55	8.34 ± 0.17	8.45
9	60 (0)	70 (1)	120 (1)	38.34 ± 0.96	38.63	8.58 ± 0.20	8.60
10	50 (-1)	70 (1)	90 (0)	38.96 ± 0.45	39.02	9.06 ± 0.19	8.94
11	70 (1)	60 (1)	60 (-1)	37.89 ± 0.17	38.24	9.31 ± 0.55	9.21
12	50 (-1)	60 (0)	60 (-1)	37.67 ± 0.04	37.94	9.17 ± 0.28	9.29
13	60 (0)	70 (1)	60 (-1)	38.30 ± 0.18	37.97	9.28 ± 0.20	9.28
14	60 (0)	50 (-1)	60 (-1)	39.21 ± 0.31	38.92	9.39 ± 0.56	9.37
15	50 (-1)	50 (-1)	90 (0)	38.91 ± 0.51	38.93	9.57 ± 0.14	9.46
16	70 (1)	60 (0)	120 (1)	37.29 ± 0.08	37.02	8.83 ± 0.14	8.71
17	60 (0)	60 (0)	90 (0)	40.16 ± 0.18	40.18	9.33 ± 0.63	9.48
18	70 (1)	50 (-1)	90 (0)	38.45 ± 0.12	38.39	9.01 ± 0.38	9.13

Note: "*" = Mean of duplicate runs.

where X_1, X_2, and X_3 are independent variables and b_0, b_1, b_2,... b_9 are offset, interaction, and squared effects. The selection model was mainly based on the R^2 value obtained from the regression.

Phytochemical Screening Assays

The CBP extract was tested for the presence of bioactive compounds, including tannin, flavonoid, alkaloid, saponin, and glycoside compounds, using the following standard procedures[26,27] (Table 2).

Total Phenol Content Analysis

The Folin-Ciocalteu assay was used for this determination.[28] The CBP extract (2 g) was dissolved in 100 mL of 99.99%

ethanol to a concentration of 20 mg/mL. The gallic acid (ranging from 10 to 100 µg/mL) or diluted extract (1 mL) was added to 2.5 mL of 10% Folin-Ciocalteu reagent and mixed thoroughly for 1 min. To the solution, 2 mL of 2% (w/w) sodium carbonate was added, and the mixture was allowed to stand for 15 min at room temperature. The absorbances of the reaction solutions containing polyphenol compounds extracted from the extracts and Folin-Ciocalteu reagent were measured at 765 nm. TPC values were calculated as milligramme gallic acid equivalent per gramme of dry material (mgGAE/g) using a calibration curve ($y = 0.0117x + 0.0037$, $R^2 = 0.9969$).

Total Flavonoid Content Analysis

The total flavonoid content of the extracts was determined using the aluminium trichloride colorimetric method.[29] The quercetin

Table 2. Qualitative tests for phytochemical screening.

Compound	Procedure	Indicating Positive Test
Tannin	1 mL of diluted extract (200 mg/mL) + a few drops of 1% gelatin solution containing sodium chloride	A white precipitate
Flavonoid	1 mL of diluted extract (200 mg/mL) + a few drops of 10% lead acetate solution	A yellow colour precipitate
Alkaloid	1 mL of diluted extract (200 mg/mL) + a few drops of Mayer's reagent (Potassium Mercuric Iodide)	A yellow colour precipitate
Saponin	0.5 g of crude extract was shaken with 2 mL of purified water	The foam produced persists for 10 min
Glycoside	1 mL of diluted extract (200 mg/mL) + 1 mL of pyridine + 1 mL of sodium nitroprusside solution and made alkaline using 10% sodium hydroxide solution	A pink to blood red colour

(ranging from 20 to 200 µg/mL) or diluted extract (20 mg/mL) with 0.5 mL was added to 1.5 mL of methanol, 0.1 mL of 10% aluminium chloride solution, 0.1 mL of 1M potassium acetate solution, and 2.8 mL of distilled water and mixed thoroughly for 1 min. The mixture was allowed to stand for 30 min at room temperature. The reaction formed a yellow solution, which was recorded at 415 nm. TFC values were calculated as mg of quercetin equivalent per gramme of dry material (mgQE/g) using a calibration curve ($y = 0.0049x + 0.0345$, $R^2 = 0.9953$).

Antioxidant Activity by the DPPH Radical Scavenging Assay

The free radical scavenging activity of the CBP extract was determined using the DPPH assay, according to the method described by Navghare and Dhawale.[30] The crude extract was diluted with methanol to concentrations of 200, 100, 50, and 25 µg/mL. As a positive control, an antioxidant standard, ascorbic acid (vitamin C), was prepared at the same concentrations. Then, 1 mL of the diluted extract or ascorbic acid solution was mixed with 3 mL of 0.1 mM DPPH in methanol. A blank sample was also prepared by mixing 3 mL of the methanol DPPH solution with 1 mL of methanol. The mixtures were incubated for 30 min in the dark at room temperature, and the decrease in absorbance was measured at 517 nm. The ability to scavenge DPPH radicals was calculated using the following formula:

$$\%Inhibition = \frac{A_{blank} - A_{sample}}{A_{blank}} \times 100\% \qquad (3)$$

where A_{blank} is the absorbance of DPPH without a sample (control); A_{sample} is the absorbance of the sample and DPPH (test sample) at 517 nm wavelength.

Each experiment was run in triplicate, and the average of the three inhibition values at each concentration was calculated. The graphs of averaged inhibition values against extract concentrations were used to produce a linear regression line to determine the half-maximal inhibitory concentration (IC_{50}).

Antibacterial Activity

Bacterial Cultures

Two pure cultures of the pathogenic bacteria strains *Staphylococcus aureus* WDCM 00195 and *Escherichia coli* WDCM 00196 were obtained from the Vietnam Academy of Science and Technology in Hanoi, Vietnam. The organisms were stored in Tryptic soy agar (TSA) nutrient slants at 4°C until needed for use.

Preparation of Standard Culture Inoculums of Test Organisms

Five colonies of each bacterial strain were inoculated in 15 mL sterile Mueller-Hinton broth (MHB) for approximately 24 h at 37°C, adjusted to a McFarland scale 0.5 ($\sim 10^8$ colony-forming units (cfu) per mL) with a spectrophotometer at 625 nm to reach an optical density of 0.08–0.10, and diluted 1:100 in sterile MHB to obtain final inoculums containing 10^6 cfu/mL. The standardised inoculum suspension was inoculated within 15-20 min.[31]

Antibiotic Susceptibility Testing

The paper disc diffusion method was used to determine the antibacterial activity of the CBP extract.[32] One hundred microliters (100 µL) of suspension of each bacterial strain was

swabbed onto Mueller-Hinton agar (MHA) media using a sterile cotton swab. Three sterile philtre discs of Whatman No. 1 paper (6 mm in diameter) was impregnated with the CBP extract at a concentration of 20 mg/mL in 5 μL volumes, placed on the inoculated agar plates, and gently pressed down with the help of a sterile forceps to ensure complete contact of the disc with the agar surface. Tetracycline at a concentration of 2 mg/mL was used as a positive control, whereas discs with a solution of 30% (v/v) DMSO served as a negative reference (5 μL each in separate Petri plates). Then, inoculated plates were incubated at 37°C for 24 h. The next day, the diameter of the inhibition zone was measured in millimetres around the discs in each plate. The size (diameter) of the inhibition zone was used to classify antibacterial activity, as shown in Table 3. The average inhibition zone diameter was categorised as very severe for diameters >20 mm; severe for diameters 10-20 mm, moderate for diameters 5-10 mm, and weak for diameters <5 mm.[33]

Determination of Minimum Inhibitory Concentration (MIC) and Minimum Bactericidal Concentration (MBC)

The MIC of the CBP extract was determined by the dilution method as described by Cheesbrough.[34] A double-fold serial dilution was performed using 30% DMSO solution (v/v). The following extract concentrations were obtained: 20, 10, 5, 2.5, and 1.25 mg/mL. Equal volumes of the extract solution and minimum bactericidal concentration (MHB) (2 mL) were dispensed into sterilised test tubes, and 100 μL of standardised inoculum (10^6 cfu/mL) was added to each test tube, which was aerobically incubated at 37°C for 24 h. A tube containing only broth and inoculum without extract was used as the organism control, whereas a tube containing broth and extract without inoculum served as the extract control. The minimum inhibitory concentration (MIC) value is defined as the lowest dilution that showed no growth in the MHB medium.

Sterile MHA plates were transferred with 10 μL of sample from each test tube that showed a complete absence of growth in the MIC test. The agar plates were then incubated at 37 ℃ for 24 h. The lowest concentration of the extract that yielded no growth was considered the MBC value.

Statistical Analysis

The significance of differences was determined using one-way ANOVA and the Tukey test ($p<0.05$) with Statgraphics Centurion XV software.

RESULTS

Optimisation of Extraction of Phenolic Compounds from CBP Powder

Based on our previous study, a 60% ethanol concentration showed a high extraction efficiency of phenolics in banana peel extract. Its water content was sufficient to soften the cell walls, increase the extraction efficiency, be safe for human consumption, and easily evaporate. Tai et al.[25] for phenolic extraction from "Xiem" banana peel collected in Vietnam reported a similar result. Therefore, a solvent with 60% ethanol concentration was chosen for this experiment. The table below displays the optimisation experience plan and the corresponding test results as mean values (Table 1).

RSM was used to analyse the impact of extraction conditions on the extraction of phenolic compounds from the CBP powder. The results of this analysis are shown in Figures 2 and 3, which display the response surface plots. The regression equation for the selected model, along with the measured levels of phenolics and flavonoids and their adjusted R^2, is as follows:

$TPC = 40.18\ 0.46AC + 0.48BC - 0.94A^2 - 0.58B^2 - 1.31C^2$, with $R^2 = 93.80\%$, R^2 (adj.) = 86.83%, SEE = 0.38,

$TFC = 9.48\ 0.34C + 0.22AB - 0.16A^2 - 0.41C^2$, with $R^2 = 93.41\%$, R^2 (adj.) = 85.99%, SEE = 0.10,

On the basis of the response surface plots and regression model analysis results, the optimal extraction mixture condition for the total phenolic and flavonoid content was determined to be a ratio of 60% aqueous ethanol volume to the banana peel powder weight of 58:1 (mL/g), a temperature of 56°C, and a processing time of 76 min. A comparison between the maximum experimental values of phenolic compounds and extraction conditions and the predicted values (Table 4) revealed that the two sets of values were close. Indeed, the maximum values for TPC (prediction: 40.15 mgGAE/g, experimental: 38.42 mgQE/g) and TFC (prediction: 9.54 mgGAE/g, experimental: 9.75 mgQE/g) were obtained using the same extraction conditions in both the experimental and predicted models. These results demonstrate the validity of the experimental model, as there is a high degree of agreement between the observed values and those predicted by the regression model. Therefore, this response surface modelling approach can effectively predict the extraction of phenolic compounds from CBP powder.

Physical Properties, TPC, TFC, and Phytochemical Screening Results of the CBP Extract

Organoleptically, the crude extract obtained from the CBP powder was dark brown, with a slightly sticky texture, a bitter taste, and an intense odour of ripe banana. The equivalent yield of the extract was 13.01% (Table 5) compared with the mass of dried banana peel powder (100 g). In terms of total phenolic and flavonoid content, this extract sample showed high TPC and TFC values of 543.48 mgGAE/g and 158.96 mgQE/g, respectively. The results of phytochemical screening of the crude extract from the peel of Cau banana, as shown in Table 5, confirmed the presence of active compounds such as tannins, flavonoids, alkaloids, saponins, and glycosides. These compounds have beneficial effects on human health.

Table 3. Categorization based on the diameter of the inhibition zone formed.[31]

Average inhibition zone diameter (mm)	Inhibitory strength
>20	Very Severe
10–20	Severe
5–10	Moderate
<5	Weak
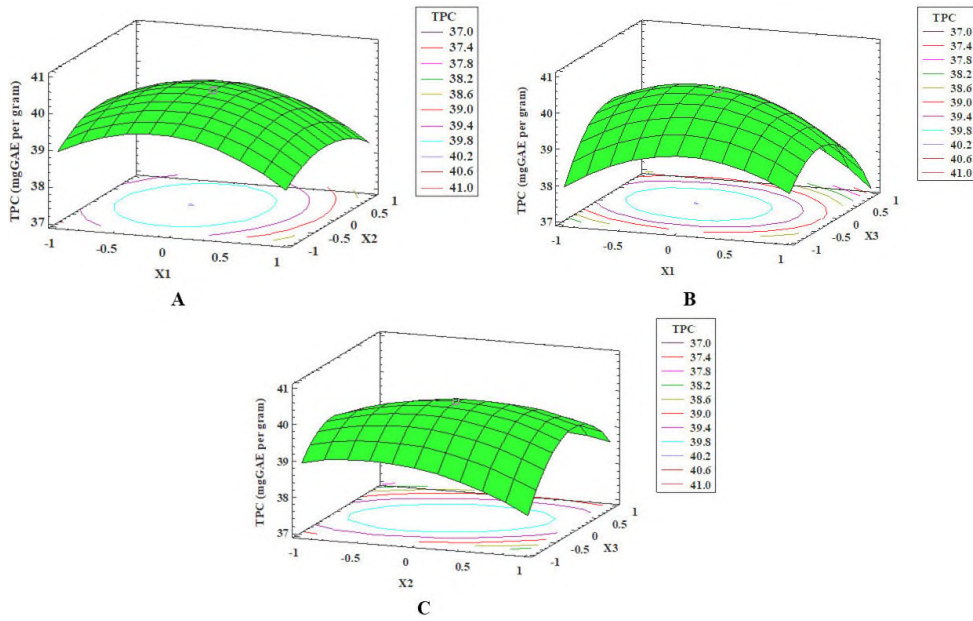
Figure 2. Impact of process conditions on the TPC of extraction. (A) Ethanol volume and temperature. (B) Ethanol volume and time. (C) Temperature and time.
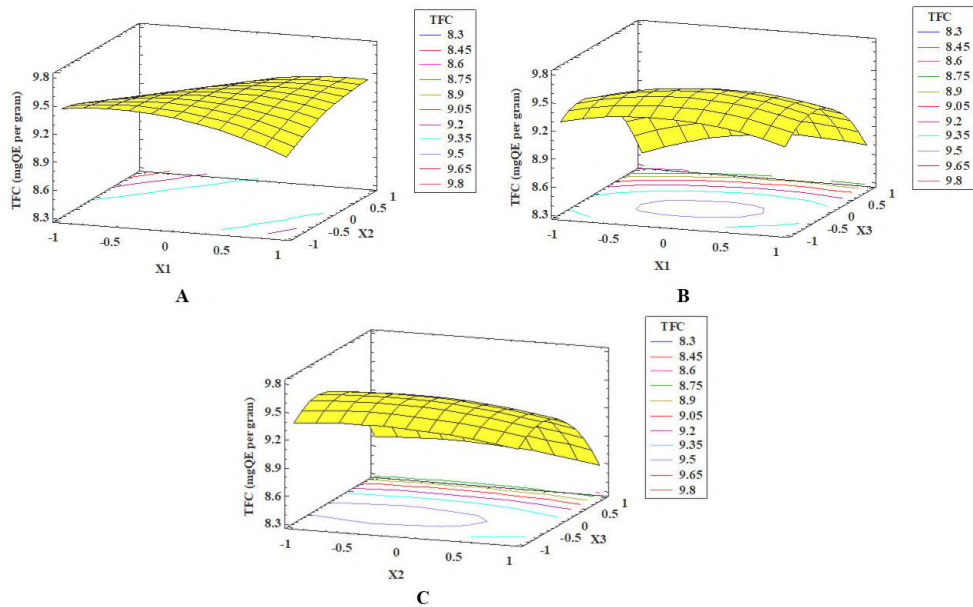
Figure 3. Impact of process conditions on the TFC of extraction. (A) Ethanol volume and temperature. (B) Ethanol volume and time. (C) Temperature and time.

Table 4. Experimental data of the validation of predicted values at optimal process conditions.

Response	Predicted value	Confidence interval (95%)		Experimental value
		Minimum	Maximum	
Y_1 - TPC (mgGAE/g)	40.15	39.79	40.51	38.42
Y_2 - TFC (mgQE/g)	9.54	9.41	9.67	9.75

TPC:total polyphenol content; TFC: total flavonoid content.

Table 5. The properties of the Cau banana peel extract.

Parameters	Result
Yield (%)	13.01
Moisture (%)	6.64 ± 0.47
TPC (mgGAE/g)	543.48 ± 1.08
TFC (mgQE/g)	158.96 ± 1.43
Tannins	+
Flavonoids	+
Alkaloids	+
Saponins	+
Glycosides	+

Note: "+" = Present. TPC:total polyphenol content; TFC: total flavonoid content.

Antioxidant Activity of the CBP Extract

The DPPH radical scavenging assay is a widely accepted method for determining the overall antioxidant capacity of plant extracts. In this study, the ethanolic extract from the CBP powder exhibited significant DPPH free radical scavenging activity, as illustrated in Figure 4.

Overall, the DPPH free radical scavenging activity of both the ethanolic extract of the CBP powder and ascorbic acid showed a dose-dependent relationship, with higher concentrations resulting in increased activity. Specifically, the percentage of inhibition of DPPH radicals for the four different concentrations of extract used in this study (25, 50, 100, and 200 µg/mL) was 24.64%, 32.55%, 54.89%, and 74.16%, respectively. In comparison, ascorbic acid at the same concentrations showed inhibition rates of 29.84%, 39.12%, 61.34%, and 90.24%. Based on the obtained percentage of inhibition, graphs were plotted to estimate the IC_{50} value using linear regression analysis. The linearity (R^2) of the extracted sample and ascorbic acid were 0.9616 and 0.9898, respectively. The IC_{50} values for quenching DPPH free radicals were found to be 105.85 µg/mL for the extract and 78.89 µg/mL for ascorbic acid. The CBP extract has approximately 1.34 times lower activity than ascorbic acid.

Antibacterial Activities of the CBP Extract

The results of the antibacterial activity of the CBP extract against the two tested pathogenic microorganisms are presented in Figure 5 and Table 6.

The zone of inhibition of bacterial growth was found to be dependent on the relative antimicrobial potency of the extract. At a concentration of 20 mg/mL, the extracted sample exhibited significant antimicrobial activity against only *S. aureus* by a larger zone of clearance observed as 15.00 mm compared with *E. coli* (0 mm) ($p < 0.05$). However, it was found to be less effective than the standard antibiotic tetracycline, whereas no inhibitory effect was noted for the negative reference (DMSO).
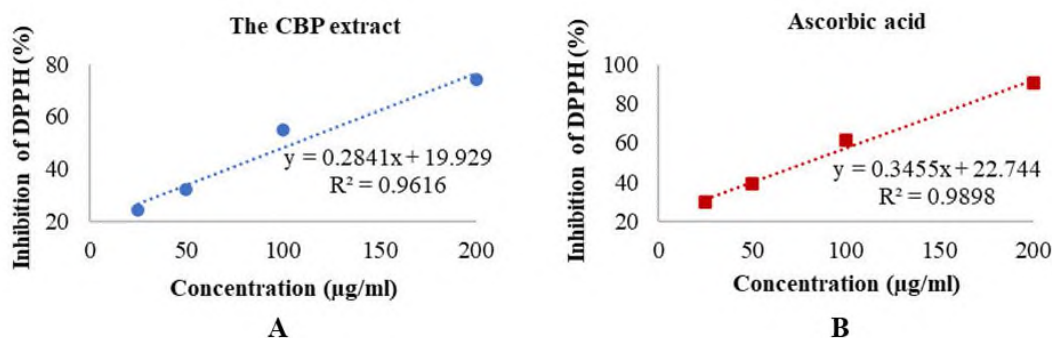
Figure 4. Percentage of DPPH inhibition by the CBP extract (A) and ascorbic acid (B) at different concentrations
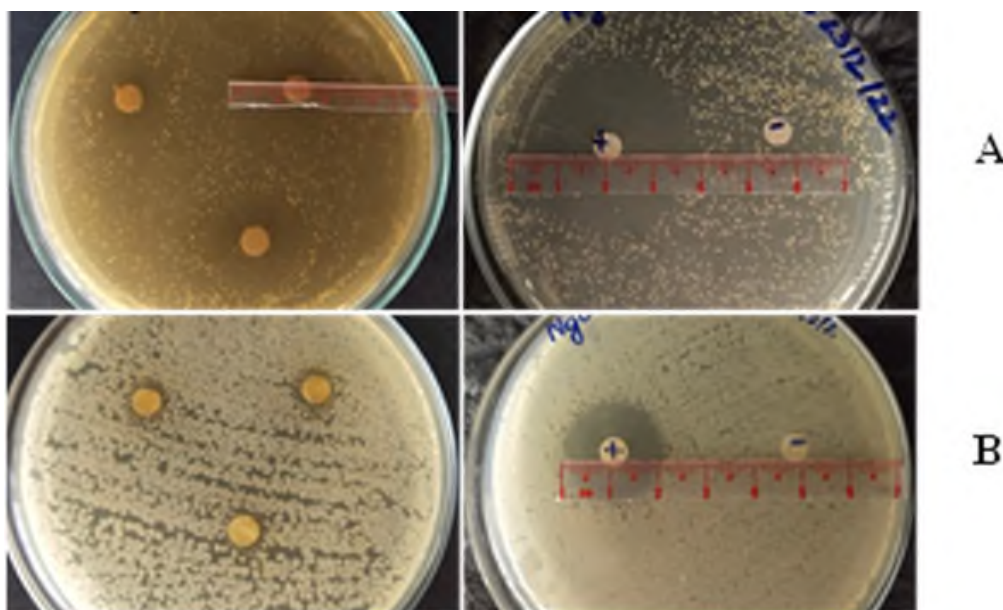
Figure 5. The inhibition of bacterial effects of the CBP extract at 20 mg/mL and controls A. The effect on *S. aureus* of the CBP extract (left) and the controls (right) B. The effect on *E. coli* of the CBP extract (left) and the controls (right).

Table 6. Antibacterial activity of the CBP extract at 20 mg/mL.

Test organisms	Zone of clearance (mm) ± SD			MIC (mg/mL)	MBC (mg/mL)
	The extract	Tetracycline	DMSO		
S. aureus	15.00 ± 0.50^a	33.83 ± 0.76^a	0^a	2.50^a	2.50^b
E. coli	0^b	21.47 ± 0.67^b	0^a	2.50^a	5.00^a

Note: Different letters (a, b,...) next to the mean values in each column indicate significant difference (Tukey test, $p<0.05$); MIC: Minimum inhibitory concentration; MBC: Minimum bactericidal concentration.

Continuously, MIC and MBC values of the CBP extract was determined. The potent antibacterial effect of the extract is also shown in Table 6. An interesting result, the same MIC values of the extract against *S. aureus* and *E. coli* were 2.50 mg/mL, whereas the MBC values were different, they were 2.50 mg/mL for *S. aureus* and 5.00 mg/mL for *E. coli*. The MIC and MBC values obtained after susceptibility tests indicated the good antimicrobial activity of the CBP extract against both tested pathogens. The MBC/MIC ratios were calculated at 1.0 and 2.0 for extthe extractainst *S. aureus* and *E. coli*, respectively, which were both bactericidal agents.

DISCUSSION

In recent years, several reports have been published on the effects of various extraction techniques on the recovery of bioactive compounds from banana peels, as well as the antioxidant and antibacterial properties of the resulting extract.[35-38] However, the specific impact of using aqueous ethanol as an extraction method for phenolic compounds from has not yet been thoroughly investigated. Ishak et al.[36] optimised the periodic extraction of flavonoids from unripe Cavendish banana peel using aqueous ethanol solution with ultrasound-assisted techniques. Their research demonstrated a high recovery rate of flavonoids from banana peel (29 mgQE/g) and a reduced extraction time (only 30 min) when using ultrasound-assisted extraction. Although this method has many advantages, such as increased efficiency and reduced extraction time, it can also be relatively expensive due to the cost of equipment installation.

Our extraction yield was higher than the previous yield obtained from *M. acuminata Colla* AAA in Thailand (11.26%).[36] González-Montelongo et al.[1] discovered that banana peels contain considerable amounts of extractable compounds. In addition, the moisture content of the extracted sample did not exceed the reference value of the water content in the crude extracts from plants (<10%), this characterisation is necessary for safe storage and longer shelf life because it can inhibit the growth of bacteria and deteriorate the content of the bioactive compounds due to polyphenol oxidase activity, which adversely affects plant extract quality.[39,40] The TPC value was much higher than that previously reported by Anal et al.[38], who found the TPC in banana peel extract to range from 18.21 to 35.06 mgGAE/g, but it was lower than that extracted from peels of three banana varieties grown in West Java, Indonesia (1460-4630 mgGAE/g).[41] Next, the extracted sample had a TFC value lower than that in previous research of 196.05 mgQE/g.[38] However, they were higher than those discovered by Salim et al.[42], who recorded 10.92 mg QE/g. The TPC and TFC values in banana peel extracts vary depending on the variety, growing region, and ripeness as well as the methods used for sample preparation, extraction, and determination.[1,43] The high TPC and TFC values of banana peel are responsible for the strong antioxidant and microbial capacities.

Phenolic compounds, including tannins and flavonoids, are naturally occurring antioxidants and antibacterial agents found in plants. Tannins, in particular, are believed to be responsible for promoting haemostasis, treating diarrhoea, relieving pain, and promoting thrombolysis.[44] However, their low taste and odour can limit their use in the food industry. On the other hand, flavonoids have lipid-lowering, antiatherogenic, anti-inflammatory, and antimicrobial properties, making them beneficial in reducing the risk of atherosclerosis and related diseases.[45] The presence of alkaloids in these plants has been traditionally used in herbal medicines, teas, and potions.[46] One of the most notable biological properties of these ac-

tive compounds is their cytotoxicity.[47] Saponins, known for their bitterness and ability to foam in aqueous solutions, had activities such as haemolysis and cholesterol-binding.[48] They have also been reported to have various pharmacological actions, including anti-inflammatory, anti-obesity, immunostimulant, hypocholesterolemic, hypoglycaemic, antifungal, and anticancer effects.[49] Glycosides, another active compound found in this plant extract, have shown great potential in treating a variety of illnesses, including cardiovascular, antibacterial, anticancer, anti-inflammatory, and neurodegenerative conditions.[50] These findings agree with previous research that identified tannins, flavonoids, alkaloids, saponins, and glycosides in banana peels from the Musa genus (*Musaceae*). Flavonoids, alkaloids, and saponins have antibacterial properties, whereas tannins and phenols have antioxidant potential.[51]

Our extract has strong antioxidant activity, as classified by the IC_{50} value given by Molyneux.[52] Our ethanolic extract from the CBP powder showed even greater DPPH scavenging power compared with other banana peels and fruit peels, such as the *M. cavendish* peel ($IC_{50} = 232.08$ µg/mL) and the *M. acuminata* peel ($IC_{50} = 139.50$ µg/mL),[30] as well as the Ambonese banana (*M. paradisiaca*) peel ($IC_{50} = 114.00$ µg/mL) and orange (*Citrus reticulata*) peel ($IC_{50} = 222.00$ µg/mL).[53] This is due to the high concentration of phytochemical compounds in banana peel, which are known for their antioxidant properties. Several previous studies have observed a positive association between the bioactive compound content and the DPPH radical scavenging activity of banana peel.[54] GC-MS analysis indicated the presence of potential antioxidant phenolic and flavonoid compounds in the ethanolic *M. paradisiaca* peel extract, including ellagic acid, gallic acid, rutin, myricetin, naringenin, epicatechin, gallocatechin, octadecenamide, β-sitosterol, stigmasterol, estragole, and vitamin E.[55,56] These bioactive compounds have the potential to remove free radicals and active oxygen species through active oxygen species (AOS) detoxifying enzymes, superoxide dismutase (SOD), and peroxidases, implying that they may play a protective role against oxidative damage.[11] The antioxidant activity found in CBP extract allows several potential uses to be suggested, including cosmetic use in the prevention of premature skin ageing[57,58] and chemoprevention of cancers and other chronic diseases at low cost.[59,60]

The 15.00 mm in diameter clear inhibition area to *S. aureus* was classified as severe actions.[61] Furthermore, plant extracts with activity at concentrations of 1000 µg extract per disc or lower are considered promising bioactive agents for further study.[62] MBC/MIC ratio ≤ 2.0 and ≤ 4.0 implies bactericidal and bacteriostatic effects, respectively.[63] Fortunately, the MBC/MIC ratios were calculated at to be 1.0 and 2.0 for extract against *S. aureus* and *E. coli*, respectively, which were both bactericidal agents. The results of this study indicated that the CBP extract is more effective against Gram-positive than Gram-negative bacteria at the same concentration. Similar findings have also been reported, and differences in sensitivity

could be attributed to the different morphological constitutions of Gram-positive and Gram-negative bacteria strains.[64,65] According to Fajrih et al.,[66] Gram-negative bacteria have an effective permeability barrier comprising a thick cell wall with three layers, including lipoprotein, outer membrane, and a thin lipopolysaccharide, and high lipid contents of 11-22%, which limited the penetration of antibacterial substances, while Gram-positive bacteria have lower lipid contents ranging from 1% to 4%. Another interesting point is that although Gram-positive bacteria have a thicker peptidoglycan layer than Gram-negative bacteria, this macromolecule is a mesh-like framework. As a result, antibacterial substances found it easier to penetrate.[67,68]

In the present study, the integration of phytochemicals in CBP extract was demonstrated, and their presence might be responsible for the potential antibacterial activity of CBP extract. Tannins are believed to have antibacterial activities by damaging components of cell membranes, cell walls, enzymes, genetic material, and other protein components of bacteria.[69] Flavonoids could play a role in forming complexes with soluble proteins or not on the cell surface and with the bacterial cell wall.[69,70] The more lipophilic a flavonoid its ability to damage the cell wall of the bacteria will be more powerful. Next, most alkaloids are strongly bactericidal agents with different mechanisms.[71] The alkaloids as pergularinine and tylophorinidine deactivated dihydrofolate reductase, an essential enzyme for bacterial nucleic acid synthesis. In addition, flavonoids and alkaloids can also kill bacteria by preventing the formation of their cell layers.[72] Meanwhile, saponins can disturb bacterial outer membrane permeability.[73] This result could be responsible for the popular use of banana peel to accelerate the wound-healing process and act as an inflammatory modulator in acne vulgarisbecause ofo the presence of antioxidant, antibacteria, and antiinflammatory substances.[74,75] They can suppress the growth of pathogenic bacteria and prevent infection of the wound.

The ethanolic extract from the CBP powder (*M. paradisiaca*) in this study showed antimicrobial activity greater than that in the previous study by Okorondu et al.[76] Reported that the water extract of *M. paradisiaca* peel did not exert any antimicrobial effect against the bacterial strains. In contrast, Asoso et al.[77] stated that the *M. paradisiaca* peel extract showed activity against *E. coli* ATCC 35218 (17 mm), *Salmonella typhi* ATCC 22648 (17 mm), *Shigella dysenteriae* ATCC 24162 (22 mm), *Klebsiella pneumonia* ATCC 34089 (17 mm), *S. aureus* ATCC 25923 (17 mm), and *Bacillus subtilis* ATCC 21332 (27 mm). Therefore, the antibacterial potency of *M. paradisiaca* extracts is controversial. It could depend on the nature of the varieties, extracted sample (solvent and concentration used), and microorganisms used.

CONCLUSION

In conclusion, the results of this study exceeded our expectations. The RSM was effectively and accurately applied to predict the TPC and TFC in the extract from the powder of Cau banana (*M. paradisiaca*) peel in Tien Giang province, Vietnam. The crude extract was confirmed to contain various chemical groups based on its phytochemical composition. The existence of all these compounds in the extracted sample was a major contributor to their potential to act as natural antioxidants and antibacterials against the growth of the tested pathogens *S. aureus* and *E. coli*. These results highlight the richness of Cau banana peel in secondary metabolites and its potential as a new-generation drug. Furthermore, it would be interesting to test more different bacterial pathogens, including *K. pneumoniae*, *Yersinia*, and *S. typhimurium*, as well as identify different phenolic molecules and test them *in vitro* and *in vivo by* exploiting animal models.

ORCID IDs of the Authors

Truong Quoc Tat   0009-0005-7839-3910
Nguyen Duy Khanh   0009-0003-3873-6726

REFERENCES

1. González-Montelongo R, Lobo MG, González M. Antioxidant activity in banana peel extracts: Testing extraction conditions and related bioactive compounds. *Food Chem*. 2010;119(3):1030-1039.

2. Isibika A, Vinneras B, Kibazohi O, Zurbrügg C, Lalander C. Co-composting of banana peel and orange peel waste with fish waste to improve conversion by black soldier fly (*Hermetia illucens* (L.), Diptera: Stratiomyidae) larvae. *J Clean Prod*. 2021;318:128570. doi:10.1016/j.jclepro.2021.128570

3. Budhalakoti N. Extraction of protein from banana by-product and its characterization. *J Food Meas Charact*. 2021;15(3):2202-2210.

4. Palacios AS, Llyina A, Ramos-González R, et al. Ethanol production from banana peels at high pretreated substrate loading: comparison of two operational strategies. *Biomass Conv Bioref*. 2021;11:1587-1596.

5. Unakal C, Kallur RI, Kaliwal BB. Production of α-amylase using banana waste by *Bacillus subtilis* under solid state fermentation. *Eur J Exp Biol*. 2012;2:1044-1052.

6. Eshak NS. Sensory evaluation and nutritional value of balady flat bread supplemented with banana peels as a natural source of dietary fiber. *Ann Agric Sci*. 2016;61(2):229-235.

7. Kumar KS, Bhowmik D, Duraivel S, Umadevi M. Traditional and medicinal uses of banana. *J Pharmacogn Phytochem*. 2012;1(3):51-63.

8. Hikal WM, Ahl SA, Hussein AH et al. Banana peels: A waste treasure for human being. *Evid Based Complement Alternat Med*. 2022;7616452. doi:10.1155/2022/7616452

9. Vu HT, Scarlett CJ, Vuong QV. Phenolic compounds within banana peel and their potential uses: A review. *J Funct Foods*. 2018;40:238-248.

10. Zaini HM, Roslan J, Saallah S, et al. Banana peels as a bioactive ingredient and its potential application in the food industry. *J Funct Foods*. 2022;92:105054. doi:10.1016/j.jff.2022.105054.

11. Sundaram S, Anjum S, Dwivedi P, Rai GK. Antioxidant activity and protective effect of banana peel against oxidative hemolysis of human erythrocyte at different stages of ripening. *Biotechnol Appl Biochem*. 2011;64:1192-1206.

12. Yan L, Fernando WM, Brennan M, et al. Effect of extraction method and ripening stage on banana peel pigments. *Int J Food Sci Technol*. 2016;51(6):1449-1456.

13. Hikal WM, Said-Al, Ahl HA. Banana peels as possible antioxidant and antimicrobial agents. *Asian J Res Rev Agrc*. 2021;3(3):35-45.

14. Alam MJ, Akter S, Afroze S, Islam MT, Sayeem EH. Development of fiber and mineral enriched cookies by utilization of banana and banana peel flour. *J Microbiol Biotechnol Food Sci*. 2020;10(3):329-334.

15. Singh B, Singh JP, Kaur A, Singh N. Bioactive compounds in banana and their associated health benefits-A review. *Food Chem*. 2016;206:1-11.

16. Crozie A, Jaganath IB, Clifford MN. Phenols, polyphenols and tannins: an overview. Plant secondary metabolites: Occurrence, structure and role in the human diet 2006;1:1-25.

17. Pereira GA, Molina G, Arruda HS, Pastore GM. Optimizing the homogenizer-assisted extraction (HAE) of total phenolic compounds from banana peel. *J Food Process Eng*. 2017;40(3):e12438. doi:10.1111/jfpe.12438

18. Anhwange BA, Ugye TJ, Nyiaatagher TD. Chemical composition of *Musa sapientum* (banana) peels. *Electron J Environ Agr Food Chem*. 2009;8(6):437-442.

19. Chinemerem ND, Ugwu MC, Oliseloke AC, et al. Antibiotic resistance: The challenges and some emerging strategies for tackling a global menace. *J Clin Lab Anal*. 2022;36(9):e24655. doi:10.1002/jcla.24655

20. Atef NM, Shanab SM, Negm SI, Abbas YA. Evaluation of antimicrobial activity of some plant extracts against antibiotic susceptible and resistant bacterial strains causing wound infection. *Bull Natl Res Cent*. 2019;43(1):1-11.

21. Mpharm SR. Anti-inflammatory and antioxidant activities of extracts from *Musa sapientum* peel. *J Med Assoc Thai*. 2012;95(1):142-146.

22. Kumari P, Pillai VV, Benedetto A. Mechanisms of action of ionic liquids on living cells: The state of the art. *Biophys Rev*. 2020;12(5):1187-1215.

23. Kapadia SP, Pudakalkatti S, Shivanaikar S. Detection of antimicrobial activity of banana peel (*Musa paradisiaca* L.) on *Porphyromonas gingivalis* and *Aggregatibacter actinomycetemcomitans*: An *in vitro* study. *Contemp Clin Dent*. 2015;6(4):496-499.

24. Tai NV, Minh VQ, Thuy NM. Food processing waste in Vietnam: Utilization and prospects in food industry for sustainability development. *J Microbiol Biotechnol Food Sci*. 2023;13(1):e9926. doi:10.55251/jmbfs.9926

25. Tai NV, Linh MN, Thuy NM. Optimization of extraction conditions of phytochemical compounds in "Xiem" banana peel powder using response surface methodology. *J App Biol Biotech*. 2021;9(6):56-62.

26. Sofowora A. Screening plants for bioactive agents. Medicinal Plants and Traditional Medicinal in Africa. 2nd Ed. Spectrum Books Ltd, Sunshine House, Ibadan, Nigeria, 1993:134-156.

27. Tiwari P, Kumar B, Kaur M, Kaur GH. Phytochemical screening and extraction: A review. *Int Pharm Sci*. 2011;1(1): 98-106.

28. Yadav RNS, Agarwala M. Phytochemical analysis of some medicinal plants. *J Phytol*. 2011;3(12):10-14.

29. Mandal B, Madan S. Preliminary phytochemical screening and evaluation of free radical scavenging activity of *Stevia rebaudiana* Bertoni from different geographical sources. *J Pharmacogn Phytochem*. 2013;2(1):14-19.

30. Navghare VV, Dhawale SC. *In vitro* antioxidant, hypoglycemic and oral glucose tolerance test of banana peels. *Alex J Med*. 2017;53(3):237-243.

31. Natta L, Orapin K, Krittika N, Pantip B. Essential oil from five Zingiberaceae for anti food-borne bacteria. *Int Food Res J*. 2008;15(3):337-46.

32. Setyowati WAE, Susanti VHE. Antibacterial activity of natural paper from banana peel (*Musa paradisiaca* Linn.) with additive essential oils. In *IOP Conference Series: Materials Science and Engineering*. 2019;*578*(1):012048. IOP Publishing.

33. Indriani V, Chiuman L, Wijaya LL, *et al*. Antibacterial effect of *Curcuma zedoaria* extract on *Bacillus cereus* and *Staphylococcus epidermidis*. *Althea Med J*. 2020;7(1):6-10.

34. Cheesbrough M. *District laboratory practice in tropical countries, Part 2*. Cambridge university Press, United Kingdom 2005.

35. Singhal M, Ratra P. Antioxidant activity, total flavonoid and total phenolic content of *Musa acuminate* peel extracts. *Global J Pharmacol*. 2013;7(2):118-122.

36. Ishak NA, Raza NAA, Dek SP, Baharuddin AS. Production of high tannin content and antioxidant activity extract from an unripe peel of *Musa acuminata* (Cavendish) using ultrasound-assisted extraction (UAE). BioRes. 2020;15(1):1877-1893.

37. Said FM, Gan JY, Sulaiman J. Correlation between response surface methodology and artificial neural network in the prediction of bioactive compounds of unripe *Musa acuminata* peel. *Eng Sci Technol Int*. 2020;*3*(4):781-787.

38. Anal AK, Jaisanti S, Noomhorm A. Enhanced yield of phenolic extracts from banana peels (*Musa acuminata* Colla AAA) and cinnamon barks (*Cinnamomum varum*) and their antioxidative potentials in fish oil. *J Food Sci Technol*. 2014;51:2632-2639.

39. Lavelli V, Caronni P. Polyphenol oxidase activity and implications on the quality of intermediate moisture and dried apples. *Eur Food Res Technol*. 2010;231:93-100.

40. Sulastri E, Zubair MS, Anas NI, et al. Total phenolic, total flavonoid, quercetin content and antioxidant activity of standardized extract of *Moringa oleifera* leaf from regions with different elevation. *Pharmacogn J*. 2018;10(6):104-108.

41. Fidrianny I, Suhendy H, Insanu M. Correlation of phytochemical content with antioxidant potential of various sweet potato (*Ipomoea batatas*) in West Java, Indonesia. *Asian Pac J Trop Biomed*. 2018;8(1):25-30.

42. Salim E. Dried samples characterization and determination of total phenol and flavonoid of ethanol extract from *Musa paradisiaca* L. fruit peel. *Na J Adv Res Rev.* 2022;16(3):941-946.

43. Kabir MR, Hasan MM, Islam MR, et al. Formulation of yogurt with banana peel extracts to enhance storability and bioactive properties. *J Food Process Preserv.* 2021;45(3):e15191. doi:10.1111/jfpp.15191

44. Sharma K, Kumar V, Kaur J, et al. Health effects, sources, utilization and safety of tannins: A critical review. *Toxin Rev.* 2021;40(4):432-444.

45. Salvamani S, Gunasekaran B, Shaharuddin NA, et al. Antiartherosclerotic effects of plant flavonoids. *Biomed Res Int.* 2014;480258. doi:10.1155/2014/480258

46. Bribi N. Pharmacological activity of alkaloids: A review. *Asian J Bot.* 2018;1(1):1-6.

47. Zarin MA, Wan HY, Isha A, Armania, N. Antioxidant, antimicrobial and cytotoxic potential of condensed tannins from *Leucaena leucocephala* hybrid-Rendang. *Food Sci Hum Wellness.* 2016;5(2):65-75.

48. Sharmin F, Koyama T, Koyama H, Ishizaki S. Cholesterol-binding ability of saponin from Japanese starfish. *J Food Sci Technol.* 2021;58:3056-3064.

49. Marrelli M, Conforti F, Araniti F, Statti GA. Effects of saponins on lipid metabolism: A review of potential health benefits in the treatment of obesity. *Molecules.* 2016;21(10):1404. doi:10.3390/molecules21101404

50. Riaz T, Akram M, Laila U, et al. Therapeutic applications of glycosides obtained from medicinal plants. *Int Arch Integr Med.* 2023;10(8):30-38.

51. Siddique S, Nawaz S, Muhammad F, et al. Phytochemical screening and in-vitro evaluation of pharmacological activities of peels of *Musa sapientum* and *Carica papaya* fruit. *Nat Prod Res.* 2018;32(11):1333-1336.

52. Molyneux P. The use of the stable free radical diphenylpicrylhydrazyl (DPPH) for estimating antioxidant activity. *Songklanakarin. J Sci Technol.* 2004;26(2):211-219.

53. Ariani N, Nurani LH. The antioxidant activity analysis of the ethanolic extract of banana peel (*Musa paradisiaca* forma typica) with DPPH method. In *Proceedings of the 1st Muhammadiyah International Conference on Health and Pharmaceutical Development.* 2018;2018, 44-47.

54. Rit WS, Swantara IMD, Asih IARA, Puspawati NM. Antibacterial activity and antioxidant capacity of selected local banana peel (*Musa* sp.) methanol extracts cultivated in Bali. *Int J Agri Env Biotech.* 2020;5(03):242-251.

55. Behiry SI, Okla MK, Alamri SA, et al. Antifungal and antibacterial activities of *Musa paradisiaca* L. peel Extract: HPLC analysis of phenolic and flavonoid contents. *Processes.* 2019;7:215. doi:10.3390/pr7040215

56. Abdel Aziz SM, Ahmed OM, Abd EL-Twab SM, et al. Antihyperglycemic effects and mode of actions of *Musa paradisiaca* leaf and fruit peel hydroethanolic extracts in nicotinamide/streptozotocin-induced diabetic rats. *Evid Based Complement Alternat Med.* 2020;2020:9276343. doi:10.1155/2020/9276343

57. Kumari PS, Ranjitha R, Vidhya N. Revitalizing property of banana peel extracts by antioxidant activity and antibacterial activity against acne causing *Staphylococcus epidermidis. Ann Phytomed.* 2020;9(2):215-222.

58. Hashim M, Hamid Z, Gul Z, Akbar A. Functional, nutritional and medicinal potential of banana peel. *Pure Appl Bio.* 2023;12(1):470-490.

59. Ruangtong J, Jiraroj T, T-Thienpraser NP. Green synthesized ZnO nanosheets from banana peel extract possess antibacterial activity and anti-cancer activity. *Mater Today Commun.* 2020;24:101224. doi:10.1016/j.mtcomm.2020.101224

60. 60. Azarudeen AM, Nithya R. Pharmaceutical aspects of banana peel: A review. *J Pharm Sci Res.* 2021;13(2):112-117.

61. Indriani V, Chiuman L, Wijaya LL, et al. Antibacterial effect of *Curcuma zedoaria* extract on *Bacillus cereus* and *Staphylococcus epidermidis. Althea Med J.* 2020;7(1):6-10.

62. Mitscher LA, Leu RP, Bathal MS, et al. Antimicrobial agents from higher plants. I. Introduction, rationale, and methodology. *Lloydia.* 1972;35(2):157-166.

63. Gas EN, Aho HS, Borquaye LS. Peptide extract from *Olivancillaria hiatula* exhibits broad-spectrum antibacterial activity. *Biomed Res Int.* 2018;2018:6010572. doi:10.1155/2018/6010572

64. Balouiri M, Sadiki M, Ibnsouda SK. Methods for *in vitro* evaluating antimicrobial activity: A review. *J Pharm Anal.* 2016;6:71-79.

65. Mekinic IG, Skroza D, Ljubenkov I, et al. Antioxidant and antimicrobial potential of phenolic metabolites from traditionally used mediterranean herbs and spices. *Foods.* 2019;8:1-16.

66. Fajrih N, Wiryawan KG, Sumiati S, et al. Identification of bioactive compounds of banana corm (*Musa paradisiaca*) using GC-MS and its inhibitory effect against pathogenic bacteria. *Biodiv J Biol Div.* 2022;23(1):195-204.

67. Vollmer W. "Peptidoglycan." Molecular Medical Microbiology. Academic Press, 2015. 105-124.

68. Yahaya A, Ali M, EL-Hassan FI, Jido BA. Antibacterial activity of guava (*Psidium guajava* L.) extracts on *Staphylococcus aureus* isolated from patients with urinary tract infections attending a tertiary-care hospital. *Sci World J.* 2019;14(1):47-51.

69. Sabir A. Antibacterial activity of flavonoid from propolis trigona sp against *Streptococcus mutans* bacteria (*in vitro*). *Dent J.* 2005;38(3):135-141.

70. Cushnie TT, Lamb AJ. Recent advances in understanding the antibacterial properties of flavonoids. *Int J Antimicrob Agents.* 2011;38:99-107.

71. Thawabteh A, Juma S, Bader M, et al. The biological activity of natural alkaloids against herbivores, cancerous cells and pathogens. *Toxins.* 2019;11:1-28.

72. Sandhiutami NMD, Fahleni F, Miftahurrohmah N, et al. Enhanced wound healing effect of *Areca catechu* L. ointment via antibacterial activity and anti-inflammatory process at grade IIA burns in rats. *J Herbmed Pharmacol.* 2023;12(3):388-398.

73. Arabski M, Wasik S, Dworecki K, Kaca W. Laser interferometric and cultivation methods for measurement of colistin/ampicilin and saponin interactions with smooth and rough of *Proteus mirabilis* lipopolysaccharides and cells. *J Microbiol Methods.* 2009;77:178-83.

74. Meliawaty F, Fadilah RPN, Mentari P. Ambon banana peel extract gel (*Musa paradisiaca* var. Sapientum (L.) Kunt) accelarates of wistar rats gingiva wound healing. *J Health Dent Sci.* 2021;1(1):90-100.

75. Savitri D, Djawad K, Hatta M, et al. Active compounds in kepok banana peel as anti-inflammatory in acne vulgaris: Review article. *Ann Med Surg (Lond).* 2022;84:104868. doi:10.1016/j.amsu.2022.104868

76. Okorondu SI, Mepba HD, Okorondu MMO, Aririat LE. Antibacterial properties of *Musa paradisiaca* peel extract. *Curr Trends Microbiol*. 2010;6:21-26.

77. Asoso O, Akharaiyi FC, Animba L. Antibacterial activities of plantain (*Musa paradisiaca*) peel and fruit. *Der Pharm Lett*. 2016;8(5):5-11.

How to cite this article

Effect of the Ethanolic Extract of *Eryngium billardieri* on the Viability of the Triple-Negative Breast Cancer Cell Line (MDA-MB-231) and *CDKN2A, MDM2*, and *HER2* Expression

Azadeh Hekmat[1] (ID), Elaheh Ghanbari[1] (ID), Saeed Hesami Tackallou[2] (ID)

[1]Department of Biology, Science and Research Branch, Islamic Azad University, Tehran, Iran
[2]Department of Biology, Central Tehran Branch, Islamic Azad University, Tehran, Iran

ABSTRACT

Objective: Currently, treating triple-negative breast cancer (TNBC) poses a significant challenge. *Eryngium billardierei* is widely employed as a medicinal plant, particularly for the treatment of cancers. However, there is a notable shortage of research investigating the effects of *E. billardierei* on TNBC. This study seeks to evaluate the anticancer capabilities of the ethanolic extract of *E. billardierei* concerning TNBC, as well as its impact on the expression of *CDKN2A, MDM2*, and *HER2*.

Materials and Methods: The MTT assay, N-acetyl-L-cysteine (NAC) assay, AO/EtBr dual staining, and flow cytometry were utilized to assess the anticancer potential of the extract of *E. billardierei* against the MDA-MB-231 cell line. In addition, the impact of *E. billardierei* extract on the expression of *CDKN2A, MDM2*, and *HER2* was examined using real-time PCR.

Results: The results conclusively demonstrated that the extract of *E. billardierei* exhibited a dose-dependent suppression of the growth of MDA-MB-231 cells. Moreover, treatment with the extract induced apoptosis in cancer cells. The inhibitory effect on growth was attributed to the generation of ROS, leading to a significant upregulation ($P<0.01$) of *CDKN2A* expression and a downregulation ($P<0.05$) of *MDM2* expression. Conversely, the expression of HER2 remained unaffected following extract treatment.

Conclusion: The outcomes of this study provide a foundation for considering the use of *E. billardierei* extract in the treatment of TNBC. However, additional research is warranted to investigate the mechanisms of *E. billardierei* extract across a broader spectrum of TNBC cell lines.

Keywords: *Eryngium billardierei*, Triple-negative breast cancer, *CDKN2A, MDM2, HER2*

INTRODUCTION

Breast cancer is a widespread disease that affects numerous women globally. It is a complex disease comprising various subtypes, each yielding distinct responses to clinical interventions. Among the several subtypes of breast cancer, triple-negative breast cancer (TNBC) stands out as one of the most challenging cancers to treat. Triple-negative is a categorization in immuno-histochemistry for breast cancers that do not express human epidermal growth factor receptor 2 (HER2), progesterone receptor (PR), and estrogen receptor (ER). These receptors play a pivotal role in the proliferation and development of cancer cells. HER2 is a membrane receptor of tyrosine kinases (RTKs) and is encoded by the *HER2* oncogene located on chromosome 17. In the majority of cases, aberrations in *HER2* expression, whether at the protein or gene level, have been associated with

an unfavourable prognosis in both lymph node-positive and lymph node-negative breast malignancy.[1] TNBC is also characterised by overexpression of P-cadherin, fascin, caveolin 1 and 2, epidermal growth factor receptor (EGFR), and alpha-beta crystallin.[2]

A tumour suppressor protein frequently inactivated in cancer is p16INK4a, which is encoded by the cyclin-dependent kinase inhibitor 2A (*CDKN2A*) gene. The *CDKN2A* gene (8.5 kb full length) includes three exons and two introns. Inactivation of p16[INK4a] has been documented as a potential contributor to cancer progression. Frequently, this inactivation is observed through promoter hypermethylation, homozygous deletion, or point mutations and has been identified in numerous cancers. Hence, managing abnormalities in CDKN2A regulation has potential benefits for cancer therapy.[3] CDKN2A is capable of ac-

tivating the p53 tumour surveillance pathway by inhibiting and interacting with the p53 antagonist and murine double minute 2 (MDM2).[4] The MDM2 homologue protein is encoded by the proto-oncogene gene *MDM2*. The human *MDM2* gene is on the long arm of chromosome 12, specifically at the 13-14 position (12q13-14). The overexpression of MDM2 can be identified in several malignancies like colorectal, esophagogastric, lung, liver, and breast cancers.[5]

Nowadays, although recent methods of breast cancer therapy, such as surgery, radiation therapy, and chemotherapy, have made substantial developments in improving patient outcomes, there is growing interest in discovering complementary or alternative treatment options.[2] Recently, several researches focussed on the potential of plant-based compounds in breast cancer treatment. Countless natural plants contain functional components that can act as anticancer agents. Moreover, when compared with synthetic substances, natural products have been recognised as cost-effective, relatively non-toxic, and suitable for ingestion.[6] *Eryngium*, belonging to the Umbelliferae family, comprises 274 species, nine of which are native to Iran. Remarkably, *E. billardierei* is widely utilised as a medicinal plant globally for treating several ailments.

Earlier studies have shown that extracts derived from both the aerial and root components of *E. billardierei* exhibit antibacterial, anti-inflammatory, antinociceptive, and antioxidant impacts.[7,8] Several research studies have shown that *E. billardieri* has cytotoxic effects on diverse cancerous cell lines. Roshanravan et al. demonstrated that n-hexane and dichloromethane extracts of *E. billardieri* significantly induced apoptosis in pancreatic cancer cells by incrementing Bax and reducing cyclin D1 mRNA expression.[7] The cytotoxic effects of *E. billardieri* on hepatocellular carcinoma (HepG-2), breast adenocarcinoma (MCF-7), lung carcinoma (A-549), and colorectal adenocarcinoma (HT-29) cell lines were also confirmed.[9] In a recent study by Hasanbeiglu et al., it was detected that non-terpenoid compounds present in *E. billardierei* could be accountable for the cytotoxic impacts observed in the aerial part extracts of this plant on MCF-7 and musculus skin melanoma (B16) cell lines.[10]

Although previous studies have emphasised the anticancer impacts of *Eryngium* species in certain cancerous cell lines,[7, 9-11] research specifically addressing the impact of *E. billardierei* on TNBC remains limited. Therefore, the objective of this study was to assess the anticancer potential of the ethanolic extract of *E. billardierei* against the MDA-MB-231 cell line and to explore its impact on *CDKN2A, MDM2,* and *HER2* expression. The findings from this study could offer a foundation for considering the use of *E. billardierei* for treating TNBC.

MATERIALS AND METHODS

Materials

The TNBC cell line MDA-MB-231 (ATCC® HTB-26™, USA) was purchased from the Iranian Biological Resource Centre (IBRC), Iran. The cells were stored in a 5% CO_2 humidified atmosphere incubator at 37 °C. MTT (Dimethylthiazol-2-yl]-2, 5-diphenyltetrazolium bromide) and acridine orange (AO) were acquired from Sigma-Aldrich Co., USA. The Annexin FITC kit was purchased from IQ Product, Netherlands. Dimethyl sulfoxide (DMSO), ethidium bromide (EtBr), and N-acetyl-cysteine (NAC) were obtained from Merck, Germany. The fetal bovine serum (FBS), streptomycin, penicillin, and RPMI-1640 medium were prepared from BioIdea, Iran. The plant materials were acquired from a local market in Tehran, Iran. The voucher specimen (No. IAUH-12161) was authenticated by the Avicenna Herbarium, Azad University, Iran. An easy cDNA synthesis kit was purchased from Parstous Co., Iran. RNX-Plus was obtained from Sinaclon Co., Iran. From Ampliqon. (Odense, Denmark), the SYBR Green real-time Master Mix kit was obtained.

Preparation of the Ethanolic Extract

The extraction procedure was modified on the basis of methodologies outlined in prior research.[12] In summary, the petal and sepal portions of *E. billardieri* were dried in an oven and ground into a fine powder using a mechanical grinder (Retsch, Germany). Subsequently, 50 g of plant powder was macerated in 500 mL of ethanol (70% v/v), covered with aluminium foil, and placed in a shaker at 25 °C. After 72 h, the extract was filtered through Whatman filter papers and then centrifuged at 3500 rpm for 20 min. Condensation was performed using a rotary evaporator (Heidolph, Germany). The supernatant was then dried at 37 °C, resulting in a semisolid mass stored at 4 °C for further analyses.

Samples Preparation

MDA-MB-231 cells in the log phase were trypsinize with trypsin-EDTA and seeded in 96-well plates. Afterward, the cells were washed with PBS buffer, and 10^5 cells/well were seeded into 96-well plates, and after that 180 µL growth medium was added to each well. The cells were randomly divided into three groups, consisting of one control group and two experimental groups. The experimental groups were exposed to varying concentrations (10, 20, 30, 40, 50, 75, 100, 250, 500, and 1000 µg/mL) of the ethanolic extract of *E. billardierei* for 24 and 48 h.

Cell Viability Assay

After treating MDA-MB-231 cells in both control and experimental groups for 24 and 48 h, 0.5 mg/mL MTT (20 µL) was

added to each well of 96-well plates. Subsequently, the cells were incubated for 3 h in a CO$_2$ incubator at 37 °C. Following incubation, the formed insoluble formazan was dissolved in 100 µL of DMSO and thoroughly mixed. The optical density (OD) of each well at 570 nm was measured against a reagent blank using an ELISA reader (Model 680, Bio-Rad Inc., USA). Each experiment was replicated three times.

Measurement of Reactive Oxygen Species (ROS) Generation

The influence of the *E. billardieri* extract on ROS generation, both in the absence and presence of NAC, was investigated. NAC powder was dissolved in RPMI 1640, and subsequently, MDA-MB-231 cells were pretreated with 5 mM NAC for 3 h in a CO$_2$ incubator at 37 °C. Following this pre-treatment, the cells were exposed to the *E. billardieri* extract. After a 48-h treatment of the cells, 0.5 mg/mL MTT (20 µL) was introduced into each well of 96-well plates, and cell viability was examined.

Flow Cytometry Analysis

A total of 10^6 cells/well were seeded into 6-well plates for 48 h and subsequently treated with *E. billardieri* extract. Following treatment, the cells were collected by centrifugation at 1000 g for 5 min and washed twice with PBS buffer (0.01 M, pH 7.4). Subsequently, the cells were suspended in 100 µL of Annexin V binding buffer. The cells underwent double staining with a 5 µL solution of PI (Propidium iodide) and a 5 µL solution of FITC-labelled Annexin V. Samples were then incubated for 30 min in the dark at 25 °C and later analysed via flow cytometry applying BD FACSCalibur™, BD Biosciences Inc., USA.

AO/EtBr Dual Staining

MDA-MB-231 cells, cultivated in 6-well plates at a density of 10^4 cells/well, were treated with *E. billardieri* extract. The cells were then washed three times with PBS, and 9 µL of the cell suspension was stained with 1 µL of a dye mixture (100 mg/mL EtBr and 100 mg/mL AO in PBS). The stained cell suspension (10 µL) was applied to a clean microscope slide and promptly observed using an Axoscope 2 plus fluorescence microscope (Zeiss, Germany).

Extraction of RNA

Total RNA was extracted from MDA-MB-231 cells treated with the ethanolic extract of *E. billardierei* using an RNA isolation kit. The extracted RNA was immediately frozen in liquid nitrogen and stored at 75 °C. The purity of purified RNA was determined by measuring absorbances at wavelengths of 260 and 280 nm using a UV spectrophotometer. The ratio of absorbances was calculated to assess total RNA purity. Furthermore, agarose gel electrophoresis (1.2% w/v) of the extracted

RNA (15 µL) was conducted in 1X TBE buffer at 80 V for 30 min. The gel was stained with a solution of EtBr and visualised under UV illumination.

cDNA Synthesis and Real-Time Quantitative PCR

The expression of *CDKN2A, MDM2*, and *HER2* genes was evaluated in both control and experimental samples. A total of 1 µg of RNA was utilised for cDNA synthesis, and real-time PCR was conducted using the SYBR Green real-time Master Mix kit. The PCR conditions included an initial denaturation at 95 ºC for 2 min, followed by 40 cycles of denaturation at 95 ºC for 15-20 sec, and annealing at 55-65 ºC for 60 s. The relative expression was calculated by applying the REST 2009 software (version 2.0.13). Gene-specific primers were designed using Primer Express 3.0 software and confirmed for specificity through a BLAST search. Each primer was synthesised by Yekta Tajhiz, Iran. Two negative controls were included in each PCR reaction, one without RT (reverse transcription) treatment (minus-RT) and one without cDNA template. From the same RNA, the experiments were repeated with a cDNA template synthesised three times. For each sample, the mRNA levels represent the mean value of data obtained from three independent real-time PCR trials. Lastly, alterations in fold expression were analysed using the comparative CT method,[13] with normalisation performed through the *GAPDH* (glyceraldehyde-3-phosphate dehydrogenase) gene serving as the housekeeping gene (Eq. 1). The comparative CT method makes various assumptions, including that the efficiency of the PCR is close to 1 and that the PCR efficiency of the interest gene (here are *CDKN2A, HER2*, and *MDM2*) is similar to the internal control gene.

$$\text{Fold change} = 2^{-\Delta\Delta C_T} = \big[(C_T\text{gene of interest} - C_T GAPDH)$$
$$\text{(1)}$$
$$\text{sample with extract} - (C_T\text{gene of interest} - C_T GAPDH)\big]$$

Primers for CDKN2A, HER2, MDM2, and GAPDH were as follows: CDKN2A, forward 5'-CTCGTGCTGATGCTACTGAGGA-3' and reverse 5'-GGTCGGCGCAGTTGGGCTCC-3'; HER2, forward 5'-TGTGACTGCCTGTCCCTACAA-3' and reverse 5'-CCAGACCATAGCACACTCGG-3'; MDM2, forward 5'-TAATTGAAGGGTCATGCCTAAGTGT-3' and reverse 5'-GCTGCCTCCGACTTAACTGC-3'; and GAPDH, forward 5'-GGAAGGTGAAGGTCGGAGTCA-3' and reverse 5'-TCATTGATGGCAACAATATCCACT-3'.

Statistical Analysis

Significant differences were assessed using the t-test in Graph-Pad Prism Software (Version 8.4.3, GraphPad Software Inc., USA). FlowJo software (Version 7.6.1.) was used for the analysis of flow cytometry data. All data are presented as the mean

± standard deviation (SD). The symbol * indicates a significant difference, where * and # signify *P*<0.05 and ** and ## indicate *P*<0.01.

RESULTS

UV-Vis Spectroscopy Results

The ethanolic extraction of *E. billardierei* was subjected to UV-Vis spectroscopy, which revealed a prominent absorption band with a maximum wavelength (λmax) of approximately 266 nm, as illustrated in Figure 1. In line with the existing literature, it is noteworthy that the spectra of flavonoids and phenolic acids regularly demonstrate distinct λmax values around 270 or 340 nm.[14] In addition, phenolic acids characterised by the benzoic acid carbon framework display their λmax within the range of 200–290 nm.[15] Consequently, the extract from *E. billardierei* showed significant levels of total flavonoids and phenolics.
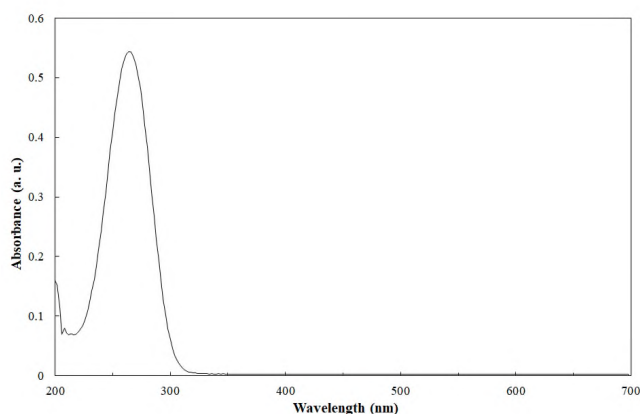
Figure 1. The UV-Vis spectrum of the *E. billardierei* ethanolic extract.

Growth Rates of MDA-MB-231 Cells

Because cell cultures serve as prominent biological systems for examining the effect of drugs or compounds on cell proliferation rates, the initial step involved utilising the MTT assay to measure the influence of the *E. billardierei* extract on the growth of MDA-MB-231 cells. The MTT assay results confirmed that the *E. billardierei* extract displayed a dose-response suppression effect on the growth of MDA-MB-231 cells (Figure 2). Hence, the IC50 (50% inhibition concentration) of *E. billardierei* extract after 24 and 48 h of incubation were determined to be 400.3 and 104.9 µg/mL. The type of solvent used for extracting plants is important. Polar solvents such as ethanol and water are employed in polar compound extraction. Ethanol, in particular, is non-toxic at low concentrations and possesses self-preservative properties when its concentration exceeds 20%.[16] In addition, prior studies have proposed that the ethanolic extract of certain plants may have a potential therapeutic impact on TNBC.[17-19]

Therefore, in this study, we utilised the ethanolic extract of *E. billardierei*. Hence, after cells were cultured, the EtOH solution was added, and the proliferation effects of the solvent alone were determined. As shown in Figure 2, EtOH had no impact on the viability of the cells. A previous study also confirmed that EtOH at a lower concentration is a good solvent choice because it has low toxicity in the MDA-MB-231 cell line.[20] Hence, it can be concluded that the dose-dependent inhibitory effects observed after the treatment of cells with *E. billardierei* extract are a result of the plant extract contents.
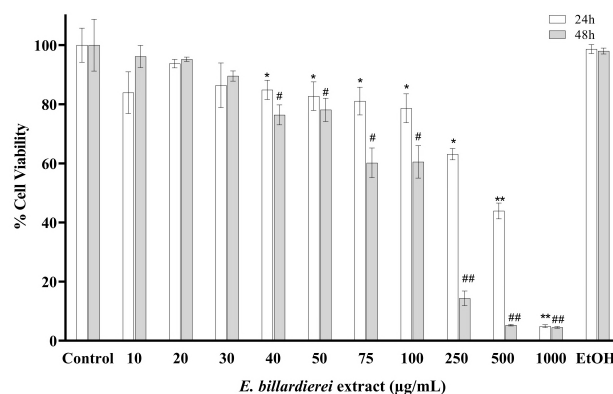
Figure 2. MTT assay of MDA-MB-231 cells after treatment with diverse concentrations of *E. billardierei* ethanolic extract after 24 and 48 h. Values are mean ± standard deviation; * *P*<0.05 vs. control, ** P<0.01 vs. control, # *P*<0.05 vs. control, ## P<0.01 vs. control.

As can be observed, after 48 h, the IC50 decreased significantly. The doubling time of MDA-MB-231 is ca. 25-35 hours[21], thus, our results indicated that the effect of *E. billardieri* can be dependent on cell doubling time. Consequently, a concentration of 104.9 µg/mL (lower IC$_{50}$) of the extract and 48-h treatment was chosen for further studies.

Measurement of ROS Levels

To investigate whether oxidative stress plays a role in the antiproliferative effects of the *E. billardierei* extract, cells were treated with the extract and NAC. As shown in Figure 3, compared with the control, pretreatment with NAC abolished *E. billardierei* extract–induced cytotoxicity in MDA-MB-231 cells significantly. This result implied that *E. billardierei* extract could produce ROS in cells, which could inhibit cell proliferation.

Flow Cytometry Results

The determination of necrotic and apoptotic cell values involved the measurement of membrane integrity and phosphatidylserine externalisation. This was accomplished through double staining with Annexin V and PI and analysed via flow cytometry. As shown in Figure 4 and Table 1, the amount of
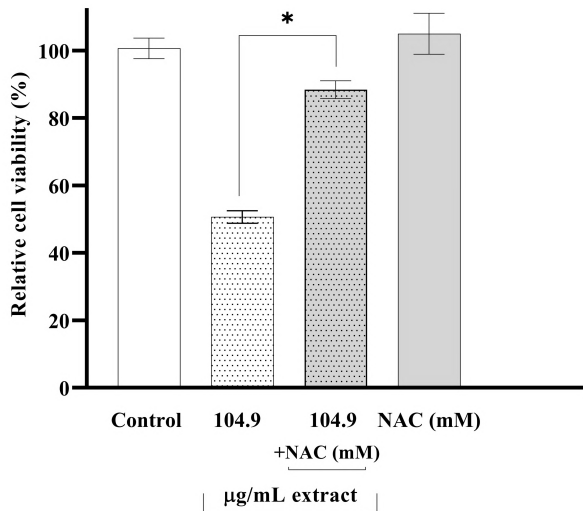
Figure 3. Measurement of ROS generation. MDA-MB-231 cells were pre-treated with NAC and then treated with *E. billardierei* ethanolic extract after 48 h. Values are mean ± standard deviation; * indicates $P<0.05$.

necrotic cells was higher than the control cell ($P<0.05$). In addition, the proportions of total cell apoptosis (late apoptotic cells+early apoptotic cells) were enhanced significantly after treatment with *E. billardierei* extract ($P<0.05$) compared with the control group.
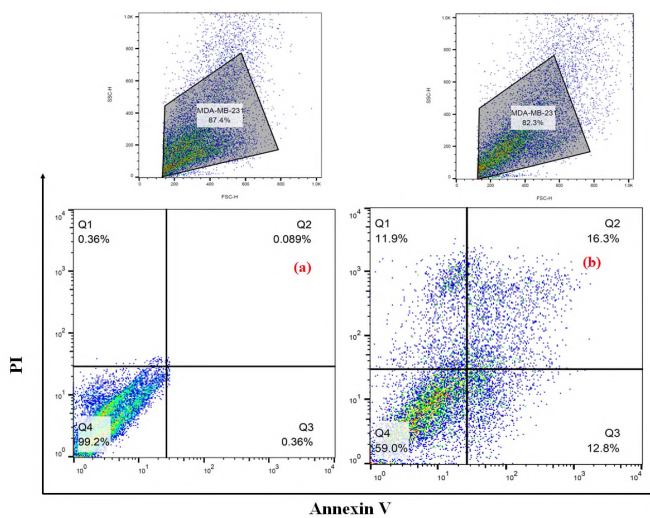
Figure 4. Flow cytometry analyses of MDA-MB-231 cells: (a) control cells and (b) cells treated with 104.9 µg/mL of *E. billardierei* ethanolic extract. Cells were gated on forward (FSC) vs. side scatter (SSC) to select the cell population (The upper graphs). Harvested cells were stained with Annexin V-FITC (x-axis) and PI (y-axis).

AO/EtBr Double-Staining Results

For a comprehensive understanding of the effects of the *E. billardierei* extract, the morphology of MDA-MB-231 cells

was examined using the AO/EtBr double staining assay. As shown in Figure 5, no significant change and apoptosis were detected in the control group. In AO/EtBr staining, living cells display a normal green nucleus.[22] After 48 h of treatment with the extract, early-stage apoptotic cells, characterised by crescent-shaped or granular yellow-green AO nuclear staining, were recognised. In addition, late-stage apoptotic cells, distinguished by concentrated and asymmetrically localised orange nuclear EtBr staining, were observed following a 48-h treatment with the ethanolic extract of *E. billardierei*. Note that an enhancement in volume and the presence of uneven orange-red fluorescence at the periphery were monitored in necrotic cells. However, it is important to mention that the number of necrotic cells was insignificant. These results indicate that the *E. billardierei* extract can induce nuclear fragmentation and chromatin condensation in MDA-MB-231 cells.
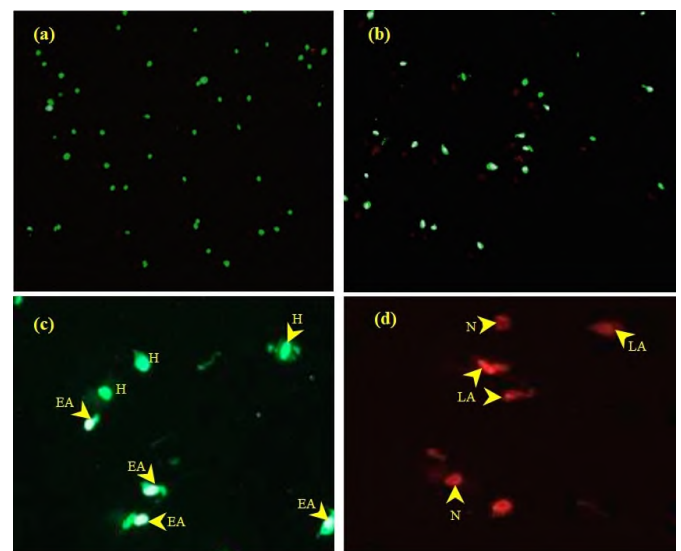
Figure 5. Apoptosis analysis by AO/EtBr: (a) Negative control group (H); (b) cells treated with *E. billardierei* extract (×10). (c) Nuclei showed yellow-green fluorescence by AO staining (×40), and (d) showed orange fluorescence by EtBr (×40). H: live cell, EA: early apoptotic cells, LA: late apoptotic cells, and N: necrotic cell.

Results about *CDKN2A, MDM2*, and *HER2* Gene Expression

Real-time qPCR was employed to assess the influence of the *E. billardierei* extract on *CDKN2A* and *HER2* expression in MDA-MB-231 cells. As shown in Figure 6, compared with the control group, after 48 h of treatment with *E. billardierei* extract, the expression of *HER2* did not alter. However, the expression of *CDKN2A* increased slightly notably (P<0.01) after treatment with *E. billardierei* extract. Conversely, the expression of *MDM2* was reduced notably (P<0.05) after treatment with *E. billardierei* extract. In summary, the statistical analysis revealed a significant correlation between the expression of *CDKN2A* and *MDM2* following treatment with the *E. billardierei* extract for 48 h.

Table 1. Relative number (in %) of living, early and late apoptotic, and necrotic cells in the control and sample treated with *E. billardierei* extract (Mean±SEM, n=3, * P<0.05, and ** P<0.01).

Sample	Live cells (Q4: PI⁻/FITC⁻)	Early apoptotic cells (Q3: PI⁻/FITC⁺)	Late apoptotic cells (Q2: PI⁺/FITC⁺)	Necrotic cells (Q1: PI⁺/FITC⁻)
Control	99.2±0.20	0.36±0.42	0.089±0.15	0.36±0.55
Treated with the *E. billardierei* extract	59.0±2.38**	12.8±0.55*	16.3±2.70*	11.9±1.01*
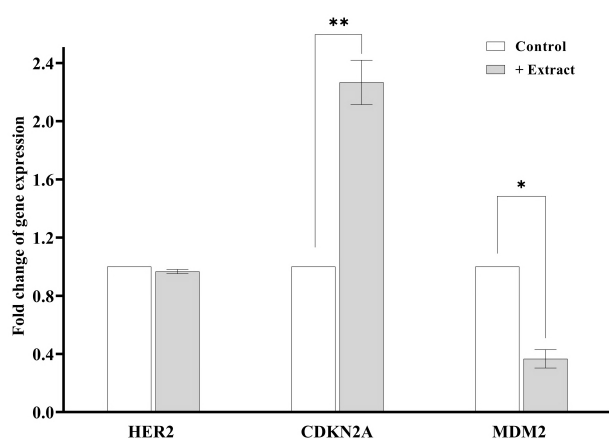
Figure 6. Fold changes in the gene expression levels of *HER2, CDKN2A,* and *MDM2* in cells treated with 104.9 µg/mL of *E. billardierei* extract after 48 h compared with the control groups. The fold change in gene expression was calculated according to the comparative CT method as described in the Materials and Methods section. Values are mean ± standard deviation; *indicates *P*<0.05 and ** indicates *P*<0.01.

DISCUSSION

TNBC represents the most aggressive subtype of breast cancer, constituting ~15 to 20% of all breast cancers globally. Recently, various research focussed on the potential of plant-based compounds in breast cancer treatment. The current study implies that the proliferation of MDA-MB-231 cells could be inhibited by *E. billardierei* extract in a time- and dose-dependent manner. Previous studies have confirmed the anticancer effect of *Eryngium* species, but the IC$_{50}$ value in different cells was different depending on the type of solvent and time of treatment. For example, Paşayeva *et al.* found the cytotoxic effects of *E. billardieri* extract with IC$_{50}$=99.50 µg/mL) on the MCF7 cell line.[23] Results of Hasanbeiglu et al. confirmed that the dichloromethane extract of *E. billardieri* could inhibit MCF7 growth with IC$_{50}$ = 110.30 and 31.37 µg/mL after 24- and 48-h treatment, respectively.[10] The preceding study further confirmed that the methanolic extract of *E. thyrsoideum* inhibited the growth of MDA-MB-231 cells, yielding IC$_{50}$ values of 78.46 and 47.51 µg/mL after 24- and 48-h treatment, respectively.[17]

Flow cytometry analysis revealed that the treatment of cells with *E. billardierei* extract induced apoptosis, pushing MDA-MB-231 cells into both early and late apoptosis stages. The flow cytometry results of Hasanbeiglu et al. also showed that *E. billardieri* extract caused apoptosis in MCF7 cells.[10] The fluorescence microscopic image also proved that the majority of the *E. billardieri* extract-treated cells were at the apoptosis stage (early and late stage). In addition, as cells in the necrotic stage display an orange colouration with normal nuclear morphology and no condensed chromatin, our data implied that the predominant response of MDA-MB-231 cells to *E. billardierei* extract treatment was late apoptosis. These data are in agreement with the flow cytometry results.

Control of intracellular ROS levels is important for maintaining cellular homeostasis. At low levels, ROS function as signalling molecules, whereas at elevated levels, they could induce cell damage and lead to cell death. The results revealed that *E. billardieri* extract inhibited proliferation and promoted the ROS-mediated endogenous apoptotic pathway in MDA-MB-231 cells. Oxidative stress has the potential to disrupt the equilibrium between ROS production and radical scavenging, ultimately triggering cellular apoptosis.[24, 25] Thus, our findings imply that ROS play a role as effectors in the *E. billardieri* extract-induced inhibition of MDA-MB-231 cell viability. Elevated ROS levels may activate several signalling molecules in tumour cells, leading to cell cycle arrest and apoptosis.[24]

After 48 h of treatment with *E. billardierei* extract, *HER2* expression was not affected. It has been demonstrated that HER2 can inhibit p53 through two indirect pathways, both of which are mediated by protein kinase B (PKB), also known as AKT. The initial mechanism entails AKT-mediated suppression of the Alternate Reading Frame Protein (ARF). Typically, ARF interacts with and inhibits MDM2, preventing its interaction with p53. In cells overexpressing *HER2*, a decrease in *ARF* expression was detected in an AKT-dependent manner, leading to heightened MDM2 activity and diminished p53 levels. In addition, it was detected that AKT or HER2 activation decreased the expression and nuclear localisation of p53. As a result, a hypothesis was developed suggesting that AKT directly phosphorylates the MDM2 protein, guiding it to the nucleus.

Once in the nucleus, MDM2 can ubiquitinate p53, facilitating its degradation.[26] In addition, our data revealed that the *CDKN2A* and *MDM2* expression was pregulated and downregulated, respectively, following *E. billardierei* extract treatment. As previously mentioned, MDM2 serves as the primary cellular antagonist of p53, which restrains the growth-suppressive function of p53 in unstressed cells. Clinical and preclinical data on MDM2 inhibitors in the context of human cancer treatment have shown that targeting MDM2 could present an innovative approach to improving the efficacy of tumour therapeutics. MDM2 inhibitors exert their effects by obstructing the binding between p53 and MDM2 through competitive binding to region I of the MDM2 protein. This disruption results in increased p53 levels and activation of the p53 signalling pathway. Accordingly, MDM2 inhibitors can foster cell apoptosis and impede cell growth.[5] In contrast, an augmented expression of CDKN2A can trigger growth arrest, demonstrating one of the distinctive features of premature senescence.[27] CDKN2A can also facilitate the degradation of MDM2 and physically obstruct the interaction between MDM2 and p53. This process results in the stabilisation of p53.[4] An earlier study showed that the extract of *E. billardierei* could upregulate *Bax* and *p53* expression in MCF7 cells[10], which is in agreement with our present data.

In previous studies, it has been confirmed that the ethanolic extract of *E. billardierei* contains significant total flavonoids and phenolics.[8,28] Flavonoids exhibit a dual role in maintaining ROS homeostasis. They act as antioxidants under normal condition. However, in cancer cells, they have significant prooxidant properties. Flavonoids can restrain the proliferation of tumour cells by inhibiting several pathways, including PKB, nuclear factor kappa-light-chain-enhancer of activated B cells (NF-κB), phosphatidylinositide 3-kinases (PI3K), and the epidermal growth factor receptor/mitogen-activated protein kinase (EGFR/MAPK) pathway.[29] Several flavones have also been found to regulate the cell cycle at different points.[30] Phenolic compounds extracted from plant sources have been shown to have inhibitory effects on the proliferation of tumour cells, including breast cancer cells.[31] Thus, it could be concluded that flavonoids and phenolics play a significant role in the anticancer properties of *E. billardierei* extract. Nonetheless, this study is solely a preliminary *in vitro* investigation. Subsequent studies, particularly *in vivo* experiments, are necessary to validate the potential low toxicity of the *E. billardierei* extract.

CONCLUSION

In summary, the current study demonstrated a robust growth-inhibitory effect of *E. billardierei* extract on human TNBC MDA-MB-231 cells. Moreover, treatment with *E. billardierei* extract was found to induce apoptosis in cancer cells. Following a 48-h treatment with *E. billardierei* extract, no significant effect on *HER2* expression was observed. The growth-inhibitory

effect was associated with the generation of ROS, influencing the upregulation of *CDKN2A* and the downregulation of *MDM2* expression. These findings suggest that *E. billardierei* extract holds promise for development into an innovative and effective anticancer drug against TNBC. However, further research and validation, including *in vivo* studies, are warranted to verify its potential therapeutic application.

ORCID IDs of the authors

Azadeh Hekmat   0000-0003-0123-1575
Elaheh Ghanbari   0009-0001-0998-1218
Saeed Hesami Tackallou   0000-0002-9492-3038

REFERENCES

1. Subramaniyan V, Fuloria S, Gupta G, et al. A review on epidermal growth factor receptor's role in breast and non-small cell lung cancer. *Chem Biol Interact*. 2022;351:109735. doi:10.1016/j.cbi.2021.109735

2. Hekmat A, Saso L, Lather V, Pandita D, Kostova I, Saboury AA. Recent advances in nanomaterials of group XIV elements of periodic table in breast cancer treatment. *Pharmaceutics*. 2022;14(12):2640. doi: 10.3390/pharmaceutics14122640

3. Zhao R, Choi BY, Lee M-H, Bode AM, Dong Z. Implications of genetic and epigenetic alterations of CDKN2A (p16INK4a) in cancer. *E Bio Medicine*. 2016;8:30-39.

4. Al-Saran N, Subash-Babu P, Al-Nouri DM, Alfawaz HA, Alshatwi AA. Zinc enhances CDKN2A, pRb1 expression and regulates functional apoptosis via upregulation of p53 and p21 expression in human breast cancer MCF-7 cell. *Environ Toxicol Pharmacol*. 2016;47:19-27.

5. Hou H, Sun D, Zhang X. The role of MDM2 amplification and overexpression in therapeutic resistance of malignant tumors. *Cancer Cell Int*. 2019;19(1):216. doi:10.1186/s12935-019-0937-4

6. McGrowder DA, Miller FG, Nwokocha CR, et al. Medicinal herbs used in traditional management of breast cancer: Mechanisms of action. *Medicines*. 2020;7(8):47. doi:10.3390/medicines7080047

7. Roshanravan N, Asgharian P, Dariushnejad H, et al. *Eryngium billardieri* induces apoptosis via bax gene expression in pancreatic cancer cells. *Adv Pharm Bull*. 2018;8(4):667-674.

8. Daneshzadeh MS, Abbaspour H, Amjad L, Nafchi AM. An investigation on phytochemical, antioxidant and antibacterial properties of extract from *Eryngium billardieri* F. Delaroche. *J Food*

Meas Charact. 2020;14:708-715.

9. Esmaeili S, Irani M, Moazzeni Zehan H, Keramatian B, Tavakoli Harandi Z, Hamzeloo-Moghadam M. Cytotoxic activity of some ethnic medicinal plants from southwest of Iran. *J Pharmacognosy Res*. 2016;3:43-47.

10. Hasanbeiglu S, Hosseini K, Molavi O, Asgharian P, Tarhriz V. *Eryngium billardieri* extract and fractions induce apoptosis in cancerous cells. *Anticancer Agents Med Chem*. 2022;22(11):2189-2201.

11. Forouhandeh H, Rezaei Param Z, Molavi O, Asgharian P, Tarhriz V. Evaluation of anti-proliferative activity of *Eryngium caucasicum* on melanoma cancer cells. *BMC Complement Med Ther*. 2022; 22(1):134. doi:10.1186/s12906-022-03618-w

12. Afshari M, Malayeri AR, Mohammadshahi M. Effects of *Eryngium caucasicum* extract on testosterone, inflammation and oxidative status of nicotinamide-streptozotocin induced type-2 diabetes in male rats. *J Contemp Med Sci*. 2019;5(2):77-81.

13. Schmittgen TD, Livak KJ. Analyzing real-time PCR data by the comparative *C*T method. *Nat Protoc*. 2008;3(6):1101-1108.

14. Jarzębski M, Siejak P, Smułek W, et al. Plant extracts containing saponins affects the stability and biological activity of hempseed oil emulsion system. *Molecules*. 2020;25(11):2696. doi:10.3390/molecules25112696

15. Robbins RJ. Phenolic acids in foods: An overview of analytical methodology. *J Agric Food Chem*. 2003;51(10):2866-2887.

16. Abubakar AR, Haque M. Preparation of medicinal plants: Basic extraction and fractionation procedures for experimental purposes. *J Pharm Bioallied Sci*. 2020;12(1):1-12.

17. Hosseini K, Ariya MP, Molavi O, Asgharian P, Tarhriz V. The fractions of *Eryngium thyrsoideum* extract sensitize breast cancer cells to apoptosis. *J Nat Pharm Prod*. 2022;17(3):118888. doi:10.5812/jjnpp.118888

18. Nordin FJ, Pearanpan L, Chan KM, et al. Immunomodulatory potential of *Clinacanthus nutans* extracts in the co-culture of triple-negative breast cancer cells, MDA-MB-231, and THP-1 macrophages. *PLoS One*. 2021;16(8):e0256012. doi:10.1371/journal.pone.0256012

19. Alshaeri HK, Alasmari MM, Natto ZS, Pino-Figueroa A. Effects of *Annona muricata* extract on triple-negative breast cancer cells mediated through EGFR signaling. *Cancer Manag Res*. 2020;12:12519-12526.

20. Nguyen ST, Nguyen HT-L, Truong KD. Comparative cytotoxic effects of methanol, ethanol and DMSO on human cancer cell lines. *Biomed Res Ther*. 2020;7(7):3855-3859.

21. Samson J, Derlipanska M, Zaheed O, Dean K. Molecular and cellular characterization of two patient-derived ductal carcinoma in situ (DCIS) cell lines, ETCC-006 and ETCC-010. *BMC Cancer*. 2021;21(1):1-20.

22. Hekmat A, Rabizadeh M, Safavi M, Hajebrahimi Z. The comparison of the apoptosis effects of titanium dioxide nanoparticles into MDA-MB-231 cell line in microgravity and gravity conditions. *Nanomed J*. 2019;6(2):120-127.

23. Paşayeva L, Köngül E, Geylan R, Karatoprak GŞ, Tugay O, editors. Analysis of the cytotoxic effects of *Eryngium billardieri* Delar. Extracts on MCF7 Cell Line. *Proceedings*. 2017;1:1055. doi:10.3390/proceedings1101055

24. Khan MA, Siddiqui S, Ahmad I, et al. Phytochemicals from Ajwa dates pulp extract induce apoptosis in human triple-negative breast cancer by inhibiting AKT/mTOR pathway and modulating Bcl-2 family proteins. *Sci Rep*. 2021;11(1):10322. doi:10.1038/s41598-021-89420-z

25. Zahedian S, Hekmat A, Tackallou SH, Ghoranneviss M. The impacts of prepared plasma-activated medium (PAM) combined with doxorubicin on the viability of MCF-7 breast cancer cells: a new cancer treatment strategy. *Rep Biochem Mol Biol*. 2022;10(4):640-652.

26. Carpenter RL, Lo H-W. Regulation of apoptosis by HER2 in breast cancer. *J Carcinog Mutagen Res*. 2013;2013:1-13. doi:10.4172/2157-2518.S7-003

27. Vousden KH, Prives C. Blinded by the light: the growing complexity of p53. *Cell*. 2009;137(3):413-431.

28. Yavari S, Hekmat A, Saedari S. The ethanolic extract of *Eryngium billardierei* F. Delaroche restrains protein glycation in human serum albumin: An *in vitro* study. *J Serb Chem Soc*. 2023, November, doi:10.2298/JSC230725091Y

29. Kopustinskiene DM, Jakstas V, Savickas A, Bernatoniene J. Flavonoids as anticancer agents. *Nutrients*. 2020;12(2):457. doi:10.3390/nu12020457

30. Khan AU, Dagur HS, Khan M, Malik N, Alam M, Mushtaque M. Therapeutic role of flavonoids and in cancer prevention: Current trends and future perspectives. *Eur J Med Chem Rep*. 2021;3:100010. doi:10.1016/j.ejmcr.2021.100010

31. Fabiani R. Anti-cancer properties of olive oil secoiridoid phenols: A systematic review of *in vivo* studies. *Food Funct*. 2016;7(10):4145-4159.

How to cite this article

Upregulated Acute Systemic Inflammation-Related Genes based on Endotoxin Exposure Provide "Survival Benefit" or Create "High Risk of Death" in Leukaemia and Colon Cancer

Gizem Ayna Duran[1] iD

[1]Izmir University of Economics, Faculty of Engineering, Biomedical Engineering Department, Izmir, Türkiye

ABSTRACT

Objective: Although endotoxin exposure has been shown to trigger innate immune responses and promote cancer, it has also been shown to prevent cancer formation. In our study, survival analysis was performed to determine whether the upregulated genes triggered by endotoxins have hazardous effects on cancers or provide a survival benefit.

Materials and Methods: Gene intensity values of control and bacterial endotoxin-administered individuals were obtained from the Gene Expression Omnibus database. Using the R "Linear Models for Microarray Data" package, differentially expressed gene analyses were conducted to determine genes that differ between healthy and bacterial endotoxin-administered samples. "ShinyGo 0.80" web-based tool was used to determine the disease types indicated by these genes. The "Kaplan-Meier Plotter" web-based tool was used to conduct survival analysis.

Results: Genes that create an innate immune response to bacterial endotoxin exposure and are upregulated differently than in individuals without exposure were identified. According to gene enrichment analyses, the two main types of cancer identified were leukaemia/lymoma and colon cancer. We detected that *MLF1, STAT5B,* and *BCL3* genes led to poor survival; however, the *ARHGAP26* gene was protective for acute myeloid leukaemia patients. In the case of colon cancer, *SMAD7* and *TLR2* genes were determined as leading to "high risk of death".

Conclusion: Once the systemic inflammation-related genes identified in our study are confirmed through laboratory experiments in samples taken from solid tissue in the case of colon cancer and at the level of genes obtained from blood samples in leukemias, genetically targeted treatments will also be possible.

Keywords: Cancer, Endotoxin, Systemic inflammation, Bioinformatics, Survival

INTRODUCTION

Bacterial endotoxins (lipopolysaccharide, LPS) are a part of the outer wall of Gramme-negative bacteria with the biologically active part lipid-A. After the bacteria die and their bacterial outer walls disintegrate, they appear in materials containing cellulose, called organic dust, and appear in a way that we can even be exposed to in our daily lives.[1] Health problems that occur as a result of exposure to bacterial endotoxins vary depending on the LPS concentration. While septic shock and serious life-threatening effects may occur as a result of exposure to high doses of LPS, there are even cases where it can be considered beneficial for the host because of the low level of triggering of the innate immune system as a result of exposure to low doses.[2,3] In addition to studies showing that endotoxin-mediated inflammatory responses have a triggering effect on cancer, there are studies showing that they have host-protective effects on cancer. For example, in a study showing that LPS, which is more abundant in the colon flora compared with normal intestinal flora, regulates gene expression in human colon cancer cell lines, it was shown at the genetic level that LPS does not affect cell viability but contributes to inflammatory responses and cancer development.[4] In a study published in 2021, it was shown at the molecular level that LPS triggers metastasis in colorectal cancers using cell lines and clinical samples.[5] In addition, there are studies on the relationship of gut microbiota with many cancers other than colon cancer. Some studies have also shown that endotoxins (mainly LPS) have protective effects against cancer. For example, in a review article published in 2023, where current and comprehensive publications were scanned, publications sharing information on whether the gut

microbiota, consisting of different types of bacteria, promote or inhibit cancers in different human and murine cancer models were summarized.[6] There are limited number of studies conducted on mouse models and mouse/human cell lines, showing that gut microbiota inhibits cancer formation in colorectal and colon cancers. It has been shown that mostly colorectal or colon cancer gut microbiota promote cancer.[6-9] In another study, it was shown that acute myeloid leukaemia (AML) caused cancer progression in vivo and in vitro through the effect of gut-derived LPS in mouse models.[10]

In clinics, local and systemic inflammation is decisive in the diagnostic phase of cancers and in terms of response to treatment.[11] Studies have shown that inflammatory responses play a role in tumour progression and survival in cancer patients. For example, in a study conducted in 2018 that included randomized clinical trials, the effect of systemic inflammatory responses on the survival rates of cancer patients was investigated. As seen in the study, a limited number of studies are possible in leukaemia and colon cancer patients.[12] In another study, we attempted to determine pre-diagnostic systemic inflammation markers for many types of cancer based on cancer incidence using UK Biobank data. These markers include the systemic immune-inflammation index, neutrophil-to-lymphocyte ratio, platelet-to-lymphocyte ratio, and lymphocyte-to-monocyte ratio.[13] In another study in which meta-analyses were conducted in 2021, a study was conducted on the creation of a systemic inflammation response index in cancer patients.[14]

As can be seen from the studies summarized in the literature above, there is no research on how endotoxin-mediated systemic inflammation affects cancer formation and survival at the gene level. In this context, our study provides novel findings. Our aim in our study was to identify upregulated genes associated with systemic inflammation through bioinformatic analysis and to identify the cancers with which these genes are associated. In our study, the effect of genes upregulated in certain types of cancer on the survival (protective or triggering) of patients was also investigated.

MATERIALS AND METHODS

Data Acquisition and Processing

In this study, gene intensity values of control and bacterial endotoxin-administered individuals were obtained from the Gene Expression Omnibus (GEO) database (GSE3284) [HG-U133_Plus_2] Affymetrix Human Genome U133 Plus 2.0 Array (GPL96 and GPL97) platforms with 22.283 and 22645 probes, respectively. According to the overall design of the dataset, genes of blood leukocytes of individuals were analysed before (0 hour as an internal control) and at 2, 4, 6, 9, and 24 h upon bacterial endotoxin administration using Affymetrix GeneChip arrays.[15-18] Additionally, gene intensity values of

24 healthy individuals (from GSE9006) were used as the control for samples obtained from all bacterial endotoxin administered hours, including hour 0 from the GSE3284 dataset. Using these datasets, differentially expressed gene (DEG) analysis was achieved; thus, only genes that were commonly upregulated at 2, 4, 6, 9, and 24 h after bacterial endotoxin administration were identified.

Statistical Analysis

In this study, raw data of GSE3284 and GSE9006 (24 healthy controls) as CEL files were used, and "Robust Multi-Array Average" normalization was achieved using the Bioconductor R packages. Using the linear modelling method included in the R LIMMA (version 4.2.2) package separately for all datasets, genes that differed between healthy samples and bacterial endotoxin-administered samples were identified. A p-value of <0.01 was set as the threshold value for determining statistical significance. Following DEG analyses, upregulated genes were determined in bacterial endotoxin-administered individuals at 2, 4, 6, 9, and 24 h (GSE3284) (16 individuals for 2, 9, 24 h and 14 individuals for 4 and 9 h), which were different from the genes obtained from the other 16 control individuals (0 h before administration) and healthy individuals (obtained from GSE9006).

Gene Enrichment Analysis

"ShinyGo 0.80" web-based tool was used to determine the disease types indicated by the genes that are commonly upregulated in individuals who were administered bacterial endotoxin, according to healthy internal control and 0 h samples, by selecting the "Disease. OMIM.Disease" option (http://bioinformatics.sdstate.edu/go80/).[19]

Survival Analysis

The "Kaplan-Meier (KM) Plotter" web-based tool was used to determine how the genes found to be commonly upregulated in people administered bacterial endotoxin compared with healthy controls affected survival [event-free survival (EFS) for AML and multiple myeloma (MM); relapse-free survival (RFS) for colon cancer) in cancer types (leukaemia and colorectal cancers) determined in gene enrichment analysis (https://kmplot.com/analysis/).[20] Hazard Ratio (HR) is a ratio that indicates the probability of an event (in the case of survival, this is death) in a group of cancer patients relative to the probability in a control group over a unit of time. In our study, HR was obtained as a result of survival analysis, and HR greater than 1 in KM plots means that the relevant upregulated gene has a hazardous effect on survival. When HR is less than 1, the relevant upregulated gene provides survival benefit.

RESULTS

In our study, DEG analyses were performed to determine the genes that were upregulated in individuals administered bacterial endotoxin compared with controls. As a result of the DEG analysis performed with the gene intensity data obtained from both platforms in the GSE3284 dataset, there were 415 upregulated genes obtained from the GPL96 platform, whereas this number was 202 from the GPL97 platform. After the common genes were determined, this number was determined to be 617. Gene enrichment analysis was performed using the 617 genes obtained using the ShinyGo 0.80 "Disease. OMIM.Disease" option. According to our results, the most common cancer types are leukaemia, lymphoma, and colorectal cancer (Figure 1). As seen in Table 1, the genes indicated by the detected cancer types are *MLF1, ARHGAP26, BCL3, MYB, STAT5B, KIT,* and *IKZF1* genes for leukaemia and *BCL3* and *MAD1L1* genes for lymphoma. For colon cancer, *SMAD7, MLH3*, and *TLR2* genes were determined according to the results of gene enrichment analysis.
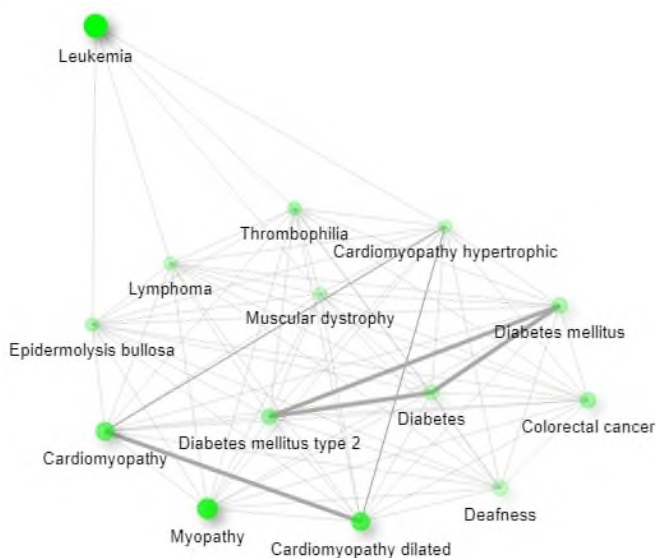
Figure 1. Upregulated acute systemic inflammation-related DEGs indicate various disease types, including cancers such as leukaemia, lymphoma, and colorectal cancers. The network figure obtained from ShinyGO 0.80 webtool using the "Disease. OMIM.Disease" option mentioned mainly leukaemia, lymphoma, and colon cancers. In the interactive plot, two pathways (nodes) are connected if they share 20% (default) or more genes. Darker nodes are associated with more significantly enriched gene sets. Bigger nodes represent larger gene sets. Thicker edges represent more overlapping genes (http://bioinformatics.sdstate.edu/go80/).

Table 1 shows the genes specific to leukaemia, lymphoma, and colorectal cancers obtained from gene enrichment analyses. The aim of our study was to determine whether genes specific to these cancers affect survival in cancer patients. Therefore, survival analysis was performed one by one for genes for AML, MM, and colon cancers using the "KM-Plotter" tool, which

also includes high patient numbers. The number of patients and information about the relevant genes are shared in Table 2.

According to the results obtained from survival analysis, *SMAD7* and *TLR2*, among the three genes determined in colon cancer patients, affect survival (EFS) in a statistically significant way, and since HR value is above 1, its effect on survival is considered as "high risk of death" (Figure 2). In addition, it was determined that the *MLH3* gene did not significantly affect the survival of patients (data not shown).
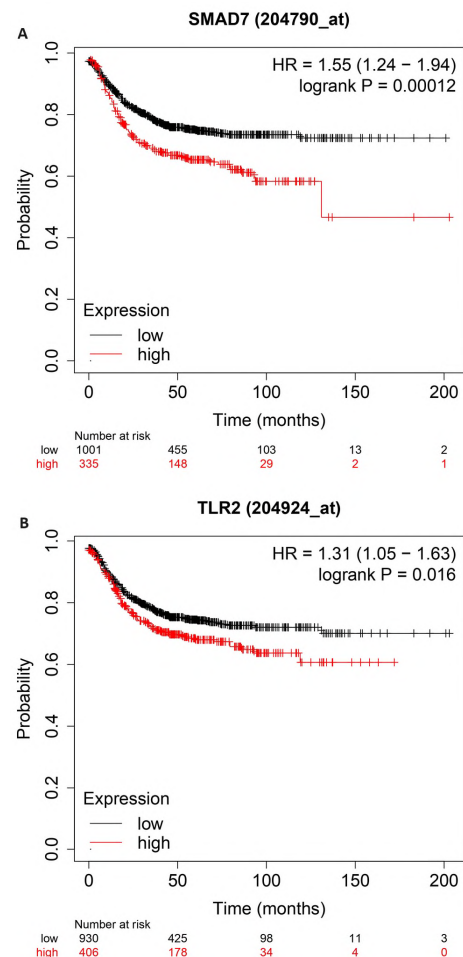
Figure 2. Upregulated *SMAD7* and *TLR2* genes indicate "high risk of death" in colon cancer patients. (A) Hazardous effect of *SMAD7* gene on RFS shown by Kaplan-Meier plot (B) Hazardous effect of *TLR2* gene on RFS shown by Kaplan-Meier plot HR > 1 means DEGs have hazardous effects on survival, HR<1 means DEGs lead to survival benefit in patients.

In our study, using the data of AML patients in KM-Plotter, survival analysis was performed with the genes determined for leukaemia according to the results of gene enrichment analyses. According to our results, while *MLF-1, STAT5B*, and *BCL3* genes had hazardous effects on survival in AML patients, *ARHGAP26* gene had a protective effect on survival (Figure 3). In addition, it was determined that the *PBT*, hlk-1 (IKZF1), and *MYB* genes did not significantly affect the survival of patients (data not shown).

Table 1. Leukaemia, lymphoma, and colorectal cancer-related upregulated genes in individuals with acute systemic inflammation.

Enrichment FDR	Number of Genes	Pathway Genes	Fold Enrichment	Pathway	Genes
3.65897672044697e-05	7	57	12.53132832	Leukemia	*MLF1, ARHGAP26, BCL3, MYB, STAT5B, KIT, IKZF1*
0.038128527	2	17	12.00480192	Lymphoma	*BCL3, MAD1L1*
0.016862797	3	31	9.874917709	Colorectal cancer	*SMAD7, MLH3,*

Explanations of all gene abbreviations are explained in Table-2.

Table 2. Number of cancer patients included in survival analysis of commonly upregulated genes in individuals with acute systemic inflammation.

	Genes and Affy IDs	Gene Description	Number of MM patients	Number of AML patients
AML and MM	*MLF1* (204783_at)	myeloid leukemia factor 1	801	525
	ARHGAP26 (226576_at)	Rho GTPase activating protein 26	559	353
	BCL3 (204907_s_at)	BCL3 transcription coactivator	801	525
	MYB (204798_at)	MYB proto-oncogene, transcription factor	801	525
	STAT5B (205026_at)	signal transducer and activator of transcription 5B	559	353
	KIT (PBT) (205051_s_at)	KIT ligand	801	525
	IKZF1 (hlk-1) (205039_s_at)	IKAROS family zinc finger 1	559	353
Colon Cancer	**Genes and Affy IDs**	**Gene Description**	**Number of CC patients**	
	SMAD7 (204790_at)	SMAD family member 7	1296	
	MLH3 (204838_s_at)	mutL homolog 3	1296	
	TLR2 (204924_at)	toll like receptor 2	1296	

MM: Multiple Myeloma; AML: Acute Myeloid Leukemia; CC: Colon Cancer; Affy IDs: Affymetrix probe IDs
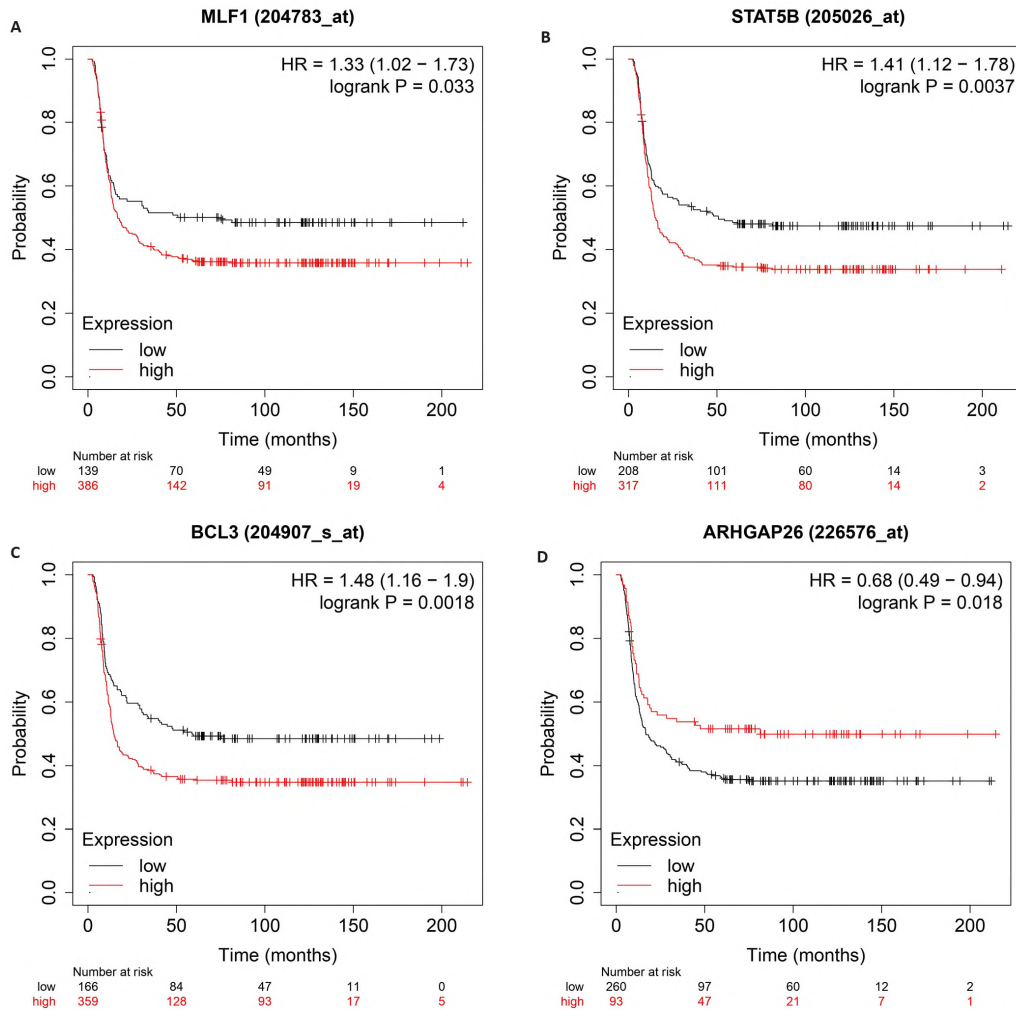
Figure 3. Upregulated *MLF-1, STAT5B*, and *BCL3* genes indicate a "high risk of death" and upregulated *ARHGAP26* gene provides "survival benefit" in AML patients. (A) Hazardous effect of *MLF1* gene on event-free survival (EFS) shown by Kaplan-Meier plot (B) Hazardous effect of *STAT5B* gene on EFS shown by Kaplan-Meier plot. (C) Hazardous effect of *BCL3* gene on EFS shown by Kaplan-Meier plot. (D) Protective effect of *ARHGAP26* gene on EFS shown by Kaplan-Meier plot. HR > 1 indicates that DEGs have hazardous effects on survival, HR<1 means DEGs lead to survival benefit in patients.

In our study, survival analysis was also performed using the genes determined for leukaemia, using the data of MM patients in KM-Plotter. According to our results, *BCL3*, *MYB*, and *IKZF1* genes had hazardous effects on survival in patients with MM, whereas *MLF-1, ARHGAP26, STSD5B*, and *PBT* genes were found to have a protective effect on survival (Figure 4).

DISCUSSION

The gene intensity data (GSE3284) of the people whose data were used in our study were originally taken from a study conducted on the genetic analysis of the acute systemic inflammation responses of human blood leukocyte cells after infection with bacterial endotoxin (LPS).[15] There are studies in literature examining the role of inflammatory responses caused by endotoxin exposure in cancer development. As summarised in a recent review article published by Jiaao Sun et al., it has been shown that endotoxin exposure triggers innate immune responses and promotes cancer in some cancers and inhibits it in some cancers.[6] In our study, the aim was to determine whether the upregulated genes triggered by endotoxins have a hazardous (high risk of death) effect on cancers or provide a survival benefit.

More than 100 trillion beneficial intestinal bacteria in the human body contribute to human health by maintaining metabolic balance. However, the situation changes when microbiome disturbance called dysbiosis occurs and exposure to crude microbial metabolites triggers cancer as well as some metabolic diseases (such as type 2 diabetes, non-alcoholic liver disease).[21-23] Studies have shown that the bacteria that make up our natural flora in the colon contribute positively or negatively to the formation and development of gastrointestinal cancers such as colon, hepatocellular and pancreatic cancers, and cholangiocarcinoma.[24] There are studies conducted on mouse models and mouse/human cell lines, albeit limited in number, showing that gut microbiota inhibits cancer formation in colorectal or colon cancers. On the other hand, it has also been
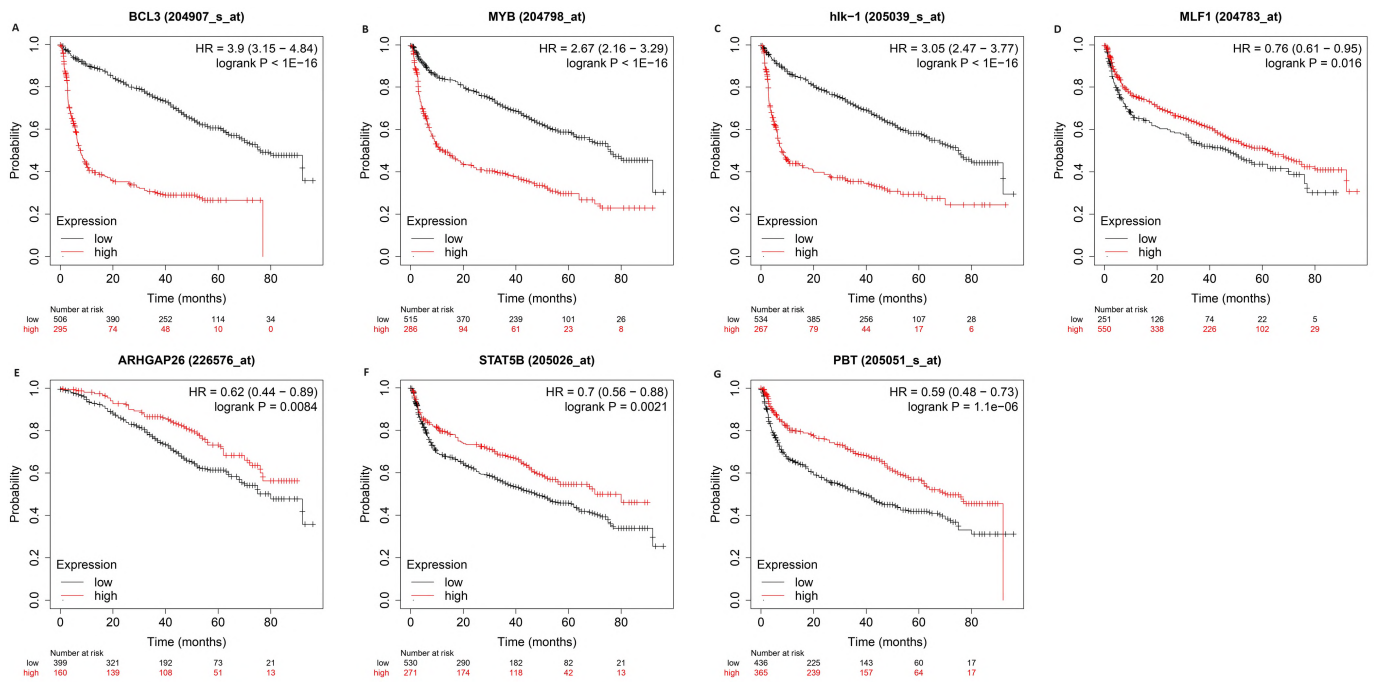
Figure 4. Upregulated *BCL3, MYB*, and *hlk-1 (IKZF1)* genes indicate "high risk of death" and upregulated *MLF-1, ARHGAP26, STSD5B*, and *PBT* genes provide "survival benefit" in MM patients. (A) Hazardous effect of *BCL3* gene on event-free survival (EFS) shown by Kaplan-Meier plot. (B) Hazardous effect of *MYB* gene on EFS shown by Kaplan-Meier plot. (C) Hazardous effect of *IKZF1 (hlk-1)* gene on EFS shown by Kaplan-Meier plot (D) Protective effect of *MLF1* gene on EFS shown by Kaplan-Meier plot (E) Protective effect of *ARHGAP26* gene on EFS shown by Kaplan-Meier plot (F) Protective effect of *STAT5B* gene on EFS shown by Kaplan-Meier plot (G) Protective effect of *PBT* gene on EFS shown by Kaplan-Meier plot HR>1 means DEGs has hazardous effects on survival, HR<1 means DEGs lead to survival benefit in patients.

shown that gut microbiota promotes cancer, mostly in colorectal cancers.[6-9] In our study, it was shown that among the genes that were upregulated in people with endotoxin exposure compared with people without endotoxin exposure, *SMAD7* and *TLR2* genes, which were found to be significant in colon cancer, negatively affected survival. Although how a gene affects survival does not mean how it affects cancer processes, it has been accepted that the detected upregulated genes have a hazardous effect on cancer development in colon cancer patients. It has been shown in the literature that the product of the *SMAD7* gene, known as an inhibitor of the transforming growth factor (TGF)-β1 signalling process in colon cancer, increases as a result of chronic intestinal inflammation and causes poorer survival.[25] In addition, while it was mentioned in this study that the *SMAD7* gene increased as a result of inflammatory bowel disease and contributed to cancer by this mechanism, its relationship with gut microflora and endotoxin exposure was not mentioned. In this respect, our study contains novel findings.[25] Another gene detected in our study is *TLR2*. In the literature, it has been shown that this gene, as a single component of the gut microbiota in mouse models, reduces the incidence of colitis-induced colon cancer by acting as a TLR agonist of *A. muciniphila*.[6,26] According to our findings, when the *TLR2* gene increases with endotoxin exposure, it causes a decrease in the survival rate of colon cancer patients; in other words, it has an increasing effect on the incidence of cancer. In addition,

laboratory studies should be conducted to determine the effect of each type of bacteria in the gut microbiota on colon cancer.

According to our findings, the second type of cancer we focussed on is leukaemia. In this context, it has been shown in the literature that AML causes cancer progression *in vivo* and *in vitro* in mouse models with the effect of gut-derived LPS.[27] Additionally, restored and intact gut microbiota was found to protect genetically predisposed mice against leukaemia.[28] Studies are limited to mouse models. In addition, as summarised in a review article published in 2023, it has been shown in Phase 2 clinical trials that dysbiosis complications can be prevented by transplantation of autologous gut microbiome in cancer treatments and AML, and restoration of the microbiota has been found to be important in the effectiveness of cancer therapies.[6] To the best of our knowledge, there are no studies in the literature that identify genetic levels between endotoxin exposure and leukaemia survival rate; therefore, the results of our study contain novel findings. Although *MLF-1, STAT5B*, and *BCL3* genes have not yet been related to endotoxin exposure in AML patients, alterations in these genes have contributed to survival rates of AML patients. For instance, Yuna Niu et al. indicated that *BCL3* gene overexpression is not only a promising potential prognostic marker for chronic lymphocytic leukaemia but also for AML.[29] Furthermore, *STAT* genes including *STAT5B* and its protein product have been shown to contribute to the malignancy of cells in AML patients. *STAT5B* and its protein

are also accepted as potential targets for therapies through the JAK/STAT pathway.[30,31] Furthermore, *MLF-1* gene may play roles in AML as either tumour suppressor gene or an oncogene depending on the context of the cell.[32] For instance, overexpression of *MLF-1* gene led to poor prognosis in AML.[33]

In our study, MM was also indicated as a result of gene enrichment analysis. Similar to AML patients[29], upregulated *BCL3* and *MYB* oncogenes have been associated with high proliferative capacity in myeloma cells of MM patients.[34,35] Lastly, high expression of the hlk-1 (*IKZF1*) gene has been associated with poor prognosis and low survival rates in MM patients.[36] These genes are also not related to endotoxin exposure, and further studies should be conducted.

Our study also has some limitations. For example, genes obtained from gene enrichment analyses indicate leukaemia/lymoma and colorectal cancers. However, survival analysis was performed for AML and MM cancers and colon cancer, for which data were available in the KM-plotter tool. Survival analysis should also be performed for other leukaemia types (e.g. lymphoma) and colorectal cancers for relevant genes.

CONCLUSION

In summary, the genes upregulated because of endotoxin exposure detected in our study may be targetable genes that can increase treatment efficiency in colon cancer and leukaemia, depending on how they affect survival. The genes triggered by immune responses as a result of systemic inflammation need to be confirmed by laboratory experiments in solid tissue samples in the case of colon cancer and at the level of genes obtained from peripheral blood mononuclear cells in leukaemia. Thus, treatments targeted at the genetic level will also be possible.

ORCID IDs of the author

Gizem Ayna Duran   0000-0002-2168-753X

REFERENCES

1. Heine H, Rietschel ET, Ulmer AJ. The biology of endotoxin. *Mol Biotechnol*. 2001;19:279–296.

2. Kellum JA, Ronco C. The role of endotoxin in septic shock. *Crit Care*. 2023;27: 400. doi: 10.1186/s13054-023-04690-5

3. Vogel SN, Hogan MM. Role of cytokines in endotoxin mediated host responses. In: Oppenheim JJ, Shevach EM, Eds. Immunophysiology. The roles of cells and cytokines in immunity and inflammation. 1990; p.238-258.

4. Cao H. Bacterial endotoxin lipopolysaccharides regulate gene expression in human colon cancer cells. *BMC Res Notes*. 2023;13:16(1):216. doi: 10.1186/s13104-023-06506-9

5. Wu X, Qian S, Zhang J, et al. Lipopolysaccharide promotes metastasis via acceleration of glycolysis by the nuclear factor-κB/snail/hexokinase3 signaling axis in colorectal cancer. *Cancer Metab*. 2021;12:9(1):23. doi: 10.1186/s40170-021-00260-x

6. Sun J, Chen F, Wu G. Potential effects of gut microbiota on host cancers: Focus on immunity, DNA damage, cellular pathways, and anticancer therapy. *ISME J*. 2023;17(10):1535-1551.

7. Roberti MP, Yonekura S, Duong CPM, et al. Chemotherapy-induced ileal crypt apoptosis and the ileal microbiome shape immunosurveillance and prognosis of proximal colon cancer. *Nat Med*. 2020;26(6):919-931.

8. Goodwin AC, Destefano Shields CE, Wu S, et al. Polyamine catabolism contributes to enterotoxigenic Bacteroides fragilis induced colon tumorigenesis. *Proc Natl Acad Sci USA*. 2011;108:15354–15359.

9. Mager LF, Burkhard R, Pett N, et al. Microbiome-derived inosine modulates response to checkpoint inhibitor immunotherapy. *Science*. 2020;18:369(6510):1481-1489.

10. Wang R, Yang X, Liu J, et al. Gut microbiota regulates acute myeloid leukaemia via alteration of intestinal barrier function mediated by butyrate. *Nat Commun*. 2022;9:13(1):2522. doi: 10.1038/s41467-022-30240-8

11. Diakos CI, Charles KA, McMillan DC, Clarke SJ. Cancer-related inflammation and treatment effectiveness. *Lancet Oncol*. 2014;15(11):e493-503. doi: 10.1016/S1470-2045(14)70263-3.

12. Dolan RD, Laird BJA, Horgan PG, McMillan DC. The prognostic value of the systemic inflammatory response in randomised clinical trials in cancer: A systematic review. *Crit Rev Oncol Hematol*. 2018;132:130-137.

13. Nøst TH, Alcala K, Urbarova I, Byrne KS, et al. Systemic inflammation markers and cancer incidence in the UK Biobank. *Eur J Epidemiol*. 2021;36(8):841-848.

14. Zhou Q, Su S, You W, Wang T, Ren T, Zhu L. Systemic inflammation response index as a prognostic marker in cancer patients: A systematic review and meta-analysis of 38 cohorts. *Dose Response*. 2021;15:19(4):1-14.

15. Calvano SE, Xiao W, Richards DR, et al. A network-based analysis of systemic inflammation in humans. *Nature*. 2005;13:437(7061):1032-1037.

16. Foteinou PT, Calvano SE, Lowry SF, Androulakis IP. Multiscale model for the assessment of autonomic dysfunction in human endotoxemia. *Physiol Genomics*. 2010;42(1):5-19.

17. Foteinou PT, Calvano SE, Lowry SF, Androulakis IP. *In silico* simulation of corticosteroids effect on an NFkB- dependent physicochemical model of systemic inflammation. *PLoS One*. 2009;4(3):e4706. doi: 10.1371/journal.pone.0004706

18. Nguyen TT, Calvano SE, Lowry SF, Androulakis IP. An agent-based model of cellular dynamics and circadian variability in human endotoxemia. *PLoS One*. 2013;8(1):e55550. doi: 10.1371/journal.pone.0055550

19. Ge SX, Jung D, Yao R. ShinyGO: A graphical gene-set enrichment tool for animals and plants. *Bioinformatics*. 2020; 36:2628–2629.

20. Kovács SA, Fekete JT, Győrffy B. Predictive biomarkers of immunotherapy response with pharmacological applications in solid tumors. *Acta Pharmacol Sin*. 2023;44(9):1879-1889.

21. Fan Y, Pedersen O. Gut microbiota in human metabolic health and disease. *Nat Rev Microbiol*. 2021;19(1):55-71.

22. Rinninella E, Raoul P, Cintoni M, et al. What is the healthy gut microbiota composition? A changing ecosystem across age, environment, diet, and diseases. *Microorganisms*. 2019;10;7(1):14. doi: 10.3390/microorganisms7010014

23. Thursby E, Juge N. Introduction to the human gut microbiota. *Biochem J*. 2017;16;474(11):1823-1836.

24. Liu Y, Baba Y, Ishimoto T, et al. Gut microbiome in gastrointestinal cancer: A friend or foe? *Int J Biol Sci*. 2022;21;18(10):4101-4117.

25. Troncone E, Monteleone G. Smad7 and colorectal carcinogenesis: A double-edged sword. *Cancers (Basel)*. 2019;1;11(5):612. doi: 10.3390/cancers11050612

26. Wang L, Tang L, Feng Y, et al. A purified membrane protein from *Akkermansia muciniphila* or the pasteurised bacterium blunts colitis associated tumourigenesis by modulation of CD8+ T cells in mice. *Gut*. 2020;69(11):1988-1997.

27. Wang R, Yang X, Liu J, et al. Gut microbiota regulates acute myeloid leukaemia via alteration of intestinal barrier function mediated by butyrate. *Nat Commun*. 2022;9;13(1):2522. doi: 10.1038/s41467-022-30240-8

28. Vicente-Dueñas C, Janssen S, Oldenburg M, et al. An intact gut microbiome protects genetically predisposed mice against leukemia. *Blood*. 2020;29;136(18):2003-2017.

29. Niu Y, Yang X, Chen Y, et al. BCL3 expression is a potential prognostic and predictive biomarker in acute myeloid leukemia of FAB subtype M2. *Pathol Oncol Res*. 2019; 25(2):541-548.

30. Almajali B, Johan MF, Al-Wajeeh AS, et al. Gene expression profiling and protein analysis reveal suppression of the C-Myc oncogene and inhibition JAK/STAT and PI3K/AKT/mTOR signaling by thymoquinone in acute myeloid leukemia cells. *Pharmaceuticals (Basel)*. 2022; 3;15(3):307. doi: 10.3390/ph15030307

31. Wingelhofer B, Maurer B, Heyes EC, et al. Pharmacologic inhibition of STAT5 in acute myeloid leukemia. *Leukemia*. 2018; 32(5):1135-1146.

32. Li Z, Yang Y, Wu K, et al. Myeloid leukemia factor 1: A "double-edged sword" in health and disease. *Front Oncol*. 2023;13:1124978. doi: 10.3389/fonc.2023.1124978

33. Matsumoto N, Yoneda-Kato N, Iguchi T, et al. Elevated *Mlf1* expression correlates with malignant progression from myelodysplastic syndrome. *Leukemia*. 2000;14(10):1757–1765.

34. Cao L, Mitra P, Gonda TJ. The mechanism of MYB transcriptional regulation by MLL-AF9 oncoprotein. *Sci Rep*. 2019;27;9(1):20084. doi: 10.1038/s41598-019-56426-7

35. Brenne AT, Fagerli UM, Shaughnessy JD Jr, et al. High expression of BCL3 in human myeloma cells is associated with increased proliferation and inferior prognosis. *Eur J Haematol*. 2009; 82(5):354-363.

36. Davis KL. Ikaros: Master of hematopoiesis, agent of leukemia. *Ther Adv Hematol*. 2011;2(6):359-368.

How to cite this article

Using Chloroplast Regions *accD, matK, rbcL,* and *ycf-1* for Phylogeny Construction in *Polyspora huongiana* Orel, Curry & Luu

Nguyen Trung Quan[1], Hoang Thanh Chi[2], Phung My Trung[3], Truong Quang Cuong[4], Tran Thi Cam Thi[5], Hoang Kim Son[1], Bui Thi Kim Ly[2]

[1]Viet Nam National University, Department of Biology - Biotechnology, VNU-HCM, Ho Chi Minh City, Vietnam

[2]Thu Dau Mot University, Department of Medicine and Pharmacy, Thu Dau Mot City, Binh Duong Province, Vietnam

[3]Unaffiliated, 9A Dong Khoi Stress, Tam Hoa Ward, Bien Hoa City, Vietnam

[4]Bidoup Nui Ba National Park, Tran Hung Dao str. 5E, Dalat, Vietnam

[5]Ho Chi Minh City University of Technology – HCMUT, Faculty of Chemical Engineering, VNU-HCM, Ho Chi Minh City, Vietnam

ABSTRACT

Objective: Theaceae is a commodity with high economic value. The diversity of Theaceae species present in Southeast Asia, especially Vietnam, provides an excellent supply source for promoting the development of related industries. Nearly 130 species of Theaceae, many of which are highly endemic, were discovered in Vietnam, including 13 *Polyspora* species. *Polyspora huongiana* was discovered in Bidoup-Nui Ba National Park, Vietnam, on January 7, 2010. Because they are native species and lack data, studies are needed to provide genetic data for ecological assessment and original identification of the plant.

Materials and Methods: Sanger sequencing, data collection, and nucleotide analysis of the genetic data of *accD, matK, rbcL,* and *ycf1* in *P. huongiana* were provided.

Results: The results showed that combinations of two sequences could separate the *Polyspora* genus, whereas at least three sequences were necessary to identify *P. huongiana*, which was genetically closely related to *Polyspora axillaris* and *Polyspora hainanensis*.

Conclusion: *P. huongiana* is closely related to *Polyspora axillaris* and *Hainanensis*. The combination of 3–4 sequences allowed reliable identification of *P. huongiana*.

Keywords: *Polyspora huongiana*, Phylogeny, *matK, rbcL, accD, ycf1*.

INTRODUCTION

The tea family (Theaceae) comprises approximately 460 species, which are mainly distributed in East and Southeast Asia. *Camellia* is the largest tea genus, comprising more than 300 species worldwide.[1,2] Thus far, nearly 130 Theaceae species belonging 5 genera have been found in Vietnam, namely 95 species of *Camellia*, 13 species of *Polyspora*, 8 species of *Pyrenaria*, 7 species of *Schima*, and 3 species of Stewartia.[1] Many endemic *Polyspora* species have recently been discovered and described for the first time, such as *Polyspora congii, Polyspora bidoupensis*, and *Polyspora huongiana*.[2-4] The number of species and endemism reflect the biodiversity of tea species in Vietnam.[5] Conservation and sustainable exploitation of tea species is crucial in both the economy and the ecology.[6]

Theaceae species often share the same physical characteristics, especially *Polyspora* and *Camellia*.[7] The similarity of the two genera makes it difficult to distinguish them.[8,9] Ecologists can rely on winged seed morphology to differentiate if this plant is *Polyspora* or *Camellia*, and the result is hardly conclusive based on limited information.[10] The development of technology has provided new approaches to solving problems using molecular biology techniques. The DNA fingerprint method is considered an independent tool in forensic investigations, research, plant identification, and many other fields.[11] DNA Barcoding was born after the emergence of PCR and Sequencing methods and quickly became a promising aid in classifying species and individuals.[11-13] In addition, NGS techniques are currently widely used in classifying and studying the ecology of species, currently.[11,13] DNA barcoding was first described in 2003, and it refers to short gene sequence elements that can be used for species identification.[11] Since its inception, DNA barcoding has become a robust technique that has been

dramatically developed to replace DNA fingerprints in ecological research. In 2004, The Consortium for the Barcode of Life (CBOL) was founded to develop orientations and standards in the barcode research and management system of living things. In 2007, the DNA barcode standard for terrestrial plants was announced by CBOL, and plant identification became easier.

In recent years, genetic analysis studies on *Polyspora* species have gained attention; comparative research and genetic analysis among the species have been conducted. The chloroplastic genome is weighed up a sequence region that is highly conserved throughout evolution. Hence, it is a source for comparing and identifying plant species. The chloroplastic structure of *Polyspora* was analysed and included 132 genes encoding 87 proteins, 37 tRNS, and 8 rRNA. Among them, *matK* (metabolite of the maturase K) and *rbcL* (Ribulose-bisphosphate carboxylase) are the two main regions suggested by CBOL for plant identification; *accD* (Acetyl-CoA carboxylase beta subunit) and *ycf1* (ycf1 is the second largest gene in the plastid genome) are potential sequences with high nucleotide diversity.[9] In this study, marker regions, including *rbcL* and *matK*, were used to indicate the genetic relationship between *P. huongiana* and *Polyspora* and *Camellia* published DNA data.[14] *accD* and *ycf1*, regions of inconsistency in plants, were also evaluated as species-identifying factors.[15,16]

MATERIALS AND METHODS

Plant Sample and Sample Preparation

Polyspora huongiana Orel, Curry & Luu were collected from TK89, Đạ Chais village, Lạc Dương district, Lâm Đồng province, Vietnam, by Truong Quang Cuong. The plant was identified and tagged voucher number 210622PHU. The leaves were double-washed with distilled water before being stored at -20ºC until analysis.

DNA Extraction and Amplification

The leaves were ground in liquid nitrogen, and DNA was extracted using the cetyltrimethylammonium bromide (CTAB) method.[17] Amplicons were amplified using MyTaq mix (Meridian, USA) with the chloroplast primers listed in Table 1.[13] The PCR reactions were prepared as follows: 10 µL MyTaq mix 2X, 400 nMol primers (PhuSaBiochem, Vietnam), 50 ng template, and nuclease-free water (Promega, AUS) up to 20 µL. The PCR cycles were conducted using a DTlite instrument (DNA-Technology, Russia) with the temperature programme of 95ºC for 2 min, 35 cycles of 10 sec at 95ºC, 10 sec at 60ºC, 60 sec at 72ºC, and an additional 2 min of 72ºC for once. A human beta-globin template (Medick Ltd Co., Vietnam) was used as a positive control (PCR using Beta globin primers) and negative control (PCR using chloroplast primers).

Product Purification and Sequencing

Electrophoresis in 1% agarose (Bio-Helix, Taiwan) for 45 min at 90 V confirmed the PCR products. An ExactMark 100 bp DNA ladder (1st BASE, Malaysia) was used for product length determination. The PCR products were purified by adding ExoSAP IT (ThermoFisher, USA) at a ratio of 5:2 and incubating for 15 min at 37ºC and 15 min at 80ºC. The purified products were subjected to PCR with BigDye Terminator Cycle Sequencing (Applied Biosystem, USA) and sequenced using an ABI 3500 analyser (Applied Biosystem, USA). The obtained sequences were trimmed for 20–50 nucleotides on both sides for noise signal elimination and analysed using Snapgen V5.3.2. The forward and reverse sequences were aligned and united.

Reducing Power Measurement

The DNA sequences of *accD, matK, rbcL*, and *ycf1* were checked using the NCBI database's BLAST (Basic local alignment search tools) tool. Each sequence's 100 most related sequences were chosen for further analysis (Table 2). DNA sequences were aligned in the Mega11 programme with the Clustal W algorithm.[18] Sequences were randomly assembled to form sequence combinations using Mega11 and DnaSP version 6.12.03.[18,19] The phylogeny of *P. huongiana* was determined by maximum likelihood estimation with 1000 bootstrap replications and was considered strong (frequency above 85%), moderate (50 - 85%), and weak (below 50%).[20] The neighbour-joining algorithm built the phylogenetic trees.[21]

Statistical Analysis

The data were stored and statistically analysed using GraphPad Prism version 9.0.0 software. Data expressed as mean $\pm$ standard deviation. The unpaired Student's t-test and One-way ANOVA followed by Tukey's post hoc test were applied for statistical comparisons with an alpha value of 0.05.

RESULTS

Estimation of Sequence Divergence

The DNA polymorphisms of the *accD, matK, rbcL*, and *ycf1* regions within *Polyspora* were computed on 10 random sequences, which further clarified the DNA divergence compared with the *Camellia* genus (Figure 1 and Table 3). The nucleotide diversity (π) and the average number of nucleotide differences of the regions are presented in Table 4, which varied from 0.00164 to 0.00531 for *Polyspora* and from 0.0004 to 0.10650 for

Table 1. The primers used for amplified the marker regions.

Target	Forward primer	Reverse primer
accD	CAGAGCGAGGCCAGTGAAAGTGAAGATCCG	GCCACTGGTACAGCCTCGGTTAATCCTG
matK	CAGAGCGAGGCGTACAGTACTTTTGTGTTTACGAG	GCCACTGGTAACCCAGTCCATCTGGAAATCTTGGTTC
rbcL	CAGAGCGAGGATGTCACCACAAACAGAGACTAAAGC	GCCACTGGTAGTAAAATCAAGTCCACCRCG
ycf1	CAGAGCGAGGTCTCGACGAAAATCAGATTGTTGTGAAT	GCCACTGGTACGATGGAATCGACCGTTGCG
Beta globin	ATGCCTCTTTGCACCATTCT	CAGTTTAGTAGTTGGACTTAG

Table 2. Sequence region locations on the chloroplast genome of gene regions were analyzed.

Accession No.	Species	Nucleotide position			
		accD	*matK*	*rbcL*	*ycf1*
NC_061599.1	*Camellia limonia*	58626 - 60367	1948 - 3647	56669 - 58296	125931 - 131552
NC_057956.1	*Camellia achrysantha*	102947 - 104688	46278 - 47977	100090 - 102617	13691 - 19412
NC_041672.1	*Camellia renshanxiangiae*	58647 - 60388	1947 - 3646	56694 - 58321	125959 - 131754
NC_039645.1	*Camellia nitidissima*	59123 - 60864	2034 - 2733	57165 - 58792	126423 - 132238
NC_035652.1	*Camellia elongata*	58719 - 60460	1947 - 3646	56759 - 58386	126052 – 131840
OP580978.1	*Camellia euryoides*	59134 - 60824	2020 - 3719	57126 - 58753	126393 - 132214
OQ630970.1	*Camellia cordifolia*	58751 - 60441	1953 - 3652	56744 - 58371	126067 - 131861
ON208849.1	*Camellia pingguoensis*	58956 - 60697	1947 - 3646	56998 - 58625	126196 - 132002
ON208848.1	*Camellia ptilosperma*	58934 - 60675	1947 - 3652	56976 - 58603	126244 - 132065
NC_069227.1	*Camellia tamdaoensis*	58628 - 60369	1941 - 3640	56671 - 58298	111129 - 116944
ON755230.1	*Polyspora axillaris*	58628 - 60369	1944 - 3637	56673 - 58300	126004 - 131825
NC_035645.1	*Polyspora axillaris*	58624 - 60325	1945 – 3638	56669 - 58296	126034 - 131855
MW801387.1	*Polyspora chrysandra*	58290 - 60031	1944 - 3637	56334 - 57961	125695 - 131516
NC_035648.1	*Polyspora dalgleishiana*	58360 - 60092	1945 - 2638	56404 - 58031	125657 – 131394
MK994520.1	*Polyspora hainanensis*	58229 - 59919	1945 - 3638	56221 - 57848	125578 – 131390
ON755225.1	*Polyspora longicarpa*	59057 - 60798	1980 - 3673	57101 - 58728	126321 - 131936
NC_059950.1	*Polyspora penangensis*	58976 - 60717	1946 - 3639	57028 - 58655	126240 - 132061
ON755229.1	*Polyspora speciosa*	59004 - 60745	1945 - 3645	57047 - 58674	126334 - 132155
NC_053889.1	*Polyspora tiantangensis*	59057 - 60798	1980 - 3673	57101 - 58728	126321 - 132136
NC_067734.1	*Polyspora tonkinensis*	59020 - 60761	1946 - 3639	57064 - 58691	126377 - 132186

Camellia, respectively. *ycf1* was the most variable chloroplastic sequence region compared within the genus in both *Polyspora* and *Camellia*.

P. huongiana Chloroplast DNA Markers

The selected regions for analysis included sequences with high nucleotide diversity values and were limited to two conserved regions of primers hybridising. The initial half sequences of *accD* and *rbcL*, the central *matK* gene, and the second half of *ycf1* were selected for analysis of *P. huongiana*. The sequences were submitted to NCBI (National Centre for Biotechnology Information, USA) with accession numbers OR525840, OR52584, OR52584, and OR525843 for *accD, matK, rbcL*, and *ycf1* of *P. huongiana*, respectively. The dynamic DNA quick response coding (DDQR) algorithm was provided by the Central China Normal University and Institute of Medicinal Plant Development, Chinese Academy of Medical Science, China (www.1kmpg.cn/ddqr/), which created

DDQR for the sequences obtained in this work (Figure 2).[22]

A Phylogenetic Tree Built from a Single Sequence

The sequences of *accD* and *ycf1* showed the greatest similarity to *Camellia weiningensis* (MK820035.1) and *Polyspora axillaris* (ON755230.1); the sequences of *matK* and *rbcL* showed the greatest resemblance to *Polyspora hainanensis* (NC_035693.1).[23-25] The 100 most related sequences were collected for further analysis. The branches show the clustered associated taxa. The initial trees for the heuristic search were generated automatically by applying Neighbour-Join and BioNJ algorithms to a matrix of pairwise distances estimated using the fixed model. The topology obtained the highest log likelihood value. The sequences set up codon positions, including 3 frames and noncoding. The best-fixed models for *accD, matK*, and *ycf1* were the Tamura 3-parameter

Table 3. *Polyspora huongiana*-related sequences obtained by the BLAST tool and corresponding accession numbers.

Accession No.	Species	accD	matK	rbcL	ycf1
KJ197940.1	*Apterosperma oblata*		x		
NC 035641.1	*Apterosperma oblata* voucher YangSX 4361			x	
NC 057956.1	*Camellia achrysantha*	x			
KX216453.1	*Camellia albogigas*		x		
MK994520.1	*Polyspora hainanensis*		x	x	x
NC 050354.1	*Camellia anlungensis* voucher CANLU20191106	x			
MN078085.1	*Camellia vietnamensis*		x	x	
KY406793.1	*Camellia reticulata*	x			x
KY626042.1	*Camellia luteoflora*	x			x
MZ618349.1	*Camellia chrysanthoides*	x	x	x	
NC 024663.1	*Camellia reticulata*	x			x
MW256435.1	*Camellia brevistyla*				x
NC 052752.1	*Camellia brevistyla*				x
NC 072329.1	*Camellia caudata*				x
NC 058854.1	*Camellia confusa*				x
ON000202.1	*Camellia confusa*			x	
NC 067053.1	*Camellia connata*	x		x	
MN078088.1	*Camellia meiocarpa*			x	x
NC 061904.1	*Camellia costata*				x
NC 024541.1	*Camellia crapnelliana*				x
NC 022459.1	*Camellia cuspidata* voucher HKAS:S.X.Yang3159	x			
MN078090.1	*Camellia oleifera*		x	x	
MT123282.1	*Camellia suaveolens*		x	x	
NC 035643.1	*Polyspora speciosa* voucher YXQ145	x	x	x	x
NC 035645.1	*Polyspora axillaris* voucher YXQ099	x	x	x	x
KU669077.1	*Camellia chrysanthoides* voucher Y.Q.Liufu 1529				x
MT663341.1	*Camellia chuongtsoensis*				x
MZ151355.1	*Camellia oleifera* var. oleifera			x	x
NC 035652.1	*Camellia elongata* voucher YangSX 5065	x			
OL405564.1	*Camellia euphlebia*	x			
MZ151356.1	*Camellia oleifera* var. oleifera			x	x
NC 053896.1	*Camellia fascicularis*	x			
OM868265.1	*Camellia fascicularis*	x		x	
KU669083.2	*Camellia fascicularis* voucher S.X.Yang 93527				x
MZ189740.1	*Camellia oleifera* var. oleifera			x	x
MZ665482.1	*Camellia meiocarpa*			x	x
NC 050388.1	*Camellia fraterna*				x
MW801387.1	*Polyspora chrysandra* voucher FZF		x	x	x
NC 038181.1	*Camellia granthamiana*		x		
MZ054232.1	*Camellia gigantocarpa*				x
NC 058879.1	*Camellia gigantocarpa*				x
KX216461.1	*Camellia handelii*		x		
MZ151357.1	*Camellia oleifera*		x	x	
KY626040.1	*Camellia huana*	x			
NC 022461.1	*Camellia impressinervis* voucher	x			
MT157620.1	*Camellia indochinensis*	x			
NC 035693.1	*Polyspora hainanensis* voucher YXQ097	x	x	x	x
OK135162.1	*Camellia indochinensis* var. tunghinensis	x			
NC 058646.1	*Camellia micrantha*	x	x	x	x
NC 059950.1	*Polyspora penangensis* voucher SING2015-178	x	x	x	x
LC679291.1	*Camellia japonica* voucher TF<JPN>:TW021201		x		
LC678549.1	*Camellia japonica* voucher TF<JPN>:TW023656		x		
LC678986.1	*Camellia japonica* voucher TF<JPN>:TW024624		x		
LC679132.1	*Camellia japonica* voucher TF<JPN>:TW024751		x		
LC678314.1	*Camellia japonica* voucher TF<JPN>:TW025361		x		
LC689760.1	*Camellia japonica* voucher TF<JPN>:TW026076			x	
LC677835.1	*Camellia japonica* voucher TF<JPN>:YK0056		x		
NC 079935.1	*Camellia jinshajiangica*	x			
NC 035648.1	*Polyspora dalglieshiana* voucher BROWP 501		x	x	x
NC 035689.1	*Polyspora longicarpa* voucher YangSX 4779		x	x	x
NC 054364.1	*Camellia perpetua*	x			x
NC 057957.1	*Camellia chrysanthoides*	x			x
NC 053889.1	*Polyspora tiantangensis* voucher Ma 15701		x	x	x
KX216414.1	*Camellia longipedicellata*		x		
NC 065391.1	*Camellia longipedicellata*				x

Table 3. Continued

NC 061051.1	*Camellia pingguoensis*	x	x	x	
NC 067609.1	*Camellia longissima* voucher S. X. Yang5079			x	
NC 061599.1	*Camellia limonia*	x	x		x
NC 061600.1	*Camellia petelotii* var. microcarpa	x	x	x	
MN579509.2	*Camellia lungzhouensis*	x			
NC 060777.1	*Camellia polyodonta*		x	x	x
NC 061610.1	*Camellia amplexifolia*	x	x	x	x
KU669092.2	*Camellia luteoflora* voucher Y.Q.Liufu1534				x
NC 062050.1	*Camellia aurea*	x	x	x	
NC 035688.1	*Camellia mairei* voucher YangSX 5054	x			
NC 065391.1	*Camellia longipedicellata* voucher YangSX 5001	x	x	x	x
MT956593.1	*Camellia meiocarpa*				x
NC 067082.1	*Camellia saluenensis*	x			x
NC 067088.1	*Camellia pingguoensis* var. terminalis	x	x	x	
NC 058881.1	*Camellia meiocarpa* clone 3				x
NC 067085.1	*Camellia bambusifolia*	x			x
NC 067090.1	*Camellia ptilosperma*	x	x	x	
KU669078.1	*Camellia micrantha* voucher Q.Q.Ye 1314				x
NC 065198.1	*Camellia formosensis*			x	x
NC 039645.1	*Camellia nitidissima*	x			
MT157617.1	*Camellia nitidissima* var. nitidissima	x			
NC 063576.1	*Camellia suaveolens*		x	x	
NC 067086.1	*Camellia lienshanensis*	x			x
NC 067081.1	*Camellia edithae*		x	x	x
NC 067087.1	*Camellia subintegra*		x	x	x
NC 067091.1	*Camellia indochinensis* var. tunghinensis	x	x	x	
NC 067089.1	*Camellia parvipetala*		x	x	x
NC 067092.1	*Camellia wumingensis*	x	x	x	
NC 067734.1	*Polyspora tonkinensis* voucher FZF20220217	x	x	x	x
NC 068780.1	*Camellia flavida*	x	x	x	
OP953554.1	*Camellia oleifera*		x	x	
NC 067613.1	*Camellia lipingensis*	x		x	x
NC 068781.1	*Camellia longzhouensis*	x	x	x	
NC 067764.1	*Camellia lanceoleosa*	x		x	x
NC 080228.1	*Camellia oligophlebia*	x			
NC 069227.1	*Camellia tamdaoensis*	x	x	x	
NC 069309.1	*Camellia insularis*	x	x	x	x
KU669079.1	*Camellia parvipetala* voucher Q.Q.Ye 1316				x
MT157621.1	*Camellia perpetua*	x			
NC 069310.1	*Camellia minima*	x		x	x
KU669085.1	*Camellia perpetua* voucher Y.Q.Liufu 1531				x
MT157619.1	*Camellia petelotii* var. microcarpa	x			
NC 070214.1	*Camellia pyxidiacea*	x	x	x	
NC 068785.1	*Camellia obtusifolia*		x	x	x
NC 080274.1	*Camellia uraku*	x	x	x	x
NC 072608.1	*Camellia lungshenensis*	x			x
ON208849.1	*Camellia pingguoensis*	x		x	
OK046127.1	*Camellia leyensis*	x	x	x	
OK149109.1	*Camellia pingguoensis* var. terminalis	x			
OK235334.1	*Camellia petelotii* var. microcarpa	x	x	x	
AB207877.1	*Camellia pitardii*	x			
OP709388.1	*Camellia pitardii* var. alba	x			
NC 079666.1	*Camellia brevipetiolata*	x			x
NC 080233.1	*Camellia omeiensis*	x			x
NC 022462.1	*Camellia pitardii* voucher HKAS:S.X.Yang3148				x
OK546696.1	*Camellia luteocalpandria*	x	x	x	
NC 080884.1	*Camellia bailinshanica*	x			x
NC 072174.1	*Camellia hongkongensis*		x	x	x
NC 081063.1	*Camellia magniflora*	x			x
OL450398.1	*Camellia pingguoensis* var. terminalis	x	x		
KU669091.1	*Camellia ptilosperma* voucher Q.Q.Ye 1315				x
KU669075.1	*Camellia ptilosperma* voucher Y.Q.Liufu 1530				x
MW543444.1	*Camellia pubipetala*	x			
NC 054365.1	*Camellia pubipetala*	x			
OK181904.1	*Camellia trichosperma*		x	x	
MW629114.1	*Camellia pyxidiacea* var. rubituberculata	x			
MZ424202.1	*Camellia pyxidiacea* var. rubituberculata	x			

Table 3. Continued

MZ766253.1	*Camellia pyxidiacea* var. rubituberculata	x		x	
NC 041672.1	*Camellia renshanxiangiae*	x			
OK377261.1	*Camellia polyodonta*	x			x
OL685018.1	*Camellia sp. 'longruiensis'*	x	x	x	
NC 050389.1	*Camellia rhytidophylla*	x			
OM935753.1	*Camellia chrysanthoides*	x	x		
NC 041473.1	*Camellia sasanqua*				x
OL689015.1	*Camellia gauchowensis*			x	x
MZ403753.1	*Camellia semiserrata*				x
NC 058880.1	*Camellia semiserrata*				x
ON208846.1	*Camellia indochinensis* var. tunghinensis	x	x	x	
ON208847.1	*Camellia petelotii* var. petelotii	x	x	x	
OL689023.1	*Camellia semiserrata* var GN1				x
MZ359672.1	*Camellia semiserrata* var. magnocarpa	x			
OP404083.1	*Camellia sinensis*	x			
OL840044.1	*Camellia sinensis* var. assamica			x	
OM677554.1	*Camellia sinensis* var. assamica voucher TCM172K-		x		
OM677553.1	*Camellia sinensis* var. assamica voucher TCM170K-		x		
OL944068.1	*Camellia sinensis* var. assamica voucher TCM193K-		x		
OM677563.1	*Camellia sinensis* var. assamica voucher TCM196K-		x		
OM677583.1	*Camellia sinensis* var. assamica voucher TCM238K-		x		
ON208848.1	*Camellia ptilosperma*	x	x	x	x
OQ281601.1	*Camellia sinensis* var. sinensis	x			
ON208850.1	*Camellia wumingensis*	x	x	x	
MZ128138.1	*Camellia sp.* XJ-2021		x		
OL689014.1	*Camellia chekiangoleosa*		x	x	
OL689016.1	*Camellia meiocarpa* cultivar X3			x	x
OL689018.1	*Camellia oleifera*		x	x	x
OL689019.1	*Camellia oleifera*		x	x	x
OL689020.1	*Camellia oleifera*		x	x	
OL689021.1	*Camellia oleifera*		x	x	x
NC 035651.1	*Camellia szechuanensis* voucher YangSX 5066				x
AF380052.1	*Camellia taliensis*			x	
AF380095.1	*Camellia taliensis*		x		
OL689024.1	*Camellia vietnamensis*		x	x	x
OK405020.1	*Camellia tetracocca*			x	
AB207882.1	*Camellia tsaii*	x			
OL742653.1	*Camellia polyodonta*		x	x	x
ON755226.1	*Polyspora hainanensis* voucher FZF20220110	x	x	x	x
MN078084.1	*Camellia vietnamensis*			x	
ON755227.1	*Polyspora speciosa* voucher FZF20220121	x	x	x	x
NC 060778.1	*Camellia vietnamensis*			x	
ON755229.1	*Polyspora speciosa* voucher FZF20220310	x	x	x	x
OL689022.1	*Camellia sasanqua*			x	x
MK820035.1	*Camellia weiningensis*	x			
ON755230.1	*Polyspora axillaris* voucher FZF20220406	x	x	x	x
ON367462.1	*Camellia semiserrata*		x	x	
KU669080.1	*Camellia xiashiensis* voucher Y.Q.Liufu 1528				x
ON072481.1	*Camellia yokdonensis* cultivar Dung & Hakoda		x		
OL689025.1	*Camellia yuhsienensis*			x	x
NC 058253.1	*Camellia zhaiana* voucher YangSX 6023	x			
MH332607.1	*Gordonia sp.* gp-413		x		
AF089716.1	*Polyspora axillaris*			x	
AF380047.1	*Polyspora axillaris*			x	
AF380090.1	*Polyspora axillaris*		x		
AF421092.1	*Polyspora axillaris*			x	
KJ440031.1	*Polyspora axillaris*			x	
KJ510931.1	*Polyspora axillaris*		x		
OM262114.1	*Camellia sinensis* var. pubilimba		x		x
OL537881.1	*Polyspora axillaris* voucher BRIT:Gostel593		x		
ON418964.1	*Camellia meiocarpa*		x	x	x
AF380091.1	*Polyspora chrysandra*		x		
ON418963.1	*Camellia suaveolens*			x	x
ON418965.1	*Camellia sp.* XJ-2021		x	x	x
AF380092.1	*Polyspora hainanensis*		x		
KJ197938.1	*Polyspora hainanensis*		x		
ON755225.1	*Polyspora longicarpa* voucher FZF20211220		x	x	x

<div align="center">Table 3. Continued</div>

OP580978.1	*Camellia euryoides*	x	x	x	x
OP936137.1	*Camellia sp.* XJ-2021	x	x	x	x
AF380051.1	*Polyspora longicarpa*			x	
AF380094.1	*Polyspora longicarpa*		x		
KJ197937.1	*Polyspora longicarpa*		x		
OP723864.1	*Camellia pitardii* var. cryptoneura	x			x
OQ630970.1	*Camellia cordifolia*	x	x	x	
OP953553.1	*Camellia semiserrata*	x			x
AF380093.1	*Polyspora speciosa*		x		
OP036120.1	*Camellia oleifera*			x	x
OP953555.1	*Camellia vietnamensis*	x		x	x
OP953554.1	*Camellia oleifera*		x	x	
OQ707217.1	*Camellia borealiyunnanica*	x	x		
NC 067734.1	*Polyspora tonkinensis*			x	
OQ538305.1	*Camellia pitardii* var. compressa	x			x
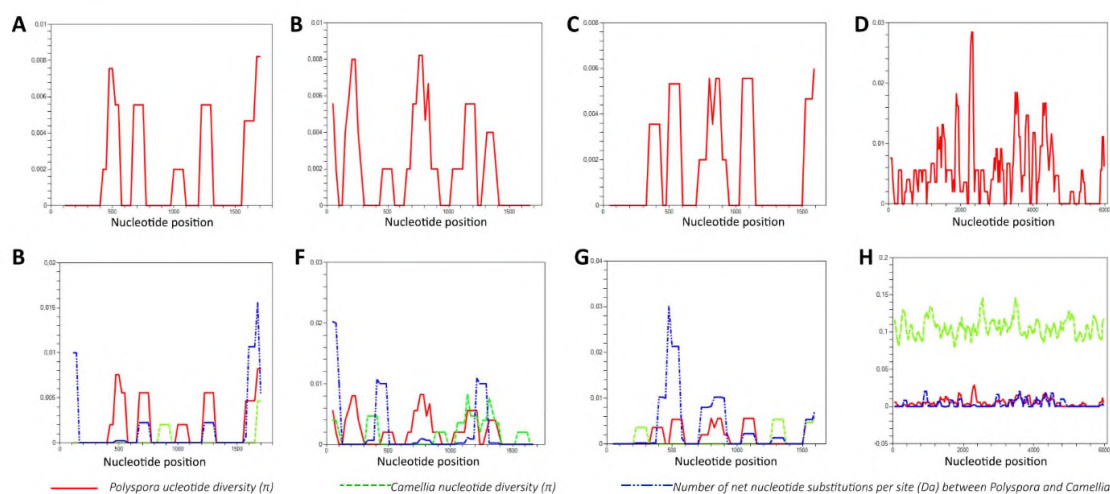
Figure 1. The DNA polymorphism of the *Polyspora* and *Camellia* sequences. The nucleotide diversity of *accD* (A), *matK* (B), *rbcL* (C), and *ycf1* (D) genes with peripheral 100 nucleotides supplement of the genus of *Polyspora*. The DNA polymorphism of of *accD* (E), *matK* (F), *rbcL* (G), and *ycf1* (H) genes comparing between *Polyspora* and *Camellia* genera.

<div align="center">Table 4. Genetic parameters of evaluated Polyspora and Camellia populations.</div>

Values	Populations		Sequences			
	Polyspora	*Camellia*	*accD*	*matK*	*rbcL*	*ycf1*
Nucleotide diversity (π)	x		0.0020	0.00232	0.00164	0.00531
		x	0.0004	0.00168	0.00083	0.10650
	x	x	0.00217	0.00334	0.00314	0.05768
Average number of nucleotide differences (k)	x		3.356	3.933	2.667	29.222
		x	0.667	2.844	1.356	585.622
	x	x	3.637	5.658	5.111	317.163
The average number of nucleotide differences between populations	x	x	5.100	7.700	7.900	325.930
The average number of nucleotide substitutions per site between populations (Dxy)	x	x	0.00304	0.00455	0.00485	0.05927
The number of net nucleotide substitutions per site between populations	x	x	0.00184	0.00254	0.00362	0.00337

model (T92), and the one for *rbcL* was the Jukes–Cantor model (JC). The phylogenic trees were constructed with maximum likelihood in 1000 bootstraps (Figure 3). The *rbcL* and *ycf1* sequences clearly separated the *Polyspora* species population (Figure 3).
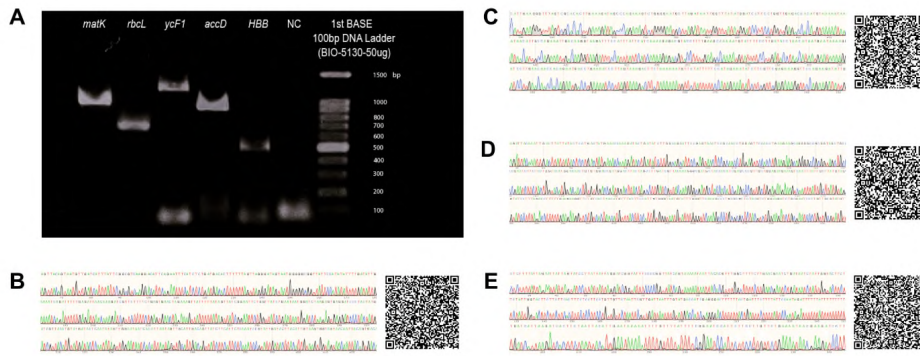
Figure 2. The amplicons of the evaluated marker genes. The amplicons were tested for quality by gel electrophoresis with the positive markers (A). The nucleotide signals by Sanger sequencing and the DDQR codes of the sequences of *accD* (B), *matK* (C), *rbcL* (D), and *ycf1* (E).
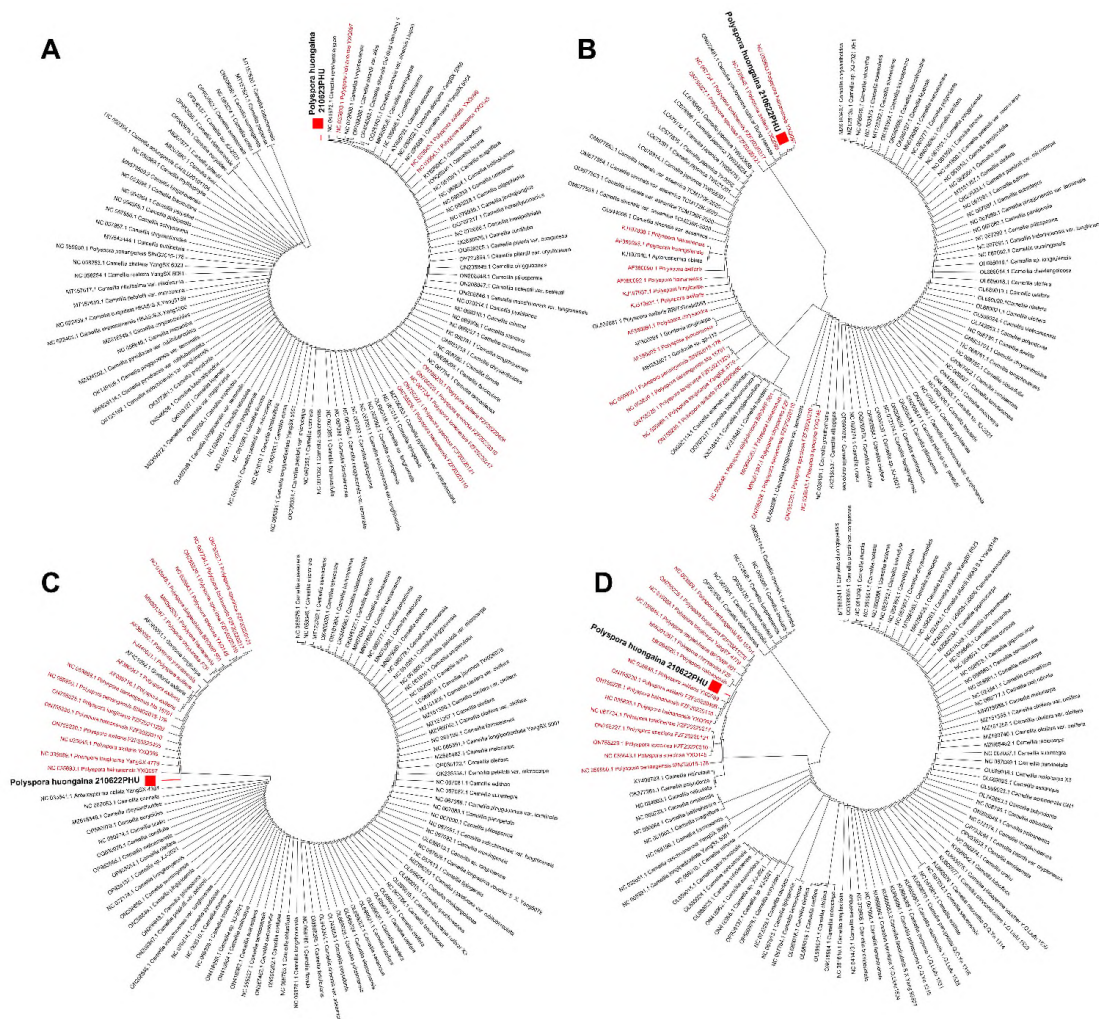
Figure 3. The topology trees built from single-sequence. The topology trees of *accD* (A), *matK* (B), *rbcL* (C), and *ycf1* (D) were conducted from the 100 most related sequences by using Maximum Likelihood algorithm with 1000 bootstraps and a fixed model. *Polyspora* species were in red.

A Phylogenetic Tree Built from Multiple Sequences

Sequence combinations were performed using Snapgene V5.3.2 and were coded into DDQR codes (Figure 4). The combination sequences were coalesced by two, three, or four markers, further contributing to phylogenetic tree conduction (Figures 5-7). The combination demonstrated

the ability to distinguish genera better than the single factor mentioned above.

Two-sequence coherence revealed the authentic separation of the *Polyspora* out of the *Camellia*. The nucleotide diversities between populations of *Polyspora* and *Camellia* were respectively recorded as 0.00582, 0.00121, 0.05682, 0.00969, 0.0376, and 0.04222 for the fusions of *accD + matK, accD + rbcL, accD + ycf1, matK + rbcL, matK + ycf1,* and *rbcL + ycf1*. Evolutionary analysis with maximum likelihood and the T92 model were performed on the fused sequences, with the exception of *rbcL + ycf1*.[26] The T92 evolutionarily invariable (+I, 40,03% sites) model was chosen for the *rbcL + ycf1* evolutionary analyses.[26,27] The topology of *accD + matK* showed that *P. huongiana* had the most related sequence to *Camellia pingguoensis* (OL450398.1), while the rest of the analysis reflexed *P. axillaris* and *P. hainanensis*.[28] *AcD + matK + rbcL, matK + rbcL + ycf1, rbcL + ycf1 + accD,* and *ycf1 + accD + matK* were obtained by assembling sequences from *P. huongiana* and the most-sequence-related collection. The nucleotide diversity were 0.00105 ± 0.00019, 0.00170 ± 0.01135, 0.0442 ± 0.02269, and 0.02712 ± 0.01989 for the fusions in the order. The pairwise distances from *P. huongiana* to *Camellia* (from 0.0005998 ± 0.0005010 to 0.005519 ± 0.002343) and that within *Polyspora* (from 0.001701 ± 0.0001957 to 0.008859 ± 0.001912) indicated a significant difference, p-value < 0.0001 (Figure 7). The *accD + matK + rbcL, matK + rbcL + ycf1,* and *rbcL + ycf1 + accD* algorithms were built evolutionary using the T92 model and Maximum likelihood applying Neighbour-joining and BioNJ algorithms.[26] The *ycf1 + accD + matK* were analysed by the T92 with a discrete Gamma distribution (+G, parameter = 0.3937) model featuring evolutionary rate differences among sites (Figure 6).

The combination of the four sequence regions allowed the distinction of two genera at large genetic distances (Figure 8). There was a significant difference between the pairwise distances from *P. huongiana* within *Polyspora* (0.003725 ± 0.002167) and to *Camellia* (0.007074 ± 0.0003353), p-value = 0.0013; the analysis was based on the T92+G model with 1000 bootstrap replication.[26,29] The nucleotide diversity of the populations was 0.02234 ± 0.01563 in the *Polyspora* and Camellia combination and was 0.00344 ± 0.00037 only in the *Polyspora* genus. The phylogenic tree was obtained using the T92+G model. *P. huongiana* was separated from the most related species *P. axillaris and P. hainanensis* with a frequency of 94% bootstraps.

DISCUSSION

matK and *rbcL* are two commonly used plant classification genes suggested by CBOL.[11] The sequence of *matK* has been recorded to have the fastest evolution in chloroplasts, so it is often used in analysing the evolution and phylogeny of plant species.[30,31] However, the analysis of closely related plant families requires a strong method for identification, as the two sequence regions are not strong enough to distinguish between *Camellia* and *Polyspora*. Nucleotide variation at loci >0.035 is considered highly polymorphic, and it was recorded through the nucleotide density values.[32,33] Based on the analysis of this study, the *matK* and *rbcL* markers did not meet the value. Therefore, two other proposed sequences were added to improve species identity, namely *accD* and *ycf1*.[15] In particular, the *accD* sequence was determined to have low genetic variability, thereby helping to ensure the specific identification of species within the genus. On the other hand, the *ycf1* sequence exhibited high polymorphism in both *Polyspora* and *Camellia* genera, enhancing the ability to separate species between genera.[16] DNA polymorphism in *accD* sequences was higher among *Polyspora* species than within *Camellia species*, which was also detected in *rbcL* and *matK* genes. The *ycf1* sequence exhibited high genetic variability and was evenly distributed throughout the gene region. the DNA variability of *ycf1* was significantly higher in *Camellia* than in *Polyspora*. Most of the nucleotide differences between *Polyspora* and *Camellia* were located in the first half of the *matK* and *rbcL* genes but in the two ends of the *accD* gene. The length-appropriate sequences were selected based on nucleotide diversity distributed according to the nucleotide position to perform Sanger sequencing. The sequences and fusions of *P. huongiana* were translated into DDQR for easy retrieval.

The results showed that *Camellia weiningensis (accD* sequence), *P. hainanensis (rbcL* and *matK fusion),* and *P. axillaris (ycf1* sequence) had the most similar genetic sequences. These two genera of plants are often confused with each other due to common morphological characteristics; for example, *Polyspora (Gordonia) yunnanensis* Hu (wfo-0001219828) and *Camellia taliensis* (wfo-0000582705) have been still considered two names for the same species. All 100 most compatible sequences observed in this study belonged to the genera *Camellia* and *Polyspora*, indicating a deep genetic connection. Using a single sequence to distinguish these two genera faced many obstacles. Hence, sequence combination is necessary for differentiated augments. The combination of two or more sequences allowed for better separation of *Polyposra* from *Camellia*. The two-gene markers proved effective; these results were also analysed for other plant species,
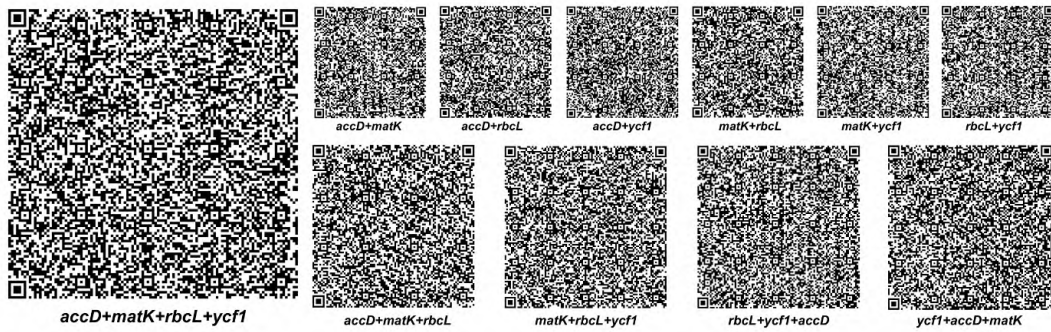
Figure 4. The DDQR codes for the sequence combinations of *P. huongiana*.
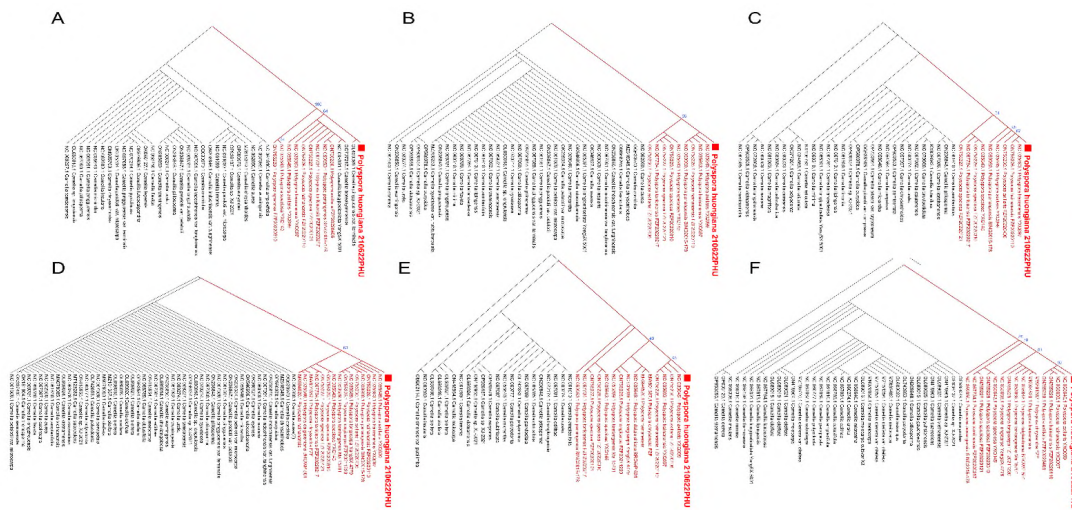
Figure 5. The topology trees of the two-region combinations. Topology trees of the combinations of *accD+matK* (A), *accD+rbcL* (B), *accD+ycf1* (C), *matK+rbcL* (D), *matK+ycf1*(E), and *rbcL+ycf1* (F) were built up by using Maximum Likelihood algorithm with 1000 bootstraps and a fixed model. *Polyspora* species were in red.
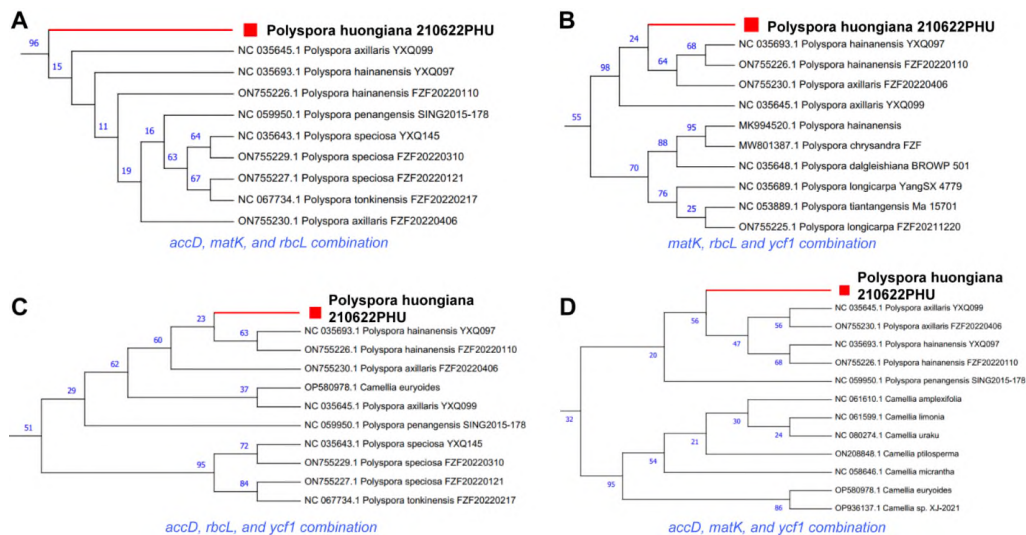
Figure 6. The topology trees of the tri-sequence fusions. Topology trees of the combinations of *accD+matK+rbcL* (A), *matK+rbcL+ycf1* (B), *rbcL+ycf1+accD* (C), and *ycf1+accD+matK* (D) were conducted by using Maximum Likelihood algorithm with 1000 bootstraps and a fixed model.
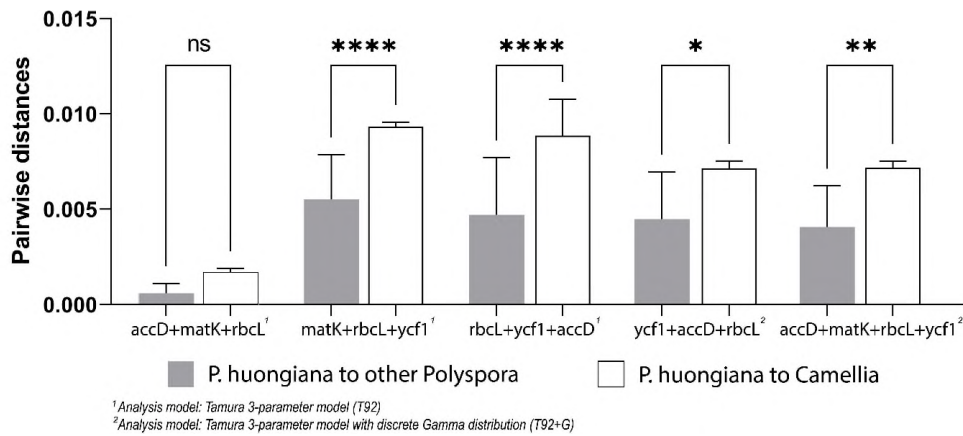
Figure 7. The genetic distances were measured from *P. huongiana* to the other evaluated. The genetic distances of *P. huongiana* to the others were determined by using the best-fixed model conducted by Mega 11 software. The P-values expressed as "ns" for not statistically significant, "*", "**", and "****" for the values less than 0.03, 0.002, and 0.0001, respectively.
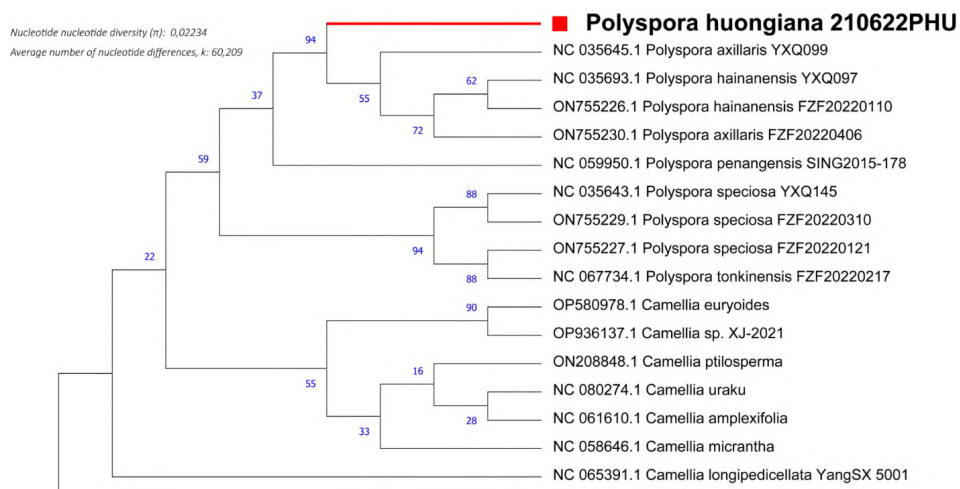
Figure 8. The topology tree of the quart-sequence fusion of *accD+matK+rbcL+ycf1*. The *accD+matK+rbcL+ycf1* topology tree was conducted by using the Maximum Likelihood algorithm with 1000 bootstraps and the T92+G model.

such as jewel orchids, in previous research.[20,34] The combination of the three sequences provided good species discrimination within the genus *Polyspora*, and the most effective combination was *rbcL + ycf1 + accD*. Similarly, combining all four sequence regions gave a large genetic distance and separation between the *Camellia* and *Polyspora* populations, besides, it illustrated good species discrimination within the genus.

The genetic distances between individuals can be used as an element to identify individuals with species, genera, families, and orders.[29,35,36] In this study, the genetic distance between *P. huongiana* and the closest neighbour ranged from 0.0016 to 0.008 in tri- or quant-sequence fusion analysis. *P. axillaris* and *P. hainanensis* were the most connected species published in the NCBI database to *P. huongiana*, based on nucleotide analysis of four investigated regions. Thus far, the plants were judged to share common characteristics and have a deep relationship with

the species native to Vietnam, namely *P. bidoupensis, P. gigantiflora, P. intricata, P. balansae, P. tonkinensis, P. axillaris*.[3,14] The close relative relationship between *P. huongiana* and P. axillaris was genetically confirmed in this study. However, the lack of genetic data on endemic species in Vietnam, especially native tea species, has prevented an in-depth analysis. Research on the genetic diversity of plant species has required attention and implementation plans to address the issue of the lack of genetic information; it helps determine the relationships among phytosociological factors, thereby helping to define the interaction between species.[37] As a result, the most effective exploitation, use, and conservation strategies for plant species in general and area-highly specific plant species, in particular, will be deployed.

CONCLUSION

The combination of two or more of the sequences *accD, matK, rbcL*, and *ycf1* can be considered as a strategy to recognise the *Polyspora* or *Camellia* genera. It is suggested that the tri-sequence or quat-sequence fusion of the mentioned regions can be used to identify *Polyspora* species, including *P. huongiana*, which have a close genetic relationship with *Polyspora axillaris* and *Polyspora hainanensis*. The combination of genetic markers in accurately identifying *P. huongiana* species will contribute positively to the rapid identification and conservation of this rare tea species.

ORCID IDs of the authors

Nguyen Trung Quan	0000-0002-6436-4693
Hoang Thanh Chi	0000-0002-6638-1235
Phung My Trung	0000-0001-7086-8110
Truong Quang Cuong	0000-0001-9159-1018
Tran Thi Cam Thi	0009-0005-6732-2930
Hoang Kim Son	0009-0004-0468-8305
Bui Thi Kim Ly	0000-0002-8433-7035

REFERENCES

1. Nguyet Hai Ninh L, Luong V, Nguyen Van C, et al. An updated checklist of Theaceae and a new species of *Polyspora* from Vietnam. *Taiwania*. 2020;65(2):216-227.

2. Dũng LV, Liễu NT, Cuong TQ, Thanh NT. Đa tu tra la nho (*Polyspora microphylla* Luong, Nguyen et Truong) mot loai moi thuoc ho Ch (Theaceae) o Viet Nam. JS: NST. 2016;32(2):1-5.

3. Orel G, Wilson PG, Curry AS, Luu HT. *Polyspora huongiana* sp. nov. (Theaceae) from Vietnam and notes on related species. *Nord J Bot*. 2012;30(1):47-52.

4. Beech E, Barstow M, Rivers M. The Red List of Theaceae. 2017.

5. Le S, Lesueur D, Herrmann L, et al. Sustainable tea production through agroecological management practices in Vietnam: A review. *J Environ Sustain*. 2021;4:589–604.

6. Romprasert S. Sweet green tea consumption with health economics matter. *Int J Econ Res*. 2017;14:193-202.

7. Zhang W, Kan S-l, Zhao H, Li Z-y, Wang X-q. Molecular phylogeny of *Tribe theeae* (Theaceae s.s.) and its implications for generic delimitation. *PLoS One*. 2014;9(5):e98133. doi: 10.1371/journal.pone.0098133

8. Cheng L, Li M, Han Q, et al. Phylogenomics resolves the phylogeny of Theaceae by using low-copy and multi-copy nuclear gene makers and uncovers a fast radiation event contributing to tea plants diversity. *Biology (Basel)*. 2022;11(7). doi: 10.3390/biology11071007

9. Fan Z-F, Ma C-L. Comparative chloroplast genome and phylogenetic analyses of Chinese *Polyspora*. *Sci Rep*. 2022;12(1):15984. doi: 10.1038/s41598-022-16290-4

10. Erdei B, Hably L. Fossil Gordonia (s.l.)–like (Theaceae) winged seeds from the early Miocene of the Mecsek Mts, W Hungary. *Paleobiodivers Paleoenviron*. 2021;101(1):59-67.

11. Sucher N, Hennell J, Carles M. DNA Fingerprinting, DNA barcoding, and next generation sequencing technology in plants. *Methods Mol Biol*. 2012;862:13-22.

12. Ankola K, Mahadevegowda L, Melichar T, Boregowda MH. Chapter 18 - DNA barcoding: nucleotide signature for identification and authentication of livestock. In: Mondal S, Singh RL, editors. Advances in Animal Genomics: Academic Press; 2021. p. 299-308.

13. Kress W, Erickson D. DNA Barcodes: Methods and Protocols. *Methods Mol Biol*. 2012;858:3-8.

14. Orel G, Wilson PG, Curry AS, Luu HT. *Polyspora huongiana* sp. nov. (Theaceae) from Vietnam and notes on related species. *Nord J Bot*. 2012;30(1):47-52.

15. Huang H, Shi C, Liu Y, Mao SY, Gao LZ. Thirteen *Camellia* chloroplast genome sequences determined by high-throughput sequencing: Genome structure and phylogenetic relationships. *BMC Evol Biol*. 2014;14:151. doi: 10.1186/1471-2148-14-151

16. Li W, Zhang C, Guo X, Liu Q, Wang K. Complete chloroplast genome of *Camellia japonica* genome structures, comparative and phylogenetic analysis. *PLoS One*. 2019;14(5):e0216645-e. doi: 10.1371/journal.pone.0216645

17. Aboul-Maaty NA-F, Oraby HA-S. Extraction of high-quality genomic DNA from different plant orders applying a modified CTAB-based method. *BNRC*. 2019;43(1):25. doi: 10.1186/s42269-019-0066-1

18. Tamura K, Stecher G, Kumar S. MEGA11: Molecular Evolutionary Genetics Analysis Version 11. *Mol Biol Evol*. 2021;38(7):3022-3027. doi: 10.1093/molbev/msab120

19. Rozas J, Ferrer-Mata A, Sánchez-DelBarrio JC, et al. DnaSP 6: DNA sequence polymorphism analysis of large data sets. *Mol Biol Evol*. 2017;34(12):3299-3302.

20. Ho VT, Tran TKP, Vu TTT, Widiarsih S. Comparison of matK and rbcL DNA barcodes for genetic classification of jewel orchid accessions in Vietnam. *J Genet Eng Biotechnol*. 2021;19(1):93. doi: 10.1186/s43141-021-00188-1

21. Saitou N, Nei M. The neighbor-joining A new method for reconstructing phylogenetic trees. *Mol Biol Evol*. 1987;4(4):406-425.

22. Wang Y, Yao X, Liu R, Liu C. DDQR (dynamic DNA QR coding): An efficient algorithm to represent DNA barcode sequences. *PLoS One*. 2023;18(1):e0279994. doi: 10.1371/journal.pone.0279994

23. Li Q, Guo Q, Gao C, Li H. Characterization of complete chloroplast genome of *Camellia weiningensis* in Weining, Guizhou Province. *J Acta Horticulturae Sinica*. 2020;47:779-787.

24. Zheng H, Wei S. Complete chloroplast genomes of *Camellia pubipetala* Y. Wan et S. Z. Huang and *Camellia debaoensis* R. C. Hu et Y. Q. Liufu. *Mitochondrial DNA B Resour*. 2021;6(8):2381-2382.

25. Yu XQ, Gao LM, Soltis DE, et al. Insights into the historical assembly of East Asian subtropical evergreen broadleaved forests revealed by the temporal history of the tea family. *New Phytol*. 2017;215(3):1235-1248.

26. Tamura K. Estimation of the number of nucleotide substitutions when there are strong transition-transversion and G+C-content biases. *Mol Biol Evol*. 1992;9(4):678-687.

27. Buckley TR, Simon C, Chambers GK. Exploring among-site rate variation models in a maximum likelihood framework using empirical data: effects of model assumptions on estimates of topology, branch lengths, and bootstrap support. *Syst Biol*. 2001;50(1):67-86.

28. Wei S-J, Liufu Y-Q, Zheng H-W, et al. Using phylogenomics to untangle the taxonomic incongruence of yellow-flowered *Camellia* species (Theaceae) in China. *J Syst Evol*. 2023;61(5):748-763.

29. Enan M, Al-Deeb M, Fawzi N, Amiri K. DNA Barcoding of *Ricinus communis* from different geographical origin by using chloroplast matk and internal transcribed spacers. *Am J Plant Sci*. 2012;03:1304-1310.

30. Kang Y, Deng Z, Zang R, Long W. DNA barcoding analysis and phylogenetic relationships of tree species in tropical cloud forests. *Sci Rep*. 2017;7(1):12564. doi: 10.1038/s41598-017-13057-0

31. Patwardhan A, Ray S, Roy A. Molecular Markers in Phylogenetic studies-A review. *J Phylogen Evolution Biol*. 2014;2:2. doi: 10.4172/2329-9002.1000131

32. Meyer CP, Paulay G. DNA barcoding: Error rates based on comprehensive sampling. *PLoS Biol*. 2005;3(12):e422. doi: 10.1371/journal.pbio.0030422

33. Liao M, Gao X, Zhang J, Deng H-N, Xu B. Comparative chloroplast genomics of *Sophora* species: Evolution and phylogenetic relationships in the early-diverging legume subfamily *Papilionoideae* (Fabaceae). *Front Plant Sci*. 2021;12:778933. doi: 10.3389/fpls.2021.778933

34. Li H, Xiao W, Tong T, et al. The specific DNA barcodes based on chloroplast genes for species identification of Orchidaceae plants. *Sci Rep*. 2021;11(1):1424. doi: 10.1038/s41598-021-81087-w

35. Birch JL, Walsh NG, Cantrill DJ, Holmes GD, Murphy DJ. Testing efficacy of distance and tree-based methods for DNA barcoding of grasses (*Poaceae tribe* Poeae) in Australia. *PLoS One*. 2017;12(10):e0186259. doi: 10.1371/journal.pone.0186259

36. Hebert PD, Cywinska A, Ball SL, deWaard JR. Biological identifications through DNA barcodes. *Proc Biol Sci*. 2003;270(1512):313-321.

37. Abbas A, Ali A, Hussain A, et al. Assessment of genetic variability and evolutionary relationships of *Rhizoctonia solani* inherent in legume crops. *Plants*. 2023;12(13):2515. doi: 10.3390/plants12132515

Biodegradation of Chlorpyrifos in Paddy Rice Soil in the Mekong Delta, Vietnam

Truong Quoc Tat[1]

[1]Dong Thap University, Faculty of Technology and Engineering, Department of Biotechnology and Food, Dong Thap-Vietnam

ABSTRACT

Objective: Chlorpyrifos (CP) is an organophosphate insecticide. High toxicity makes it a potential source of soil pollution when used in agriculture. This study aimed to assess the anaerobic digestion of CP, the diversity of chlorpyrifos-degrading bacteria in soil, and the mechanism of CP decomposition.

Materials and Methods: Four soil samples were collected from paddy rice fields in Vietnam to evaluate the degradation of CP by anaerobic bacteria. The experiment was conducted in 50 mL microcosms containing 30 mL mineral salt medium, 10 g soil, and 35 mg/kg CP. The concentration of CP was determined using an high performance liquid chromatography.The intermediate products of CP were identified using a gas chromatography–mass spectrometry.

Results: Our bacterial communities in the soil samples anaerobically degraded CP. The rate of CP degradation was doubled after increasing the bacterial density during incubation. The percentage of CP degradation within a 4-month incubation period was significantly higher in the two bacterial communities isolated from alluvial soil than in acid soil. Four bacterial communities were found to degrade CP through the anaerobic reduction of chloride. The intermediate products resulting from the decomposition of CP by these soil bacterial communities were identified as O, O-diethyl-3, 6-dichloro-2-pyridyl phosphorothioate; 3,5,6-trichloro-2-pyridinol; O, O-diethyl-O (3,5,6-trichloro-2-pyridyl) phosphate. This shows the presence of the *Chloroflexi* bacterial phylum in the soil samples.

Conclusion: There is the presence of a group of anaerobic bacteria capable of decomposing CP in soil specialised in rice cultivation, opening up the potential to improve polluted soil by biological means.

Keywords: Anaerobic bacteria, Chlorpyrifos, *Chloroflexi*, DGGE, HPLC, GC/MS.

INTRODUCTION

Chlorpyrifos [*O*, *O*-diethyl *O*-(3,5,6-trichloro-2-pyridyl) phosphorothioate-CP] is an organophosphate insecticide widely used by farmers for insect pest control in agriculture. It is also used, to a lesser extent, for indoor pest control in homes and buildings, and for soil treatment to manage subterranean termites.[1-7] Some reports indicate that CP bioaccumulate in blue-green algae,[8-10] mosquito fish,[11] aquatic plants, and goldfish.[12] In soil, slow resolution CP, soil persistence, and half-life (DT50) range from 60 to 100 days. The organic carbon adsorption coefficient of CP ranged from 652 L/kg for little soil organic matter (1.35% organic matter) to 30.381 L/kg for organic-rich soil (3.41% organic carbon).[13] The common use of CP caused air pollution, soil pollution, and contamination of surface water, rivers, streams, ponds, and lakes.[14] In soil, microorganisms play an important role in promoting CP breakdown. There have been many studies on the decomposition of CP, but most have focused on issues related to CP decomposition under aerobic conditions. However, the anaerobic bacteria can decompose CP in their respiratory process. In the world as well as in Vietnam, the anaerobic digestion of CP has not been studied. However, there are many studies on the anaerobic microbial decomposition of toxic substances containing -chlor, such as *Clostridium butyricum*, *Clostridium pasteurianum*, and *Citrobacter freundii*, which are capable of reducing -chlor hexachlorocyclohexane isomers.[15,16] The results of research on biodegradable dioxins showed reduced activity of some groups, and -chlor anaerobic bacteria play a crucial role in the decomposition of polychlorinated dibenzo-p-dioxins.[16] Other studies showed that soil samples collected from areas with more polluted areas in Vietnam had reduced activity of the chloro-good dibenzo-p-dioxin anaerobic bacteria.[17] In the Mekong Delta of Vietnam, the situation in the paddy soil is often favourable conditions for anaerobic bacteria involved in metabolic pathways and decomposition of soil organic toxins. Therefore, the

theory is still capable of decomposing CP as well as other organic toxins when supplemented with organic acids. This is a matter of electronics. Bacteria can use it to remove chlorine from CP. Therefore, this study was performed to evaluate the decomposition of CP by anaerobic bacterial communities in paddy soil.

MATERIALS AND METHODS

Soil Samples

Soil samples were collected at a depth of 0–30 cm in paddy soils under flooded conditions after rice was harvested. The experiment was conducted with 4 soil samples coded as PH01, PH02, CL01, and CL02. The soil sample origins and characteristics are presented in Table 1. Each soil sample was a completely random layout including 5 treatments, each treatment was repeated 3 times, and the components of each treatment are presented in Table 2. Each soil sample was placed in a 50 mL glass vial and incubated. Before adding 10 g of soil to each vial, CP at a concentration of 35 ppm was dissolved in acetone, and 1 g of finely ground dry soil was added. The acetone was then allowed to evaporate naturally in a fume hood. Next, 30 mL of an anaerobic solution was added. This solution was prepared as described by Christoph et al.[18] and includes macro, trace, and essential vitamins that promote the activity of anaerobic Cl-reducing bacteria. These ingredients include D-biotin, folic acid, riboflavin, pyridoxine hydrochloride, vitamin B12, nicotinamide, and a mixture of organic acids such as pyruvic acid (pyruvate), acetic acid (acetate), butyric acid (butyrate), lactic acid (lactate), and propionic acid (propionate) at a concentration of 250 µM each. After mixing, the solution was aerated with N_2 and vacuumed to remove the O_2. The macromineral solution (1 L) should be supplemented with trace minerals (1 mL), vitamins (0.1 mL), and an organic acid mixture (4 mL). The anaerobic level of the solution can be checked by adding 1 mL of a resazurin anaerobic reagent. If the solution turns blue or purple-green, it indicates that the solution is indeed anaerobic (Figure 1). CP was added after 11 months of incubation: CP was added to the incubated samples to an enriched number of bacteria. 70 mg/L of CP was added to each incubated sample. CP was added for 1, 4, and 5 days. After 330 days, the incubated jars were supplemented with CP to enrich the bacterial population. The concentration of added drug was equivalent to the initial CP concentration of 35 ppm. Before adding the CP, an appropriate amount of anaerobic solution should be added to return the incubation bottle to its original volume of 40 mL. To add CP, a 3 mL medical syringe should be used to inject 1 mL of CP at a concentration of 1400 ppm into NT1, NT4, and NT5. no medicine should be added to live control treatments (NT2, NT3).
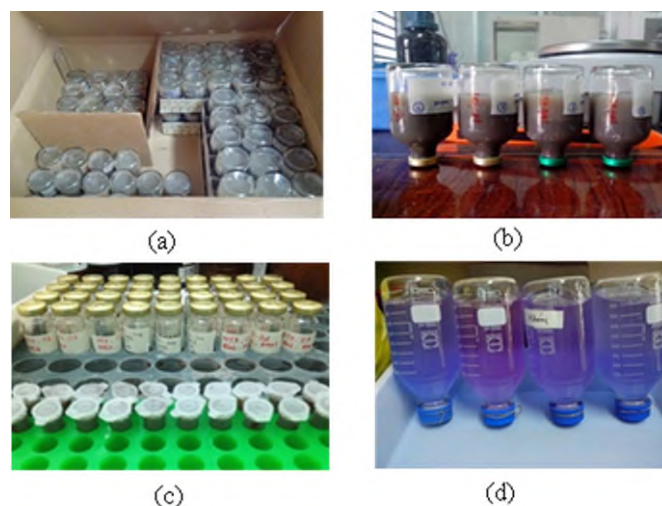
Figure 1. Experimental setup for anaerobic conditions. (a) Incubation vials are stored for measurements every 60 days, (b) Samples are incubated in 50 mL pi vials, (c) Chemical and biological measurements are taken, (d) Anaerobic solution is blue or blue-violet in color.

Samples were taken at 60, 120, 180, 300, 330, 350, and 450 days to determine the CP content, analyse biodiversity, and detect by products present.

Shake the incubation bottle well, use a sterile medical syringe to remove the fluid from the 1 mL incubation bottle, and put it into the 10 mL pi bottle. The syringe was blown with nitrogen gas to expel all the oxygen before sampling. The incubation bottle was gently shaken during the sampling process to make the sample more even and accurate.

The extraction was performed three times using a mixture of toluene and acetone at a ratio of 2:1. After extraction, the samples were allowed to naturally evaporate until they reached a volume of 1 mL. The resulting sample was then filtered and passed through an alumina column for further purification. The concentration of CP was determined using an HPLC (High-Performance Liquid Chromatography) machine equipped with a C18 column measuring 25 cm in length and 4.6 mm in diameter with a particle size of 5 µm. The mobile phase was a mixture of methanol and water in a ratio of 80:20, the detection wavelength was set to 230 nm, the flow rate was 1 mL, and the retention time was 17.7 min. The chromatograms of the baseline and standard are shown in Figures 2 and 3, respectively. The standard curve equation is $y = 20767x - 692.89$ with a linear range of 0.1-300 ppb. The limit of detection (LOD) is 0.1 ppm and the limit of quantification (LOQ) is 0.33 ppm.

The intermediate products of CP were identified using a Shimadzu GC/MS QP2010 Plus chromatography column, specifically, an Rxi 5SilMS 30 m x 0.32 mm chromatography column with a 0.25 µm film. The sample injection chamber temperature was set to 250 ℃, while the gas chromatography (GC)–mass spectrometry (MS) communication points and ion source were set to 250 ℃ and 200 ℃, respectively. A sample volume of 1 µL

Table 1. The origin and characteristics of soil samples used in the experiments.

Province	Code	Number crop/year	Depth (cm)	Soil characteristics			Organic content (%)	pH
				Clay (%)	Loam (%)	Sand (%)		
Tien Giang	CL01	2		67	31	2	7.62	5.70
	CL02	3	0 – 20					
Hau Giang	PH01	3		73	27	0.2	4.90	5.06
	PH02	3						

Table 2. Ingredient of treatments.

Treatments	Ingredient
1- Negative control (NT1)	Use 10 g of sterile soil, 70 mg/L of CP, 30 mL of mineral salt minimum
2 - Positive control (NT2)	Use 10 g of non-sterile soil, no additional CP, 30 mL of mineral salt minimum, vitamin supplements and an organic acid mixture
3 - Positive control (NT3)	Use 10 g of non-sterile soil, no additional CP, 30 mL of mineral salt minimum, no additional vitamin and organic acid mixture
4 - (NT4)	Use 10 g of non-sterile soil, 70 mg/L of CP, 30 mL of mineral salt minimum, vitamin supplements and an organic acid mixture
5 - (NT5)	Use 10 g of non-sterile soil, 70 mg/L of CP, 30 mL of mineral salt minimum, no additional vitamin and organic acid mixture
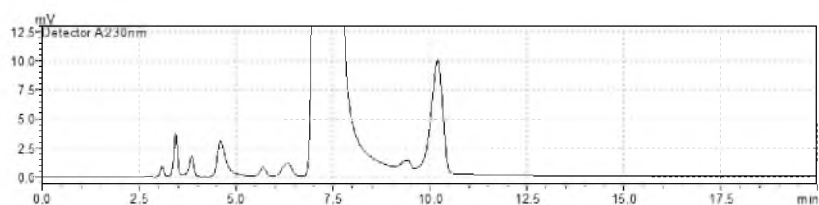
Figure 2. Chromatogram of baseline (blank sample).
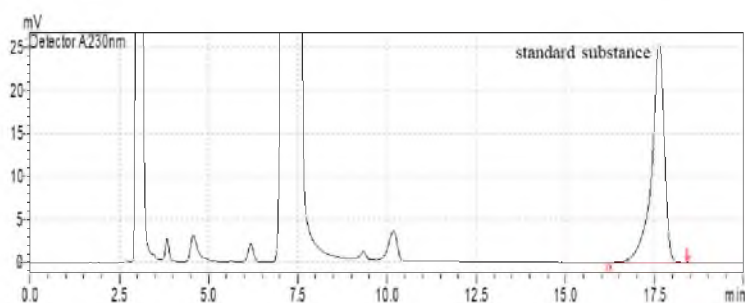
Figure 3. Chromatogram of standard substance.

175

was injected using the splitless injection mode. This method was selected for its accuracy in identifying intermediate CP products.

Soil samples of bacterial communities coded as PH01 after incubation for 2 months were used to extract DNA and perform PCR-denaturing gradient gel electrophoresis (DGGE). The DNA of bacterial communities was extracted using DNA extraction methods from the soil of PowerSoil (R) Isolation. The DNA product was amplified by PCR 2 times. The first PCR was performed using 338F/Chlor1101R primers.[19,20] This PCR product was generated using 341F-GC/534R primers.[21] The primer sequence is shown in Table 3. Then, the DGGE method was used to assess the diversity of the bacterial communities. To use the Cluster and Gel Compare software to analyse the electrophoresis images and compare similarities between bacterial communities.

Table 3. Oligonucleotide sequences of primer.

Gene	Primer sequence, 5'- 3'
338F	ACT CCT ACG GG AGG CAG CAG
Chl1101R	CTC GCK AGA AMA TKT AAC TAG CAAC
341F-GC	CGC CCG CCG CGC GC GGC GGG CGG GGC GG GGG CAC GG GGG CAC GGG GGG CCT ACG GGA GGC AGC AG
534R	ATT ACC GCG GCT GC TGG

Methods of Data Processing, Analysis, and Statistics

Microsoft Excel was used to calculate the percentage of decomposition and graph. The significance of differences was determined using one-way ANOVA and the Tukey test ($p < 0.05$) with Minitab 16 software.

RESULTS

Evaluation of the Potential of Chlorpyrifos Degradation by Anaerobic Bacterial Communities

In the Hau Giang and Tien Giang provinces, four soil samples were collected from paddy soils and used in experiments to evaluate the degradation ability of CP by anaerobic bacterial communities. The results showed that all treatments were biodegradable for CP. After 2 months of incubation, the remaining concentration of CP in the treatment ranged from 3% to 45% of the initial concentration. The decomposition rate of CP increased after supplementation because the number of anaerobic bacteria increased. After 20 days of incubation, the remaining concentration of CP in the treatment ranged from 4.9% to 48.3% of the initial concentration. After 4 months of incubation, the remaining concentration of CP in the treatment

ranged from 0.8% to 1.5% of the initial concentration (Figures 4 and 5).

On the other hand, at 4 months after the addition of CP, the decomposition rate CP of 2 bacterial communities was coded as CL01, and CL02 (the remaining CP from 1% to 1.5% compared to the control), which were higher than 2 communities were coded as PH01 and PH02 (the remaining of CP from 1% to 16% compared to the control).

Identification of Intermediate CP Products

The intermediate products generated during the decomposition of CP by soil anaerobic bacteria were identified.This results in the production of various metabolic byproducts, including a chlorine decomposition product at position 5 on the pyridine ring, namely O, O-diethyl-3,6-dichlo-2 pyridyl phosphorothioate. Another by-product formed is the ester radical decomposition product, which leads to the formation of 3,5,6-trichloro-2-pyridinol (TCP). Further analysis revealed the presence of O, O-diethyl-O (3,5,6-trichloro-2-pyridyl) phosphate (Chlorpyrifos oxon). Treatment without the addition of organic acids enhances the ability of bacteria to use CP for subproduct analysis. Specifically, the sample obtained at 60 days showed daughter products that were identical to those in the treatment with added organic acids (one-chlorine reduction product, TCP, and Chlorpyrifos oxon). However, the 330-day sample exhibited only the formation of chlorine-based decomposition products. In the analytical results, we were unable to determine the carbon cleavage product of CP. This shows that in a farming environment in which only CP is added to promote bacterial utilisation, dechlorination products are still formed. The content of dechlorinated CP was higher than that of TCP (Figure 6).

Anaerobic Bacterial Diversity in Soil

The results of PCR using 338F/Chl1101R primers showed that *Chloroflexi* phylum was present in soil samples. Besides, the results of PCR using 341F-GC/534R primers showed that all samples had a band of DNA at a position of 200 bp. The results of DGGE showed that each band on the gel represents a different bacterial species. To determine whether the chlor-reduction bacteria group in the experiment could be identified from the new DNA bands that appeared in samples supplemented with CP compared with the control treatment with no additional CP. Because the incubation period had passed, bacteria could increase the number. This leads to the formation of a new band in the treatments (Figure 7). The PCR-DGGE results showed that the structure of bacterial communities (was coded as PH01) diversity among treatment complements did not supplement the organic acid, and the control treatment (no additional CP) had a high degree of similarity, 90%-96% (Figure 8).
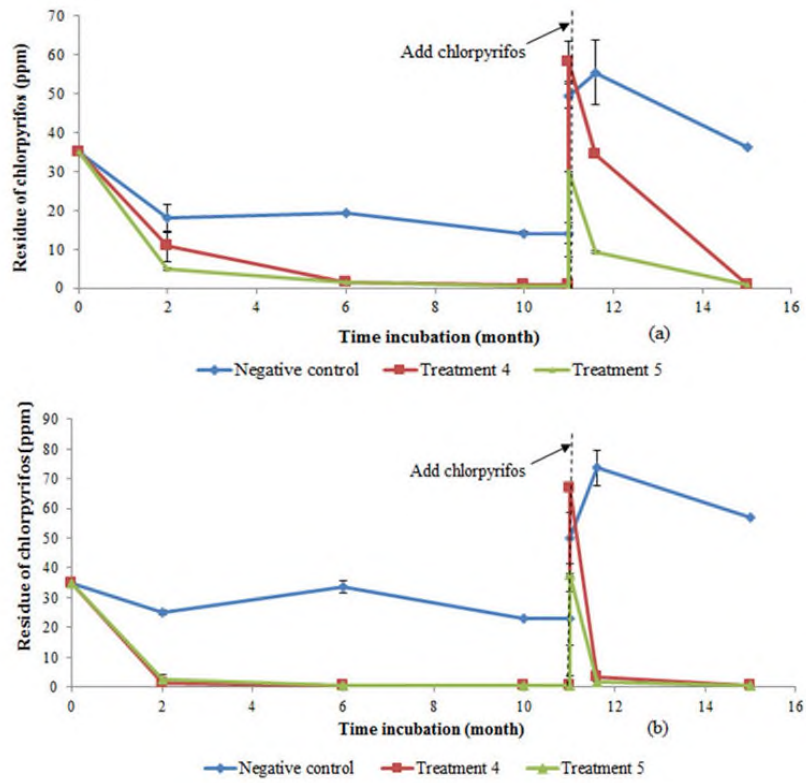
Figure 4. Chlorpyrifos degradability of bacterial comunities CL01 (a) and CL02 (b) (n = 3, standard error).
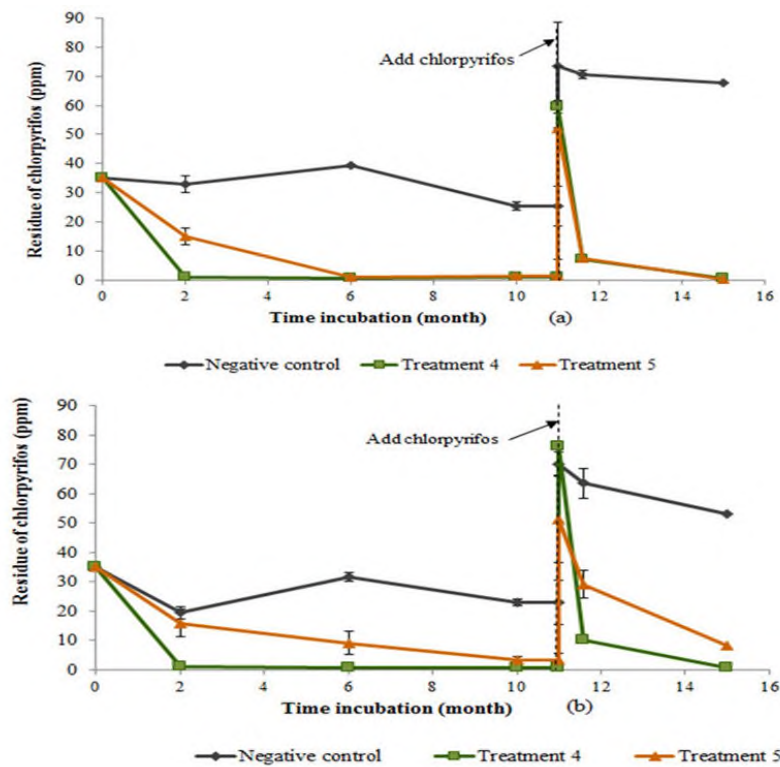
Figure 5. Chlorpyrifos degradability of bacterial comunities PH01 (a) and PH02 (b) (n = 3, standard error).
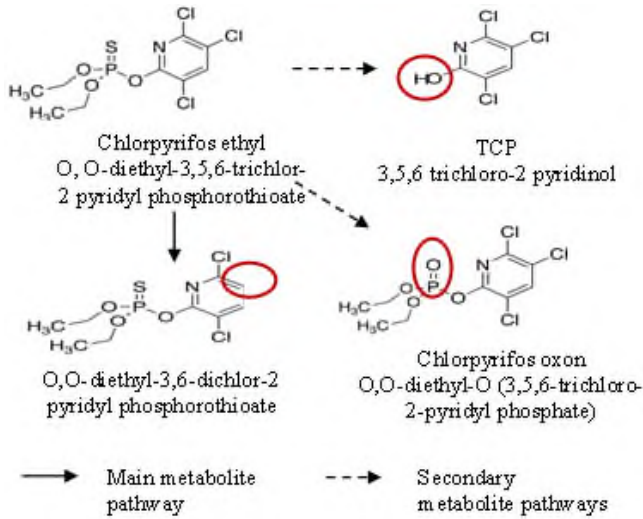
Figure 6. Metabolism diagram of chlorpyrifos in organic acid supplementation treatment.
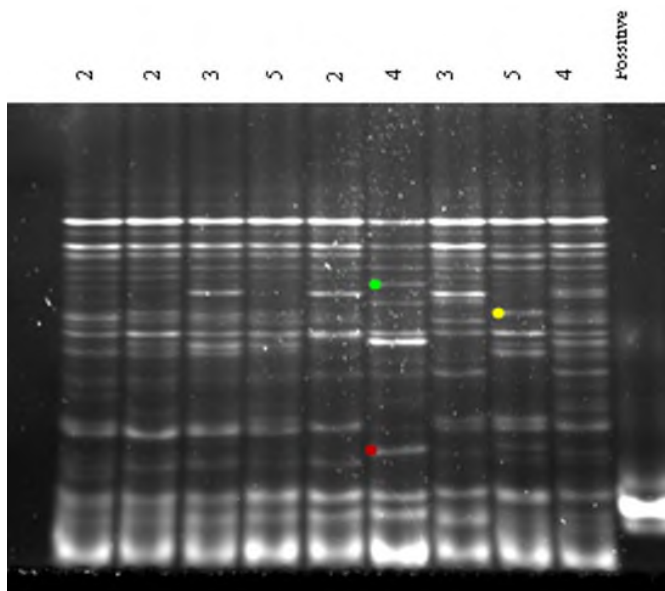
Figure 7. Electrophoresis map PCR-DGGE product of treatments in soil sample PH01.

Figure 8. The similarity of the bacteria *Chloroflexi phylum* in soil samples PH01.

Thus, *Chloroflexi phylum* bacteria were present in 4 soil samples, and the bacterial communities had a high degree of similarity. This result is consistent with the test results for intermediate metabolic products of the CP decomposition route by anaerobic bacterial communities. Intermediate products generated during the decomposition of CP by soil bacterial communities were determined as O, O-diethyl-3, and 6-dichloro-2 pyridyl phosphorothioate.

DISCUSSION

In recent years, there has been a growing interest in the microbial biodegradation of pollutants as a means of finding sustainable ways to clean up contaminated environments. One effective approach is to enhance the growth of microbes that may already be present at the contaminated site and to introduce specialised microbes with the ability to degrade specific contaminants. This technique is known as bioremediation and has become increasingly common. One particularly efficient method is reductive dehalogenation, which rapidly detoxifies chlorinated compounds. However, the complete degradation of organochlorine contaminants under anaerobic conditions requires a consortium of many microorganisms to work together, with complex interrelationships.[22]

In the soil environment, CP can decompose and metabolise in various ways, including adsorption into the soil, infiltration into groundwater, evaporation into the air, and absorption and decomposition by soil microorganisms (both aerobic and anaerobic). In soil, CP decomposition via hydrolysis and photolysis is slow. Therefore, microorganisms play a crucial role in promoting drug decomposition. Although numerous studies have been conducted on the decomposition of CP, most have focused on aerobic conditions. Some notable studies on aerobic decomposition include Singh et al.,[23] who isolated *Enterobater* B14 strain, and Yang et al.,[24] who successfully studied the ability of *Alcaligenes faecalis* DSP3 strain to decompose both CP and its byproduct TCP. Ghanem et al.[25] isolated Klebsiella sp. for their study. Additionally, Anwar et al.[26] Isolated *Bacillus pumilus* C2A1 strains that decompose both CP and TCP. This strain decomposed up to 90% of TCP at a concentration of 300 ppm after only 8 days of incubation.

Numerous studies have been conducted on the decomposition of organic compounds containing chlorine in an anaerobic environment. Among these compounds, some are considered highly toxic, such as Dioxins. According to Duong et al.,[17] bacteria belonging to the genera *Clostridium, Chromium, Bacteroidetes*, and *Chloroflexi* can reduce chlorine content in these compounds. The *Chloroflexi* phylum is one of the most extensively studied genera due to its ability to degrade organochlorine compounds, which are highly toxic and persistent in soil and sediments. Within this phylum, *Dehalococcoides mccartyi* is strictly anaerobic bacteria that are well-known for their

ability to obtain energy through the reductive dehalogenation of organic chlorinated compounds. All known *D. mccartyi* species use hydrogen as an electron donor, acetate as a carbon source, and halogenated aliphatic or aromatic compounds as respiratory electron acceptors. For example, strain 195 can use perchloroethene (PCE), 1,2,3,4-tetrachlorodibenzo-p-dioxin, and hexachlorobenzene as electron acceptors in its respiratory process.[27-29] Similarly, strain CBDB1 has been shown to grow with hexachlorobenzene and dioxins as well.[30,31] For 1,2,3,4-TCDD, chlorine is reduced at both the parent site (para) and the branch site, resulting in the formation of products such as 1,2,3-trCDD, 1,2,4-trCDD, and diCDD. In the case of 2,3,7,8-TCDD, the product formed is 2,3,7-trCDD. The bacterial species examined in the experiment are considered quite diverse and differ from known chlorine-reducing bacterial species found elsewhere in the world. In addition to dioxins, other organic toxins have been successfully investigated. Jagnow et al.[15] Has shown that certain bacteria, such as *Clostridium, Bacillaceae*, and *Enterobacteriaceae*, can decompose γ-hexachlorocyclohexane (γ-HCH) under anaerobic conditions. Specifically, *Clostridium butyricum, C. pasteurianum*, and *Citrobacter freundii* were found to effectively reduce chlorine radicals attached to the gamma position within 4 to 6 days of incubation. However, other facultative anaerobic species, such as *Lactobacillaceae* and *Propionibacterium*, do not exhibit decomposition activity. The main byproduct of this process is γ-tetrachlorocyclohexene (γ-TCH), an important intermediate in the degradation of γ-HCH. Daniel (1990)[32] conducted a study on the degradation of polychlorinated biphenyls (PCBs). The focus of this research was on the biodegradation of PCBs under aerobic and anaerobic conditions. The PCB decomposition system includes aerobic bacteria living in oxidising environments and anaerobic bacteria living in oxygen-free environments, such as aquatic sediments. Drug decomposition experiments follow two different mechanisms. Aerobic bacteria can decompose PCBs by breaking their structure and opening carbon rings. On the other hand, anaerobic bacteria retain the biphenyl ring and reduce the chlorine radicals in the molecule, forming various derivatives of PCBs. These two natural processes complement each other and contribute to the decomposition of the most commonly used PCB mixtures. Other organophosphate pesticides, such as CP, have also been the subjects of research. The pesticide sumithion (o,o-dimethyl-o-(3-methyl-4-nitro) phosphorothioate) was tested for biodegradation using microorganisms isolated from sludge under anaerobic conditions. Analysis of drug concentrations using liquid and gas chromatography revealed that the bacterial system was able to decompose sumithion at concentrations of 20, 50, and 100 ppm in 15, 25, and 45 days, respectively. After 2 years of isolation, the bacterial strain was identified as SY, which can be easily produced and used to treat sumithion-contaminated soil.[33] Similar to other organic substances, CP also contains chlorine radicals attached to the aromatic rings. The successful decomposition of the aforementioned substances demonstrates the potential of the anaerobic decomposition of CP.

In the present study, after conducting the survey, all four bacterial systems (CL01, CL02, PH01, and PH02) effectively decomposed CP under anaerobic conditions. Upon the addition of CP, the bacterial systems could completely utilise the drug. Over 20 days, there was no significant difference in the rate of drug decomposition between the treatments with and without organic acid supplementation for all four bacterial systems (CL01, CL02, PH01, and PH02). However, the decomposition times of the four bacterial systems were shorter than those of the initial experimental setup, indicating an increase in the number of bacteria involved in the decomposition process. According to the National Registration Authority in 2000,[34] the hydrolysis of CP is slower in moderately acidic soils but faster in alkaline environments, because of having 2 types of soil in Tien Giang and Hau Giang provinces. In Tien Giang province, the soil has 7.62% organic matter content which is higher than the soil (having organic matter content of 4.9%) in Hau Giang province. Therefore, in the soil of Tien Giang province, the ability of CP hydrolysis and the decomposition of bacteria CP is better.

In this study, we examined the intermediate products produced during the decomposition of CP by anaerobic bacteria. Our findings revealed that the primary intermediate products were a chlorine decomposition product at position 5 on the pyridine ring, namely O, O-diethyl-3,6-dichloro-2 pyridyl phosphorothioate, TCP, and O, O-diethyl-O (3,5,6-trichloro-2-pyridyl) phosphate (Chlorpyrifos oxon). Chlorpyrifos oxon hydrolysis rate is significantly faster than that of the original CP properties. Therefore, the formation of chlorpyrifos oxons is a crucial intermediate step in promoting the decomposition of CP.[9] However, the concentrations of TCP and chlorpyrifos oxons were found to be very low, indicating that the main decomposition process is still the formation of dechlorination products. The findings of the investigation into the metabolism of CP are partially consistent with those of the Racke[35] study on the overall metabolic pathway of the compound. Both studies found that TCP and chlorpyrifos oxons are formed during metabolism. However, this study also discovered a new product, the dechlorination product at position 5 on the pyridine ring, which is the most abundant metabolite in the anaerobic digestion of CP. This product was not observed in the Racke[35] study on CP metabolic products. Thus, in each treatment with or without organic acids, bacteria used CP as an electron acceptor during respiration. Particularly for treatments without added organic acids, it is not possible to conclude from the analysis results whether or not the bacteria can use CP as their sole carbon source. Analysis of the control samples revealed CP in the soil samples used for testing. Of these samples, half showed evidence of TCP formation at low concentrations. The survey of CP decomposition activity and analysis of metabolic products indicated the presence of anaerobic bacteria in the natural environment that are capable of breaking down CP. Moreover,

the results of the analysis of bacterial diversity are consistent with the results of by-product testing using GC/MS. This shows that the presence of organic acid in the soil does not affect the products identified in the presence and absence of organic acid supplementation. This indicates that there was no difference in the drug decomposition mechanism between the two treatments, indicating a similar structure in the bacterial system. However, in treatments NT2 and NT3, only a small number of daughter products were detected, with only TCP appearing in half of the analysed samples. This could be due to the low concentration of the products, which renders them difficult to detect. Despite this, CP was still present, indicating the possibility of dechlorination activity in both treatments, regardless of the presence of additional organic acid sources. This finding could explain the high similarity between all treatments.

CONCLUSION

Analysis of CP during anaerobic incubation revealed that all four bacterial communities from the four soil samples possessed the ability to effectively decompose CP. Furthermore, the rate of degradation was found to double when the bacterial density was increased during incubation. Interestingly, the decomposition rate of CP over the 4-month incubation period was higher in the two bacterial communities from alluvial soil than in those from acid soil. It was observed that all four bacterial communities utilised anaerobic respiration to degrade CP by reducing –chlor. This shows the presence of *Chloroflexi* bacteria in the soil samples.

Ethics Committee Approval: Ethics committee approval is not required for the study.

Peer Review: Externally peer-reviewed.

Conflict of Interest: Author declared no conflict of interest.

Financial Disclosure: Author declared no financial support.

ORCID IDs of the author

Truong Quoc Tat   0009-0005-7839-3910

REFERENCES

1. Guardino X, Obiols J, Rosell MG, Farran A, Serra C. Determination of chlorpyrifos in air, leaves and soil from a greenhouse by gas-chromatography with nitrogen–phosphorus detection, high performance liquid chromatography and capillary electrophoresis. *J Chromatogr A*. 1998;823:91-96.

2. Kale SP, Carvalho FP, Raghu K, Sherkhane PD, Pandit GG, Mohan Rao A. Studies on degradation of 14C-chlorpyrifos in the marine environment. *Chemosphere*. 1999;39:969-976.

3. Sundaram B, Rai SK, Ravendra N. Degradation of bifenthrin, chlorpyrifos and imidacloprid in soil and bedding materials at termiticidal application rates. *Pestic Sci*. 1999;55:1222-1228.

4. Subhani A, Liano M, Huang CY, Xie ZM. Impact of some agronomic practices on paddy field soil health under varied ecological condition: Influence of soil moisture. *Pedosphere*. 2001;11:38-48.

5. Wang LG, Jiang X, Wang F, Bian YR, Stephan F, Dieter M. Separation of chlorinated hydrocarbons and organophosphorus, pyrethroid pesticides by silicagel fractionation chromatography and their simultaneous determination by GC-MS. *J Environ Sci*. 2004;16:268-271.

6. Wang LG, Jiang X, Yan DY. Comparison of two procedures for extraction and cleanup of organophosphorus and pyrethroid pesticides in sediment. *Pedosphere*. 2004;14:229-234.

7. Pandey S, Singh DK. Total bacterial and fungal population after chlorpyrifos and quinalphos treatments in groundnut (*Arachis hypogaea* L.) soil. *Chemosphere*. 2004;55:197-205.

8. Lal S, Lal R. Bioaccumulation, metabolism and effects of DDT, fenitrothion and chlorpyrifos on *Saccharomyces cerevisiae*. *Arch Environ Contam Toxicol*. 1987;16:753-757.

9. Lal S, Saxena DM, Lal R. Uptake, metabolism and effects of DDT, fenitrothion and chlorpyrifos on *Tetrahymena pyriformis*. *Pestic Sci*. 1987a;21:181-191.

10. Lal R. Bioconcentration and metabolism of DDT, fenitrothion and chlorpyrifos by the blue-green algae *Anabaena* sp. and *Aulosira fertilissima*. *Environ Pollut*. 1987b;46:187-196.

11. Metcalf RL. A laboratory model ecosystem to evaluate "compounds" producing biological magnification. *Essays Toxicol*. 1974;5:17-28.

12. Spacie A, Hamelink JL. Bioaccumulation. In: Rand PM, Petrocelli SR (Eds.), Fundamentals of aquatic toxicology: Methods and applications. Hemisphere Publishers, NY, 1985:497-534.

13. Gebremariam SY. Mineralization, sorption and desorption of chlorpyrifos in aquatic sediments and soils. Doctor of Philosophy, Washington State University. United States. 2012;198.

14. Fenske RA, Lu C, Barr D, Needham L. Children's exposure to chlorpyrifos and parathion in an agricultural community in central Washington State. *Environ Health Perspect*. 2002;110(5):549-553.

15. Jagnow G, Haider K, Ellwardt PC. Anaerobic dechlorination and degradation of hexachlorocyclohexane isomers by anaerobic and facultative anaerobic bacteria. *Arch Microbiol*. 1977;115(3):285-292.

16. Bunge M., Adrian L, Kraus A, et al. Reductive dehalogenation of chlorinated dioxins by an anaerobic bacterium. *Nature*. 2003;421:357-360.

17. Duong V, Tran, DV, Nguyen NK, Häggblom MM, Springael D. Diversity of dibenzofuran-degrading bacteria isolated from dioxin-polluted areas in Vietnam. Abstract Q-008. *ASM*. 2009;109:17-21.

18. Christoph EH, Umlauf GCK, Bidoglio G. "PCDD/Fs and Dioxinlike PCBs in Soils after the Flooding of River Elbe and Mulde in 2002". DIOXIN 2004-24th Intern. Symposium on Halogenated Environmental Organic Pollutants and POPs, 6-10 September 2004. Berlin.

19. Park JW, Krumins V, Kjellerup B, et al. The effect of co-substrate activation on indigenous and bioaugmented PCB dechlorinating bacterial communities in sediment microcosms. *Appl Microbiol Biotechnol*. 2011;89(6):2005-2017.

20. Lane DJ. 16S/23S rRNA Sequencing. In: Stackebrandt, E., Goodfellow, M. (Eds.), Nucleic Acid Techniques in Bacterial Systematics. Wiley, Chichester, New York, 1991;115-175.

21. Muyzer G, Dewaal EC, Uiterlinden AG. Profiling of complex microbial-populations by denaturing gradient gel-electrophoresis

of polymerase chain reaction-ampli fied genes-coding for 16S ribosomal-RNA. *Appl Environ Microbiol*. 1993;59:695-700.

22. McCarty PL. Breathing with chlorinated solvents. *Sci*. 1997;276(5318):1521-1532.

23. Singh BK, Walker A, Morgan JAW, Wright DJ. Biodegradation of chlorpyrifos by *Enterobacter* strain B-14 and its use in bioremediation of contaminated Soils. *Appl Environ Microbiol*. 2004;70:4855-4863.

24. Yang L, Zhao Y, Zhan B, Yang CH, Zhang X. Isolation and characterization of a chlorpyrifos and 3,5,6-trichloro-2-pyridinol degrading bacterium. *FEMS Microbiol Lett*. 2005;251(1):67-73.

25. Ghanem M, Orfi, Shamma M. Biodegration of Chlorpyrifos by *Kepsiella* sp. Isolated an active sluge sample of waste water Treatment plant in Damascus. *Folia Microbiol*. 2007;52(4):423-427.

26. Anwar S, Liaquat F, Khan QM, Kalid ZM, Iqal S. Biodegradation of chlorpyrifos and its hydrolysis product 3,5,6-trichloro-2-pyridinol by *Bacillus pumilus* strain C2A1. *J Hazard Mater*. 2009;168(1):400-405.

27. Maymo-Gatell X, Chien YT, Gossett JM, Zinder SH. Isolation of a bacterium that reductively dechlorinates tetrachloroethene to ethene. *Science*. 1997;276(5318):1568-1579.

28. Fennell DE, Nijenhuis I, Wilson SF, Zinder SH, Haggblom MM. *Dehalococcoides ethenogenes* Strain 195 Reductively Dechlorinates Diverse Chlorinated Aromatic Pollutants. *Environ Sci Technol*. 2004;38(7):2075-2081.

29. Adrian L, Hansen SK, Fung JM, Gorisch H, Zinder SH. Growth of *Dehalococcoides* strains with chlorophenols as electron acceptors. *Environ Sci Technol*. 2007;41(7):2318-2323.

30. Adrian L, Szewzyk U, Wecke J, Gorisch H. Bacterial dehalorespiration with chlorinated ben zenes. *Nature*. 2000;408(6812):580-583.

31. Bunge M, Adrian L, Kraus A., et al., Reductive dehalogenation of chlorinated dioxins by an anaerobic bacterium. *Nature*. 2003;421(6921):357-360.

32. Daniel A. Abramowicz. Aerobic and anaerobic biodegradation of PCBs: A review. *Crit Rev Biotechnol*. 1990;10(3):241-251.

33. Savadogo PW, Ouattara AS, Sedogo MP, Traoré S. Anaerobic biodegradation of Sumithion an organophosphorus insecticide used in Burkina Faso agriculture by acclimatized indigenous bacteria. *Pak J Biol Sci*. 2007;10(11):1896-905.

34. National Registration Authority (NRA). The NRA review of chlorpyrifos. NRA, Australia, 2000:80.

35. Racke KD. Environmental fate of Chlorpyrifos. *Rev Environ Contam Toxicol*. 1993;131:1-151.

How cite this article

Crude Extracts of Three *Iris* Species as Sources of MRSA Antimicrobial Compounds

Belmina Šarić Medić[1] ⓘ, Anesa Jerković-Mujkić[2] ⓘ, Berina Cubara[2] ⓘ, Adaleta Durmić-Pašić[1] ⓘ, Jasna Hanjalić Kurtović[1] ⓘ, Kasim Bajrović[1] ⓘ, Elma Omeragić[3] ⓘ, Mirza Dedić[3] ⓘ, Faruk Bogunić[4] ⓘ, Lejla Pojskić[1] ⓘ

[1]University of Sarajevo, Institute for Genetic Engineering and Biotechnology, Sarajevo-Bosnia and Herzegovina
[2]University of Sarajevo, Faculty of Science, Department of Biology, Sarajevo-Bosnia and Herzegovina
[3]University of Sarajevo, Faculty of Pharmacy, Department of Natural Sciences, Sarajevo-Bosnia and Herzegovina
[4]University of Sarajevo, Faculty of Forestry, Sarajevo-Bosnia and Herzegovina

ABSTRACT

Objective: *Iris* species are widely used in pharmaceutical and cosmetic applications owing to their high content of bioactive compounds with anti-inflammatory and antimicrobial properties. This study aimed to investigate the potential antibacterial effect of crude extracts (aqueous, 50% and 80% ethanol) of three *Iris* species (*I. pumila*, while *I. reichenbachii* and *I. illyrica* are endemic) from Bosnia and Herzegovina against the multiresistant bacterial strain methicillin-resistant *Staphylococcus aureus subsp. aureus* ATCC 33591 (MRSA strain).

Materials and Methods: The antimicrobial compounds in the crude extracts were identified using High-performance liquid chromatography (HPLC), and their effects on the MRSA strain were tested using agar well diffusion and broth microdilution method. The binding affinities were analysed using molecular docking simulations.

Results: We identified bioactive targeted compounds in these extracts, mainly flavonoids named isorhamnetin, hesperidin, quercetin, fisetin, genistein, and kaempferol. Antibacterial assays showed that extracts of all three *Iris* species inhibited MRSA. The binding affinity analysis showed that isorhamnetin and hesperidin had the highest affinity scores, stronger (isorhamnetin) or the same (hesperidin) as the positive control ceftobiprole.

Conclusion: This *in vitro* and *in silico* study showed that *Iris* species represent a valuable source of bioactive compounds that can be used against multidrug-resistant strains such as MRSA. The potential use of these agents in multiple drugs is warranted, and further evaluation for human application is needed.

Keywords: Plant bioactive compounds, Methicillin-resistant *Staphylococcus aureus*, Molecular docking, Minimum inhibitory concentration.

INTRODUCTION

Staphylococcus aureus is a Gram-positive facultative anaerobic bacterium commonly found in the body as part of its microbiota.[1] During the production of virulence factors, such as extracellular toxins and enzymes or cell surface protein expression, *S. aureus* can promote infections by becoming a pathogenic strain.[2] These high lethality rates can include infections of the skin and soft tissues, endovascular infections, pneumonia, endocarditis, sepsis, and similar.[3] It is one of the most important human bacterial pathogens that can cause infection in almost any human tissue. The treatment of these infections can be problematic due to the presence of antibiotic-resistant

S. aureus. A subgroup that has developed drug resistance primarily to β-lactams is methicillin-resistant *S. aureus* (MRSA). Decreased affinity for β-lactams or β-lactams resistance of *S. aureus* has been developed due to the presence of *mecA*, which encodes penicillin-binding protein 2a (PBP2a).[4] MRSA has become one of the greatest threats in clinical medicine, resulting in difficult prediction and expensive treatment.

Despite intensive research and development of a new broad range of antibiotics, there is still a need for their effectiveness confirmation.[5] The progress in combating antimicrobial resistance is greatly reduced because of the effects of the pandemic.[6] Thus, the incidence of the increased number of drug-resistant

pathogens is highlighted as a primary investigation field by various pharmaceutical and scientific communities; they recognised the potential in alternative treatments with the usage and drug repurposing of plant-derived substances.[3] Because natural compounds constitute the majority of currently used clinical antibiotics, numerous plant extracts are continuously important sources of antimicrobials.[3,7]

Worldwide, many endemic plant species have shown significant antimicrobial activity.[8-11] These studies highlight the potential of endemic plants as sources of new antimicrobial agents. Within the Iridaceae family, *Iris spp.* represent the largest genus and one of the most significant families of flowering plants, ranging throughout Eurasia and North America, with a vast diversity of species.[12] Many secondary metabolites that have been identified from *Iris* species have demonstrated various biological properties, including antimicrobial, antioxidant, anti-inflammatory, antitumor, and immunomodulatory effects.[13] The unique chemical compounds that endemic plants often produce are potential sources of novel antimicrobial agents that may be effective against resistant strains of bacteria and fungi.[14] Research on the medicinal properties of endemic plants also highlights their ecological importance and promotes conservation efforts that are crucial for maintaining biodiversity and protecting ecosystems.[15]

This study explored the antimicrobial *in vitro* activity of different *Iris* plant extracts from Bosnia and Herzegovina, including dwarf iris, *Iris pumila* L., *Iris reichenbachii* Heuff., and Illyrian iris, *Iris illyrica* Tomm., against methicillin-resistant *S. aureus*, as well as the confirmation of their potential antimicrobial properties using molecular docking simulation studies.

MATERIALS AND METHODS

Preparation of Plant Extracts

Plant material from three different *Iris* species was collected in the period of April-June 2021 in different regions of Bosnia and Herzegovina (*I. pumila*-Kalinovik region, *I. reichenbachii*-Kladanj region, and *I. illyrica*-Neretva Canyon). Clean and air-dried rhizomes were macerated and pulverised using an IKA mill and dissolved in a 1:1 volume ratio of the solvents (distilled water, 50% ethanol, or 80% ethanol). Following evaporation, the extracts were dissolved in absolute ethanol and filtered through a PTFE syringe sterile filter (Lab-Expert, Slovenia, 0.45 µm) under sterile conditions. The final concentration of the crude extract was 330 mg/mL.

Componential Analysis of Target Compounds

High-performance liquid chromatography (HPLC) was used to identify potential antimicrobial compounds in *Iris* species plant extracts using an Agilent Infinity II 1260 HPLC system. Analysis was performed at a constant temperature of 40°C during a 55

min run. HPLC standards for the targeted compounds (fisetin, quercetin, kaempferol, isorhamnetin, genistein, and hesperidin) were acquired from Sigma-Aldrich, USA.

Evaluation of Antibacterial Activity

The antimicrobial properties of *Iris* species extracts were tested against the multi-drug-resistant bacteria *Staphylococcus aureus* subsp. *aureus* ATCC 33591 (MRSA strain) using agar well diffusion and broth microdilution. The MRSA strain was cultivated on Mueller–Hinton (MH) medium overnight at 37°C as part of the agar well diffusion method.[16] The cultured MRSA strain was used at 1-2 x 10^8 CFU/mL as the inoculum, obtaining uniform homogeneous turbidity corresponding to 0.5 McFarland.[17] Then, 50 µL of each extract was added to the wells made by drilling the plates with a sterile borer. Tests were performed in triplicate. Clear inhibition zones were measured after incubation at 37°C for 24 h. We used several antibiotics as positive controls: Colistin (10 µg), Streptomycin (10 µg), Ampicillin (10 µg), and Amoxicillin (25 µg), all made by Oxoid™, Great Britain. The broth microdilution method[18] was used to determine the minimum inhibitory concentration (MIC) and minimum bactericidal concentration (MBC). The 50 µL of liquid Mueller–Hinton Broth (Sigma Aldrich) was added to every well in a sterile microtiter plate, except in the wells of the first column. Subsequently, serial two-fold dilutions of the tested Iris species extracts were added in the 165-0.32 mg/mL range. After that, 50 µL of the MRSA suspension was added to the first eleven columns, at approx. 5x10^5 CFU/mL concentration. The eleventh column contained only the standard inoculum used as the positive control, while the twelfth column contained the negative control sterile liquid MHB. After incubation for 16-18 h at 37°C, 30 µl of 0.015% resazurin (Sigma-Aldrich, USA) was added to each well and left for another 2-4 h of incubation. At the end of the analysis, the wells without visible change represented the concentration of the extract above the MIC value.[19] MBCs were determined by plating well contents with concentrations higher than the MIC and incubating at 37°C for 24 h aerobically. Each test was performed twice.

Receptor-Ligand Binding Evaluation

To elucidate the potential antibacterial effect against multi-drug bacteria, we analysed the binding affinity of determined bioactive compounds in *Iris* species extracts (fisetin, quercetin, kaempferol, isorhamnetin, genistein, and hesperidin) to the SauPBP2a active site—the protein responsible for MRSA resistance to β-lactams. The obtained affinity values were compared against ceftobiprole, which is a high-affinity reference molecule, and methicillin, which has a low affinity to the SauPBP2a active site.[20] The three-dimensional (3D) crystal structure of SauPBP2a was retrieved from the Protein Data Bank (PDB) database (RCSB Protein Data Bank) (PDB

ID: 1MWT). The structure data files (SDF) were obtained from the PubChem database (isorhamnetin CID:5281654; hesperidin CID:10621; ceftobiprole CID: 135413542; quercetin CID: 5280343; fisetin CID: 5281614; genistein CID:5280961; kaempferol CID:5280863; methicillin CID:6087). The SDF ligand files were converted to PDB 3D format using PyMOL 2.4. (https://pymol.org/2/), whereas the preparation of target proteins and ligands and their conversion to the PDBQT format was performed using AutoDock Tools software (http://mgltools.scripps.edu/downloads). Selection and determination of the catalytic binding site of SauPBP2a (amino acid residues within chain B named Ser403, Lys406, Tyr446, Ser462, Asn464, Ser598, Gly599, and Thr600) were based on reference data, and also PrankWeb.[21] Grid box dimensions were based on data from the literature. Molecular docking followed standard procedures that require AutoDock Vina 1.1.2. software.[22] To identify the molecular interactions, we used PyMOL 2.4.

Statistical Analysis

Mean values ± standard deviation (SD) were calculated using Microsoft Office 2019 (Excel (Microsoft Corporation, USA). One-way ANOVA ($P<0.05$ and $P<0.01$) and Tukey's multiple comparison test were calculated using software STATISTICA 10; StatSoft. Inc.

RESULTS

In Vitro Antimicrobial Activity of Identified Bioactive Compounds

HPLC revealed that targeted bioactive compounds in *I. pumila, I. reichenbachii*, and *I. illyrica* extracts (aqueous, 50% ethanol, and 80% ethanol) were present in *Iris* species extracts at different concentrations, in a range from 0.223647 to 292.6555, expressed in mg.g^{-1} DW. Fisetin was not present in all *I. pumila* extracts, kaempferol, and hesperidin in *I. illyrica* extracts, whereas genistein was identified only in the aqueous and 50% ethanolic extracts of *I. pumila* (Table 1).

The results of the antibacterial assay (agar well diffusion method) showed that all tested extracts of *Iris* spp. had antibacterial effects against the MRSA strain. The aqueous extract of *I. pumila* had the greatest inhibitory effect against this multidrug-resistant strain (20.00±1.73), although the other values of the effects of the extracts were also not negligible. The potential antimicrobial properties of the extracts were also evaluated using MIC and MBC as parameters (Table 2). None of the four antibiotics tested (colistin, ampicillin, streptomycin, and amoxicillin), did not cause the growth inhibition, whereas most extracts had MIC values between 10.31 and 20.63 mg/mL.

In Silico Molecular Docking Simulation

A molecular docking study revealed that the best binding affinity (rmsd l.b. 0.000; rmsd u.b. 0.000) to the SauPBP2a site was for isorhamnetin (-8.3), following the hesperidin (-8.1) as well as the positive control of binding ceftobiprole (-8.1), followed by quercetin (-7.9), fisetin (-7.8), genistein (-7.5), kaempferol (-7.3) and methicillin (-5.3), all expressed in kcal/mol. It was noted that all compounds had better scores than the negative control of binding affinity methicillin.

After acquiring binding affinity results, we analysed intermolecular interactions of ligands with better or the same binding scores as the positive controls ceftobiprole (isorhamnetin and hesperidin) and the target protein SauPBP2a. These data revealed interactions between amino acid residues and selected compounds in terms of the formation of good hydrogen bonds. Isorhamentin formed five hydrogen bonds in total, including three with the amino acid residue Ser403 (2.9 Å; 2.2 Å; 2.0 Å), one with Asn464 (3.2 Å), and Ser462 (2.5 Å). The bioactive component hesperidin exhibited hydrogen bonding with the amino acid residues: Ser494 (2.2 Å), Asn500 (2.3 Å), and Gly282 (2.4 Å). The positive control for binding affinity, ceftobiprole, formed two hydrogen bonds with the amino acid residues Ser598 (2.7 Å) and Thr600 (2.0 Å) (Figure 1).

DISCUSSION

Iris species are well known for their use in the pharmaceutical, cosmetic, and food industries, but they also have various potential applications as antioxidant, anticancer, hepatoprotective, anti-inflammatory, and antimicrobial agents.[13,23] Some are widely used in traditional medicine for inflammation, bacterial, and viral infections, and in some cases as adjuvant therapy for cancer treatment.[24] These biological activities are the result of numerous bioactive compounds present, such as xanthones, quinones, flavonoids and their derivates, terpenes, and simple phenolics.[23-25] In the present study, we examined the potential antibacterial effect of crude extracts of *Iris* species (*I. pumila, I. reichenbachii*, and *I. illyrica*) obtained using different solvents against the MRSA strain. Using HPLC, we identified bioactive targeted compounds (isorhamnetin, hesperidin, quercetin, fisetin, genistein, and kaempferol). Isorhamnetin, quercetin, fisetin, and kaempferol belong to the class of flavonoids named flavanols; hesperidin is in the flavanone group of flavonoids, while genistein is an isoflavone. To our knowledge, the results from our research represent the first report on the phytochemical composition of three *Iris* species crude extracts from the Bosnia and Herzegovina area, characterised via HPLC technique. Other phytochemical studies of *Iris* spp. have revealed the presence of different flavonoids in their composition.[26,27]

Table 1. Compound contents of the examined extracts were determined using HPLC.

Plant species	The type of extraction	Compound content (mg/1 g DW)					
		Fisetin	Quercetin	Kaempferol	Isorhamnetin	Genistein	Hesperidin
Iris reichenbachii Heuff.	aqueous	81.31115	48.4339	0	6.97005	0	10.35255
	50 % ethanol	218.0028	18.08235	0.1995659	0.469365	0	46.45055
	80 % ethanol	292.65555	22.1808	0.87237	0.933755	0	76.9613
Iris pumila L.	aqueous	0	53.02175	10.16585	25.4444	0	15.16575
	50 % ethanol	0	12.9293	0.922625	2.075675	0.113647	58.0301
	80 % ethanol	0	9.2454	0.894715	2.20035	0.132236	48.0050
Iris ilyirica Tomm.	aqueous	65.8556	15.81085	0	14.5912	0	0
	50 % ethanol	84.4289	7.905	0	2.651465	0	0
	80 % ethanol	168.878735	14.96365	0	8.1085	0	0

Table 2. Minimum inhibitory concentration (MIC) and minimum bactericidal concentration (MBC) of tested extracts and control and diameter of inhibition zones* (mm) obtained through the agar well diffusion method.

Plant species	The type of extraction	*Staphylococcus aureus* subsp. *aureus* ATCC 33591 (MRSA strain)		
		MIC• (mg/mL)	MBC• (mg/mL)	Diameter of inhibition zones (mm)
Iris reichenbachii Heuff.	aqueous	10.31	20.63	18.00±0.00
	50 % ethanol	10.31	20.63	19.00±1.00 [* c, f]
	80 % ethanol	10.31	20.63	16.30±0.57 [* b,h,i **d]
Iris pumila L.	aqueous	10.31	20.63	20.00±1.73 [** c,e.f]
	50 % ethanol	10.31	20.63	16.70±0.57 [** d]
	80 % ethanol	10.31	20.63	16.30±0.57 [* b,h,i **d]
Iris illyrica Tomm.	aqueous	10.31	20.63	18.00±0.00
	50 % ethanol	10.31	20.63	19.00±1.00 [* c,f]
	80 % ethanol	20.63	41.25	19.00±0.00 [* c,f]
Control (mg/mL)	Amoxicillin, initial concentration = 0.512 mg/mL	NI	NI	N/A

•Same values obtained through duplicates
* Note: The data are given as mean ± standard deviation (SD) of triplicate experiments. Results were subjected to One-way ANOVA, and mean comparisons were performed using Tukey's multiple comparison test.
Different superscripts in the column indicate significant differences (**$P<0.01$ and *$P<0.05$).
NI=No inhibition
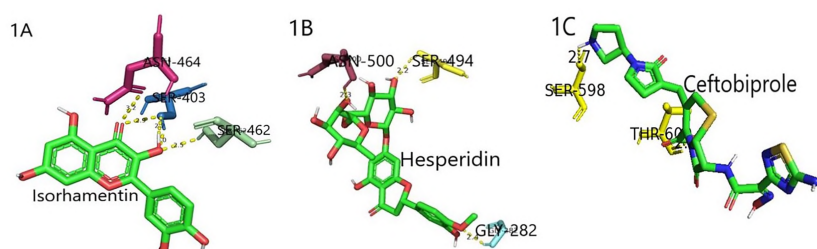
Figure 1. Results of intermolecular bonding (H-bond yellow dots) between ligands (1A-isorhamnetin; 1B-hesperidin; positive control 1C-ceftobiprole) and amino acid residues of the SauPBP2a active site.

Many *in vitro* or *in vivo* studies have pointed out that these flavonoids have prominent antimicrobial effects[28,29], whereas some of those studies emphasised the antibacterial effect against MRSA. For instance, some studies indicated the inhibitory effects of kaempferol and quercetin against MRSA[30], hesperidin inhibited biofilm formation of MRSA[31], genistein was highlighted as a promising drug for MRSA-induced osteomyelitis.[32] These are just a few of the studies that are being conducted to explore the potential of research-targeted bioactive compounds against multiresistant MRSA. They are positively correlated with our findings; potential antimicrobial effects of compounds mentioned above were found in the *Iris* species examined in this study.

A molecular docking analysis of binding affinity showed that isorhamnetin had the highest affinity score, even higher than the positive control ceftobiprole, whereas hesperidin had the same binding affinity as ceftobiprole. The binding energies of the analysed ligands were ranged from -5.3 to -8.3 kcal/mol. Alhadrami et al. analysed the antimicrobial effect of certain flavonoids against MRSA, i.e., the PBP2a receptor. Their results and data obtained through *in silico* analysis, followed by *in vitro* studies on the bacterial MRSA strain, suggested that, apart from the other compounds, quercetin, kaempferol, and hesperidin had antimicrobial potential, whereas hesperidin showed a synergistic effect.[27] In the present study, kaempferol had higher binding affinity than negative control methicillin. However, compared to the other ligands, it had the lowest score. Ceftobiprole had a slightly better binding score than quercetin. The study of Kalalo et al. showed that quercetin (-8,5 kcal/mol) and kaempferol (-8,3 kcal/mol) had the potential to inhibit MRSA.[33] Both ligands, isorhamnetin, and hesperidin, interacted within residues that are in the transpeptidase domain of PBP2a protein (residues 327-668)[34], which suggests that these compounds have the potential to bind to the PBP2a active site, which could ultimately have an impact on cell wall synthesis.

According to the results of the agar well diffusion test, all extracts showed strong inhibitory activity against MRSA.[35] The highest antibacterial activity with an inhibition zone value of 20 mm was observed for the aqueous extract of *I. pumila*, and the statistical analyses revealed that it was significantly greater (P<0.01) than the inhibition zone values for 50% and 80% ethanol extracts of *I. pumila* and 80% ethanol extract of *I. reichenbachii*. Additionally, positive effects against the MRSA strain were recorded for the 50% ethanol extract of *I. reichenbachii* and 50% and 80% ethanol extracts of *I. illyrica* (19 mm), with statistically significant differences (P<0.05) when compared with the 50% and 80% ethanol extracts of *I. pumila*. According to Gold et al., absolute ethanol has no microbiocidal effect; therefore, its antimicrobial effect cannot be attributed to the solvent but mostly to the components that possess antimicrobial potential, as recorded in the literature.[36] In the existing literature, there are no data on the effects of these three species of the genus *Iris* on multiresistant MRSA,

but studies are available on other *Iris* species. A study by Hoang et al. (2020) showed that *Iris* spp. of the Iridaceae family have antimicrobial potential against *S. aureus*, whereby the methanol extracts showed also the anti-biofilm formation effect.[37]

CONCLUSION

Our study using *in vitro* and *in silico* methods showed that *Iris* species from Bosnia and Herzegovina have the potential to be a valuable source of antimicrobial compounds, particularly against multiresistant bacterial strains such as MRSA. However, further studies are needed to confirm the mechanism of action and possible cytotoxic and genotoxic effects for initial use in pharmacotherapy. This study can serve as a basis for exploring the health-based properties of endemic plants from the Balkan peninsula.

ORCID IDs of the authors

Belmina Šarić Medić	0000-0001-8593-4678
Anesa Jerković-Mujkić	0000-0002-7769-4181
Berina Cubara	0009-0007-1965-3297
Adaleta Durmić-Pašić	0000-0002-5022-6185
Jasna Hanjalić Kurtović	0000-0002-8693-7886
Kasim Bajrović	0000-0002-7927-2417
Elma Omeragić	0000-0002-5996-4926
Mirza Dedić	0000-0002-4951-7516
Faruk Bogunić	0000-0002-7636-3559
Lejla Pojskić	0000-0003-2260-318X

REFERENCES

1. Masimen MAA, Harun NA, Maulidiani M, Ismail WIW. Overcoming methicillin-resistant *Staphylococcus aureus* (MRSA) using antimicrobial peptides-silver nanoparticles. *Antibiotics (Basel)*. 2022;11(7):951. doi: 10.3390/antibiotics11070951

2. Lowy FD. *Staphylococcus aureus* infections. *N Engl J Med*. 1998;339(8):520-532.

3. Ahmad-Mansour N, Loubet P, Pouget C, et al.

Staphylococcus aureus toxins: An update on their pathogenic properties and potential treatments. *Toxins (Basel)*. 2021;13(10):677. doi: 10.3390/toxins13100677

4. Baek KT, Gründling A, Mogensen RG, et al. β-Lactam resistance in methicillin-resistant *Staphylococcus aureus* USA300 is increased by inactivation of the ClpXP protease. *Antimicrob Agents Chemother*. 2014;58(8):4593-4603.

5. Brown NM, Goodman AL, Horner C, Jenkins A, Brown EM. Treatment of methicillin-resistant *Staphylococcus aureus* (MRSA): Updated guidelines from the UK. *JAC-Antimicrob Resist*. 2021;3(1):dlaa114. doi: 10.1093/jacamr/dlaa114

6. CDC. Special report: COVID-19 U.S. Impact on antimicrobial resistance. 2022; Available: https://www.cdc.gov/drugresistance/pdf/covid19-impact-report-508.pdf

7. Johnston CW, Badran AH. Natural and engineered precision antibiotics in the context of resistance. *Curr Opin Chem Biol*. 2022;69:102160. doi: 10.1016/j.cbpa.2022.102160

8. Rakotofina HME, Donno D, Tombozara N, et al. Chemical composition, antimicrobial activity, and antioxidant capacity of *Micromeria flagellaris* Baker and *M. madagascariensis* Baker: Two endemic species from Madagascar as sources of essential oils. *Heliyon*. 2024;10(5):e26865. doi: 10.1016/j.heliyon.2024.e26865

9. Dini S, Chen Q, Fatemi F, Asri Y. Phytochemical and biological activities of some Iranian medicinal plants. *Pharm Biol*. 2022;60(1):664-689.

10. İnanir M, Uçar E, Tüzün B, Eruygur N, Ataş M, Akpulat HA. The pharmacological properties of *Gypsophila eriocalyx*: The endemic medicinal plant of northern central Turkey. *Int J Biol Macromol*. 2024;266(Pt2):130943. doi: 10.1016/j.ijbiomac.2024.130943

11. Alam K, Ahmad N, Ahmad I, Nafees M. Pharmacological activities of *Rhododendron afghanicum*; An endemic species of Khyber Pakhtunkhwa, Pakistan. *Chem Biodivers*. 2023;20(12):e202301273. doi: 10.1002/cbdv.202301273

12. Fan L, Gao Y, Hasenstein KH, Wang L. 'Flower Angel': A new *Iris sanguinea* cultivar. *HortSci*. 2021;56:617-618.

13. Khatib S, Faraloni C, Bouissane L. Exploring the use of *Iris* species: Antioxidant properties, phytochemistry, medicinal and industrial applications. *Antioxidants (Basel)*. 2022;11(3):526. doi: 10.3390/antiox11030526

14. Abdallah EM, Alhatlani BY, de Paula Menezes R, Martins CHG. Back to nature: Medicinal plants as promising sources for antibacterial drugs in the post-antibiotic era. *Plants*. 2023;12(17):3077. doi: 10.3390/plants12173077

15. Volenzo T, Odiyo J. Integrating endemic medicinal plants into the global value chains: The ecological degradation challenges and opportunities. *Heliyon*. 2020;6(9):e04970. doi: 10.1016/j.heliyon.2020.e04970

16. Nigussie D, Davey G, Legesse BA, Fekadu A, Makonnen E. Antibacterial activity of methanol extracts of the leaves of three medicinal plants against selected bacteria isolated from wounds of lymphoedema patients. *BMC Complement Med Ther*. 2021;21(1):2. doi: 10.1186/s12906-020-03183-0

17. European Committee on Antimicrobial Susceptibility Testing. EUCAST guidelines for detection of resistance mechanisms and specific resistances of clinical and/or epidemiological importance. EUCAST, Basel, Switzerland (2017).

18. CLSI, Clinical and Laboratory Standards Institute. MO7: Methods for dilution antimicrobial susceptibility test for bacteria that grow aerobically, 11th ed. Wayne, PA: USA (2018).

19. Elshikh M, Ahmed S, Funston S, et al. Resazurin-based 96-well plate microdilution method for the determination of minimum inhibitory concentration of biosurfactants. *Biotechnol Lett*. 2016;38(6):1015-1019.

20. Masumi M, Noormohammadi F, Kianisaba F, Nouri F, Taheri M, Taherkhani A. Methicillin-Resistant *Staphylococcus aureus*: Docking-based virtual screening and molecular dynamics simulations to identify potential inhibitors of penicillin-binding protein 2a in natural flavonoids. *Int J Microbiol*. 2022;9130700. doi: 10.1155/2022/9130700

21. Jendele L, Krivak R, Skoda P, Novotny M, Hoksza D. PrankWeb: A web server for ligand binding site prediction and visualization. *Nucleic Acid Res*. 2019;47(1):W345-W349.

22. Trott O, Olson A. AutoDock Vina: Improving the speed and accuracy of docking with a new scoring function, efficient optimization and multithreading. *J Comput Chem*. 2010;31(2):455-461.

23. Kaššák P. Secondary metabolites of the choosen genus *Iris* species. *Acta Univ Agric et Silvic Mendel Brun*. 2012;60(8):269-280.

24. Amin HIM, Hussain FHS, Najmaldin SK, et al. Phytochemistry and biological activities of Iris species growing in Iraqi Kurdistan and phenolic constituents of the traditional plant *Iris postii*. *Molecules*. 2021;26(2):264. doi: 10.3390/molecules26020264

25. Periferakis A, Periferakis K, Badarau IA, et al. Kaempferol: Antimicrobial properties, sources, clinical and traditional applications. *Int J Mol Sci*. 2022;23(23):15054. doi: 10.3390/ijms232315054

26. Unver T, Uslu H, Gurhan I, Goktas B. Screening of phenolic components and antimicrobial properties of *Iris persica* L. subsp. *persica* extracts by *in vitro* and *in silico* methods. *Food Sci Nutr*. 2024; 00:1–17. doi:10.1002/fsn3.4251

27. Alhadrami HA, Hamed AA, Hassan HM, Belbahri L, Rateb ME, Sayed AM. Flavonoids as potential anti-MRSA agents through modulation of PBP2a: A computational and experimental study. *Antibiotics* (Basel). 2020;9(9):562. doi: 10.3390/antibiotics9090562

28. Pyrzynska K. Hesperidin: A Review on extraction methods, stability and biological activities. *Nutrients*. 2022;14(12):2387. doi: 10.3390/nu14122387

29. Xu HX, Lee SF. Activity of plant flavonoids against antibiotic-resistant bacteria. *Phytother Res*. 2001;15(1):39-43.

30. Yin N, Yang X, Wang L, et al. Kaempferol inhibits the expression of α-hemolysin and protects mice from methicillin-resistant *Staphylococcus aureus*-induced lethal pneumonia. *Microb Pathog*. 2022;162:105336. doi: 10.1016/j.micpath.2021.105336

31. Vijayakumar K, Muhilvannan S, Vignesh MA. Hesperidin inhibits biofilm formation, virulence and staphyloxanthin synthesis in methicillin resistant *Staphylococcus aureus* by targeting SarA and CrtM: an *in vitro* and *in silico* approach. *World J Microbiol Biotechnol*. 2022;38(3):44. doi: 10.1007/s11274-022-03232-5

32. Guo X. Antibacterial and anti-inflammatory effects of genistein in *Staphylococcus aureus* induced osteomyelitis in rats. *J Biochem Mol Toxicol*. 2023;37(4):e23298. doi: 10.1002/jbt.23298

33. Kalalo MJ, Fatimawali, F, Kalalo, T, Rambi CIJ. Tea bioactive compounds as inhibitor of MRSA penicillin binding protein 2a (PBP2a): A molecular docking study. *J Farm Medica*. 2020; 3(2):70-75. Doi: 10.35799/pmj.3.2.2020.32878

34. Fishovitz, J, Hermoso, JA, Chang, M, Mobashery, S. Penicillin-binding protein 2a of methicillin-resistant *Staphylococcus aureus*. *IUBMB Life*. 2014; 66(8):572-7. doi: 10.1002/iub.1289

35. Iwashina T, Mizuno T. Flavonoids and Xanthones from the genus

Iris: Phytochemistry, relationships with flower colors and taxonomy, and activities and function. *Nat Prod Commun*. 2020;15(10). doi:10.1177/1934578X20937

36. Gold, NA, Mirza TM, Avva U. Alcohol sanitizers. In: StatPearls [Internet]. Treasure Island (FL): StatPearls Publishing; 2024. PMID: 30020626

37. Hoang L, Beneš F, Fenclová M, et al. Phytochemical composition and *in vitro* biological activity of *Iris spp.* (Iridaceae): A new source of bioactive constituents for the inhibition of oral bacterial biofilms. *Antibiotics (Basel)*. 2020;9(7):403. doi: 10.3390/antibiotics9070403

How to cite this article

RESEARCH ARTICLE

Anatomical and Histological Structures of the Female Reproductive System of the Adult Lucerne Leaf Beetle *Gonioctena fornicata* (Brüggemann, 1873) (Coleoptera: Chrysomelidae)

Nurcan Ozyurt Kocakoglu[1] (iD), Hicret Arslan[1] (iD), Selami Candan[1] (iD)

[1]Gazi University, Science Faculty, Department of Biology, Yenimahalle, Ankara, Türkiye

ABSTRACT

Objective: The aim of this study was to determine the anatomical and histological structures of the female reproductive system of *Gonioctena fornicata* (Brüggemann, 1873) (Coleoptera: Chrysomelidae), an economically important alfalfa pest, and to contribute to studies in this field.

Materials and Methods: The anatomy and histology of the female reproductive system and egg structure of adult *G. fornicata* were described using stereo, light, and scanning electron microscopy.

Results: The female reproductive system of *G. fornicata* comprises a pair of ovaries, lateral oviducts, a spermatheca, and a common oviduct. Each ovary contains 14 telotrophic ovarioles with terminal filaments. Just below the terminal filament is the germarium. The germarium surface is smooth and has a pear-shaped appearance. There is a single oocyte in the vitellarium region, located next to the germarium. The oocyte, which completes its development, passes into the pedicel, the last part of the ovariole. The ovarioles are connected to the lateral oviduct via pedicels. Polygonal shapes are observed on the chorion surface of eggs in the lateral oviduct. A pair of lateral oviducts opens into a common oviduct. Spines extend from the intima layer of the lateral and common oviducts towards the lumen. *G. fornicata* eggs laid outside are yellowish in colour and have a cylindrical appearance. The chorion is extremely thin and has polygonal shapes on its surface.

Conclusion: The female reproductive systems of *G. fornicata* are generally similar to those of other species in the subfamily Chrysomelinae.

Keywords: Ovariol, Ovary, Trophocyte, Light microscope, Scanning electron microscope.

INTRODUCTION

The family Chrysomelidae comprises most species-rich and important families.[1,2] This family includes approximately 19 subfamilies and >2,000 genera, and the total number of species is estimated to exceed 50,000. The Palaearctic region is represented approximately 3,500 Chrysomelidae species[3-9] although recent studies indicate that the region is home to approximately 9,293 species. In Turkey, approximately 968 Chrysomelidae species have been identified, representing 11 subfamilies and 113 genera.[10] Chrysomelinae includes important pests and biological control agents and is one of the largest subfamilies in Chrysomelidae.[11,12]

One of the pest species included in the Chrysomelinae is the lucerne leaf beetle *Gonioctena fornicata* (Brüggemann, 1873), which is a pest of plants in the Fabaceae family, especially alfalfa. Both the adult and larval stages of *G. fornicata*

(Chrysomelidae) are highly damaging, causing crop losses and significant damage to alfalfa. Adults and larvae of these species feed on the leaves, flowers, leaf buds, young shoots, and stem tips of alfalfa.[13-15]

In the Coleoptera female reproductive system, the ovaries are divided into two or more ovarioles that open into the oviduct.[16] There are terminal filaments, germarium, vitellarium, and pedicel in each ovariol.[17-20] Whereas the division of germ cells and detection of oocyte and follicle formation occur in the germarium, the growth of oocytes and egg formation occur in the vitellarium.[21] There are very few studies on the reproductive systems of the different species belonging to the family Chrysomelidae, which is of great importance for the reproductive system and the classification.[17,22-26] The aim of this study was to determine the female reproductive system and egg structure of *G. fornicata* (Chrysomelidae) anatomically and histo-

logically and to contribute to the development of more effective control methods against this pest.

MATERIALS AND METHODS

Lucerne Leaf Beetle Samples

The 20 adult female specimens of *G. fornicata* (Chrysomelidae) used in this study were collected in May 2022 from an agricultural field in Elazığ, Türkiye.

Stereo Microscopy

The female reproductive organs of insects anaesthetised with ethyl acetate smoke and dissected in 0.1 M sodium phosphate buffer at pH 7.2, examined, and photographed under an Olympus SZX7 stereomicroscope.

Light Microscopy

For histological examination, 10 female reproductive systems were dissected and fixed in 10% neutral formalin for 24 h. After fixation, the specimens were rinsed with tap water and dehydrated in an ethanol gradient from 50% to 100%. They were then clarified in two batches of xylene for 15 min each and gradually switched from xylene to paraffin. The tissues were then definitively embedded in liquid paraffin at 65°C and solidified at room temperature. 5-6 µm thick sections were obtained from these paraffin blocks using a Microm HM 310 microtome. Finally, sections were stained with Haematoxylin and eosin (H&E) and Mallory's trichrome (M) and visualised and photographed using an Olympus BX51 LM microscope.

Scanning Electron Microscopy (SEM)

For SEM examination, initially, 10 samples were fixed in 2.5% glutaraldehyde and then rinsed with sodium phosphate buffer (pH 7.2). The samples were then dehydrated using a series of ethanol solutions ranging from 50% to 100%. Subsequently, the samples were air-dried using hexamethyldisilazane. Finally, the specimens, which were affixed to SEM stubs with double-sided tape, received a thin gold coating using a Polaron SC 502 sputter coater before examination. Images were captured using a JEOL JEM 6060 LV SEM at 5 kV.

RESULTS

The female reproductive system of *G. fornicata* comprises one pair of ovaries, one pair of lateral oviducts, and one common oviduct. Each ovary consists of four parts; terminal filament, germarium, vitellarium, and pedicel. The ovary consists of 14 telotrophic ovarioles with terminal filaments (Figure 1). The ovariole ends with a terminal filament (Figures 2a and 2b). The germarium is located in the second half of the ovariole. When histological sections are examined, it is seen that the trophocyte proximal to the germarium had large spherical and basophilic nuclei (Figures 2b, 2c and 2d). Germarium has a pear-shaped appearance and a smooth surface (Figure 2e). The germarium

length is 291 µm and width is 144 µm, and the width of the terminal filament is 12.9 µm. At the same time, trophocyte were found in the broken samples (Figure 2f).

Figure 1. General view of *Gonioctena fornicata* female reproductive system under steromicroscope. co: common oviduct, lo: lateral oviduct, ov: ovariole.
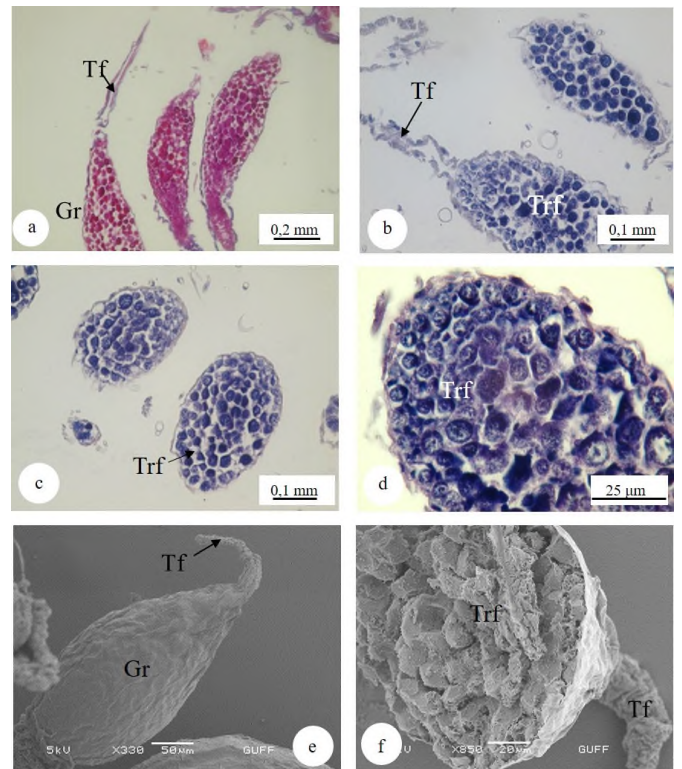
Figure 2. (a) Terminal filament extending from the germarium under light microscope: Haematoxylin and eosin (H&E) and Mallory's trichrome (M) staining. (**c,d**). Germarium under light microscope: H&E staining (**e**). Germarium and terminal filament general view under scanning electron microscope. (**f**). Nutrient granules in germarium under scanning electron microscope. Gr: Germarium, Tf: Terminal filament, Trf: Trophocyte.

The germarium contains trophocyte (large nurse cells), young oocytes, and prefollicular cells (Figure 3a). There is a single oocyte in the vitellarium region, located next to the germarium.

The previtellogenic oocyte is surrounded by several layers of follicular epithelium. No nutrients were stored in the ooplasm (Figure 3b). The vitellogenic oocyte is surrounded by a single-layered cylindrical follicle epithelium. Nutrients began to be stored in the ooplasm (Figures 3c and 3d). When examined under a scanning electron microscope, nutrient granules were observed in the ooplasm of the choriogenic oocyte, and the chorion layer was formed (Figure 3e). At this stage, polygonal shapes are distinguished on the chorion surface (Figure 3f).
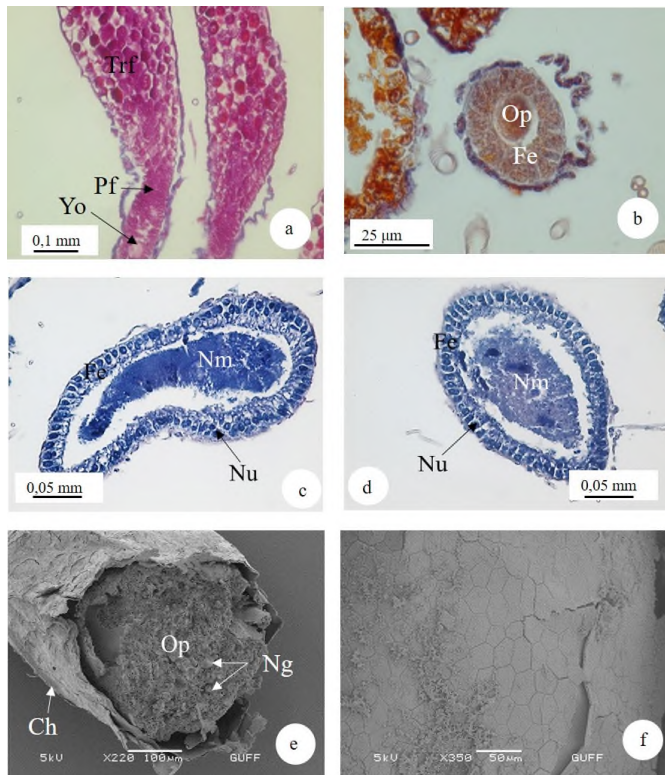
Figure 3. (a) General appearance of trophocytes, prefollicular cells, and young oocytes in the germarium under light microscope: Mallory's trichrome (M) staining. (**b**). Section of previtellogenic oocytes under light microscope: M staining, (**c,d**). Vitellogenesis under light microscope: Haematoxylin and eosin staining. (**e**). Choriogenic oocyte under scanning electron microscope. (**f**). The surface of choriogenic oocyte, under scanning electron microscope. Ch: Chorion, Fe: Follicular epithelium, Nm: Nutrient material, Nu: Nucleus, Ng: Nutrient granules, Op: Ooplasma, Pf: Prefollicular cells, Trf: Trophocyte, Yo: Young oocytes.

The choriogenic oocyte passes into the pedicel, which is the last part of the ovariole. The ovarioles are connected to the lateral oviduct by pedicels (Figure 4a). The last part of the ovarioles is the pedicel, which is surrounded by a single-layer epithelium (Figures 4a and 4b). The pedicels connect to the lateral oviduct, which has a wider lumen (Figure 4a). Histological sections are examined, it is seen that it is surrounded by a single-layer epithelial layer and forms folds towards the lumen (Figures 4c and 4d). The oval nuclei are located towards the middle of the epithelium. When histological sections taken from the lateral oviduct were examined, abundant spine-like structures were observed on the intima (Figures 4c and 4d).
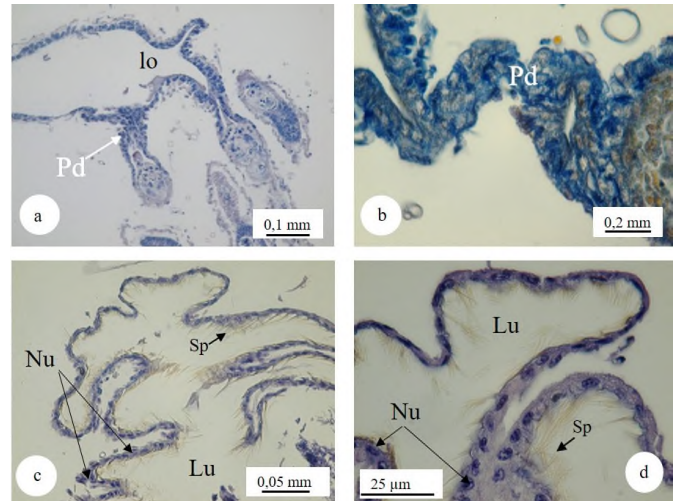
Figure 4. (a) Attachment of the pedicels to the lateral oviduct under light microscope: Haematoxylin and eosin (H&E) staining. (**b**) Longitudinal section of the pedicel under light microscope: Mallory's trichrome staining, (**c,d**). Spines located in the lateral oviduct under light microscope: H&E staining. Sp: Spins, lo: lateral oviduct, Lu: Lumen, Nu: Nucleus, Pd: Pedicel.
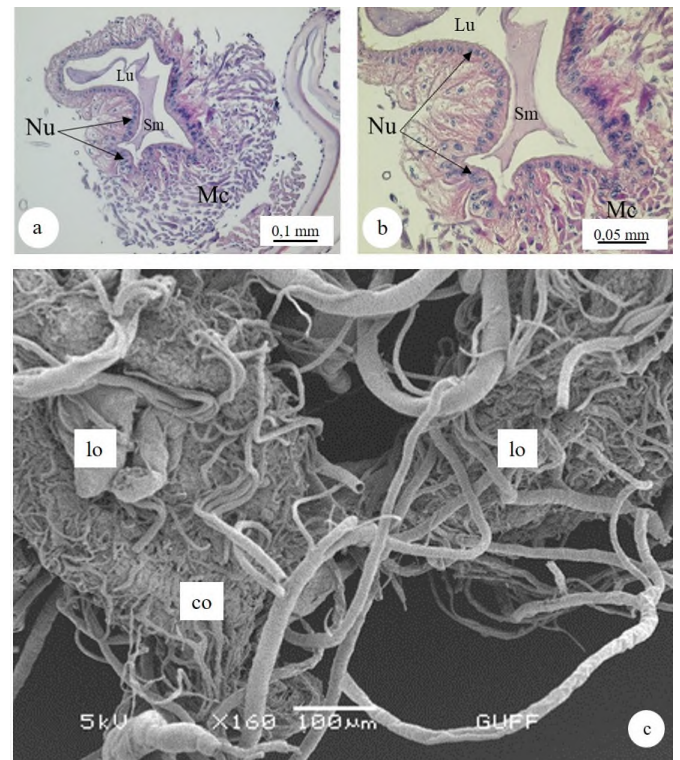
Figure 5. (a,b) Common oviduct histological section under light microscope: Haematoxylin and eosin staining. (**c**). Connection of the lateral oviduct to the common oviduct under scanning electron microscope. co: common oviduct, lo: lateral oviduct, Lu: Lumen, Nu: Nucleus, Sm: Secretory materials, Mc: Muscles.

The lateral oviduct open into the common oviduct, and in the histological sections of the common oviduct, a single-layered epithelium with a round nucleus forming wide folds towards the lumen is observed. Beneath the epithelium, spines extend from the intima layer towards the lumen. Secretory material is remarkable in the lumen. There is a dense amount of muscle

around the common oviduct (Figures 5a and 5b). Numerous trachea networks can be seen on the lateral and common oviduct surfaces (Figure 5c).

G. fornicata (Chrysomelinae) eggs lying outside are yellowish in colour and have a cylindrical appearance (Figure 6a). Eggs are 1.35 mm long and 0.5 mm wide. The egg has a micropyle region (Figure 6c) and polygonal shapes on its surface (Figures 6a-6e). In the SEM image (Figure 6f), the opening made by the larva as it hatches from the egg can be distinguished. Aeropyle openings are evident on the egg side (Figures 6g and 6h). The egg chorion is very thin (~500 nm) (Figures 6i and 6j).
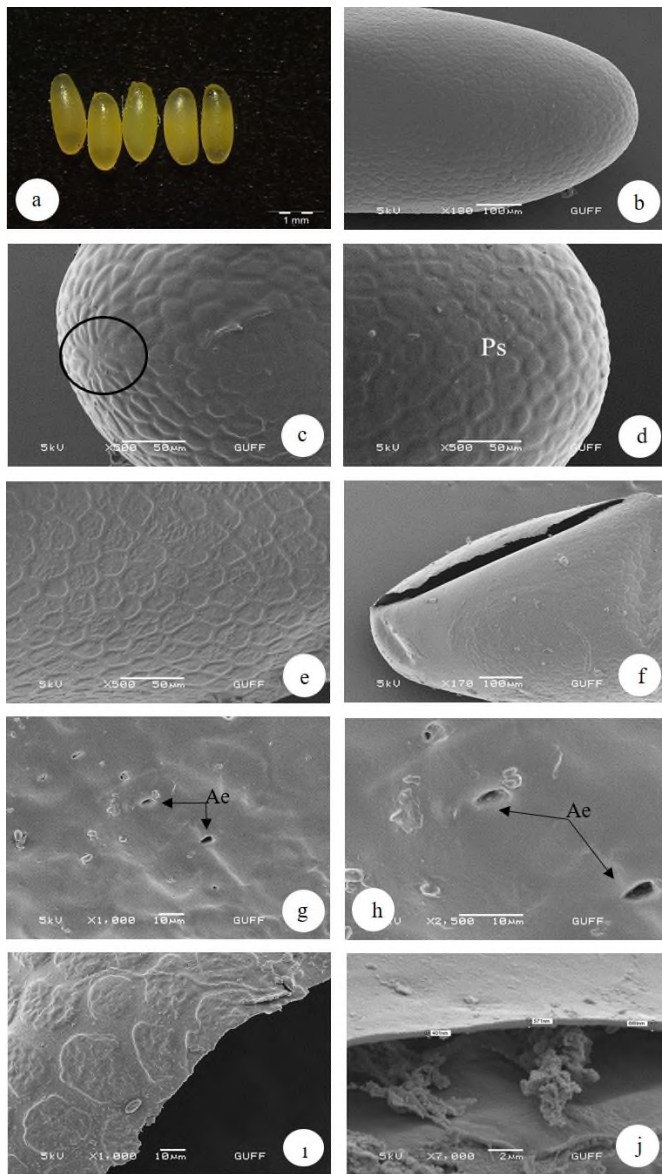
Figure 6. (a) *Gonioctena fornicata* eggs in the general view under stereomicroscope. **(b-e)**. Micropyle opening and polygonal patterns on the egg surface under scanning electron microscope. **(f)**. Opening on the surface of the egg. **(g,h)**. Aeropyles on the egg surface under scanning electron microscope. **(i,j)**. Chorionic thickness of the egg under scanning electron microscope. Ae: Aeropyle opening, Ps: Polygonal shapes.

DISCUSSION

The female reproductive systems of *G. fornicata* are generally similar to those of other Chrysomelinae species such as *Zygogramma exclamationis* (Fabricius, 1798), *Chrysomela populi* (Fabricius, 1798), *Chrysolina herbacea*, (Duftschmid 1825), and *Phaedon brassicae* (Baly, 1874).[23, 27-29]

Insect eggs develop in highly protected structures called ovarioles.[30] The ovariole is important both systematically and in terms of life history.[31,32] The number of ovarioles affects fertility because each ovary produces its own egg.[33-35] Ovariole numbers play a crucial role in reproductive fitness.[36] Taxonomists find them valuable because of the fluctuation in the ovariole counts of insects over evolutionary time, ranging from increases to decreases and stabilisation. Extreme ovariole numbers often mirror extreme egg production levels, providing insights into evolutionary adaptations.[37] When the number of ovarioles of the studied leaf beetles is analysed, it was observed that the number varied from species to species. For example, the number of ovarioles in *G. fornicata* (Chrysomelinae) consists of 14 telotrophic ovarioles. However, each ovary of *C. herbacea* (Chrysomelinae) contains 18 telotrophic ovarioles.[28] In *Stolas conspersa* (Cassidinae), each ovary contains 28 ovarioles.[17] However, in *Longitarsus nigripennis* (Galerucinae), each ovary comprises 5–7 telotrophic ovarioles.[24] Each ovary of *Callosobruchus maculatus* (Fabricius 1775), (Bruchinae) comprising 6 ovarioles.[26] The ovariole of *G. fornicata* (Chrysomelinae) consists of four parts: terminal filaments, germarium, vitellarium, and pedicel. These structures were similarly reported in *Aspidimorpha sanctaecrucis* (Fabricius, 1792) (Cassidinae), *C. populi* (Chrysomelinae), *C. herbacea* (Chrysomelinae), and *P. brassicae* (Chrysomelinae).[22,27-29]

In *G. fornicata* (Chrysomelinae), spines were observed in groups on the intima of the lateral and common oviducts. In *Chrysomela scripta* (Chrysomelinae), the lateral oviduct intima has spines.[38] In *C. populi* (Chrysomelinae), spines were observed on the intima of the common oviduct.[27]

The pedicel of *G. fornicata* exhibits a singular-layered structure with inward folds directed towards the lumen. Conversely, in *A. sanctaecrucis* (Cassidinae), the ovarian duct is enveloped by a straight forward columnar epithelium.[22]

The surface patterns and shapes of insect eggs are essential. Egg characteristics generally support higher taxonomic groups.[38-40] Additionally, egg size, colour and surface structure vary among genus and are systematically important. *G. fornicata* eggs are yellowish and cylindrical. The eggs of *Sennius bondari* (Pic,1929) (Bruchinae) and *Sennius nappi* Ribeiro-Costa & Reynaud 1998 (Bruchinae) are oval.[39] Similarly, *C. populi* (Chrysomelinae) eggs are light yellow and long.[27] *G. fornicata* (Chrysomelinae) eggs are polygonal, similar to *C. herbacea* (Chrysomelinae) eggs.[28] These structures

were similarly reported in Callosobruchus spp. (Bruchinae) and *Zabrotes subfasciatus* (Boheman, 1833), (Bruchinae) are smooth.[40] Egg size varies in different genera of the Chrysomelidae. *G. fornicata* (Chrysomelinae) egg size is 1.35 mm in length and 0.5 mm in width. *C. populi* (Chrysomelinae) is approximately 1.6 mm in length and 0.6 mm width.[27] *C. herbacea* (Chrysomelinae) eggs are 1.60 mm long and 0.75 mm in width.[28] The eggs of *S. nappi* (Bruchinae) were avoid, 0.74 mm in length and 0.39 mm wide, and were covered by an ornamented membranous composed of small triangles.[39]

CONCLUSION

The morphological structures of the female reproductive organ and egg structure of insects are relatively complex and vary from species to species. Examining these structures is crucial for the fight against these pests. Therefore, in this study, we focused on describing the female reproductive organ and egg structure of *G. fornicata* and presented its similarities and differences with other species. This study intends to contribute to female reproductive biology studies in Coleoptera and other insect order species, which may be useful for future taxonomy studies of insect histoanatomy.

ORCID IDs of the authors

Nurcan Ozyurt Kocakoglu	0000-0001-7137-8631
Hicret Arslan	0000-0002-8206-8855
Selami Candan	0000-0002-7402-1360

REFERENCES

1. Kısmalı S. İzmir ili ve çevresinde kültür bitkilerinde zarar yapan Chrysomelinae ve Halticinae (Coleoptera, Chrysomelidae) alt familyalarına ait türler, tanınmaları, konukçuları, yayılışları ve kısa biyolojileri üzerinde araştırmalar. *Ege Üniv. Ziraat Fak. Derg*. 1973;10(2):341-378.

2. Lopatin IK. *Leaf Beetles (Chrysomelidae) of Middle Asia and Kazakhstan. Nauka, Leningrad:* Zoological Institute, Academies of Sciences of the USSR, 1977.

3. Gruev B. Geographical distribution of Lamprosomatinae, Eumolpinae, Chrysomelinae, Alticinae, Hispinae ve Cassidinae (Coleoptera, Chrysomelidae) on the Balkan Peninsula. Plovdiv University Press. 512p. Plovdiv, 1992.

4. Konstantinov AS, Korotyaev BA, Volkovitsh MG. Insect biodiversity in the palaearctic region. In: Foottit RG, Adler PH. Insect biodiversity: Science & society. Chapter 7. Oxford: Wiley-Blackwell; p. 107–162, 2009.

5. Aslan EG, Ayvaz Y. Diversity of Alticinae (Coleoptera, Chrysomelidae) in the Kasnak Oak Forest Nature Reserve, Isparta, Turkey. *Turk J Zool*. 2009;33(3):251–262.

6. Aslan EG, Japoshvili G, Aslan B, Karaca İ. Flea beetles (Coleoptera: Chrysomelidae: Alticinae) were collected using the Malaise trap method in Gölcük Natural Park (Isparta, Turkey), a new record for Turkish fauna. *Arch Biol Sci*. 2012; 64;1:365–370.

7. Ghahari H. Jędryczkowski WB. A Contribution to the knowledge of leaf beetles (Coleoptera: Chrysomelidae) from Arasbaran Biosphere Reserve & its Neighboring Areas (Northwestern Iran). *Acta Zool Bulg*. 2012;64(4); 347-352.

8. Ekiz AN, Şen İ, Aslan EG, Gök A. Checklist of leaf beetles (Coleoptera: Chrysomelidae) of Turkey, Excluding Bruchinae. *J Nat Hist*. 2013;47(33-34):2213-2287. doi:10.1080/00222933.2012.763069.

9. Konstantinov A, Chamorro, M.L. Prathapan K, Ge SQ, Yang XK. Moss-inhabiting flea beetles (Coleoptera: Chrysomelidae: Galerucinae: Alticini) with description of a new genus from Cangshan, China. *J Nat Hist*. 2013;47(37-38):2459–2477. doi:10.1080/00222933.2012.763068.

10. Bezděk J, Sekerka L. *Catalogue of Palaearctic Coleoptera*. Volume 6/2. Revised and Updated Second Edition. Chrysomeloidea II (Megalopodidae, Orsodacnidae, Chrysomelidae). –Leiden: Brill, 2024.

11. Flinte V, Abejanella A, Daccordi M, RF, Macedo, MV. Chrysomelinae species (Coleoptera, Chrysomelidae) and new biological data from Rio de Janeiro, Brazil. *ZooKeys*. 2017;(720): 5. doi:10.3897/zookeys.720.13963

12. Syrett P, Fowler SV, Emberson RM. Are chrysomelid beetles effective agents for the biological control of weeds. In Proceedings of the IX International Symposium on the biological control of weeds (pp. 399-407). University of Cape Town, Stellenbosch, South Africa, 1996.

13. Barış A, Yücel C, Gök N. Distribution, density, and population monitoring of *Gonioctena fornicata* (Brüggemann, 1873) (Coleoptera: Chrysomelidae) in lucerne fields of Bolu, Zonguldak and Bartın provinces. *Plant Prot Bull*. 2021;61(1):15–20.

14. Alkan B. *Tarım Entomolojisi*. T.C. Tarım Bakanlığı Ankara Yüksek Ziraat Enstitüsü Ders Kitabı 31. Ankara Yüksek Ziraat Enstitüsü Basımevi, Ankara, 1946;232.

15. Bodenheimer FS. *Türkiye'de ziraate ve ağaçlara zararlı olan böcekler ve bunlarla savaş hakkında bir etüd*. Bayur Matbaası, Ankara, 1958;346.

16. Metcalfe ME. The structure and development of the reproductive system in the Coleoptera with notes on its homologies. *Quart J Micr Sci*. 1932;2:49–129.

17. Simões MVP. Male and female reproductive systems of *Stolas conspersa* (Germar) (Coleoptera, Chrysomelidae, Cassidinae). *Rev Bras Entomol*. 2012;56(1):19–22.

18. Salazar K, Boucher S, Serrao JE. Structure and ultrastructure of the ovary in the South American *Veturius sinuatus* (Eschscholtz) (Coleoptera, Passalidae). *Arthropod Struct Dev*. 2017;46(4):613–626.

19. Metcalfe ME. The structure and development of the reproductive

system in the Coleoptera with notes on its homologies. *Quart J Micr Sci*. 1932;2:49–129.

20. Wan Nurul 'Ain WMN, Nurul Wahida O, Yaakop S, Norefrina Shafinaz MN. Morphology and histology of reproductive organ and first screening of Wolbachia in the ovary of red palm weevil, *Rhynchophorus ferrugineus* (Coleoptera: Dryophthoridae). *Serangga*. 2018;23(2):183–193.

21. Trauner J, Büning J. Germ-cell cluster formation in the telotrophic meroistic ovary of *Tribolium castaneum* (Coleoptera,Polyphaga, Tenebrionidae) and its implication on insect phylogeny. *Dev Genes Evol*. 2007;217(1):13–27.

22. Boonyoung P, Senarat S, Kettratad J, et al. Mature gonadal histology and gametogenesis of the tortoise beetle *Aspidimorpha sanctaecrucis* (Fabricius, 1792) (Coleoptera: Cassidinae: Chrysomelidae): Histological observation. Songklanakarin. *J Sci Technol*. 2020;42(4):873-878.

23. Gerber GH, Neill GB, Westdal PH. The anatomy and histology of the internal reproductive organs of the sunflower beetle, *Zygogramma exclamationis* (Coleoptera: Chrysomelidae). *Can J Zool*. 1978;56(12):2542–2553.

24. Devasahayam S, Vidyasagar PSPV, Koya KM. A Reproductive system of pollu beetle, *Longitarsus nigripennis Motschulsky* (Coleoptera: Chrysomelidae), a major pest of black pepper, *Piper nigrum* Linnaeus. *J Entomol Res*. 1998;22(1):77–82.

25. Kumar R, Attah PK. Structure of the organs of digestion and reproduction in the Tortoise Beetle, *Aspidomorpha* spp. (Chrysomelidae: Coleoptera). *J Nat Hist*. 1977;11(1):65–76.

26. Mohamed MI, Khaled AS, Fattah HMA, Hussein MA, Salem DAM, Fawki S. Ultrastructure and histopathological alteration in the ovaries of *Callosobruchus maculatus* (F.) (Coleoptera, Chrysomelidae) induced by the solar radiation. *J Basic Appl Zool*. 2015;68:19–32.

27. Özyurt Koçakoğlu N, Candan S, Güllü M. Morphology of the reproductive tract of females of leaf beetle *Chrysomela populi* (Chrysomelidae: Coleoptera). *Biol*. 2021;76(11):3257-3265.

28. Özyurt Koçakoğlu N, Candan S, Güllü M. Structural and ultrastructural characters of the reproductive tract in females of the mint leaf beetle *Chrysolina herbacea* (Duftschmid 1825) (Coleoptera: Chrysomelidae). *Acta Zool*. 2022;103(3):365-375.

29. Wang XP, Zhou XM, Wang YY, Lei CL. Internal reproductive system and diapausing morphology of the Brassica leaf beetle *Phaedon brassicae* Baly (Coleoptera: Chrysomelidae: Chrysomelinae). *Coleopts Bull*. 2007;61(3):457–462.

30. Büning J. The insect ovary: Ultrastructure, previtellogenic growth, and evolution. Springer Netherlands. 1994.

31. Büning J. Ovariole structure supports sistergroup relationship of Neuropterida and Coleoptera. *Arthropod Syst Phylogeny*. 2006;64(2):115–126. doi:10.3897/asp.64.e31647.

32. Štys P, Biliński S. Ovariole types and the phylogeny of hexapods. *Biol Rev*.1990;65: 401–429.

33. Cohet Y, David JR. Control of the adult reproductive potential by preimaginal thermal conditions. *Oecologia*. 1978; 36(3):295–306.

34. David JR. Le nombre d'ovariles chez la Drosophila: Relation avec la fecondite et valeur adaptive. *Arch Zool Exp Gén*. 1970;111: 357–370.

35. R'kha S, Moreteau B, Coyne JA, David JR. Evolution of a lesser fitness trait: Egg production in the specialist *Drosophila sechellia*. *Genet Res*. 1997;69(1):17–23.

36. Orr HA. Fitness and its role in evolutionary genetics. *Nat Rev Genet*. 2009;10(8):531–539.

37. Robertson JG. Ovariole numbers in Coleoptera. *Can J Zool*. 1961;39(3):245–263.

38. Cheetham T. Anatomy and histology of tissues associated with egg deposition in *Chrysomela scripta* Fabr. (Coleoptera: Chrysomelidae). *J Kans Entomol* Soc. 1992;65(2):101–114.

39. Caron E, Ribeiro-Costa CS, Linzmeier AM. The egg morphology of some species of *Sennius* bridwell (Coleoptera: Chrysomelidae: Bruchinae) based on scanning electron micrographs. *Zootaxa*. 2004;556(1):1–10.doi:10.11646/zootaxa.556.1.1

40. Wightman JA, Southgate BJ. Egg morphology, host, and probable regions of origin of the bruchids (Coleoptera: Bruchidae) that infest stored pulses-an identification aid. *J Exp Agric*. 1982;10(1):95–99.

How to cite this article

Evaluation of Protective effects of Fermented *Ficus racemosa* Fruit Extract against Oxidative Stress and Hyperglycemia

Ngoc Thanh Vu[1] , Duyen Thi My Chung[2]

[1]International University-VNU HCM, School of Biotechnology, Department of Applied Chemistry, Ho Chi Minh City-Vietnam
[2]Ho Chi Minh City University of Medicine and Pharmacy, Department of Traditional Medicine, Ho Chi Minh City-Vietnam

ABSTRACT

Objective: Uncontrolled oxidative stress and diabetes are linked to multiple serious health issues. This study aimed to demonstrate the potency of *Aspergillus niger* solid-state fermentation (SSF) to enhance the preventive and therapeutic capacity of *Ficus racemosa* fruit extract (FRFE) against oxidative stress and hyperglycaemia.

Materials and Methods: SSF and post-SSF ultrasound-assisted extraction was utilised to prepare fermented FRFE (F-FRFE). F-FRFE was compared with unfermented FRFE (U-FRFE) in terms of the antioxidant activity and the protective effect against oxidative stress and hyperglycaemia. The antioxidant activity was evaluated by 2,2-diphenyl-1-picrylhydrazyl/2,2-azino-bis(3-ethylbenzothiazoline-6-sulfonic acid) radical scavenging, ferric reducing antioxidant potential, and thiobarbituric acid reactive substance assays. The protective effect against oxidative stress was evaluated in human hepatocytes treated with the oxidative stress inducer, H_2O_2. The antioxidative stress and antihyperglycemic impact was further investigated in a streptozotocin-induced diabetic mouse model.

Results: Compared with U-FRFE, F-FRFE possessed higher *in vitro* and *ex vivo* antioxidant potential. In human hepatocytes, H_2O_2 treatment induced apoptotic cell death, which was alleviated by F-FRFE at a higher extent compared with U-FRFE. In the diabetic mouse, F-FRFE but not U-FRFE treatment completely subsidised hyperglycaemia and elevated oxidative stress.

Conclusion: Our findings demonstrated the protective effectiveness of F-FRFE against oxidative stress and hyperglycaemia with prospects in pharmaceutical applications.

Keywords: *Ficus racemosa*, Antioxidant, Hyperglycaemia, Diabetes, Oxidative stress, Solid-state fermentation

INTRODUCTION

Oxidative stress occurs when intrinsic antioxidant defences are overburdened by the production of reactive oxygen species (ROS) or due to the imbalance between ROS and the antioxidant level. ROS are produced by biological organisms to regulate various cellular processes such as stress response, cell death or survival, and inflammation.[1] Excessive accumulation of ROS or increased oxidative stress has been implicated in the development of multiple health issues such as ageing, obesity, diabetes, cardiovascular disease, osteoporosis, chronic kidney disease, chronic obstructive pulmonary disease, neurodegenerative diseases, and cancer.[1] Several reports have suggested that natural compounds, especially polyphenols extracted from plant sources, can remarkably reduce oxidative stress and attenuate oxidative stress-related health disorders such as diabetes and cancer.[2] Diabetes mellitus is a metabolic disorder with persistent hyperglycaemia, caused by the failure of insulin production (type 1) or insulin resistance (type 2). Diabetes is recorded as one of the most prevalent diseases worldwide with a high rate of premature morbidity and mortality.[3] Diabetic onset is linked to increased production of ROS, resulting in oxidative stress, which further escalates the progression of diabetes mellitus and leads to the development of other severe disorders.[4] Therefore, uncontrolled or untreated diabetic patients would develop serious complications, many of which would be caused by elevated oxidative stress. The current main treatment strategy for diabetes is the use of antihyperglycemic or hypoglycaemic drugs, such as metformin, thiazolidinediones, sulfonylureas, dopamine-2 agonists, glucagon-like peptide-1 agonists, dipeptidyl peptidase-4 inhibitors, and sodium-glucose cotransporter-2 inhibitors, either alone or in combination.[2] Nevertheless, chronic treatment with these chemical agents could lead to various undesirable side effects such as abdominal pain,

nausea, and body weight gain.[5] Therefore, tremendous efforts have been made to identify alternative natural compounds in the management of hyperglycaemia and diabetes. Among these compounds, polyphenols extracted from plant sources, especially medicinal plants, are excellent candidates due to their low toxicity and high antioxidant and hypoglycaemic potential.[2]

Ficus racemosa is cultivated in various countries, including Southeast Asia, China, Malaysia, India, Sri Lanka, Pakistan, New South Wales and Australia.[6] Different parts of *F. racemosa* tree have been used as a traditional medicine in many countries and reported to possess multiple biological activities such as antioxidant, antimicrobial, anti-diabetic, anti-cancer, hepatoprotective and anti-inflammatory capability.[6] The bioactive content and biological activities of various plant extracts have been shown to be augmented via solid-state fermentation (SSF).[7-11] Therefore, this study investigated the ability of SSF to enhance the bioactive values of *F. racemosa* fruit extract (FRFE) in terms of total phenolic content (TPC), total flavonoid content (TFC), the *in vitro* and *ex vivo* antioxidant activity, the protective capacity against oxidative stress injury in hepatocytes and the antioxidative stress and anti-hyperglycaemic potential in a diabetic mouse model.

MATERIALS AND METHODS

Sample Preparation for SSF

Ficus racemosa fruit was collected from the Tien Giang province in Vietnam. The sample was available at the herbarium of the International University–VNU HCM, Vietnam. *F. racemosa* fruit was cleaned, air dried and ground into a fine powder, which was the dried material (DM) for SSF.

SSF and Post-SSF Extraction

The *Aspergillus niger* strain was obtained from the microbial library of Nguyen Tat Thanh University, Vietnam, and was identified as *A. niger* by 18s rRNA gene sequencing. SSF and post-SSF ultrasound-assisted extraction was performed as described with modifications.[7] Briefly, DM was mixed with water in an Erlenmeyer flask covered with cotton plugs to obtain a moisture content of 70%. The samples were then sterilised at 121°C for 15 min, cooled, and inoculated with a fungal spore suspension (10^7 spores/g DM). The inoculated flasks were incubated at 30°C for 5 days. Next, 95% ethanol was added at 10:1 mL/g DM, followed by ultrasonication (40 kHz and 400 W) for 20 min at 30°C. The mixture was shaken for 5 min at room temperature and then centrifuged at 8,000 rpm for 20 min. The supernatant was filtered through a 0.2 µm membrane filter and concentrated by a vacuum evaporator at 40°C for 8 h. Unfermented *F. racemosa* fruit extract (U-FRFE) was prepared in the same manner as the fermented *F. rasemosa* fruit extract (F-FRFE), except for the absence of fungi. U-FRFE or F-FRFE was dissolved in deionised water to obtain the desired concentrations for the *in vitro, ex vivo, in vivo* and cell culture experiments.

Determination of the Total Phenolic Content

The TPC of the samples was measured by the Folin–Ciocalteu method as described in a previous study.[7] Briefly, 12 µL of the samples were mixed with 100 µL of diluted Folin&Ciocalteu's phenol reagent and incubated for 5 min at room temperature, followed by the addition of 100 µL of Na_2CO_3 (60 g/L). Next, the mixture was incubated for 1 h at room temperature and the absorbance was measured at 725 nm. TPC was expressed as mg of gallic acid equivalent per 1 g of DM (mg GAE/g DM), determined from the gallic acid calibration curve. All chemicals were purchased from Sigma (USA).

Determination of the Total Flavonoid Content

The TFC was determined as described in a previous study.[7] Briefly, 50 µL of the samples were mixed with 75 µL sodium nitrite (5%) and 75 µL aluminium trichloride (10%), and the mixture was incubated for 5 min before the addition of 100 µL sodium hydroxide (1%). After incubation for 1 h, the absorbance was measured at 510 nm. The total flavonoid content was expressed as milligrams of quercetin equivalent per 1 g of DM (mg QE/g DM) based on the calibration curve for quercetin. All chemicals were purchased from Sigma (USA).

Phytochemical Screening by Colour Tests

Colour tests for the presence of different phytochemical groups were performed according to previously described procedures.[7] The groups tested were as follows: alkaloid (Dragendorff test), flavonoid (Bate-Smith and Metcalf test), glycoside (Kedde reaction), phenol, saponin (foam test), terpenoid (Salowski test), triterpenoid and steroid (Liebermann-Burchard test).

2,2'-Azino-bis (3-ethylbenzothiazoline-6-sulfonic acid (ABTS) Radical Scavenging Assay

The ABTS radical scavenging capacity was determined as previously described.[7] Briefly, the ABTS radical solution was prepared by mixing the ABTS solution (7 mM) with the potassium persulfate solution (2.45 mM). The mixture was kept in the dark at room temperature for 16 h before being diluted to obtain a working ABTS radical solution with an absorbance at 734 nm of 0.7. Then, 200 µL of the samples were added to 600 µL of ABTS radical working solution and the mixture was incubated for 30 min at room temperature in the dark. The absorbance at 734 nm was then measured. The percentage of scavenging activity (% SA) was calculated from the absorbance of the control (A_c) and ascorbic acid/extract sample (A_s) as follows: % SA = (A_c - A_s) x 100/ A_c.

The half-maximal inhibitory concentration (IC_{50}) value was

then determined based on the linear curve showing the % SA at different sample concentrations, which was the concentration at which % SA = 50. A higher IC_{50} value indicated a lower radical scavenging ability. All chemicals were purchased from Sigma (USA).

2,2-Diphenyl-1-picrylhydrazyl (DPPH) Radical Scavenging Assay

The DPPH radical scavenging capacity of FRFE was determined as previously described.[7] Briefly, 20 µL of the samples were mixed with 180 µL of DPPH (6×10^{-5} M, Sigma, USA). The mixture was incubated for an hour at room temperature in the dark, and the absorbance was measured at 517 nm. DPPH solution was used as a control. The % SA and IC_{50} were calculated as in the ABTS radical scavenging assay.

Ferric Reducing Antioxidant Potential (FRAP) Assay

The FRAP assay was performed as previously described.[7] Briefly, the FRAP working reagent was prepared by mixing 10 volumes of 300 mM acetate buffer (pH 3.6) with 1 volume of 2,4,6-tri(2-pyridyl)-s-triazine (10 mM) prepared in 40 mM hydrochloric acid and 1 volume of 20 mM ferric chloride. Then, 200 µL of the samples were added to 10 µL of the FRAP working solution and the mixture was incubated at 37°C for 30 min. The absorbance was then measured at 593 nm. The reducing power was calculated from the ferrous sulphate standard curve. FRAP values were expressed as millimoles of ferrous sulphate equivalent per 1 g of sample (mmol FSE/g). All chemicals were purchased from Sigma (USA).

Ex Vivo Lipid Peroxidation or Thiobarbituric Acid Reactive Substance (TBARS) Assay using Mouse Brain Homogenates

The assay was performed as previously described.[12] Trolox (Sigma, USA) was used as an antioxidant control. The *ex vivo* assay was based on the determination of the relative amount of malondialdehyde (MDA). The MDA level was determined based on the reaction with TBA, resulting in products with maximum absorbance at 532 nm. Briefly, mouse brains were homogenised in phosphate buffer (pH 7.4) at a 1:10 ratio at 4°C. Brain homogenates were incubated with the extract samples and $FeSO_4/H_2O_2$ mixture ($FeSO_4$ 0.1 mM:H_2O_2 15 mM at 1:1 ratio) at 37°C for 15 min. Trichloracetic acid 10% was added to the mixture, which was then centrifuged at 12,000 rpm for 5 min. The supernatant was collected and incubated with 0.8% TBA in a 2:1 ratio at 100°C for 15 min. The absorbance was measured at 532 nm and the IC_{50} was determined. All chemicals were purchased from Sigma (USA).

Cell Culture

HepG2 cells (ATCC, USA) were cultured in Dulbecco's modified Eagle's medium (DMEM, Sigma, USA) supplemented with 10% heat-inactivated foetal bovine serum (FBS, Sigma, USA), 100 U/mL penicillin (Sigma, USA), and 100 µM streptomycin (Sigma, USA). The cells were maintained in a 5% CO_2/95% air incubator at 37°C. All experiments were performed at less than 10 passages. Cells were tested for mycoplasma every 2 months (Universal Mycoplasma Detection Kit, ATCC, USA).

WST1 Cell Survival Assay

Cell viability was determined using the cell proliferation reagent WST-1 (Sigma, USA) in a 96-well plate format according to the manufacturer's instructions.

Western Immunoblotting

Protein extract preparation and subsequent sodium dodecyl-polyacrylamide gel electrophoresis (SDS-PAGE)/Western immunoblotting were performed as previously described.[13-16] Briefly, the cells were lysed in cell lytic M buffer and the protein concentration was determined by Bradford. The total protein lysate was then subjected to sodium dodecyl-polyacrylamide gel electrophoresis (SDS-PAGE) followed by Western immunoblotting for cleaved caspase-9 and β-actin as a loading control. Horseradish peroxidase-conjugated anti-rabbit or anti-mouse IgG antibodies were used as secondary antibodies. All antibodies were purchased from Cell Signalling Technology (USA).

Animal Studies and Sample Collection

Male Swiss albino mice were obtained from the Nha Trang Institute of Vaccines and Biological Products in Vietnam after six weeks of age. The mice were acclimated to standard environmental conditions for a week and fed standard rodent chow and water ad libitum. All mouse studies were conducted under the supervision and approval of the Animal Research Committee of the International University, Vietnam National University of Ho Chi Minh City (No. BT03/2023, http://crl.bio.hcmiu.edu.vn/about-us/facilities/) and according to ARRIVE (Animal Research: Reporting of *In Vivo* Experiments) guidelines and in accordance with the National Research Council's Guide for the Care and Use of Laboratory Animals.

Examination of the Acute Toxicity

To determine acute toxicity, mice (five male mice per group) were given a single oral dose of the vehicle control, U-FRFE or F-FRFE at various doses (0.2, 1 and 5 g/kg). Mortality and general behaviour were reported daily for 14 days.

Examination of the Antioxidative Stress and Antihyperglycemic Effect

Mice were IP injected with a single dose of the vehicle control or streptozotocin (STZ, 70 mg/kg BW, Sigma, USA). After 7

days of vehicle or STZ treatment, mice with blood glucose levels above 200 mg/dL were treated daily with vehicle control, U-FRFE or F-FRFE at 0.2 g/kg body weight (BW), or glibenclamide (5 mg/kg BW). The experiments were performed in two independent times and there were four mice per group in each replicate for a total of eight mice per group.

Quantification of Serum Glucose

Serum glucose levels were determined using the GOD-PAP Kit (Human Diagnostic Ltd. Co., Uganda) following the manufacturer's instructions.

Quantification of MDA in Livers in Livers and Kidneys

MDA levels in the livers and kidneys were determined as previously described.[2] Briefly, the livers and kidneys were homogenised in KCl 1.15% for 1 min at 13,000 rpm. The homogenates were then incubated with Tris-HCl (pH 7.4) at 37°C for 1 h, and TCA 10% was added to stop the reaction. The supernatant obtained by centrifugation reacted with TBA 0.8% at 100°C for 15 min and the absorbance was measured at 532 nm. The concentration of MDA was determined from the MDA standard, normalised to total liver or kidney protein (determined by Bradford) and expressed as nmol per 1 g of protein. All chemicals were purchased from Sigma (USA).

Quantification of Reduced Glutathione in Livers and Kidneys

The reduced glutathione (GSH) level in the livers and kidneys was determined as previously described.[2] Briefly, the livers and kidneys were homogenised in KCl 1.15% for 1 min at 13,000 rpm. The homogenates were then incubated with Tris-HCl (pH 7.4) at 37°C for 1 h, and TCA 10% was added to stop the reaction. The supernatant obtained from the centrifugation reacted with the Elman reagent in phosphate-EDTA buffer for 3 min at room temperature, and the absorbance was measured at 412 nm. The GSH concentration was determined from the GSH standard, normalised to total liver or kidney protein (determined by Bradford) and expressed as nmol per 1 g of protein. All chemicals were purchased from Sigma (USA).

Statistical Analysis

Student's t-test was used for significant comparisons between the two groups. ANOVA followed by the post hoc Tukey's honestly significant difference (HSD) test was used for comparisons between three or more groups. All statistical analyses were performed using the R program. A p-value of less than 0.05 was considered a significant difference.

RESULTS

Improvement of the Bioactive Phytochemical Content and Antioxidant Activity after SSF

As shown in Table 1, TPC and TFC were significantly increased after the fermentation duration of 5 days. Besides polyphenols, the levels of other bioactive phytochemicals such as terpenoids and sterols could be increased post-SSF, as indicated by the enhanced signals in the phytochemical screening (Table 2). The increased bioactive content in FRFE after SSF was congruent with the increase in *in vitro* and *ex vivo* antioxidant activity (Table 1).

FRFE with Enhanced Protective Capacity against Oxidative Stress Injury in Hepatocytes

H_2O_2 was utilised to induce oxidative stress in hepatocytes. H_2O_2 treatment resulted in decreased cell survival and increased cellular levels of the apoptotic marker, cleaved caspase-9, which was completely blocked by pretreatment with F-FRFE. In contrast, pretreatment with U-FRFE (Figure 1) partially alleviated oxidative stress-mediated apoptotic cell death.

Acute Toxicity Examination

In the acute toxicity study, no mortality, signs of toxicity, or significant behavioural changes, including grooming, hyperactivity, loss of righting reflex, sedation, and convulsions, were observed after oral administration of either U-FRFE or F-FRFE for up to 14 days, even at the highest dose of 5 g/kg BW (Table 3).

FRFE with Enhanced Protective Capability against Oxidative Stress and Hyperglycaemia in Streptozotocin-Induced Mouse Model

In mice treated with a single dose of streptozotocin, an increase in blood glucose levels (Figure 2) and oxidative stress, as indicated by increased MDA levels and decreased GSH levels in the kidneys and livers (Figure 3), were observed. GSH is considered to be one of the most important antioxidants protecting cells from ROS and oxidative stress damage. A decrease in the GSH level is therefore an indicator of increased oxidative stress. Another well-studied marker of oxidative stress is MDA, which is one of the end products of lipid peroxidation. All of these disturbances were reversed by treatment with either F-FRFE or glibenclamide, a hypoglycaemic agent commonly used for treating type 2 diabetes. However, the mitigating effect of U-FRFE on oxidative stress and hyperglycaemia was to a lesser extent compared with that of F-FRFE, suggesting SSF-mediated enhancement of the protective efficacy of FRFE against oxidative stress and hyperglycaemia.

Table 1. Total phenolic content, total flavonoid content and the antioxidant activity of unfermented and fermented *Ficus racemosa* fruit extract.

	TPC (mg GAE/g DM)	TFC (mg QE/g DM)	ABTS IC_{50} (µg/mL)	DPPH IC_{50} (µg/mL)	FRAP (mmol FSE/g)	*Ex vivo* IC_{50} (µg/mL)
U	16.30 ± 0.56	1.06 ± 0.08	126.80 ± 5.87	159.17 ± 8.94	0.28 ± 0.03	54.14 ± 4.39
F	34.13 ± 1.33*	2.33 ± 0.13*	55.18 ± 2.55*	76.53 ± 5.08*	0.75 ± 0.04*	21.45 ± 2.14*
AA	-	-	1.76 ± 0.17	2.27 ± 0.15	19.70 ± 0.79	-
Trolox	-	-	-	-	-	23.92± 1.38

TPC, total phenolic content; GAE, gallic acid equivalent; DM, dry material; TFC, total flavonoid content; QE, quercetin equivalent; ABTS, 2,2'-azino-bis(3-ethylbenzothiazoline-6-sulfonic acid); DPPH, 2,2-diphenyl-1-picrylhydrazyl; FRAP, ferric reducing antioxidant potential; FSE, ferrous sulphate equivalent; IC_{50}, half-maximal inhibitory concentration; U, unfermented *Ficus racemosa* fruit extract; F, fermented *Ficus racemosa* fruit extract (F); AA, ascorbic acid; data were means = standard deviation from 3 independent replicates; * p<0.05, compared to U.

Table 2. The presence of phytochemical groups in unfermented and fermented *Ficus racemosa* fruit extract.

Group	U	F
Alkaloid	+	-
Flavonoid	+	++
Glycoside	+	++
Phenol	+	++
Saponin	-	-
Tannin	+	++
Terpenoid	+	++
Triterpenoid and steroid	+	++

U, unfermented *F. racemosa* fruit extract; F, fermented *F. racemosa* fruit extract; (-), undetected; (+) and (++), detected; group marked with (++) had higher signal intensity in colour tests than group marked with (+).
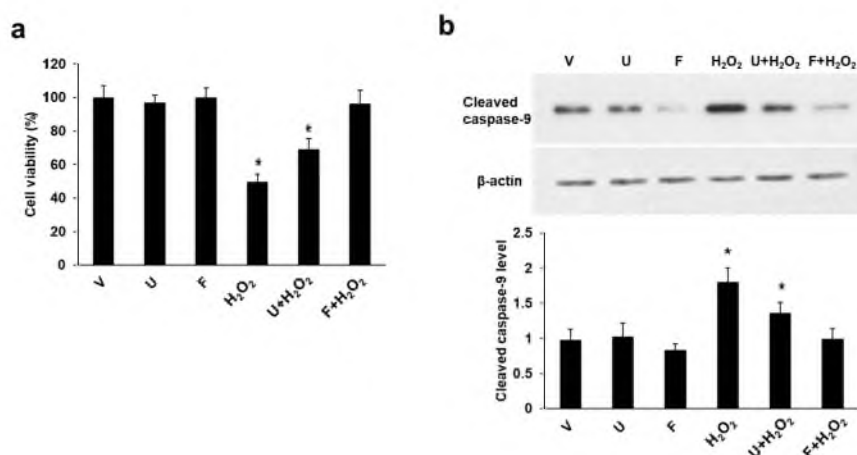
Figure 1. Protective efficacy against oxidative stress injury in hepatocytes. HepG2 cells were treated with vehicle (V), unfermented *Ficus racemosa* fruit extract (U), or fermented *Ficus racemosa* fruit extract (F) (0.2 mg/mL) for 30 min before being treated with vehicle or H_2O_2 (200 µM) for 6 h. Then, the cells were subjected to the WST1 cell viability assay (a) or Western immunoblotting for cleaved caspase-9 or β-actin (b). Data in graphs were means ± standard deviation. In (a), the cell viability for the vehicle group (V) was normalised to 100%; n = 5 from two independent occasions. In (b), the cleaved caspase-9 density was normalised to β-actin density and caspase-9/β-actin density ratio was then normalised to 1; n = 3 from two independent occasions. * p<0.05, compared to all other groups.

Table 3. Observation of the mortality and signs of toxicity after 14 days of administration of unfermented and fermented *Ficus racemosa* fruit extract.

	Dose (mg/kg BW)	Mortality	Grooming	Hyperactivity	Loss of the righting reflex	Sedation	Convulsion
	0.2	N	N	N	N	N	N
U	1	N	N	N	N	N	N
	5	N	N	N	N	N	N
	0.2	N	N	N	N	N	N
F	1	N	N	N	N	N	N
	5	N	N	N	N	N	N

BW, body weight; U, unfermented *Ficus racemose* fruit extract; F, fermented *Ficus racemose* fruit extract; N, no mortality or no abnormal sign for all five mice in a group.
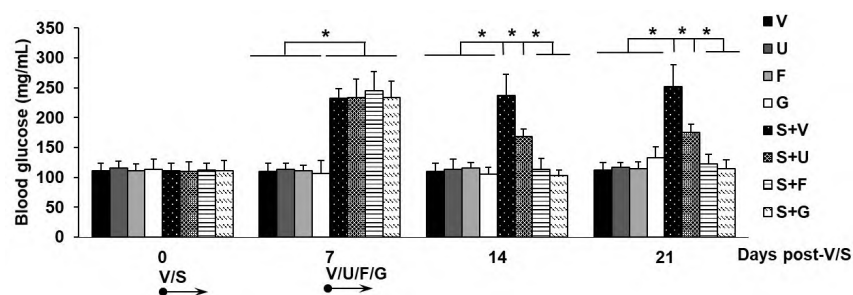
Figure 2. Protective effect against hyperglycaemia in streptozotocin-induced diabetic mouse model. After 7 days of vehicle (V) or streptozotocin (S) treatment, the mice were treated with vehicle (V), unfermented *Ficus racemosa* fruit extract (U), fermented *Ficus racemosa* fruit extract (F), or glibenclamide (G). Serum samples were collected on days 0, 7, 14, and/or 21 after V/S treatment for the determination of glucose levels. Data were means ± standard deviation; n = 8; * $p<0.05$, compared to all other groups.
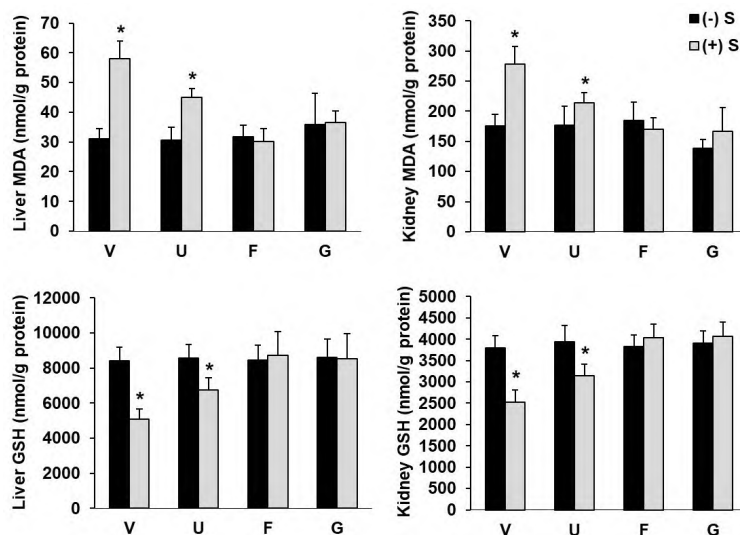
Figure 3. The protective effect against oxidative stress in a streptozotocin-induced diabetic mouse model. After 7 days of vehicle (V) or streptozotocin (S) treatment, the mice were treated with vehicle (V), unfermented *Ficus racemosa* fruit extract (U), fermented *Ficus racemosa* fruit extract (F), or glibenclamide (G). Livers and kidneys were collected on day 21 post-V/S treatment for the determination of malondialdehyde (MDA) or reduced glutathione (GSH) levels. Data were means ± standard deviation; n = 8; * $p<0.05$, compared to all other groups.

DISCUSSION

This study implicated *A. niger* SSF as an effective and environmentally friendly approach to prospectively augment the release of various bioactive compounds in FRFE. The mechanistic action of SSF for increasing the bioactive content of the plant extract has not been thoroughly investigated. It is likely that enzymatic conversion and/or cleavage of the material matrix contributes to the enhanced release of bioactive compounds in the plant extract,[7] which requires further investigation to substantiate the suggested mechanisms and determine the specific change in the phytochemical profile after SSF.

The results of the phytochemical composition and *in vitro* antioxidant activity of U-FRFE were congruent with those of a previous study[17] using FRFE prepared in the same manner. Specifically, the TPC, TFC, and DPPH IC$_{50}$ values determined in the present study, as well as the presence of alkaloids, flavonoids, tannins, and steroids, were consistent with the previous study. However, the DPPH radical scavenging activity of U-FRFE was lower than that of FRFE in another study,[18] probably due to differences in the extraction method and in the material source.

Different types of polyphenols may be associated with the antioxidant and antidiabetic potentials of the plant extract.[18] Regarding the polyphenolic profile, a previous study reported that FRFE contains significant amounts of caffeic acid, catechin, (-)-epicatechin, gallic acid, p-coumaric acid, rutin, syringic acid, trans-ferulic acid, vanillin and vanillic acid,[19] some of which may be increased after SSF. In addition to the polyphenolic compounds, other phytochemicals in FRFE may contribute to the protective capacity against oxidative stress and hyperglycaemia. Further research is essential to clarify the relationship between the change in phytochemical composition after SSF and the enhanced effect of FRFE on antioxidative stress and anti- hyperglycaemia. Since F-FRFE was shown to have higher free radical scavenging activity and increased intrinsic GSH level, it is plausible that it prevented oxidative stress or ROS accumulation through multiple actions: limiting ROS formation, removing existing ROS by direct scavenging activity and/or enhancing intrinsic antioxidant defence to limit ROS accumulation. Further studies are needed to determine the mechanistic action of F-FRFE in suppressing oxidative stress.

The human hepatoma cell line HepG2 was used in this study as a cellular model of oxidative stress injury. HepG2 is originally derived from hepatocellular carcinoma but still retains several biological characteristics of hepatocytes. It has been used to study oxidative injury induced by H_2O_2, iron arachidonic acid, CYP2E1, alcohol, and hepatitis C virus.[20] Regarding H_2O_2, it has been widely used to induce oxidative stress injury in hepatocytes and other cell types.[21-23] In particular, H_2O_2 has been reported to induce apoptotic cell death, which is consistent with the results of this study. Importantly, the induced apoptotic cell death was completely "rescued" by F-FRFE, but not by U-FRFE pretreatment, likely due to the higher antioxidant activity of F-FRFE compared to U-FRFE. H_2O_2-induced oxidative injury in HepG2 cells was also reported to be completely rescued by cocoa phenolic extract in a previous study,[24] indicating the significant effect of the antioxidant-rich extract in ameliorating oxidative injury. Regarding the mechanism of cell death suppression, it is plausible that F-FRFE prevents cell death by inhibiting the apoptotic pathway activation. However, further investigation would be required to exclude the involvement of other cell death/survival pathways in the effect of F-FRFE on cell viability.

For hyperglycaemic mouse models, STZ and alloxan, the cytotoxic glucose analogues, are the most prominent chemical agents used to induce diabetes. Alloxan has been used in previous studies to create a hyperglycaemic mouse or rat model.[17,25] In these studies, FRFE at a dose of 0.2 g/kg BW was shown to partially alleviate the hyperglycaemia, which is consistent with the observation in this study for the effect of U-FRFE at the same dose. Compared with U-FRFE, F-FRFE completely reversed the elevated blood glucose levels induced by STZ treatment, indicating a higher protective effect against hyperglycaemia.

The onset of diabetes is associated with increased oxidative stress and increased oxidative stress has been reported to accelerate the progression of diabetes and lead to the development of other serious health disorders.[4] Findings in this study also supports speculation regarding the interactive effect of F-FRFE on oxidative stress and hyperglycaemia. It is likely that FRFE stabilises blood glucose levels by reducing oxidative stress. However, the possibility of an oxidative stress-independent hypoglycaemic effect of F-FRFE could not be ruled out without further investigation. If the effect of F-FRFE on blood glucose levels depends on its antioxidant activity, another unclear mechanism is how F-FRFE modulates blood glucose levels by controlling oxidative stress. Regardless of these unrevealed mechanisms, the preventive efficacy of F-FRFE against oxidative stress injury and hyperglycaemia is conclusive, highlighting its potential applications in nutraceutical and pharmaceutical products.

CONCLUSION

Diabetes and other oxidative stress-related health disorders can potentially be alleviated by natural compounds from plant sources. F-FRFE with enhanced TPC, TFC and antioxidant capacity was demonstrated in this study to effectively protect hepatocytes from oxidative stress and subsidise the oxidative stress and hyperglycaemia in STZ-induced mouse model. The mechanistic dual action of F-FRF was also revealed: enhancement of intrinsic antioxidant defence and direct scavenging of free radicals. Most importantly, the F-FRF extract was shown to be safe, highlighting its potential to replace or reduce the use

of current chemically synthesised drugs with undesirable side effects.

ORCID IDs of the Authors

Ngoc Thanh Vu   0000-0001-7846-8162
Duyen Thi My Chung   0000-0003-0913-952X

REFERENCES

1. De Almeida AJPO, De Oliveira JCPL, Da Silva Pontes LV, et al. ROS: Basic concepts, sources, cellular signaling, and its implications in aging pathways. *Oxid Med Cell Longev*. 2022;2022:1-23. doi:10.1155/2022/1225578

2. Ghouizi AE, Ousaaid D, Laaroussi H, et al. *Ficus carica* (Linn.) leaf and bud extracts and their combination attenuates type-1 diabetes and its complications via the inhibition of oxidative stress. *Foods*. 2023;12(4):759. doi:10.3390/foods12040759

3. Sun H, Saeedi P, Karuranga S, et al. IDF Diabetes Atlas: Global, regional and country-level diabetes prevalence estimates for 2021 and projections for 2045. *Diabetes Res Clin Pract*. 2022;183:109119. doi:10.1016/j.diabres.2021.109119

4. Dabravolski SA, Sadykhov NK, Kartuesov AG, Borisov EE, Sukhorukov VN, Orekhov AN. The role of mitochondrial abnormalities in diabetic cardiomyopathy. *Int J Mol Sci*. 2022;23(14):7863. doi:10.3390/ijms23147863

5. Egbuna C, Awuchi CG, Kushwaha G, et al. Bioactive compounds effective against type 2 diabetes mellitus: A systematic review. *Curr Top Med Chem*. 2021;21(12):1067-1095.

6. Pahari N, Majumdar S, Karati D, Mazumder R. Exploring the pharmacognostic properties and pharmacological activities of phytocompounds present in *Ficus racemosa* Linn.: A concise review. *Pharmacol Res-Modern Chinese Med*. 2022;4:100137. doi:10.1016/j.prmcm.2022.100137

7. Nguyen HN, Chung DTM, Le TM, Vu NT. Fermented hylocereus undatus peel extract with enhanced antioxidant, anti-inflammatory, anti-biofilm and sun protection potential. *Waste Biomass Valori*. 2024. doi:10.1007/s12649-024-02662-6

8. Paz-Arteaga SL, Ascacio-Valdés JA, Aguilar CN, et al. Bioprocessing of pineapple waste for sustainable production of bioactive compounds using solid-state fermentation. *Innov Food Sci Emerg*. 2023;85:103313. doi:10.1016/j.ifset.2023.103313

9. Srianta I, Kuswardani I, Ristiarini S, Kusumawati N, Godelive L, Nugerahani I. Utilization of durian seed for *Monascus* fermentation and its application as a functional ingredient in yogurt. *Bioresour Bioprocess*. 2022;9(1). doi:10.1186/s40643-022-00619-y

10. Torres-León C, Ramírez-Guzmán N, Ascacio-Valdés J, et al. Solid-state fermentation with *Aspergillus niger* to enhance the phenolic contents and antioxidative activity of Mexican mango seed: A promising source of natural antioxidants. *LWT-Food Sci Technol*. 2019;112:108236. doi:10.1016/j.lwt.2019.06.003

11. Zhao Z, Hamid N, Qian L, et al. The effects of roasting on antioxidant and anticancer activities of fermented Hass avocado seeds. *Front Food Sci Technol*. 2022;2. doi:10.3389/frfst.2022.986868

12. Garcia YJ, Rodríguez-Malaver AJ, Peñaloza N. Lipid peroxidation measurement by thiobarbituric acid assay in rat cerebellar slices. *J Neurosci Methods*. 2005;144(1):127-135.

13. Kim M, Vu NT, Wang X, et al. Caspase 9b drives cellular transformation, lung inflammation, and lung tumorigenesis. *Mol Cancer Res*. 2022;20(8):1284-1294.

14. Vu NT, Kim M, Stephenson DJ, MacKnight HP, Chalfant CE. Ceramide kinase inhibition drives ferroptosis and sensitivity to cisplatin in mutant KRAS lung cancer by dysregulating VDAC-Mediated mitochondria function. *Mol Cancer Res*. 2022;20(9):1429-1442.

15. Vu NT, Park MA, Shultz JC, et al. HNRNP U enhances Caspase-9 splicing and is modulated by AKT-dependent phosphorylation of HNRNP L. *J Biol Chem*. 2013;288(12):8575-8584.

16. Vu NT, Park MA, Shultz MD, Bulut GB, Ladd AC, Chalfant CE. Caspase-9b interacts directly with cIAP1 to drive agonist-independent activation of NF-κB and lung tumorigenesis. *Cancer Res*. 2016;76(10):2977-2989.

17. Zulfiker AH, Saha M. Hypoglycemic and *in vitro* antioxidant activity of ethanolic extracts of *Ficus racemosa* Linn. fruits. *Am J Sci Res*. 2011;2(3):391-400.

18. Velayutham R, Sankaradoss N, Ahamed KN. Protective effect of tannins from *Ficus racemosa* in hypercholesterolemia and diabetes induced vascular tissue damage in rats. *Asian Pac J Trop Med*. 2012;5(5):367-373.

19. Sumi SA, Siraj MdA, Hossain A, Mia MdS, Afrin S, Rahman MdM. Investigation of the key pharmacological activities of *Ficus racemosa* and analysis of its major bioactive polyphenols by HPLC-DAD. *Evid Based Complement Alternat Med*. 2016;2016:1-9. doi:10.1155/2016/3874516

20. Lu Y, Cederbaum AI. CYP2E1 and oxidative liver injury by alcohol. *Free Radic Biol Med*. 2008;44(5):723-738.

21. Liu L, Duan JA, Tang YP, et al. The protective effects of the active fraction of shaofu zhuyu decoction on hydrogen peroxide-induced oxidative injury in vascular smooth muscle cells. *Molecules*. 2010;15(8):5066-5078.

22. Tomassoni D, Amenta F, Amantini C, et al. Brain activity of thioctic acid enantiomers: *In vitro* and *in vivo* studies in an animal model of cerebrovascular injury. *Int J Mol Sci*. 2013;14(3):4580-4595.

23. Xu Y, Ruan S, Wu X, Chen H, Zheng K, Fu B. Autophagy and apoptosis in tubular cells following unilateral ureteral obstruction are associated with mitochondrial oxidative stress. *Int J Mol Sci*. 2013;31(3):628-636.

24. Martín MA, Ramos S, Mateos R, et al. Protection of human HepG2 cells against oxidative stress by cocoa phenolic extract. *J Agric Food Chem*. 2008;56(17):7765-7772.

25. Jahan IA, Nahar N, Mosihuzzaman M, et al. Hypoglycaemic and antioxidant activities of *Ficus racemosa* Linn. fruits. *Nat Prod Res*. 2009;23(4):399-408.

How to cite this article

Etoposide Treatment of Cancer Cell Lines Results in Nuclear Localisation of Cleaved Gasdermin D

Soukaina Imlilss[1] ⬤, Zahira Ahmadi[1] ⬤, Ghita Jekki[1] ⬤, Elif Eren[1] ⬤

[1]Bahcesehir University, Faculty of Engineering and Natural Sciences Department of Molecular Biology and Genetics, Inflammasomes and Cell Death Laboratory, Besiktas, Istanbul, Türkiye

ABSTRACT

Objective: Overcoming resistance to apoptosis is one of the main goals of cancer treatment. Subversion of apoptosis to pyroptosis, an inflammatory cell death mediated by Gasdermin family members, was previously proposed as an alternative strategy for killing cancer cells. Since the pyroptotic activity of Gasdermin D has been mainly studied in the context of inflammasome activation and its association with cancer is mostly based on expression correlation, we sought to determine whether Gasdermin D-mediated pyroptosis could be triggered in response to drugs used to induce apoptosis in cancer cells.

Materials and Methods: Cancer cells were treated with different concentrations of etoposide, gemcitabine, and cisplatin, which are used as chemotherapeutic agents in various ongoing clinical trials. Membrane integrity was evaluated by measuring lactate dehydrogenase release, and Gasdermin D and Caspase activations and subcellular localisation of Gasdermin D were determined by western blotting.

Results: Upon treatment with the well-known apoptosis inducer etoposide, a necrotic form of programmed cell death was observed in different cancer cell lines even at low drug concentrations. Additionally, cleavage analysis revealed a 20-kDa-Gasdermin D fragment in the supernatant of treated cells. Surprisingly, this cleaved form was localised in the nuclei of etoposide-treated cells rather than in the well-defined cytosolic and plasma membrane localisations.

Conclusion: Overall, these results demonstrate the complex interplay between different cell death pathways and suggest that Gasdermin D generates a fragment presenting an unknown function in the nuclei of etoposide-treated cancer cell lines.

Keywords: Pyroptosis, Gasdermin D, Cancer, Etoposide, Nucleus

INTRODUCTION

Pyroptosis is an inflammatory form of necrotic cell death mediated by Gasdermin D and is required for the clearance of pathogen-infected cells and to trigger inflammation.[1–3] Gasdermin D is activated upon the recognition of pathogen-associated molecular patterns (PAMPs) and danger-associated molecular patterns (DAMPs) by the canonical and non-canonical inflammasome pathways. Gasdermin D cleavage by Caspase-1/4/5 results in the release of the 30 kDa N-terminal fragment (p30), which translocates to the plasma membrane to form pores and induces pyroptosis.[1,2] These pores serve as conduits for IL-1beta secretion into the extracellular milieu and result in membrane rupture through the activation of NINJ1.[4,5]

Before the identification of their role in pyroptosis, the expression of Gasdermin proteins was initially proposed as a prognostic marker for various cancers. For instance, Gasdermin B was shown to be highly expressed in breast cancer, and new strategies to target Gasdermin B in HER2-positive breast cancer cells are under development.[6,7] Whereas a clear correlation between Gasdermin B expression and cancer progression was made, conflicting results were obtained for Gasdermin D. Although a decrease in Gasdermin D expression was found to activate anti-tumoral immunity, other studies demonstrated that *Gasdermin D* downregulation promoted gastric tumour formation and colorectal cancer.[8–11] These data suggest that Gasdermin proteins modulate cancer through properties beyond their expression.

Interestingly, Gasdermin E, another member of the family, can also trigger pyroptosis under physiological conditions. Gasdermin E was not activated by inflammasome-related Caspases but rather by the apoptotic executioner Caspase-3 and initiator Caspase-8. Gasdermin E triggered secondary necrosis upon its cleavage by Caspase-3 in macrophages infected with vesicular stomatitis virus or treated with high concentrations of etopo-

side and localised at the mitochondrial membrane to induce the release of mitochondrial proteins.[12,13] Chemotherapeutic agents including etoposide activated Gasdermin E-dependent pyroptosis in different cancer cell lines.[14] Similarly, agents such as lobaplatin, cisplatin, and paclitaxel triggered Gasdermin E-mediated pyroptosis or secondary necrosis in lung and colon cancer cell lines.[15,16] Based on these findings, Gasdermin E is considered the main player at the crossroads of the apoptosis and pyroptosis forming a molecular determinant of pyroptosis induction and is proposed to be a key target to overcome the apoptosis resistance of cancer cells.[14,16–22]

These exciting advances establishing that Caspases involved in apoptosis can also regulate Gasdermin E-dependent pyroptosis/secondary necrosis, led to the discovery of new Gasdermin D cleavage sites. Whereas the activation of Gasdermin D in macrophages stimulated pyroptosis, when *Gasdermin D* was knocked out, Caspase-3 and Caspase-8 activations in response to inflammatory stimuli directed cells towards apoptosis.[23] Gasdermin D-mediated pyroptosis was blocked by Caspase-3 cleavage of Gasdermin D at aspartic acid 87 (Asp87) residue to form a p43 fragment in macrophages.[24] Interestingly, inhibition of TAK1 during *Yersinia* infection unmasked a Caspase-8-dependent Gasdermin D cleavage at Asp275 as well as Gasdermin E activation and pyroptosis.[25,26] Under these conditions, Caspase-3 generated the Gasdermin D p43 band which levels decreased in Caspase-3 knockout cells.[26] Taken together, these findings indicate that Caspase-8 activation in the extrinsic pathway of apoptosis results in Gasdermin D cleavage at Asp275 and pyroptosis, whereas this activation is counteracted by Caspase-3 cleavage at Asp87.[27,28]

Despite these groundbreaking findings in immune cells and under gene knockout or inhibitory conditions, the effect of the well-studied inflammasome-related Gasdermin D protein's pyroptotic activity on tumour cell death is less understood. The present study aimed to determine whether Gasdermin D-mediated pyroptosis could be triggered by treatment with drugs that induce apoptosis in cancer cells. For this purpose, we analysed pyroptosis properties such as cellular morphology, lactate dehydrogenase (LDH) release, Gasdermin D and Caspase activation, IL-1beta secretion and revealed the cellular localisation of Gasdermin D in cancer cell lines treated with etoposide, gemcitabine, and cisplatin, which are known apoptosis-inducers used alone or in combination with other drugs, in numerous ongoing clinical trials.

MATERIALS AND METHODS
Cells and Drug Treatments

A549 human lung cancer cell line, HeLa human cervical cancer cell line, THP-1 human leukaemia cell line, and 4T1 mouse breast cancer cell line were used in this study. A549 and HeLa cells were maintained in DMEM and THP-1 and 4T1 cells in RPMI, both supplemented with 10% fetal bovine serum, 1 mM penicillin/streptomycin, and 1 mM non-essential amino acids. Cells were grown at 37°C, and 5% CO_2.

2×10^6 low passage healthy cells were seeded in a 25 cm^2 flask before treatment. The next day, cells were treated with the indicated concentrations of etoposide (Sigma E1383), gemcitabine (Sigma G6423), and cisplatin (Santa Cruz sc200896) for 24 h. Dimethyl sulfoxide (DMSO)-treated cells were used as a control.

Morphological Analysis

The morphology of cells was assessed for different drugs, and images were taken at 24 h after drug treatment from randomly chosen fields with the approximate same number of total cells using an inverted light microscope (Olympus CKX41). Necrotic and apoptotic cells were identified visually based on morphological criteria, such as apoptotic body formation for apoptosis and swelling, and nucleus visibility for pyroptosis.

LDH Assay

LDH levels in fresh cell-free supernatants collected 24 h after drug treatments were measured using the CyQUANT™ LDH Cytotoxicity Assay (Invitrogen #C20301) according to the manufacturer's recommendations. Briefly, 50 µL of fresh supernatant was incubated for 30 min with 50 µL substrate mix and assay buffer, and LDH levels were measured at 490 and 680 nm after stopping the reaction with 50 µL sulphuric acid. DMSO-treated cells were used as negative controls for LDH release, and Triton-X-treated cells were used as positive controls. The percentage of cell death was calculated according to the following formula: ((LDH of the sample - LDH of the negative control))/(LDH of positive control - LDH of negative control))*100. Each condition was performed in three biological replicates, and LDH levels were measured in triplicate for each biological replicate.

Inhibition of Membrane Rupture

To inhibit NINJ1-dependent membrane rupture, cells were treated with 5 mM glycine.[29] Glycine was added to the cell supernatant at the same time with the different drugs for membrane inhibition, whereas the other cells were only treated with the drugs. All supernatants were collected 24 h after treatment for the LDH assay.

Gasdermin D and Caspase Activation

Gasdermin D and Caspase-1, Caspase-8 and Caspase-3 activations were assessed by Western blotting in total cell lysates (TCL) and supernatants (Sup.). For TCL, cells were harvested in RIPA buffer containing protease inhibitor complex and cleared via centrifugation. FBS-free supernatants from con-

trol and drug-treated cells were prepared by precipitating proteins with 10% trichloroacetic acid and acetone wash. Both TCL and the supernatants were run on 12% acrylamide gel and transferred to 0.2 µm PVDF membrane for 1 h at 100 V. Proteins were visualised by using anti-Gasdermin D (Abcam #ab209845), anti-Caspase-1 (Cell Signaling Technologies #3866), anti-Caspase-8 (Cell Signaling Technologies #9746), and anti-Caspase-3 (Abcam #ab13847) antibodies.

IL-1beta Quantification

IL-1beta levels were quantified in the cell-free supernatants of treated cells using a human IL-1beta ELISA kit (Thermo Fischer Scientific, Invitrogen #88-7261). Briefly, plates were coated with anti-IL-1beta capture antibody overnight at 4°C. The next day, after saturation, cell supernatants were added in triplicate, and after 2 h of incubation, biotin-conjugated anti-IL-1beta detection antibodies were added for 2 h. After several washes and 15 min of incubation with tetramethylbenzidine, IL-1beta levels were measured at 450 nm after stopping the reaction. Purified human IL-1beta standards were used to determine the IL-1beta concentration of the samples. Interferon gamma-primed cells infected with logarithmic phase *Salmonella typhimurium* MOI25 for 5 h were used as positive control for IL-1beta secretion.

Cell Fractionation

After 24 h of treatment, cells were collected and dissociated in 200 µL of hypotonic buffer (20 mM Tris-pH 7.4, 10 mM NaCl, 3 mM MgCl$_2$). After 15 min of incubation on ice, 12.5 µL of Triton-X100 (10%) was added, and samples were centrifuged for 10 min at 3000 rpm. The supernatant was transferred into a new tube and used as the "cytoplasmic fraction". The cell pellet was resuspended in 50 µL of complete cellular fractionation buffer (20 mM Tris-pH 7.4, 1% Triton X-100, 10 mM NaCl, 1 mM EDTA, 10% glycerol, 0.1 M SDS) and incubated for 30 min on ice. After 30 min of centrifugation at 14.000 rpm, the supernatant was transferred into a new tube and labeled as the "nuclear fraction". Equal concentration of total proteins for both nuclear and cytosolic fractions was run on gel, and the purity of each fraction was determined using anti-Lamin A/C antibody (GeneTex #GTX101126) and anti-GAPDH antibody (GeneTex #GTX100118), respectively.

Statistical Analysis

Statistical analysis was performed using GraphPad Prism version 10.2.3. The two-tailed Student's t-test was used to determine statistical significance. Results of the analysis are shown on graphics with the following symbols: ns: non-significant, *p<0,05, **p<0,01, ***p<0,001, ****p<0,0001. Each experiment was repeated at least three times. Representative images of each experiment were shown.

RESULTS

Lytic Form of Cell Death Is Induced in Etoposide-Treated Cell Lines

Etoposide, a known inducer of apoptosis[30], was also found to trigger NINJ1-dependent plasma membrane rupture and Gasdermin D and Gasdermin E cleavage-associated pyroptosis and/or secondary necrosis in macrophages in previous publications.[26] To test whether it could trigger Gasdermin D-dependent pyroptosis in cancer cells, we treated A549 human lung cancer cell lines with different concentrations of etoposide and determine whether cells could undergo a lytic form of cell death (Figure 1). Twenty-four hours after treatment, etoposide-treated cells started to show morphological characteristics of necrosis, including cell swelling, membrane rupture, and appearance of the nucleus, even at very low concentrations, whereas the DMSO-treated control cells remained intact. These phenotypes were also observed in cells treated with gemcitabine, but at a lower extend than etoposide, whereas cisplatin treatment did not induce significant morphological differences (Figure 1A).

Because the major difference between apoptosis and necrosis is the rupture of the membrane in the latter, we measured the amount of LDH, a high-molecular-weight molecule that can exit the cell only when the membrane is ruptured.[31] Etoposide treatment of A549 cells triggered the release of LDH in approximately 6%, 11%, and 26% of cells at 5, 10 and 50 µM respectively (Figure 1B). Similarly, gemcitabine treatment triggered 1%, 11%, and 13% cell death at 1, 10 and 50 µM respectively (Figure 1C). Although cisplatin is a well-defined apoptosis inducer, it has previously been shown that A549 cells are resistant to cisplatin-induced cell death.[32,33] Similarly, we did not detect any cell death at 20 µM concentration in cisplatin-treated cells or LDH release, demonstrating the absence of cell rupture (Figure 1D).

Recent publications have shown that NINJ1 is activated downstream of many necrotic cellular demises and triggers plasma membrane rupture through its insertion into the plasma membrane.[5,34,35] To further validate membrane lysis upon etoposide treatment suggested by LDH release, we pre-treated cells with or without glycine, an inhibitor of membrane rupture.[29] A statistically significant reduction in LDH levels was observed in the presence of glycine, suggesting that etoposide and gemcitabine disrupted membrane integrity (Figure 1E). To validate whether the induction of necrosis by etoposide is not specific to A549 cells, we treated THP-1 human leukaemia cell lines, HeLa human cervical cancer, and mouse 4T1 breast cancer cell lines with different concentrations of etoposide. Although at different extents, all three cell lines trig-
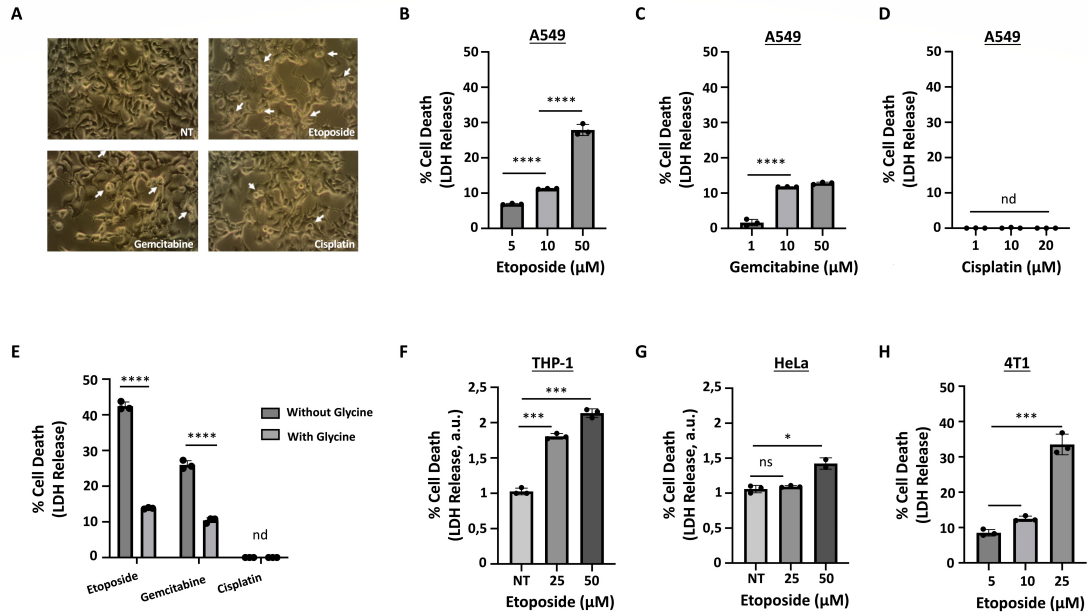
Figure 1. Etoposide induces necrotic cell death in cancer cell lines. A. Morphologies of untreated (NT), etoposide (50 µM), gemcitabine (10 µM), and cisplatin (20 µM) treated A549 cells are shown. Arrows indicate pyroptotic cells. B-D. LDH levels were determined in the cell-free supernatant of A549 cells treated with the indicated concentrations of etoposide (B), gemcitabine (C), and cisplatin (D). E. LDH levels in the presence and absence of the plasma rupture inhibitor glycine are given for A549 cells. Nd: not detected. F-H. LDH levels were determined in the cell-free supernatants of etoposide-treated HeLa (F), THP-1 (G), and 4T1 (H) cells. LDH levels were represented in arbitrary units (a.u) for HeLa and THP-1 cells, where the lowest optical density measured for the non-treated (NT) control sample was assigned and 1 arbitrary unit.
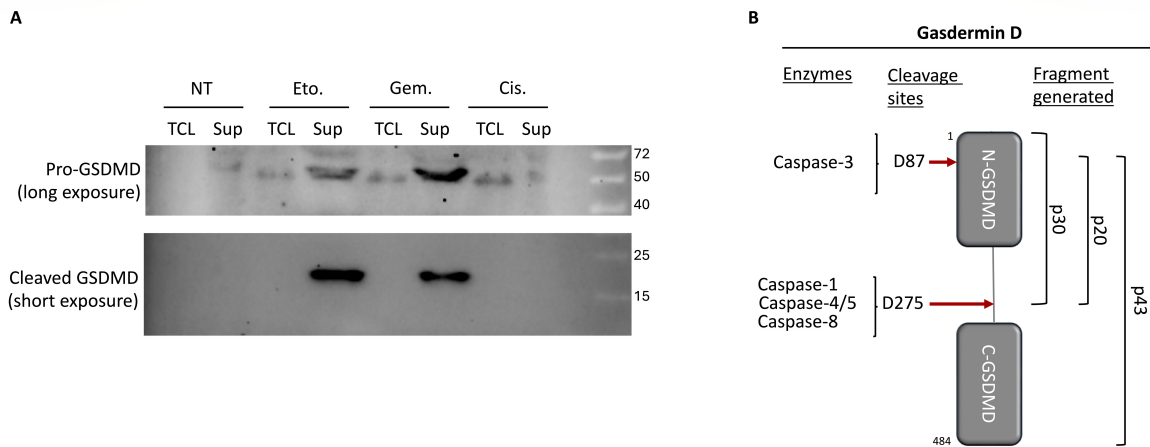
Figure 2. Etoposide triggers non-canonical Gasdermin D cleavage. **A.** Western blot analysis of Gasdermin D cleavage in total cell lysate (TCL) and cell supernatants (Sup). Etoposide and gemcitabine treatments generate a cleaved Gasdermin D band of approximately 20 kDa. A representative image of two sets of experiments is shown. B. Known cleavage sites of human Gasdermin D. Gasdermin D is cleaved at D275 (Asp275) by Caspase-1, Caspase-4/5[1,2]; by Caspase-8 at the same site[25,27], generating a p30 fragment that triggers pyroptosis. Caspase-3 cleaves human Gasdermin D at D87, resulting in a p43 fragment and p20 fragment.[23,24,27] The protein size was not scaled for the Gasdermin D representation.

gered LDH release, confirming that the phenotype observed in A549 cells is not an experimental artefact (Figure 1F-1H). These data demonstrate that etoposide and gemcitabine induce necrotic cell death resulting in plasma membrane lysis.

Etoposide Treatment Triggers Gasdermin D Cleavage

Pyroptosis is a form of cell death mediated by Gasdermin proteins.[1,2,36] To determine whether the type of necrotic cell death observed was pyroptosis, we assessed Gasdermin D activation upon apoptotic drug treatment (Figure 2A). In line with our previous results, etoposide and gemcitabine treatments induced Gasdermin D activation by cleavage (Figure 2A). The

active band was secreted outside these cells and was observed only in the supernatants. Gasdermin D has two known Caspase cleavage sites at Asp275 and Asp87 (Figure 2B). Surprisingly, although the antibody that we used recognised the N-terminal of Gasdermin D, we could only detect a cleaved band of approximatively 20 kDa (p20) instead of 30 kDa (p30) and/or 43 kDa (p43) (Figure 2A). These results suggest that etoposide treatment triggers Gasdermin D cleavage into an approximatively 20-kDa band that could be responsible for pyroptosis induction in A549 lung cancer cells.

Etoposide Treatment Activates Different Caspases but Does Not Trigger IL-1beta Secretion

In order to identify the enzyme responsible for the generation of this 20-kDa form of Gasdermin D, we analysed whether Caspase-3, Caspase-8, and Caspase-1, previously described to cleave Gasdermin D downstream different stimuli, were activated in response to apoptotic drug treatment. Caspase-3 and Caspase-8 were processed by all three drugs into their 25-kDa and 18-kDa active fragments, respectively (Figure 3A). Whereas these fragments were present in the supernatants of etoposide- and gemcitabine-treated cells, they were retained in the cell lysate of cisplatin-treated cells, demonstrating once more the absence of membrane lysis in cisplatin-treated cells (Figure 3A). On the contrary, a 20-kDa cleaved Caspase-1 band could not be detected in either cell lysates or supernatants (Figure 3A).

Besides triggering pyroptosis, the second major role of Gasdermin D is to form pores at the plasma membrane to allow the specific secretion of cleaved IL-1beta outside the cell.[4] Quantification of IL-1beta in the supernatants demonstrated that although present in high concentration in *Salmonella typhimurium-infected* cells used as positive controls, in our experimental settings triggering cleavage of Gasdermin D, IL-1beta secretion was not detected (Figure 3B). In summary, etoposide and gemcitabine treatments activated Caspase-3 and Caspase-8 without inducing Caspase-1 cleavage and IL-1beta secretion.

The Cleaved New Gasdermin D Fragment Localises To The Nucleus

Since Gasdermin D was activated in our model and showed only a 20-kDa band but did not trigger IL-1beta secretion, we hypothesised that this active Gasdermin D fragment might have another cellular function than forming pores at the plasma membrane. To determine the cellular localisation of Gasdermin D upon apoptotic drug treatment, subcellular fractionation was performed (Figure 4). Although the nuclear and cytosolic fractions of etoposide-treated cells were clean, as suggested by Lamin A/C and GAPDH blots, slight cytosolic contamination was present in non-treated cells. Surprisingly, we detected the cleaved Gasdermin D p20 fragment in the nuclear fraction of etoposide-treated cells (Figure 4). The inactive pro-form or other cleavage forms were absent. These results indicate that the cleavage fragment of Gasdermin D generated by etoposide treatment translocates to the nucleus of cancer cells.

DISCUSSION

To clarify the role of Gasdermin D-induced pyroptosis in cancer cell clearance, we treated cancer cell lines with different concentrations of drugs known to trigger apoptosis and assessed Gasdermin D activation and subcellular localisation. As suspected, the morphological characteristics of pyroptosis, plasma membrane rupture highlighted by LDH release and Gasdermin D cleavage were observed in different cancer cell lines that were used (Figures 1 and 2). To rule out an experimental artefact due to the usage of high concentrations, we lowered the drug concentration down to 10 times their IC_{50} and still observed the same phenotype, confirming plasma membrane rupture and Gasdermin D cleavage in experimental settings (Figure 1). Because prolonged exposure to apoptotic stimuli can trigger secondary necrosis and plasma membrane rupture, the role of Gasdermin E in this process cannot be neglected and must be tested. Nonetheless, these results suggest that etoposide and gemcitabine induce Gasdermin D cleavage followed by plasma membrane rupture. The use of *Gasdermin D-* and *Gasdermin E-*knockout cancer cell lines will determine whether etoposide and gemcitabine trigger pyroptosis or secondary necrosis through Gasdermin D and/or Gasdermin E activation.

Another interesting question that remains to be solved is the identification of the enzyme(s) that cleaved Gasdermin D in response to etoposide and generated the p20 fragment that we observed. According to our results, only Caspase-3 and Caspase-8 were activated in response to etoposide and gemcitabine treatment (Figure 3A). Thus, this band is probably the previously described fragment generated by Caspase-3 and Caspase-8 cleavages at Asp87 and Asp275 residues of full-length or p30 fragment of Gasdermin D.[25-28] Activation of Caspase-3 and Caspase-8 in response to apoptotic stimuli is expected. However, Gasdermin D cleavage is unusual in this context. Gasdermin D-cleaving candidate Caspases should be further confirmed by knocking them out individually or in combination or by using their specific inhibitors. Although plasma membrane rupture triggered by etoposide and gemcitabine was also observed in other cancer cell lines, we could not verify Gasdermin D cleavage in these cells (Figure 1F-1H). Use of other available anti-Gasdermin D antibodies to confirm the presence of the p20 band in other cells would support and validate our data.

Contrary to other publications on macrophages, we did not detect Caspase-1 activation nor IL-1beta cleavage and secretion in the A549 lung cancer cell line (Figure 3). IL-1beta is secreted
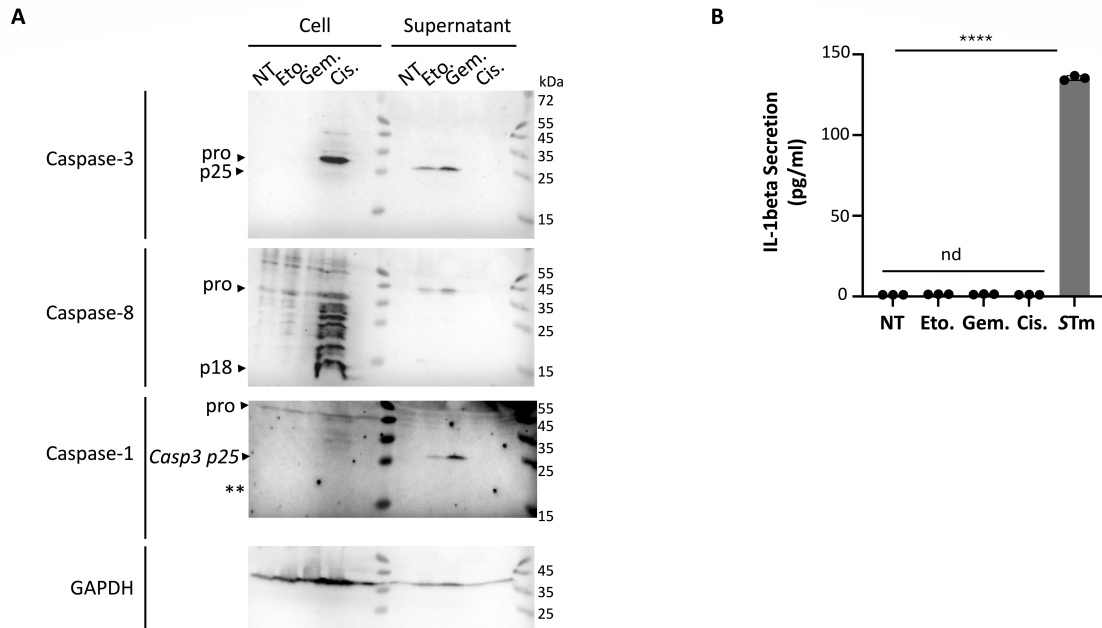
Figure 3. Etoposide treatment activates different caspases but does not trigger IL-1beta secretion. **A.** Activation of Caspase-1, Caspase-8 and Caspase-3 was assessed in the cells and supernatants of non-treated (NT), etoposide (50 µM), gemcitabine (10 µM), and cisplatin (20 µM) treated samples. Cleaved forms of Caspase-3 (p25), Caspase-8 (p18) as well as inactive Caspase-3, Caspase-8 and Caspase-1 pro-forms (32 kDa, 42 kDa and 45 kDa respectively) and GAPDH as a loading control are shown. The arrow in the Caspase-1 blot represents cleaved 25-kDa Caspase-3 bands. The expected 20 kDa band of cleaved Caspase-1 was absent. **B.** IL-1beta secretion from the supernatants of cells treated with 50 µM etoposide, 10 µM gemcitabine and 20 µM cisplatin was determined by ELISA. Supernatants of cells infected with *Salmonella typhimurium SL1344* (STm) for 5 hours were used as positive control for IL-1beta secretion. Nd: not detected. The average of three sets of independent experiments is presented.
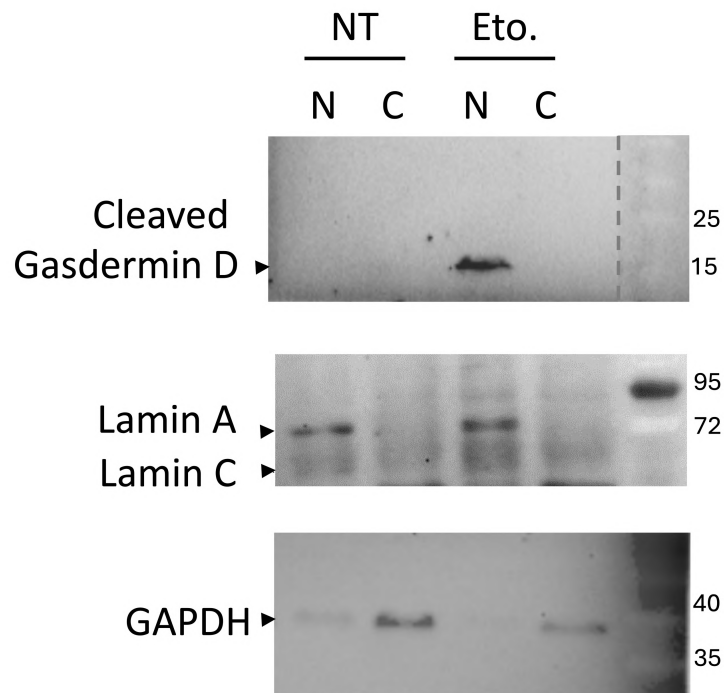
Figure 4. Cleaved Gasdermin D fragment localises to the nucleus. Nuclear (N) and cytosolic (C) fractions obtained after subcellular fractionation of non-treated (NT) and etoposide-treated cells are shown. Localisation of cleaved Gasdermin D was determined. Lamin A/C proteins were used as controls for the nuclear fraction, whereas GAPDH was used as control for the cytosolic fraction.

through Gasdermin D pores located at the plasma membrane after maturation by active cleaved Caspase-1.[4,37] The absence of Caspase-1 cleavage justifies the lack of secreted IL-1beta that is probably not cleaved either. Caspase-1 was described to be activated in an inflammasome-dependent manner. In our context, inflammasome complexes are not expected to be activated in response to etoposide treatment. Our data suggest that an inflammasome-independent pyroptosis is triggered and because IL-1beta is not cleaved, it cannot be secreted through Gasdermin pores.

Our findings demonstrated the presence of cleaved Gasdermin D in the supernatant of etoposide-treated cells. To determine whether the detected p20 Gasdermin D band was addressed to the plasma membrane, we performed subcellular fractionation and identified an unexpected nuclear localisation of this fragment (Figure 4). Thus, our data demonstrate an additional role for cleaved Gasdermin D, which was unexpectedly detected in the nucleus of etoposide-treated cancer cells. Gasdermin proteins are usually located in the cytosol of cells in their inactive state and transit to the plasma membrane when activated to form pores.[1,2] Some studies also reported the presence of Gasdermin pores in the mitochondrial membrane leading to mitochondrial membrane rupture and cell death.[13,38] To date, only two publications reported a nuclear localisation of Gasdermin D. Peng et al. demonstrated the translocation of the inactive pro-form of Gasdermin D into the nucleus under the stimulation of chemotherapy drugs in colorectal cancer.[11] In another study, immunohistochemical analysis showed the presence of Gasdermin D in the nucleus, cytoplasm, and plasma membrane of colorectal cancer.[39] Until now, the function of Gasdermin D in the nucleus has been unclear. Contrary to these publications, in our case, not the pro-form but the cleaved form of Gasdermin D was located in the nucleus of etoposide-treated lung cancer cell lines, as observed by subcellular fractionation. Immunostaining of Gasdermin D in treated cells with nuclear markers would confirm our findings.

When the Gasdermin D sequence was analysed, any nuclear localisation or nuclear retention signals could not be detected suggesting that probably a chaperon protein mediates Gasdermin D's transit to the nucleus. Characterisation of the molecular mechanisms of Gasdermin D transport to the nucleus and identification of the role of its pro- and active forms in this cellular compartment would provide significant information on the role of Gasdermin D in cancer. Finally, cancer cell lines maintained in culture were used in our study. We focused on A549 cancer cell lines that showed the highest LDH release, and all our results were based on these cell lines. We validated etoposide-induced plasma membrane rupture in other cell lines, such as THP-1 and HeLa, and both human and mouse cell lines. However, whether Gasdermin D is activated in these cells remains unclear. Determining the exact role of Gasdermin D under normal physiological conditions would provide a better understanding of crosstalk between different pathways. For instance,

tumour samples isolated from patients with cancer could be tested for Gasdermin D cleavage and nuclear localisation. At this point, our results cannot be generalised to all cancer cells. Nonetheless, in the cell line that we were using, we observed a cleaved band with a new subcellular localisation suggesting a novel role for Gasdermin D in cancer that could be masked in other cell lines.

Pyroptotic cells represented not more than 30-40% of the population in our experimental setting, demonstrating that this was not the main mechanism of cell death triggered by etoposide. Morphological analysis also revealed apoptotic cells. Our results do not exclude the induction of secondary necrosis. Even if cleaved Gasdermin D does not trigger pyroptosis or secondary necrosis, it clearly has an undefined role in the nucleus of treated cancer cells. Overall, these data put lights on an uncharacterised mechanism of cleaved Gasdermin D in the nucleus and propose an inflammasome-independent role for Gasdermin D in cancer cells.

CONCLUSION

The increasing incidence of cancer and the emergence of resistance among tumour cells to apoptosis induced by conventional therapies necessitate the exploration of novel strategies for effectively eradicating these aberrant cells. In this regard, the induction of pyroptosis appears to be a promising approach. In this study, we aimed to characterise the function of Gasdermin D in the interplay between apoptosis and pyroptosis. Similar to other studies, we found that the use of apoptosis inducer drugs triggered plasma membrane rupture in long term (24 h). Gasdermin D was cleaved in response to etoposide and gemcitabine treatments in A549 cancer cell lines, but contrary to other publications, we could only detect the p20 band in the cell supernatants of etoposide- and gemcitabine-treated cells, suggesting double cleavage by Caspase-3 at Asp87 and Caspase-8 at Asp275. Previous studies have investigated the activation of Gasdermin D by apoptotic Caspases in the context of infections and inflammasome activation in macrophages by inhibiting a pathway or knocking out a gene.[23–28] In this study, we demonstrate the cleavage of Gasdermin D into p20 fragment upon etoposide treatment in a cancer cell line. Moreover, we detected a cleaved p20 band in the nucleus of cells. Taken together, our results suggest that the Gasdermin D p20 fragment generated in response to etoposide treatment translocates to the nucleus of cancer cells. Additional experiments are needed to confirm these results, to determine whether the observed cell death is due to Gasdermin D-dependent pyroptosis or Gasdermin E-dependent secondary necrosis/pyroptosis, and to evaluate the physiological relevance of these findings. In conclusion, the present study provides evidence of the connections between different cell death pathways and the interplay between important proteins involved in the apoptosis and pyroptosis in cancer cells. Overall, we propose that Gasdermin D could be a novel

molecular switch between apoptosis and pyroptosis in cancer and unrevealed the non-canonical localisation of cleaved p20 Gasdermin D in the nucleus of etoposide-treated cancer cells.

ORCID IDs of the Authors

Soukaina Imlilss   0009-0001-9488-1931
Zahira Ahmadi   0009-0001-9394-9420
Ghita Jekki   0009-0004-4892-6803
Elif Eren   0000-0002-0328-5609

REFERENCES

1. Kayagaki N, Stowe IB, Lee BL, et al. Caspase-11 cleaves gasdermin D for non-canonical inflammasome signalling. *Nature.* Published online 2015. doi:10.1038/nature15541

2. Shi J, Zhao Y, Wang K, et al. Cleavage of GSDMD by inflammatory caspases determines pyroptotic cell death. *Nature.* 2015;526(7575):660-665. doi:10.1038/nature15514

3. Jorgensen I, Zhang Y, Krantz BA, Miao EA. Pyroptosis triggers pore-induced intracellular traps (PITs) that capture bacteria and lead to their clearance by efferocytosis. *J Exp Med.* 2016;213(10):2113-2128.

4. Heilig R, Dick MS, Sborgi L, Meunier E, Hiller S, Broz P. The Gasdermin-D pore acts as a conduit for IL-1β secretion in mice. *Eur J Immunol.* 2018;48(4):584-592.

5. Kayagaki N, Kornfeld OS, Lee BL, et al. NINJ1 mediates plasma membrane rupture during lytic cell death. *Nature.* 2021;591(7848):131-136.

6. Hergueta-Redondo M, Sarrio D, Molina-Crespo Á, et al. Gasdermin B expression predicts poor clinical outcome in HER2-positive breast cancer. *Oncotarget.* 2016;7(35):56295-56308.

7. Molina-Crespo Á, Cadete A, Sarrio D, et al. Intracellular delivery of an antibody targeting gasdermin-b reduces HER2 breast cancer aggressiveness. *Clin Cancer Res.* 2019;25(15):4846-4858.

8. Jiang Y, Yang Y, Hu Y, et al. Gasdermin D restricts antitumor immunity during PD-L1 checkpoint blockade. *Cell Rep.* 2022;41(4):111553. doi:10.1016/j.celrep.2022.111553

9. Traughber CA, Deshpande GM, Neupane K, et al. Myeloidcell-specific role of Gasdermin D in promoting lung cancer progression in mice. *iScience.* 2023;26(2):106076. doi:10.1016/j.isci.2023.106076

10. Wang WJ, Chen D, Jiang MZ, et al. Downregulation of gasdermin D promotes gastric cancer proliferation by regulating cell cyclerelated proteins. *J Dig Dis.* 2018;19(2):74-83.

11. Peng X, Na R, Zhou W, et al. Nuclear translocation of Gasdermin D sensitizes colorectal cancer to chemotherapy in a pyroptosisindependent manner. *Oncogene.* 2022;41(47):5092-5106.

12. Rogers C, Fernandes-Alnemri T, Mayes L, Alnemri D, Cingolani G, Alnemri ES. Cleavage of DFNA5 by caspase-3 during apoptosis mediates progression to secondary necrotic/pyroptotic cell death. *Nat Commun.* 2017;8:14128. doi:10.1038/ncomms14128

13. Rogers C, Erkes DA, Nardone A, Aplin AE, Fernandes-Alnemri T, Alnemri ES. Gasdermin pores permeabilize mitochondria to augment caspase-3 activation during apoptosis and inflammasome activation. *Nat Commun.* 2019;10(1):1689. doi:10.1038/s41467-019-09397-2

14. Wang Y, Gao W, Shi X, et al. Chemotherapy drugs induce pyroptosis through caspase-3 cleavage of a gasdermin. *Nature.* 2017;547(7661):99-103.

15. Yu J, Li S, Qi J, et al. Cleavage of GSDME by caspase-3 determines lobaplatin-induced pyroptosis in colon cancer cells. *Cell Death Dis.* 2019;10(3):1-20. doi:10.1038/s41419-019-1441-4

16. Zhang Z, Zhang Y, Xia S, et al. Gasdermin E suppresses tumour growth by activating anti-tumour immunity. *Nature.* 2020;579(7799):415-420.

17. Jiang M, Qi L, Li L, Li Y. The caspase-3/GSDME signal pathway as a switch between apoptosis and pyroptosis in cancer. *Cell Death Discov.* 2020;6(1):1-11.

18. Wang Q, Wang Y, Ding J, et al. A bioorthogonal system reveals antitumour immune function of pyroptosis. *Nature.* 2020;579(7799):421-426.

19. Nagarajan K, Soundarapandian K, Thorne RF, Li D, Li D. Activation of pyroptotic cell death pathways in cancer: An alternative therapeutic approach. *Transl Oncol.* 2019;12(7):925-931.

20. Hanahan D, Weinberg RA. The hallmarks of cancer. *Cell.* 2000;100(1):57-70.

21. Hanahan D, Weinberg RA. Hallmarks of Cancer: The Next Generation. *Cell.* 2011;144(5):646-674.

22. Hanahan D. Hallmarks of Cancer: New Dimensions. *Cancer Discov.* 2022;12(1):31-46.

23. He W ting, Wan H, Hu L, et al. Gasdermin D is an executor of pyroptosis and required for interleukin-1β secretion. *Cell Res.* 2015;25(12):1285-1298.

24. Taabazuing CY, Okondo MC, Bachovchin DA. Pyroptosis and apoptosis pathways engage in bidirectional crosstalk in monocytes and macrophages. *Cell Chem Biol.* 2017;24(4):507-514.e4.

25. Orning P, Weng D, Starheim K, et al. Pathogen blockade of TAK1 triggers caspase-8-dependent cleavage of gasdermin D and cell death. *Science.* 2018;362(6418):1064-1069.

26. Sarhan J, Liu BC, Muendlein HI, et al. Caspase-8 induces cleavage of gasdermin D to elicit pyroptosis during *Yersinia* infection. *Proc Natl Acad Sci U S A.* 2018;115(46):E10888-E10897.

27. Chen KW, Demarco B, Heilig R, et al. Extrinsic and intrinsic apoptosis activate pannexin-1 to drive NLRP3 inflammasome assembly. *EMBO J.* 2019;38(10):e101638. doi:10.15252/embj.2019101638

28. Demarco B, Grayczyk JP, Bjanes E, et al. Caspase-8–dependent gasdermin D cleavage promotes antimicrobial defense but confers susceptibility to TNF-induced lethality. *Sci Adv.* 2020;6(47):eabc3465. doi:10.1126/sciadv.abc3465

29. Borges JP, Sætra RS, Volchuk A, et al. Glycine inhibits NINJ1 membrane clustering to suppress plasma membrane rupture in cell death. Rothlin CV, ed. *eLife.* 2022;11:e78609. doi:10.7554/eLife.78609

30. Burden DA, Kingma PS, Froelich-Ammon SJ, et al. Topoi-somerase II.etoposide interactions direct the formation of drug-induced enzyme-DNA cleavage complexes. *J Biol Chem.* 1996;271(46):29238-29244.

31. Rayamajhi M, Zhang Y, Miao E. Detection of pyroptosis by mea-suring released lactate dehydrogenase activity. *Methods Mol Biol Clifton NJ.* 2013;1040:85-90.

32. Gao Y, Dorn P, Liu S, et al. Cisplatin-resistant A549 non-small cell lung cancer cells can be identified by increased mitochondrial mass and are sensitive to pemetrexed treatment. *Cancer Cell Int.* 2019;19(1):317. doi:10.1186/s12935-019-1037-1

33. Pan X, Chen Y, Shen Y, Tantai J. Knockdown of TRIM65 in-hibits autophagy and cisplatin resistance in A549/DDP cells by regulating miR-138-5p/ATG7. *Cell Death Dis.* 2019;10(6):1-11. doi:10.1038/s41419-019-1660-8

34. Degen M, Santos JC, Pluhackova K, et al. Structural basis of NINJ1-mediated plasma membrane rupture in cell death. *Nature.* 2023;618(7967):1065-1071.

35. Kayagaki N, Stowe IB, Alegre K, et al. Inhibiting membrane rupture with NINJ1 antibodies limits tissue injury. *Nature.* 2023;618(7967):1072-1077.

36. Cookson BT, Brennan MA. Pro-inflammatory programmed cell death. *Trends Microbiol.* 2001;9(3):113-114.

37. Xia S, Zhang Z, Magupalli VG, et al. Gasdermin D pore struc-ture reveals preferential release of mature interleukin-1. *Nature.* 2021;593(7860):607-611.

38. Miao R, Jiang C, Chang WY, et al. Gasdermin D permeabi-lization of mitochondrial inner and outer membranes accelerates and enhances pyroptosis. *Immunity.* 2023;56(11):2523-2541.e8. doi:10.1016/j.immuni.2023.10.004

39. Wang J, Kang Y, Li Y, et al. Gasdermin D in different subcel-lular locations predicts diverse progression, immune microen-vironment and prognosis in colorectal cancer. *J Inflamm Res.* 2021;14:6223-6235.

How to cite this article

Notch and Hedgehog Signalling Axis Drive Senescence in HER2-Positive Breast Cancer Resistant to Trastuzumab

Asiye Busra Boz Er[1] , Idris Er[2]

[1]Recep Tayyip Erdogan University Faculty of Medicine, Department of Medical Biology, Rize, Türkiye
[2]Karadeniz Technical University Faculty of Medicine, Department of Medical Biology, Trabzon, Türkiye

ABSTRACT

Objective: Cellular senescence halts the proliferation of damaged or preneoplastic cells, playing a vital role in cancer control. In HER2-positive breast cancer, resistance to trastuzumab, a HER2-targeted monoclonal antibody, remains a significant obstacle. Although the trastuzumab and cilengitide combination reduces stemness and epithelial-mesenchymal transition, its effect on senescence remains unclear. Additionally, inhibiting the Notch and Hedgehog pathways can induce senescence by impairing proliferation, stemness, and cell cycle progression, making them promising therapeutic targets. This study aimed to evaluate the effect of trastuzumab/cilengitide on cellular senescence in HER2-positive trastuzumab-resistant breast cancer cells and to elucidate the roles of Notch and Hedgehog signalling in this process.

Materials and Methods:: HER2-positive breast cancer cell lines HCC1954 and SKBR3, along with their trastuzumab-resistant variants, were treated with trastuzumab, cilengitide, or both. Senescence markers were assessed by real-time PCR. Notch and Hedgehog pathway activity was evaluated, with additional experiments using specific inhibitors Fli06 (Notch) and GANT61 (Hedgehog).

Results: The trastuzumab-cilengitide combination significantly upregulated senescence markers relative to monotherapy. This response was associated with a marked decrease in Notch and Hedgehog pathway activity. Further combined inhibition of these pathways enhanced senescence marker expression, underscoring their involvement in drug-induced senescence.

Conclusion: The trastuzumab-cilengitide combination induces senescence in trastuzumab-resistant HER2-positive breast cancer cells, potentially through Notch and Hedgehog inhibition. These findings support targeting senescence pathways as a novel strategy to overcome trastuzumab resistance and improve therapeutic outcomes. Further research is warranted to assess the clinical potential of such combination therapies.

Keywords: HER2-positive, Senescence, Notch, Hedgehog.

INTRODUCTION

Throughout life, cells encounter various types of damage. Depending on the severity and nature of this damage, cells can either repair themselves or activate death signalling pathways to prevent disruption of tissue homeostasis.[1] When repair mechanisms are insufficient, cells activate apoptotic signalling pathways to eliminate damaged cells and preserve tissue homeostasis. Alternatively, cells may undergo cellular senescence, a robust and irreversible cell cycle arrest, triggered by diverse stress signals. This response acts as a safeguard against the replication of aged, damaged, or preneoplastic cells, thereby limiting their potential to contribute to tumorigenesis.[2] In our previous work, we demonstrated that the combination of trastuzumab and cilengitide significantly decreased stemness[3] and epithelial-mesenchymal transition (EMT)[4] in both HER2-positive trastuzumab-resistant and -sensitive cell lines. However, the effects of this combination on senescence are unknown. Cilengitide is an arginine-glycine-aspartic acid (RGD)-containing pentapeptide that effectively blocks αvβ3 and αvβ5 integrin activation.[5] The impact of RGD-binding integrins on cellular senescence is still debated due to their presence in different combinations.[6] Recent studies have shown that CWHM12, an RGD-mimicking integrin blocker, increases senescence in hepatic stellate cells by binding to and inhibiting RGD-binding integrins.[7-12] However, the effect of RGD-binding integrin inhibitors on HER2-positive breast cancer remains unexplored. In this study, the effect of cilengitide on the

senescence of HER2-positive trastuzumab-resistant cell lines is to be investigated, and the underlying signalling mechanisms are to be elucidated.

Notch and Hedgehog signalling pathways, which are essential for development and tissue homeostasis, also significantly affect senescence in cancer cells, affecting tumour progression and therapeutic outcomes. The activation of Notch signalling pathways can induce senescence in various cancers. Notch receptors such as Notch1 and Notch2 promote senescence through the up-regulation of cyclin-dependent kinase inhibitors (CDKIs) such as p16^{INK4a} and p21^{CIP1}.[4,5] For instance, Notch activation in melanoma and breast cancer models increases p21^{CIP1} expression, leading to growth arrest and senescence induction, thereby inhibiting tumour progression.[13] Conversely, in some contexts, Notch signalling may suppress senescence and promote cancer progression. In glioblastoma and certain leukaemia cells, Notch activation correlates with enhanced cell survival and proliferation, suggesting a role in evading senescence-associated growth arrest.[14]

In previous studies Hedgehog signalling activation associated with decreased senescence in neural cells.[15] Another study revealed that Hedgehog signalling is reduced in aged endometrial stem cells, and the introduction of exogenous Hedgehog signalling has demonstrated antisenescence effects by modulating SERPINB2.[16] However, its effect and mechanism in cancer remain unknown. The crosstalk between Notch and Hedgehog signalling pathways in cancer senescence is complex and context-dependent.[12] Crosstalk between these pathways can either synergistically enhance or antagonistically regulate senescence outcomes in cancer cells, influencing tumour behaviour and therapy responses.[12,17]

HER2-positive breast cancer is characterised by overexpression of the HER2 receptor, making it a target for trastuzumab, a monoclonal antibody that inhibits HER2 signalling.[18] However, resistance to trastuzumab remains a significant challenge, leading to disease recurrence and poor prognosis. Targeting senescence pathways is gaining traction as a strategy to overcome trastuzumab resistance.[19] Trastuzumab resistance in human epidermal growth factor receptor 2-positive cancers arises from several mechanisms. One key factor is alterations in the HER2 receptor, such as truncated forms like p95HER2, which lack the extracellular domain targeted by trastuzumab, rendering it ineffective.[20] Increased HER2 expression or amplification can also saturate the drug's capacity to block all receptors. Another factor is the activation of alternative signalling pathways like the PI3K/AKT/mTOR pathway, which is often driven by PIK3CA mutations, bypassing HER2 inhibition, whereas HER family receptors, such as HER3 or EGFR, can continue oncogenic signalling.[21] The dysregulation of downstream signalling, including PTEN loss, further enhances resistance by hyperactivating these pathways. Epigenetic changes and immune evasion also play roles, altering HER2 signalling and diminishing

trastuzumab's efficacy by reducing antibody-dependent cell-mediated cytotoxicity (ADCC).[22] Additionally, upregulation of stemness pathways (e.g., Notch, Hedgehog, Wnt) and changes in cell surface integrins enable cancer cells to bypass HER2 reliance.[19] Finally, trastuzumab internalisation and degradation within lysosomes limit its availability over time.[23] Together, these mechanisms create a complex resistance landscape that requires novel therapeutic approaches.

Notch and Hedgehog signalling pathways contribute to trastuzumab resistance by promoting cell survival and proliferation. Understanding how these pathways interact with HER2 signalling in trastuzumab-resistant cells is crucial.[24] Inhibiting Notch and Hedgehog signalling has been shown to enhance the expression of senescence-associated markers, such as p16^{INK4a} and p21^{CIP1}, leading to growth arrest and reduced tumorigenicity in resistant cell lines.[25] Combining senescence-inducing agents with trastuzumab may provide a novel therapeutic approach to overcome resistance in HER2-positive breast cancer. The original value of this study can be found in its investigation of how the combination of trastuzumab and cilengitide affects cellular senescence in HER2-positive breast cancer cells that have developed resistance to trastuzumab. Previous research has focused on how these treatments reduce stemness and epithelial-mesenchymal transition (EMT)[3,4], but their effects on cellular senescence have not yet been explored in detail. This study demonstrated that this combination therapy upregulates senescence markers in trastuzumab-resistant cells and inhibits the Notch and Hedgehog signalling pathways, both of which play crucial roles in cancer progression. The involvement of specific inhibitors such as Fli06 and GANT61 to further suppress these pathways was also examined, suggesting a potential therapeutic strategy for overcoming drug resistance. The findings of this study indicate that targeting senescence pathways could be an effective strategy for addressing trastuzumab resistance in HER2-positive breast cancer, providing new directions for combination therapies. This study provides new insights into the molecular mechanisms of drug resistance and highlights a novel approach that could improve therapeutic outcomes for patients.

MATERIALS AND METHODS

Cell Culture

HCC1954 (ATCC Cat#CRL2338) and SKBR3 (ATCC Cat#HTB30) are well-known HER2-positive breast cancer cell lines, particularly recognised for their capacity to develop resistance to trastuzumab. These cell lines were cultured in DMEM supplemented with 10% FBS, 1% sodium pyruvate, and 2 mM L-glutamine. To induce trastuzumab resistance in HCC1954 and SKBR3, the cells were subjected to a gradual increase in trastuzumab concentrations (0.1–10 μM) over a period of three months. The development of resistance in these newly established cell lines was confirmed through MTT viability as-

says, with IC_{50} values calculated as described in our previous publication.[3] Chronic exposure to trastuzumab led to a marked increase in resistance, as evidenced by elevated IC_{50} values. The IC_{50} of SKBR3 cells exhibited a marked increase from approximately 0.2 μM to 2.6 μM, whereas that of HCC1954 cells, the IC_{50} dose from approximately 0.3 μM to 2.4 μM. The IC_{50} values for cilengitide were previously determined to be 0.8 μM for SKBR3-P, 0.6 μM for SKBR3-R, 0.6 μM for HCC1954-P, and 0.7 μM for HCC1954-R, as reported in earlier studies.[3,4]

Quantitative Real-Time PCR

Total RNA was isolated from SKBR3-P, SKBR3-R, HCC1954-P, and HCC1954-R cells using a Qiagen RNeasy Kit according to the manufacturer's instructions. cDNA synthesis was performed using 1 μg of RNA and the iScript Reverse Transcription Supermix for RT-qPCR (Bio-Rad). PCR amplification was conducted with the iTaq Universal SYBR Green One-Step Kit (Bio-Rad), with cycle threshold (Ct) values recorded on the ABI 7500 Real-Time PCR System (Applied Biosystems) and analysed using 7500 Software v1. The PCR protocol included an initial denaturation at 95 °C for 10 s, followed by 45 cycles of 95 °C for 10 s and 60 °C for 1 min. A subsequent melting curve analysis was carried out at 95 °C for 15 s, 60 °C for 1 min, and 95 °C for 15 s.

Real-time PCR primers were designed using the Primer3 programme and synthesised by Macrogen (sequences provided in Table 1). Each PCR reaction was performed in triplicate for each sample and primer set, and technical replicates were included. The entire experiment was independently repeated three times using different biological samples. The RT-qPCR data were normalised to the housekeeping gene GAPDH. The ΔCt value was calculated as ΔCt = Ct (target gene) Ct (housekeeping gene). Fold changes were determined using the $2^{-\Delta Ct}$ method, and relative expression levels were calculated using the $2^{-\Delta\Delta Ct}$ formula, where $2^{-\Delta Ct}$ (sample) was divided by $2^{-\Delta Ct}$ (control). The real-time PCR primers used in these experiments are listed in Table 1.

Heatmap Generation

Heatmaps were created using Python with the NumPy, Matplotlib, and Seaborn libraries. Python code was run in the Google Colab environment to produce the heatmap visualisation. Initially, the data—consisting of gene names (row labels), cell line names (column labels), and their associated quantitative values—was organised into a NumPy array. The data matrix was then visualised with the Seaborn library's heatmap function, utilising a diverging colour palette to differentiate between positive and negative values. The axes were appropriately labelled, and the heatmap was generated using Matplotlib.

Statistical Analysis

Statistical analysis was conducted with precision using two-way analysis of variance (ANOVA) to assess the interactions between the experimental variables. This was followed by Tukey's post hoc test to identify specific pairwise differences among the groups. Statistical significance was defined as follows: $*p \leq 0.05$, $**p \leq 0.01$, $***p \leq 0.001$, and $****p \leq 0.0001$. The error bars in the figures represent the mean ± standard deviation (SD), calculated from three independent experiments, each conducted in triplicate, ensuring the robustness and reproducibility of the data.

Table 1. Real-time PCR primers used in experiments.

GENE	SEQUENCE	Product length
AIF	F: GGCTGGATGAGATCAACAAGC	247
	R: TCAGGGTAGCTGAACGTCTC	
CCL3	F: TGTCCTCCTCTGCACCATG	173
	R: TGGTTAGGAAGATGACACCGG	
CST3	F: GTCGGCGAGTACAACAAAGC	194
	R: GCTTTCCTTTTCAGATGTGGC	
CSTA	F: CGCCACTCCAGAAATCCAGG	208
	R: CAAGTCCTCATTTTGTCCGGG	
CTTS	F: TGGGAGACATGACCAGTGAAG	153
	R: TCACTTCAGTAACACACCCTTTC	
CXLC8	F: TCTGTGTGAAGGTGCAGTTTTG	150
	R: ACAATAATTTCTGTGTTGGCGC	
FCER1G	F: TGGTCTTGCTCTTACTCCTTTTG	216
	R: CGTAAGTCTCCTGGTTCCTG	
FCN1	F: AGGTGTCATTGGAGAGAGAGG	175
	R: CCGGTCTAGCAGGTCCTTG	
G0S2	F: GATGGTGAAGCTGTACGTGC	193
	R: CTGCTTGCCTTTCTCCTGC	
LST1	F: CGAAGAGTAAAGAGGCTGGAG	184
	R: TGGGTTTGTTCTCAGCAATGC	
LYZ	F: AAGGTGTGAGTTGGCCAGAAC	241
	R: CAAAGCACTGCAGGATAAATGAC	
PSAP	F: TATGCTGAAGGACAATGCCAC	162
	R: CCAGGACGGCTCATTTCTCC	
S100A8	F: AATTTCCATGCCGTCTACAGG	205
	R: CTTTGTGGCTTTCTTCATGGC	
S100A9	F: ACCAATACTCTGTGAAGCTGG	230
	R: CTCGTGCATCTTCTCGTGG	
S100A11	F: ATCGAGTCCCTGATTGCTGTC	164
	R: TCCAGTTTCTTCATCATGCGG	
S100A12	F: AATACTCAGTTCGGAAGGGGC	214
	R: TGGTAATGGGCAGCCTTCAG	
SAT1	F: ATACTGCGGCTGATCAAGGAG	212
	R: TTGCCAATCCACGGGTCATAG	
SERPINA1	F: CCACGATATCATCACCAAGTTCC	202
	R: CTTATGCACGGCCTTGGAGAG	
TRYOBP	F: TAAGTGGTCTCCGTCCTGTCC	200
	R: AGTGATACGCTGTTTCCGGG	
NEAT1	F: GGCACAAGTTTCACAGGCCTACATGGG	205
	R: GCCAGAGCTGTCCGCCCAGCGAAG	

RESULTS

Trastuzumab Plus Cilengitide Combination Increases Senescence in Markers

To analyse the effect of this combination on senescence, senescence-responsive gene expression was assessed using real-time PCR in trastuzumab-resistant SKBR3 and HCC1954 cells. A panel of 20 established genes associated with human and cellular ageing was employed, including *S100A9, CXCL8, CST3, TYROBP, LST1, FCN1, FCER1G, LYZ, CCL3, S100A8, CTSS, AIF1, S100A12, SAT1, G0S2, S100A11, PSAP, NEAT1, CSTA*, and *SERPINA1* (Figure 1).

In both cell lines, combination treatment led to significant upregulation of senescence markers, with strong statistical significance. No changes were detected in the expression of dimethyle sulfoxide (DMSO) or trastuzumab alone. Although cilengitide monotherapy-induced moderate upregulation, the combination of cilengitide and trastuzumab consistently resulted in the highest levels of marker expression. These results suggest that this combination treatment exerts a synergistic effect, enhancing the upregulation of senescence markers in both SKBR3 and HCC1954 cell lines.

Trastuzumab Plus Cilengitide Combination Decreases Notch and Hedgehog-Responsive Gene Expressions

Previously, an increase in Notch and Hedgehog pathways in HER2-positive cells was demonstrated. It was also shown that Notch signalling is reduced by the combination of trastuzumab and cilengitide although its impact on the Hedgehog pathway has not been established. Given the critical crosstalk between these pathways, the effects of trastuzumab and cilengitide were assessed both individually and in combination. The results revealed that cilengitide, either alone or in combination with trastuzumab, significantly decreased Notch and Hedgehog signalling responses in SKBR3 and HCC1954–resistant cells (Figure 2). No alterations in signalling were observed with DMSO or trastuzumab alone. Additionally, cilengitide monotherapy was less effective than combination treatment in inhibiting Notch and Hedgehog signalling in both cell lines.

Combined Inhibition of Notch and Hedgehog Signalling Induce Senescence

Given the observed reduction in Notch and Hedgehog signalling pathways from the combination of trastuzumab and cilengitide, Notch and Hedgehog inhibitors were employed to investigate whether similar effects on senescence markers could be achieved. First, the effects of Notch and Hedgehog inhibitors on SKBR3 and HCC1954-resistant cells were analysed using different concentrations (0.01, 0.1, and 1 µM). To assess Notch pathway inhibition, the expression levels of *Hes, Hey, Gata3,* and *Ptcra* genes were evaluated. For Hedgehog pathway inhibition, the expression levels of *Gli1, Gli2, Hhip, Ptch1*, and *Ptch2*
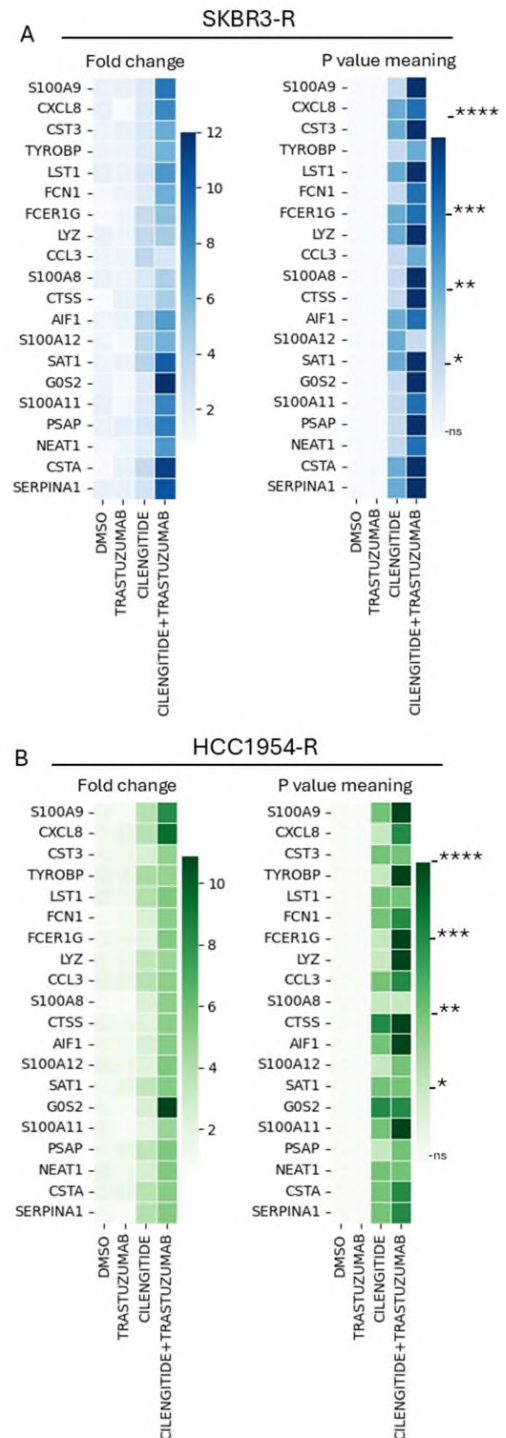
Figure 1. Senescence-responsive gene expression induced by cilengitide + trastuzumab combination therapy in HER2-positive trastuzumab-resistant cell lines. Resistance to DMSO, trastuzumab, and cilengitide monotherapy and cilengitide+trastuzumab combination therapy in (A) SKBR3 and (B) HCC1954 cells. Statistical analysis was performed using a two-way ANOVA variation test and Tukey's post hoc test to determine significance. Differences were considered significant as non-significant (ns) p > 0.05, * p≤0.05, **p≤0.01, ***p≤0.001, ****p≤0.0001, n = 3.
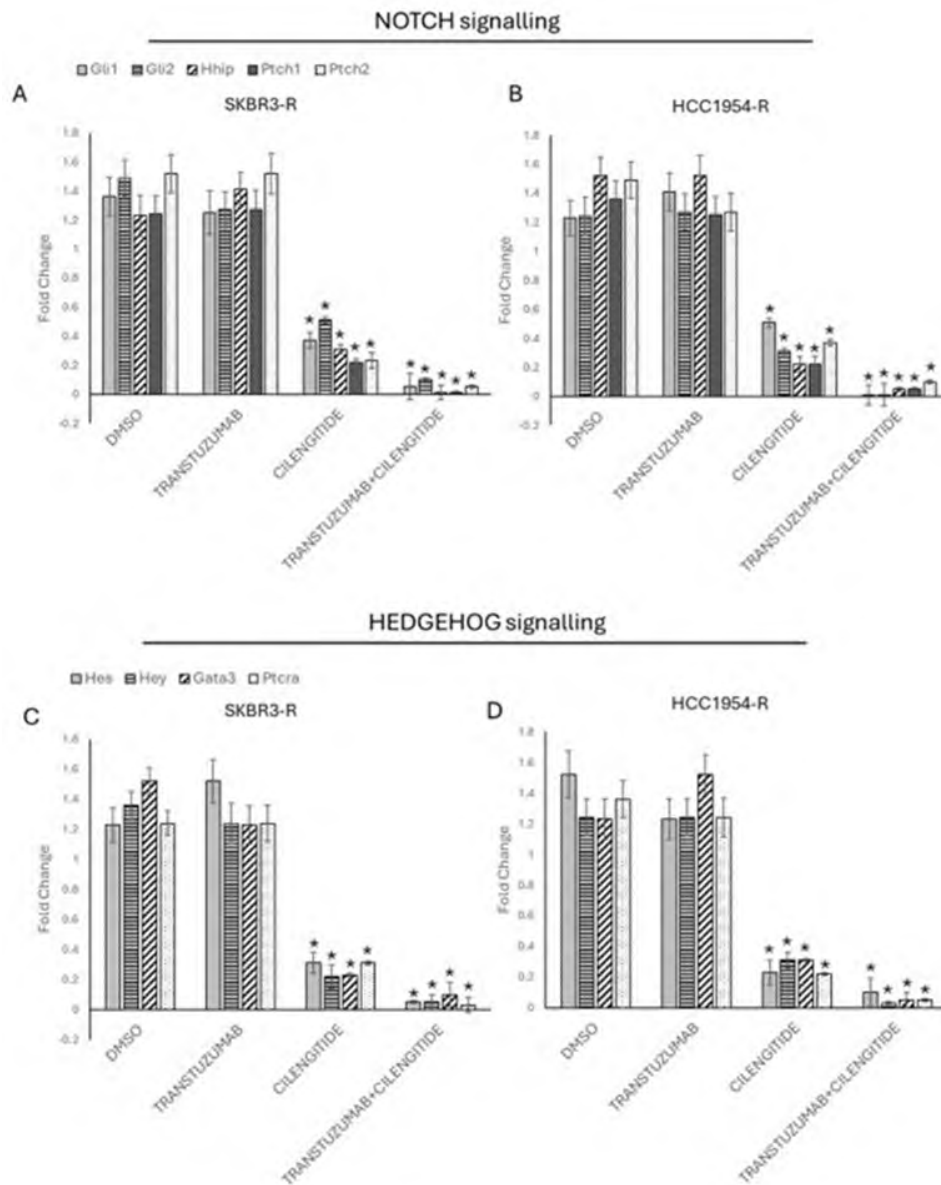
Figure 2. Trastuzumab + celangitide combination decreases NOTCH and HEDGEHOG responsive gene expressions. Cilengitide monotherapy and trastuzumab + cengitide combination decrease NOTCH-responsive gene expression in A) SKBR3-R, B) HCC1954-R cells, and Hedgehog-responsive expression in C) SKBR3-R, D) HCC1954-R cells. R: resistance. Statistical analysis was performed using a two-way ANOVA variation test and Tukey's post hoc test to show significance * $p \leq 0.05$, n=3.

genes were analysed (Figure 3). 1 µM of Fli06 and GANT61 showed significant decreases in both pathways and were used in further experiments. This study elucidated whether cilengitide and trastuzumab induce senescence markers via the Notch and Hedgehog pathways. To this end, the Notch inhibitor Fli06 and the Hedgehog inhibitor GANT61 were administered individually or in combination. RNA was collected 6 h following incubation with 1 µM Fli06 and GANT61 (Doses were determined based on their effects on the pathways as shown Figures 3A-D). While individual inhibition of Notch and Hedgehog pathways resulted in moderate increases in senescence markers, combined inhibition of both pathways led to a more pronounced up-

regulation of these markers in SKBR3- and HCC1954-resistant cells (Figure 4). DMSO-treated resistant cells were used as a control for comparison.

DISCUSSION

Senescence, characterised by irreversible cell growth arrest, plays a pivotal role in cancer biology by suppressing tumours and influencing their response to treatment.[26] Previous research has demonstrated that combining trastuzumab with cilengitide significantly reduces stemness and EMT in both trastuzumab-resistant and -sensitive HER2-positive cell lines.[4]
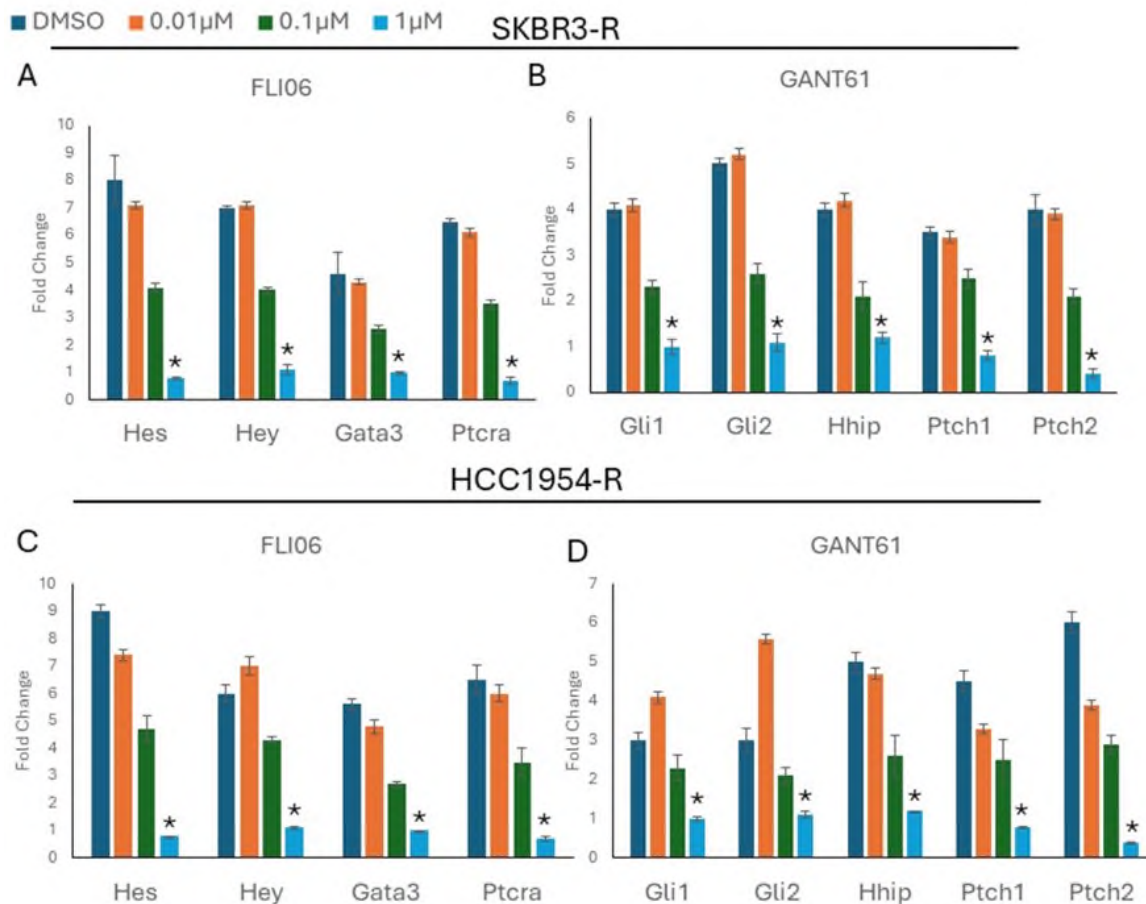
Figure 3. FLI06 decreased the Notch pathway and GANT61 decreased the Hedgehog pathway dose dependently. Notch responsive gene expressions analysed in the presence of FLI06 in a dose-dependent manner (A) in SKBR3-R, C) HCC1954-R. B) Hedgehog responsive gene expressions analysed in the presence of GANT61 in a dose-dependent manner (B) in SKBR3-R and D) HCC1954-R cells. R: resistance. Statistical analysis was performed using one-way ANOVA variation test and Tukey's post hoc test to show significance * $p \leq 0.05$, n=3.

However, the impact of this combination on senescence has not been explored. In this study, the combination of trastuzumab and cilengitide significantly upregulated senescence markers in trastuzumab-resistant HER2-positive cell lines. This finding aligns with research suggesting that targeting senescence pathways could be a novel approach to overcome cancer resistance. It has been shown that senescence can suppress tumour progression by halting the growth of resistant cells. For instance, senescence-associated secretory phenotypes (SASP) can alter the tumour microenvironment, thereby making it less favourable for tumour growth.[27]

The effects of trastuzumab and cilengitide combination on senescence were more pronounced compared with either treatment alone, suggesting a synergistic interaction between trastuzumab and cilengitide in promoting senescence. These findings underscore a promising new approach to overcoming trastuzumab resistance in HER2-positive breast cancer by

inducing cellular senescence. Cilengitide, known to influence various cellular processes such as survival, proliferation, and senescence, has been the subject of debate regarding its effects on senescence.[27] Studies have reported both pro- and antisenescent effects depending on the cellular context and specific integrins . This study contributes to the literature by demonstrating that cilengitide, an RGD-binding integrin inhibitor, can induce senescence in HER2-positive breast cancer cells. This finding agrees with other studies showing that CWHM12, another RGD-mimicking integrin blocker, enhances senescence in hepatic stellate cells.[7-10]

Further investigation into the underlying signalling pathways revealed that the combination of trastuzumab and cilengitide significantly reduces Notch and Hedgehog signalling responses in resistant cell lines.[3,4] These pathways are critical for development, tissue homeostasis, and cancer progression. The results suggest that the upregulation of senescence markers in
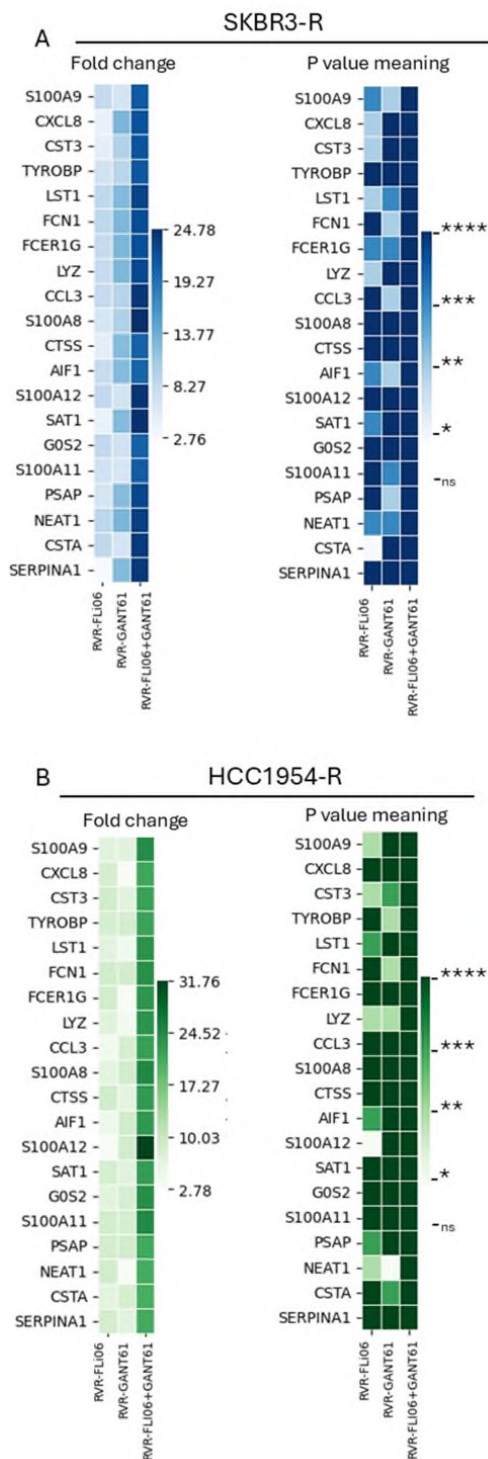
Figure 4. Senescence-responsive gene expression induced by the combined inhibition of the NOTCH and HEDGEHOG pathways in HER2-positive trastuzumab-resistant cell lines. Resistant cells compared with resistant cells treated with Fli06, GANT61, or Fli06+GANT61 in (A) SKBR3 and (B) HCC1954 cells. Statistical analysis was performed using a two-way ANOVA variation test and Tukey's post hoc test to determine significance. Differences were considered significant as non-significant (ns) $p > 0.05$, * $p \leq 0.05$, **$p \leq 0.01$, ***$p \leq 0.001$, ****$p \leq 0.0001$, n = 3.

trastuzumab-resistant cell lines is achieved through the inhibition of both Notch and Hedgehog pathways, either through the combination of trastuzumab and cilengitide or through specific inhibitors (Fli06 for Notch and GANT61 for Hedgehog). This indicates that the pro-senescent effects of the trastuzumab-cilengitide combination are, at least in part, mediated by inhibiting these pathways. This study provides new insights into how targeting these pathways can overcome trastuzumab resistance, highlighting the complex and context-dependent crosstalk between Notch and Hedgehog signalling in cancer senescence. These findings reinforce the expanding body of evidence that targeting senescence pathways is a promising strategy for overcoming trastuzumab resistance in HER2-positive breast cancer. The results clearly demonstrate that the inhibition of Notch and Hedgehog signalling pathways can drive cancer cells towards senescence, which acts as a barrier to tumour progression. Previous research supports this, indicating that the modulation of Notch signalling can either promote or suppress senescence, depending on the cancer type and context.[28,29] For instance, studies have shown that Notch1 and Notch2 upregulate p21 and p16, key regulators of senescence.[29]

Similarly, Hedgehog signalling, which maintains stem cell properties in cancer cells, plays a vital role in treatment resistance. By inhibiting this pathway with agents like GANT61, cancer cells become more sensitive to therapy, as shown in glioblastoma models.[10,17] The synergistic effect observed with the combination of trastuzumab and cilengitide, as outlined in this study, further supports the idea that integrating senescence-inducing agents into treatment regimens can significantly improve therapeutic outcomes in trastuzumab-resistant cancers.[2,19] Furthermore, the findings align with prior research indicating that integrin inhibitors like cilengitide, which target RGD-binding integrins, disrupt cancer cell adhesion and migration, thereby enhancing the effects of other therapies like trastuzumab.[1,4] This study provides compelling evidence for the clinical potential of combining trastuzumab with agents that target senescence pathways, providing a robust approach to improving treatment efficacy in patients with HER2-positive breast cancer who are resistant to current therapies.

CONCLUSION

In conclusion, the combination of trastuzumab and cilengitide induces senescence in HER2-positive trastuzumab-resistant cell lines and may be inhibited through Notch and Hedgehog signalling pathways. The data presented, not only highlight the potential of combining trastuzumab with cilengitide and underscore the need for further investigation into the crosstalk between Notch and Hedgehog signalling in the context of resistance. Ultimately, targeting senescence pathways is a compelling strategy for improving therapeutic outcomes in HER2-positive breast cancer, particularly in the setting of trastuzumab resistance. This approach could pave the way for more effective

combination therapies that enhance the durability of responses in cancer treatment.

These findings provide a promising new strategy for overcoming trastuzumab resistance in HER2-positive breast cancer and highlight the potential of senescence-inducing therapies as part of a comprehensive treatment approach. Further studies are warranted to explore the clinical implications of these findings and identify additional targets within the senescence pathways that could enhance the efficacy of current therapies.

Ethics Committee Approval: Ethics committee approval is not required for the study.

Peer Review: Externally peer-reviewed.

Author Contributions: Conception/Design of Study- I.E., A.B.B.E.; Data Acquisition- I.E., A.B.B.E.; Data Analysis/Interpretation- I.E., A.B.B.E.; Drafting Manuscript- I.E., A.B.B.E.; Critical Revision of Manuscript- I.E., A.B.B.E.; Final Approval and Accountability- I.E., A.B.B.E.

Conflict of Interest: Authors declared no conflict of interest.

Financial Disclosure: Authors declared no financial support.

ORCID IDs of the Authors

Asiye Busra Boz Er   0000-0002-1275-4470
Idris Er   0000-0003-2139-1787

REFERENCES

1. Bousset L, Gil J. Targeting senescence as an anticancer therapy. *Mol Oncol.* 2022;16(21):3855-3880.

2. McHugh D, Gil J. Senescence and aging: Causes, consequences, and therapeutic avenues. *J Cell Biol.* 2018;217(1):65-77.

3. Boz Er AB. Integrin beta3 reprogramming stemness in HER2-positive breast cancer cell lines. *Biology (Basel).* 2024;13(6). doi:10.3390/biology13060429

4. Boz Er AB, Er I. Targeting ITG3 to overcome trastuzumab resistance through epithelial–mesenchymal transition regulation in HER2-positive breast cancer. *Int J Mol Sci.* 2024;25(16):8640. doi: 10.3390/ijms25168640

5. Pan X, Yi M, Liu C, et al. Cilengitide, an alphavbeta3-integrin inhibitor, enhances the efficacy of anti-programmed cell death-1 therapy in a murine melanoma model. *Bioengineered.* 2022;13(2):4557-4572.

6. Pang X, He X, Qiu Z, et al. Targeting integrin pathways: Mechanisms and advances in therapy. *Signal Transduct Target Ther.* 2023;8(1):1. doi:10.1038/s41392-022-01259-6

7. Kitsugi K, Noritake H, Matsumoto M, et al. Inhibition of integrin binding to ligand arg-gly-asp motif induces AKT-mediated cellular senescence in hepatic stellate cells. *Mol Cell Biochem.* 2023;479(10):2697-2710.

8. Fujita M, Sasada M, Eguchi M, et al. Induction of cellular senescence in fibroblasts through beta1-integrin activation by tenascin-C-derived peptide and its protumor effect. *Am J Cancer Res.* 2021;11(9):4364-4379.

9. Rapisarda V, Borghesan M, Miguela V, et al. Integrin beta 3 regulates cellular senescence by activating the TGF-beta pathway. *Cell Rep.* 2017;18(10):2480-2493.

10. Franovic A, Elliott KC, Seguin L, Camargo MF, Weis SM, Cheresh DA. Glioblastomas require integrin alphavbeta3/PAK4 signaling to escape senescence. *Cancer Res.* 2015;75(21):4466-4473.

11. Wang B, Han J, Elisseeff JH, Demaria M. The senescence-associated secretory phenotype and its physiological and pathological implications. *Nat Rev Mol Cell Biol.* 2024. doi:10.1038/s41580-024-00727-x

12. Borah A, Kumar DS. Chapter 8 - Targeting the Hedgehog and Notch Signaling Pathways in Cancer Stem Cells. In: Dammacco F, Silvestris F, eds. *Oncogenomics.* Academic Press; 2019:103-120.

13. Yoshida Y, Hayashi Y, Suda M, et al. Notch signaling regulates the lifespan of vascular endothelial cells via a p16-dependent pathway. *PLoS One.* 2014;9(6):e100359. doi:10.1371/journal.pone.0100359

14. Lainez-Gonzalez D, Serrano-Lopez J, Alonso-Dominguez JM. Understanding the Notch signaling pathway in acute myeloid leukemia stem cells: From Hematopoiesis to Neoplasia. *Cancers (Basel).* 2022;14(6). doi:10.3390/cancers14061459

15. Zou Y, Wu S, Hu Q, et al. Sonic hedgehog restrains the ubiquitin-dependent degradation of SP1 to inhibit neuronal/glial senescence associated phenotypes in chemotherapy-induced peripheral neuropathy via the TRIM25-CXCL13 axis. *J Adv Res.* 2024. doi:10.1016/j.jare.2024.03.006

16. Cho A, Park SR, Kim SR, et al. An endogenous anti-aging factor, sonic hedgehog, suppresses endometrial stem cell aging through SERPINB2. *Mol Ther.* 2019;27(7):1286-1298.

17. Kumari R, Jat P. Mechanisms of cellular senescence: Cell cycle arrest and senescence associated secretory phenotype. *Front Cell Dev Biol.* 2021;9:645593. doi:10.3389/fcell.2021.645593

18. Swain SM, Shastry M, Hamilton E. Targeting HER2-positive breast cancer: Advances and future directions. *Nat Rev Drug Discov.* 2023;22(2):101-126.

19. Takebe N, Miele L, Harris PJ, et al. Targeting Notch, Hedgehog, and Wnt pathways in cancer stem cells: clinical update. *Nat Rev Clin Oncol.* 2015;12(8):445-464. doi:10.1038/nrclinonc.2015.61

20. Zagozdzon R, Gallagher WM, Crown J. Truncated HER2: Implications for HER2-targeted therapeutics. *Drug Discov Today.* 2011;16(17-18):810-816. doi:10.1016/j.drudis.2011.06.003

21. Prasad D, Baldelli E, Blais EM, et al. Functional activation of the AKT-mTOR signalling axis in a real-world metastatic breast cancer cohort. *Br J Cancer.* 2024;131:1543–1554

22. Khan SU, Fatima K, Aisha S, Malik F. Unveiling the mechanisms and challenges of cancer drug resistance. *Cell Commun Signal.* 2024;22(1):109. doi:10.1186/s12964-023-01302-1

23. Maass KF, Kulkarni C, Betts AM, Wittrup KD. Determination of cellular processing rates for a trastuzumab-maytansinoid antibody-drug conjugate (ADC) highlights key parameters for ADC design. *AAPS J.* 2016;18(3):635-646.

24. Ali K, Nabeel M, Mohsin F, et al. Recent developments in targeting breast cancer stem cells (BCSCs): A descriptive review of therapeutic strategies and emerging therapies. *Med Oncol.* 2024;41(5):112. doi:10.1007/s12032-024-02347-z

25. Duro-Sanchez S, Nadal-Serrano M, Lalinde-Gutierrez M, et al. Therapy-induced senescence enhances the efficacy of HER2-targeted antibody-drug conjugates in breast cancer. *Cancer Res.* 2022;82(24):4670-4679.

26. Billimoria R, Bhatt P. Senescence in cancer: Advances in detection and treatment modalities. *Biochem Pharmacol.* 2023;215:115739. doi:10.1016/j.bcp.2023.115739

27. Di Micco R, Krizhanovsky V, Baker D, d'Adda di Fagagna F. Cellular senescence in ageing: from mechanisms to therapeutic opportunities. *Nat Rev Mol Cell Biol.* 2021;22(2):75-95. doi:10.1038/s41580-020-00314-w

28. Nowell CS, Radtke F. Notch as a tumour suppressor. *Nat Rev Cancer.* 2017;17(3):145-159.

29. Andersson ER, Sandberg R, Lendahl U. Notch signaling: Simplicity in design, versatility in function. *Development.* 2011;138(17):3593-3612.

How to cite this article

Sideritis perfoliata Ethanolic Extract Mitigates Acetic Acid-Induced Ulcerative Colitis in Rats

Dilek Ozbeyli[1] ![iD], Ali Sen[2] ![iD], Naziye Ozkan Yenal[3] ![iD], Ayse Nur Hazar Yavuz[4] ![iD], Deniz Mukaddes Turet[5] ![iD], Meral Yuksel[6] ![iD], Leyla Bitis[2] ![iD], Ahmet Dogan[7] ![iD], Asli Aykac[8] ![iD]

[1]Marmara University, Vocational School of Health Services, Department of Medical Services and Techniques, Istanbul, Türkiye

[2]Marmara University, Faculty of Pharmacy, Department of Pharmacognosy, Istanbul, Türkiye

[3]Marmara University, Vocational School of Health Services, Department of Pathology Laboratory Techniques, Istanbul, Türkiye

[4]Marmara University, Faculty of Pharmacy, Department of Pharmacology, Istanbul, Türkiye

[5]Aziz Sancar Institute of Experimental Medicine, Department of Laboratory Animals Science, Istanbul University, Istanbul, Türkiye

[6]Marmara University, Vocational School of Health Services, Department of Medical Laboratory Techniques, Istanbul, Türkiye

[7]Marmara University, Faculty of Pharmacy, Department of Pharmaceutic Botanic, Istanbul, Türkiye

[8]Near East University, Vocaional School of Health Services, Department of Biophysics, Mersin, Türkiye

ABSTRACT

Objective: This study evaluated the antioxidant and anti-inflammatory effects of *Sideritis perfoliata* (SP) ethanolic extract *in vitro* and its impact on anti-inflammatory, antiapoptotic, oxidative stress, and tissue damage-related parameters in an ulcerative colitis (UC) rat model.

Materials and Methods: Dried and ground aerial parts of SP were extracted with 90% ethanol using maceration. Then, the SP extract's radical scavenging, anti-5-lipoxygenase (LOX) activities, and total secondary metabolic quantities were evaluated *in vitro*. In *in vivo* experiments, following acetic acid (AA)-induced colitis, physiological saline (PS) (1 mL, og), sulfasalazine (SS) (100 mg/kg bwt, 1mL, og), and SP extract (200 mg/kg bwt, 1mL, og) treatments were administered to AA, SS, and SP groups, respectively, once daily for three consecutive days. PS was given to the control group. At the 72nd hour, the rats were euthanized. Analyses were performed on colon tissues using ELISA, Chemiluminescence assay, Haematoxylin and Eosin staining.

Results: SP extract exhibited good antioxidant activity against 2,2'-azino-bis(3-ethylbenzthiazoline-6-sulfonic acid) (ABTS) and 2,2-diphenyl-1-picrylhydrazyl (DPPH) radicals and strong anti-5-LOX activity. The total amounts of phenol, flavonoid, and triterpene compounds in the extract were determined. Compared with the AA group, SS or SP extract treatments reduced tumour necrosis factor-α, interleukin-1β, interleukin-17, tool-like receptor-9, matrix metalloproteinases-3, caspase-9, caspase-3, luminol, and lucigenin chemiluminescence levels, macroscopic and microscopic morphological scores in colon.

Conclusion: Due to its flavonoids, phenolic acids, triterpene content, anti-5-LOX, and free radical scavenging activities, SP extract attenuates proinflammatory cytokines, mitochondrial apoptotic caspases, and oxidative stress. Our findings support the ethnopharmacological use of SP for colitis.

Keywords: *Sideritis perfoliata*, Ulcerative colitis, Cytokines, Apoptosis, Oxidative stress.

INTRODUCTION

Among the most prevalent signs of inflammatory bowel disease (IBD), a recurrent, chronic illness mediated by the immune system, are abdominal pain and bloody diarrhoea. Ulcerative colitis (UC) is one of the two most prevalent types of IBD.[1,2] It is more common in Europe and North America than globally in Africa and South America.[3] In contrast, the prevalence of the disease has increased in low-incidence countries, whereas the pace of increase in incidence has de-

clined in high-incidence countries, according to recent studies. These results underscore the potential for IBD to emerge as a worldwide health issue in the future and stress the need to promptly identify the underlying pathophysiology of the disease and determine suitable treatments.[2,3] In the hope of reducing both the physical and psychological effects of IBD, many people with IBD ($\cong$ 40%) use complementary and alternative medicines/products, the vast majority of which are herbal, in addition to their treatment.[4-6] Preclinical research highlights the therapeutic benefits of plants, which have been utilised for

millennia in conventional medicine.[7,8] According to published research, nutraceuticals high in polyphenols and antioxidants are beneficial because they can scavenge free radicals, trigger anti-inflammatory reactions, and control the gut microbiota's homeostasis.[9,10]

The most common sign of UC is inflammation of the colon's mucosal lining. The inflammatory pathway causes an increase in pro-inflammatory eukaryotic transcription factors such as activator protein-1 and nuclear factor-$\kappa\beta$, an increase in the production of pro-inflammatory cytokines (tumour necrosis factor (TNF)-α, interleukin (IL)-1β, and IL-6, and a decrease in anti-inflammatory cytokines such as IL-10. Increased levels of pro-inflammatory cytokines exacerbate inflammation and oxidative stress while decreasing antioxidant levels.[11-13] All these processes lead to increased inflammation, epithelial cell damage, neutrophil infiltration, and malfunction of the intestinal barrier.[14,15]

Among more than 140 species, *Sideritis perfoliata* (SP) is a wild plant primarily found in the Mediterranean region.[16,17] In Türkiye, the genus *Sideritis* comprises 45 species (53 taxa, more than 40 of which are endemic).[18] They are often referred to as "mountain tea" plants. Since the Dioscorides era, *Sideritis* species have been used in traditional medicine as a stimulant, carminative, appetite stimulant, and stomach stimulant.[19] *Sideritis* plants are used as tea, feed, and sweeteners. Due to its anti-inflammatory, antibacterial, anti-ulcerative, antirheumatic, wound-healing, antioxidant, antispasmodic, analgesic, stomachic, and carminative qualities, *Sideritis* species are widely utilised as traditional remedies. It is also traditionally used in Türkiye for stomach illnesses, colds, bronchitis, coughs, flu, sore throat, diabetes, and as a digestive aid.[20-24] Research reports on species of *Sideritis* have attributed these pharmacological properties to the genus due to the flavonoids, terpenoids, coumarins, sterols, and iridoids found in its chemical profile.[23,25] Previously, it procured diterpenoids, flavonoids, and phenylpropanoid glycosides from the aerial parts of SP[26,27] and SP exerted significant antioxidant and anti-inflammatory activity.[20] On the other hand, there is no information in the literature about the effects of SP on ulcerative colitis.

In light of the above information, this study investigated the antioxidant and anti-5-lipoxygenase (anti-5-LOX) effects of SP ethanolic extract *in vitro* and its impacts on anti-inflammatory, antiapoptotic, oxidative stress, and tissue damage-related parameters in acetic acid (AA)-induced UC in rats.

MATERIALS AND METHODS

Chemicals

AA, 2,2-diphenyl-1-picrylhydrazyl (DPPH), 2,2'-azino-bis(3-ethylbenzothiazoline-6-sulfonic acid) (ABTS), indomethacin, potassium persulfate, ascorbic acid, linoleic acid, trolox, lipoxidase from Glycine max (soybean), 3-Aminophthalhydrazide

(luminol), N, N'-Dimethyl-9,9'-biacridinium dinitrate (lucigenin), Folin-Ciocalteu reagent, formaldehyde, dithiothreitol (DTT), glycerol, Tris-HCl, Triton X-100, Ethylenediaminetetraacetic acid (EDTA), NaNO$_2$, AlCl$_3$·6H$_2$O, NaOH, methanol, ethanol, and aether were supplied by Sigma (Sigma-Aldrich, St. Louis, MO, USA). Sodium pentobarbital was obtained from IE Ulagay (Istanbul, Turkiye). Sulfasalazine (SS-Salazopyrin) was purchased from Pfizer (Istanbul, Turkiye). All other chemicals were of the highest quality commercially available.

Sourcing and Harvesting of Plant Materials

In July 2023, Dr. Bitis purchased the aerial parts of SP from a local plant market in the Bayramiç district of Çanakkale province and identified by Dr. Dogan. Some plant specimens were deposited at Marmara University, Faculty of Pharmacy Herbarium (International Code: MARE) (under herbarium no. 23481). The dried and ground aerial parts of SP (20.05 g) were extracted with 90% ethanol (3 x 100 mL) using the maceration method. The solvent of the extract was evaporated to dryness at a temperature not exceeding 45°C using a rotary evaporator to yield an ethanolic extract with 12.67% yield (g/g).

Validation of SP Extract's Radical Scavenging and Anti-Inflammatory Qualities *In Vitro*

The radical scavenging effects (represented by anti-ABTS and anti-DPPH radicals) of the SP extract were described by the method previously insisted on by Zou et al. (2011) as follows: 10 µL of the extract (stock solutions in the range 5000-9.77 µg/mL) dissolved in dimethyl sulfoxide (DMSO) was added to the well and mixed with ABTS or DPPH radical solution until the total volume was 200 µL.[28] After incubation (for 30 min in the dark), the mixtures on the plates (three times for each sample) were measured using 6-hydroxy-2,5,7,8-tetramethylchroman-2-carboxylic acid (Trolox) or ascorbic acid as reference standards using a spectrophotometer (517 or 734 nm).

SP extract, water (distilled), ethanol, sodium borate buffer (SBB, 0.1 M), and soybean 5-lipoxygenase (5-LOX) dissolved in SBB (10 µL, 10 µL, 20 µL, 20 µL, 25 µL, and 20,000 U/mL, respectively) were added to each well, incubated (for 5 min) and finally, linoleic acid solution (0.6 mM, 100 µL) was added to the mixture and stirred.[29] The absorbance of all samples was read at 234 nm to determine the amount of SP extract and indomethacin (reference standard) required to inhibit 5-LOX activity by 50% as IC$_{50}$ (µg/mL).

Assessment of the Total Secondary Metabolic Quantities of SP Extracts

The total phenolic content (TPC) of SP extracts was determined using the Folin-Ciocalteu colorimetric test by comparing the TPC of gallic acid (GA) (stock solutions in the range 500 - 15.63 µg/mL) (mg GA equivalent/g extract) used as the reference

standard.[30,31] The total flavonoid content (TFC) was calculated as quercetin (QUE) equivalent (mg QUE equivalent/g extract) for the SP extracts.[31,32] The determination of total triterpene content (TTC) for SP extract, which was carried out by adapting the method determined by Chang et al. (2012) to microplate, was carried out briefly with the following steps: before heating the plate at 60°C for 45 min, SP (10 µL, stock solution prepared at 5000 µg/mL concentration), vanillin-glacial AA solution (5% w/v), and perchloric acid solution (15 µL and 50 µL, respectively) were mixed in the plate.[33] The absorbance of the solutions in a plate cooled to room temperature with the help of an ice bath was evaluated at 548 nm after adding 225 µL of glacial AA. For the standard curve plot, absorbances corresponding to each concentration were determined using oleanolic acid (OLE) (1200-37.5 µg/mL). This graph was used to calculate the extract's TTC which was then expressed as milligrams of OLE equivalent per g of the SP extract.

Grouping of Rats in Experiments Based on Treatments

After obtaining approval from the Marmara University Local Ethics Committee for all experimental protocols, the rats (n=24) were obtained from the Marmara University Experimental Animal Application and Research Centre (Protocol number: 51.2023mar, Date: 2023). The male and female Wistar rats (age 3 months, 200-250 g) were randomly divided into 4 groups, with 3 males and 3 females in each group[34]: I) PS group: Sham and vehicle (Physiological saline-PS) treatment control group (n=6), II) AA group: AA-induced colitis+PS treatment group (n=6), III) SS group: AA-induced colitis+100 mg/kg bwt, SS treatment group (n=6),[35] and IV) SP group: AA-induced colitis+200 mg/kg bwt, SP extract treatment group (n=6).[36]

After an 8-hour fasting period, 5% AA (in 0.9% NaCl, pH: 3 total volume: 1 mL) was administered intrarectally (ir) with a 30% inclination using an 8-cm-long soft silicone catheter (6G) to rats in the AA, SS, and SP groups under aether anaesthesia (by inhalation). After waiting 30 s, the animals were placed back in the cage.[37] In the PS group, PS was applied to the rats in an equal volume (1 mL) and in a similar manner (ir) instead of AA. Following colitis induction, the treatment regimens (PS, SS, or SP extract) were administered via orogastric gavage (og) with a metal cannula (1 mL) and administered once a day for 3 days at the same time (at 24-hour intervals) and dosage. SS is a drug used for the treatment of active ulcerative colitis and for remission. Therefore, it is a treatment given to the positive control group in experimental studies. PS was similarly administered to the PS and AA groups (1mL/og). (Figure 1). In this model, signs of healing and regeneration of the mucosa were seen on the 7th day; therefore, we applied the treatments for 3 days in parallel with the practises in the literature.[38,39] At the end of the 72nd hour, the rats were euthanized with sodium pentobarbital (50 mg/kg bwt, ip).

In Vivo Assessment of SP Treatment Intervention in Rat Tissue from the Colon with AA-Induced UC

Lucigenin and luminol chemiluminescence levels, indicators of oxidative stress in rat colon tissue, were recorded using Mini Lumat. LB 9509 luminometer (EG&G Berthold, Germany). Counts were obtained at 1-min intervals for 5 min, as described by Haklar et al.[40]

In the colonic tissues obtained from the rat; cytokines (TNF-α, IL-1β, IL-10, IL-17), tool-like receptor-9 (TLR-9), mitochondrial-mediated apoptotic markers [caspase-3 and caspase-9], superoxide dismutase enzyme (SOD), and tissue damage indicator matrix metalloproteinase-3 enzyme (MMP-3) levels were measured using ELISA test kits which catalogue numbers are given respectively (E0764Ra, E0119Ra, E0108Ra, E0115Ra, E0082Ra, E1648Ra, E1898Ra, E1376Ra, E031Ra). These assay procedures were conducted using an Agilent Technologies Bio Tek Epoch Microplate spectrophotometer (450 nm) in compliance with the manufacturer's instructions (Bioassay Technology Laboratory (BT LAB, China).

Assessment of UC Severity and Response to Treatment Utilising Macroscopic and Microscopic Analysis

We graded the lesions that developed after harvesting and washing the 8-cm distal region of the colon using macroscopic scoring.[41] The samples were then photographed. For light microscopic evaluation, rat colonic tissue samples were fixed in 10% neutral-buffered formalin, dehydrated in a graded alcohol series, cleared with xylene, and embedded in paraffin wax. Then, 4 µm thickness sections were obtained and stained using Haematoxylin and Eosin (H&E) to study the general histological structure. The criteria for scoring and scale ranging were: damage/necrosis (0, none; 1, localised; 2, moderate; 3, severe); submucosal oedema (0, none; 1, mild; 2, moderate; 3, severe); inflammatory cell infiltration (0, none; 1, mild; 2, moderate; 3, severe); vasculitis (0, none; 1, mild; 2, moderate; 3, severe); perforation (0, absent; 1, present). The total score was 13.[42] Images were captured using a light microscope (Olympus CX21, Tokyo, Japan) and photographed using a camera (Olympus, Tokyo, Japan, BX51).

Statistical Analysis

Normality was assessed using the One-sample Kolmogorov-Smirnov test. Normally distributed data were analysed using Tukey's multiple comparison tests after analysis of one-way variance (ANOVA). Prism 6.0 (GraphPad Software, San Diego, California, USA) was used for statistical analysis. Results were expressed as mean ± S.E.M., and *p*-values of less than 0.05 were considered significant.
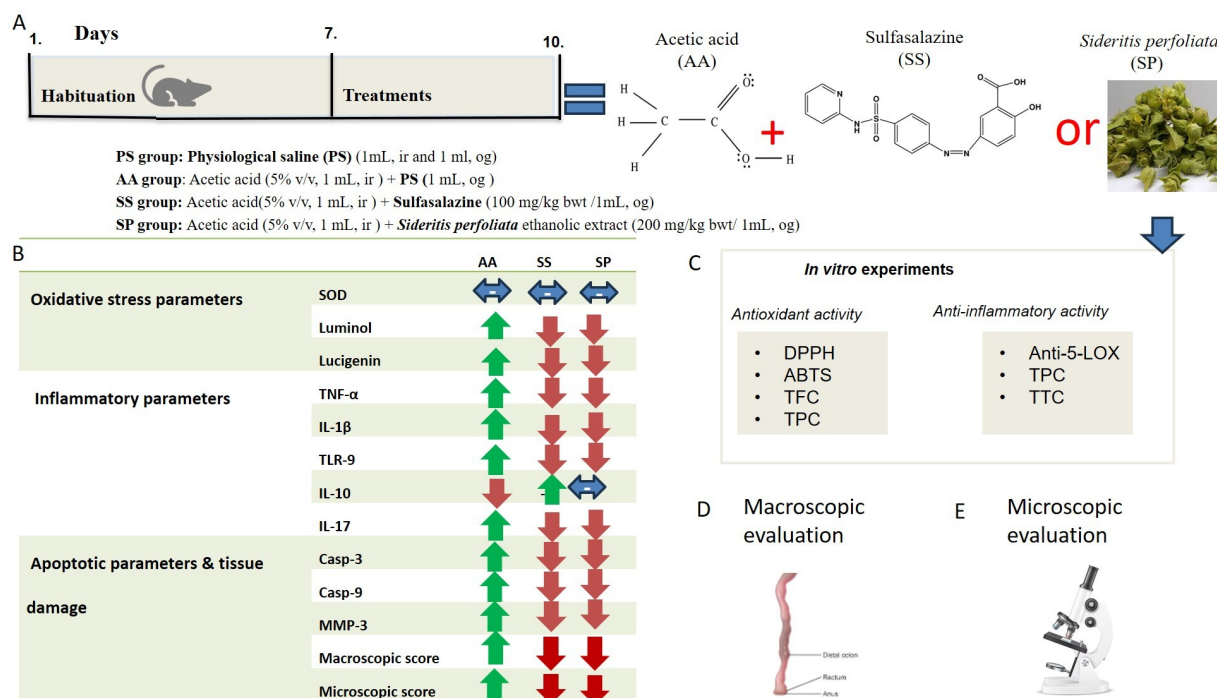
Figure 1. Experimental design. A. Following the habituation phase, the rats were randomly assigned to four experimental groups, each with 6 rats. I) PS group: Sham and vehicle (PS) treatment control group; II) AA group: AA-induced colitis+PS treatment group; III) SS group: AA-induced colitis+100 mg/kg bwt, SS treatment positive control group; IV) SP group: AA-induced colitis+200 mg/kg bwt, SP extract treatment group. After 8 h of fasting, acetic acid [1 mL 5% (v/v) in 0.9% saline] was administered intrarectally for colitis induction through a cannula. Treatments were applied for three days. B. Biochemical analyses. At the end of the 72nd h, the colon tissues of the euthanized rats were dissected for biochemical (ELISA) and other analyses. C. The radical-scavenging and anti- inflammatory properties of SP extract were verified in vitro. D. Macroscopic evaluation. E. Microscopic evaluation. **PS:** Physiological saline, **AA:** acetic acid, **SS:** Sulfasalazine, **SP:** *Sideritis perfoliata*, **ir:** intrarectally, **og:** orogastric.

RESULTS

In Vitro Evaluation of Antioxidant, Anti-Inflammatory, and Total Secondary Compounds in SP Extract

The IC_{50} values obtained because of DPPH radical analysis were determined to be 100.5±0.42 µg/mL for SP extract and 40.23±2.08 µg/g/mL for ascorbic acid used as a reference. The ABTS test results showed that the IC_{50} values for Trolox and SP extract, the reference standard, were 4.54±0.08 and 90.45±0.53, respectively. The antioxidant activity of the extract was evaluated as highly active when $IC_{50} \leq 10$ µg/mL, active when $10 < IC_{50} \leq 150$ µg/mL, moderately active when $150 < IC_{50} \leq 500$ µg/mL, and inactive when $IC_{50} > 500$ µg/mL according to the criteria proposed by Moga et al. (2021).[41] According to this criterion, SP extract was found to be active (good antioxidant activity) against DPPH and ABTS radicals.

The IC_{50} value of the extract against the 5-LOX enzyme was 17.64±0.45 µg/mL (compared to 21.42±0.48 µg/mL for conventional indomethacin), and the SP extract exhibited potent anti-inflammatory activity.

The TPC of the extract was calculated using the formula [y = 0.093x + 0.062 (R^2: 0.9987)] derived from the calibration curve defined as GA equivalent. The TPC of the extract was obtained at 140.8±1.21 mg GA equivalent per g of dried extract. The TFC of the extract was determined using the equation [y= 0.003x + 0.015 (R2: 0.9644)] obtained from the calibration curve as the QUE equivalent. The TFC of the extract was determined at 407.2±0.46 mg QUE equivalent per g of the dried extract. The TTC of the SP extract was determined using the equation [y = 0.027x + 0.016 (R2: 0.9981)] obtained from the calibration curve as the OLE equivalent. The TTC of the extract was determined at 85.97±1.66 mg OLE per g of dried extract.

In Vivo Results of Oxidative Stress, Inflammation, Apoptotic Tissue Damage, and SP Extract

The analyses revealed no statistically significant difference between the experimental groups in terms of SOD levels in colon tissue (Figure 2A). Colon luminol and lucigenin CL levels exhibited a notable increase in the AA group compared with the PS group (p<0.001). This elevation in luminol and lucigenin CL was diminished in both the SS and SP groups (p<0.001). The lucigenin level in the SS group did not deviate from the value found in the PS group, although the luminol value did not entirely revert to the PS value in the SS group (p<0.05; Figures 2B and 2C).

Compared with the PS group, colonic tissue levels of TNF-α, IL-1β, and TLR-9 in the AA group were considerably greater
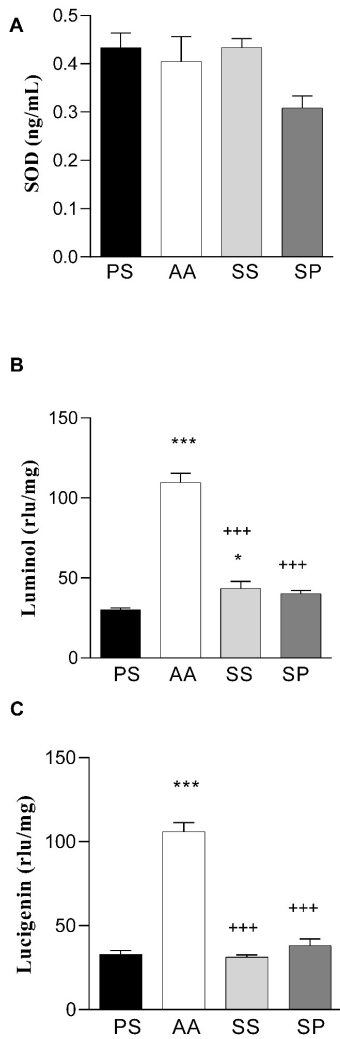
Figure 2. Evaluation of the levels of superoxide dismutase (SOD) activity (A), using ELISA method, and luminol (B), and lucigenin using CL assay (C) in colon tissue after treatments. PS, Sham, and vehicle (PS) treatment control group; AA, AA-induced colitis + PS treatment group; SS, AA-induced colitis + SS treatment positive control group; SP, AA-induced colitis + SP extract treatment group. Results were presented as mean ± S.E.M. *p<0.05, ***p<0.001 control vs. acetic acid; +++p<0.001 acetic acid vs. treatment group. **PS:** Physiological saline, **AA:** acetic acid, **SS:** Sulfasalazine, **SP:** *Sideritis perfoliata*.

Figure 3. Evaluation of the levels of TNF-α (A), IL-1β (B), TLR-9 (C), IL-10 (D), and IL-17 (E) in colon tissue after treatments in AA-induced UC rat model, using ELISA method. PS, Sham, and vehicle (PS) treatment control group; AA, AA-induced colitis+PS treatment group; SS, AA-induced colitis+SS treatment positive control group; SP, AA-induced colitis+SP extract treatment group. Results were presented as mean ± S.E.M. **p<0.01 and ***p<0.001 control vs. acetic acid; ++p<0.01 and +++p<0.001 acetic acid vs. treatment group. PS: Physiological saline, AA: acetic acid, SS: Sulfasalazine, SP: *Sideritis perfoliata*.

(p<0.001 for three markers), and the levels of these cytokines were reduced in the SS and SP groups (p<0.001) (Figure 3A-3C). IL-10 levels were significantly lower in the AA group than in the PS group (p<0.01), but increased IL-10 levels were found in the SS group than in the AA group (p<0.01) (Figure 3D). On the other hand, there were no significant differences in IL-10 levels between the SS or SP groups and the PS group (Figure 3D). Compared with the PS group, the IL-17 level was higher in the AA group (p<0.001) (Figure 3E). While a significant decrease in IL-17 levels was detected in the SS and SP groups compared with the AA group (p<0.001-p<0.01, respectively), the IL-17 level of the SP group was still higher than that of the PS group (p<0.05) (Figure 3E).

Caspase-3 and caspase-9 levels were elevated (p<0.001-p< 0.05 respectively) in the AA group; however, these elevations were attenuated in the SS (p<0.001 for both caspases) and SP (p<0.001 for both caspases) groups. There was a significant decrease in caspase-9 levels in the SP group compared with the PS group (p<0.01), while caspase-3 levels were still higher than in the PS group (p<0.01) (Figures 4A and 4B). MMP-3 activity was higher in the AA and SS groups compared with the PS group (p<0.001-p<0.05), while MMP-3 levels in the SS and SP groups were decreased compared with the AA group (p<0.05-p<0.01). In addition, no significant difference was observed between the SP and PS groups (Figure 4C).

The AA group had a higher overall macroscopic score (5.17±0.3) compared to the PS (0.00±0.1), SS (0.83±0.3), and SP (0.67±0.2) groups. The rats in the AA group had significantly higher macroscopic lesion ratings than those in the PS
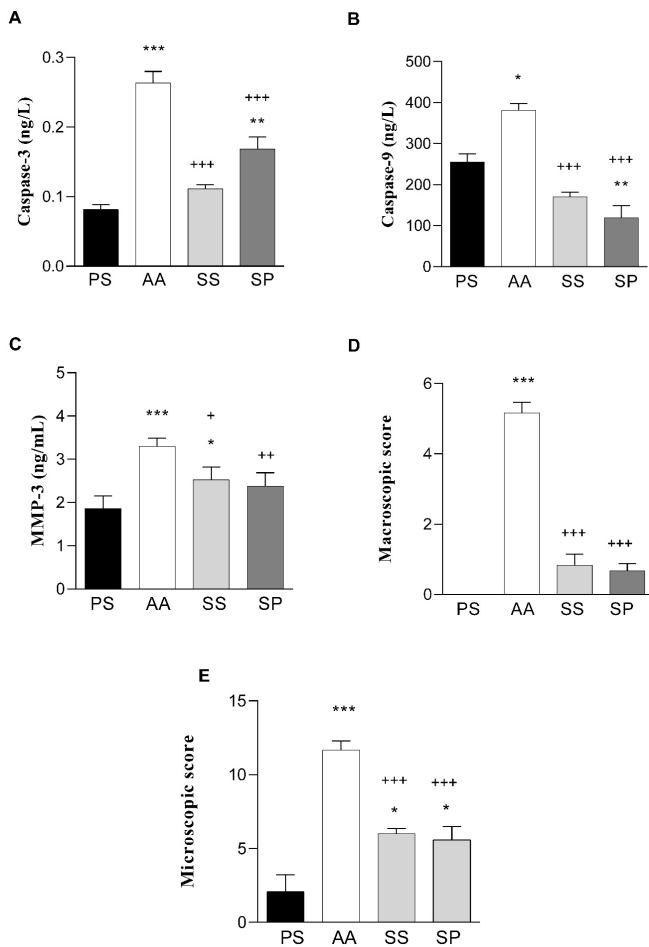
Figure 4. Evaluation of the levels of caspase-3 (A), caspase-9 (B), and MMP-3 (C), macroscopically (D), and microscopically (E) scores in colon tissue after treatments in AA-induced UC rat model. PS, Sham, and vehicle (PS) treatment control group; AA, AA-induced colitis+PS treatment group; SS, AA-induced colitis+SS treatment positive control group; SP, AA-induced colitis+SP extract treatment group; Results were presented as mean ± S.E.M. *, **: $p<0.05$, *** $p<0.001$ control vs. acetic acid; +: $p<0.05$, ++: $p<0.01$, +++$p<0.001$ acetic acid vs. treatment group. **PS:** Physiological saline, **AA:** acetic acid, **SS:** Sulfasalazine, **SP:** *Sideritis perfoliata*.

Figure 5. Effect of *Sideritis perfoliata* or sulfasalazine treatment on macroscopic images of rat colons with acetic acid-induced ulcerative colitis. A. PS Sham, and vehicle (PS) treatment control group; B. AA-induced colitis+PS treatment group; C. AA-induced colitis+SS treatment positive control group; D. AA-induced colitis+SP extract treatment group. **PS:** Physiological saline, **AA:** acetic acid, **SS:** Sulfasalazine, **SP:** *Sideritis perfoliata*.

group ($p<0.001$) (Figure 4D). The rats in the SS or SP groups showed a significant decrease in the overall macroscopic damage score compared with the AA group ($p<0.001$) (Figure 4D). The PS group's colon tissue showed standard macroscopic architecture with no signs of mucosal layer injury (Figure 5A). In contrast, the AA group (Figure 5B) exhibited significant ulcerative and oedematous mucosal lesions. Additionally, a significant reduction in mucosal damage and lesions was observed in the SS (Figure 5C) and SP (Figure 5D) groups compared with the AA group.

When colon tissues were examined for microscopic damage, the AA group was found to have a higher microscopic damage score than the control group ($p<0.001$) (Figure 4E). However, microscopic damage was significantly reduced in the SS or SP ($p<0.001$) groups (Figure 4E). On the other hand, the micro-

scopic scores of the SS and SP groups were higher than those of the control group ($p<0.05$) (Figure 4E). The Haematoxylin and eosin (H&E) stained sections of the control group revealed typical colonic histology with intact epithelium, well-preserved glands, and regular submucosal layers (Figure 6A). In contrast, the AA group exhibited pronounced damage, including a marked loss of the surface epithelial lining, glandular destruction, considerable submucosal oedema, and inflammatory cell infiltration (Figure 6B). The SS group exhibited a histological improvement with more regular epithelial surfaces and maintained glandular structures (Figure 6C). Compared with the AA group, the SP group exhibited improvements, with reduced mucosal and glandular damage, decreased submucosal oedema, and moderate inflammatory cell infiltration (Figure 6D).

DISCUSSION

In this study, SP ethanolic extract showed good antioxidant activity against ABTS and DPPH radicals and strong anti-5-LOX activity. The TPC, TFC, and TTC levels of the SP extract were also determined. Treatment with SP extract reduced macroscopic and microscopic injury scores associated with UC. The SP extract diminished TNF-α, IL-1β, IL-17, TLR-9, MMP-3, caspase-9, caspase-3, luminol, and lucigenin CL levels.

SP ethanolic extract was qualitatively proven to carry phenolic, flavonoids, and triterpene compounds with blue, orange-red, and purple colours seen in total secondary compound
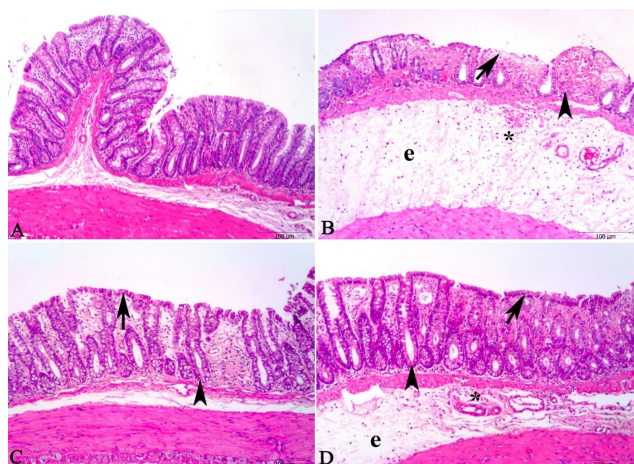
Figure 6. Light microscopic images of colonic tissue sections stained with H&E are representative examples. **A.** The PS group exhibited well-structured colonic mucosa, submucosa, and muscularis. **B.** In the AA group, there was a significant loss of colonic crypts (indicated by arrow) and glands (indicated by arrowhead), along with notable submucosal oedema (e) and inflammatory cell infiltration (marked by an asterisk). **C.** The SS group exhibited a more consistent appearance of epithelial surfaces (arrow) and preserved glandular structures (arrowhead). **D.** SP group exhibited improvements, with reduced mucosal damage (arrow), diminished glandular degeneration (arrowhead), oedema (e), and inflammatory cell infiltration (asterisk). Scale bar, 100 μm. **PS:** Physiological saline, **AA:** acetic acid, **SS:** Sulfasalazine, **SP:** *Sideritis perfoliata*.

determination tests. In addition, our quantitative analysis revealed that the compound contains high numbers of flavonoids, triterpenes, and phenolic compounds. *Sideritis* species are rich in flavonoids, terpenoids, coumarins, sterols, and iridoids, and these secondary metabolites are responsible for their pharmacological effects.[23] In addition, the extract exhibited good free radical scavenging activity against DPPH and ABTS radicals and robust anti-inflammatory activity against 5-LOX. Sarikurkcu et al. (2020) also reported that methanol and water extracts have high DPPH and ABTS radical scavenging and reducing power activities.[44] Although SP's effect on colitis is unknown, Charami et al. (2008) reported the antioxidant activity (using DPPH spectrophotometric and thiobarbituric acid lipid peroxidation measurements) and anti-soybean lipoxygenase activity of SP extracts *in vitro*.[20] Naturally derived compounds, such as flavonoids, triterpenes, and phenolic acids, have been reported to be promising agents against colitis because of their antioxidant (phenolic acids and flavonoids) and anti-inflammatory (phenolic acids, flavonoids, and triterpenes) effects.[43,45,46] Therefore, the antioxidant and anti-inflammatory properties of these compounds may be primarily responsible for the therapeutic effect of SP ethanolic extract. The consequences of our study also pointed to the 5-LOX inhibitory potential of the polar ethanolic extract. Therefore, the extract's improving impact on the UC could be attributed to the synergistic action of its constituents.

Oxidative stress causes mucosal damage accompanied by pro-inflammatory mediators in humans and animals. The AA leads to the upregulated production of free radicals and reactive oxygen species (ROS).[47] Hence, free radical scavenging and ROS elimination are essential in diminishing colon inflammation in the UC.[13] In the present study, treatment with SS and SP extract repressed the AA-induced oxidative stress, as affirmed by the declining luminol and lucigenin levels. On the other hand, no significant differences were observed between the groups in terms of SOD activity. Our *in vitro* analysis revealed that SP extract has good DPPH/ABTS radical scavenging activity, which may cause a reduction in the amount of luminol-lucigenin-enhanced CL. In addition, the antioxidant effect of flavonoids and phenolic substances in the extract also explains the low amounts of luminol and lucigenin. Therefore, reducing oxidative stress promotes biochemical and morphological colonic recovery. The antioxidant activity of *Sideritis* species was previously attributed to their high phenolic compound content, and a limited number of *in vivo* studies have been conducted to determine the anti-radical effects of extracts obtained from SP.[23] The ethanolic extract of SP displayed moderate antioxidant potential and antibacterial activity against *Prevotella intermedia*. In that study, the authors linked the plant's moderate antibacterial and antioxidant activity to the traditional use of SP for treating wounds and inflammatory conditions.[23]

The critical mediators of mucosal inflammation are cytokines and small cell-signalling molecules produced by numerous immune cells. Previous studies have demonstrated a direct correlation between cytokine levels and UC inflammation.[48,49] Colonic TNF-α, IL-1β, and IL-17 levels were upregulated as inflammation markers in male mice with UC.[50] The mucosal concentrations of pro-inflammatory cytokines IL-1β[51], TNF-α[51], and IL-17[52,53] are high in patients with UC. In the present study, AA administration increased these cytokines in the colon. Moreover, SS and SP extract treatments caused a decrease in the levels of these cytokines. Previously, SS treatment has shown a decreased effect of TNF-α, IL-1β, and IL-17 in the rat colon.[54] In our study, SP extracts reduced these cytokines similarly to SS even though TNF-α and IL-1β levels were no different from the control (PS group). This result indicates that SP mitigates cytokine responses. Only SS treatment increased the anti-inflammatory cytokine IL-10 levels, whereas SP did not cause a significant increase. We think SP's effect on IL-10 should be investigated in different colitis models.

TLR-9 levels are elevated in the colon with UC rats.[55] A relationship between the cruelty of inflammation and TLR-9 levels was shown in humans.[56,57] Our study found consistency between colonic TLR-9 levels and inflammation severity in UC rats, consistent with previous studies.[55-57] Our results suggest that SS and SP extract treatment inhibits TLR-9 levels. On the other hand, some researchers have reported that TLR-9 activation suppresses inflammation.[58,59] Therefore, more work is needed on this subject.

Suppression of caspase-9 and caspase-3 and prevention of apoptosis are potential therapeutic targets for UC.[60,61] Our

results indicated that SS and SP treatment diminished AA-induced apoptosis, partly because of reduced caspase-3 and caspase-9 activity levels. Moreover, we observed that SP extract treatment significantly improved caspase-9 levels and even reduced them to lower levels in the control group. Our findings demonstrate that SP attenuates mitochondria-associated apoptosis. Previously, medicinal or nutraceutical-based herbs have been shown to have antiapoptotic activity and to improve colitis and ulcerative lesions.[62,63] However, there is no research on the apoptotic effect of SP.

In this study, AA caused significant deterioration of macroscopic and microscopic tissue morphology and increased MMP-3 levels. Treatment with SP extract improved MMP-3 and macroscopic scoring at a level similar to control while partially improving microscopic scoring. Our *in vitro* and *in vivo* biochemical data results were reflected in the tissue and supported morphological improvements. MMPs play an essential role in connective tissue degradation and are fundamental in redundant tissue demolition in colitis.[64] MMPs are proteases that degrade all components of the extracellular matrix. Under physiological conditions, they are produced at low levels and play a role in normal tissue homeostasis. Specific inhibitors (TIMPs) inhibit their functions. However, in inflamed tissues of patients with IBD, MMPs are overproduced and TIMPs are deficient. Therefore, they contribute significantly to the mucosal degradation associated with IBD.[65] The specific inhibition of these MMPs may provide novel therapeutic options against IBD.

CONCLUSION

In conclusion, thanks to its flavonoids, phenolic acids, triterpene contents, anti-5-LOX, and free radical scavenging activities, SP extract attenuates pro-inflammatory cytokines, mitochondrial apoptotic caspases, and oxidative stress. Our findings support the ethnopharmacological use of SP for colitis.

ORCID IDs of the Authors

Dilek Ozbeyli	0000-0002-4141-6913
Ali Sen	0000-0002-2144-5741
Naziye Ozkan Yenal	0000-0003-3524-0672
Ayse Nur Hazar Yavuz	0000-0003-0784-8779
Deniz Mukaddes Turet	0000-0003-1989-9637
Meral Yuksel	0000-0002-4760-3306
Leyla Bitis	0000-0003-1167-6666
Ahmet Dogan	0000-0003-0603-5100
Asli Aykac	0000-0002-4885-5070

REFERENCES

1. Bruner LP, White AM, Proksell S. Inflammatory Bowel Disease. *Prim Care*. 2023;50(3):411-427.

2. Podolsky DK. Inflammatory bowel disease. *N Engl J Med*. 2002;347(6):417-429.

3. Agrawal M, Jess T. Implications of the changing epidemiology of inflammatory bowel disease in a changing world. *United European Gastroenterol J*. 2022;10(10):1113-1120.

4. Hilsden RJ, Verhoef MJ, Best A, Pocobelli G. Complementary and alternative medicine use by Canadian patients with inflammatory bowel disease: Results from a national survey. *Am J Gastroenterol*. 2003;98(7):1563-1568.

5. Bensoussan M, Jovenin N, Garcia B, et al. Complementary and alternative medicine use by patients with inflammatory bowel disease: Results from a postal survey. *Gastroenterol Clin Biol*. 2006;30(1):14-23.

6. Dossett ML, Davis RB, Lembo AJ, Yeh GY. Complementary and alternative medicine use by US adults with gastrointestinal conditions: Results from the 2012 National Health Interview Survey. *Am J Gastroenterol*. 2014;109(11):1705-1711.

7. Rahimi R, Shams-Ardekani MR, Abdollahi M. A review of the efficacy of traditional Iranian medicine for inflammatory bowel disease. *World J Gastroenterol*. 2010;16(36):4504-4514.

8. Ke F, Yadav PK, Ju LZ. Herbal medicine in the treatment of ulcerative colitis. *Saudi J Gastroenterol*. 2012;18(1):3-10.

9. Magrone T, Perez de Heredia F, Jirillo E, et al. Functional foods and nutraceuticals as therapeutic tools for the treatment of diet-related diseases. *Can J Physiol Pharmacol*. 2013;91(6):387-396.

10. Duda-Chodak A, Tarko T. Possible side effects of polyphenols and their interactions with medicines. *Molecules*. 2023;28(6):2536. doi: 10.3390/molecules28062536

11. Thorsteinsdottir S, Gudjonsson T, Nielsen OH, Vainer B, Seidelin JB. Pathogenesis and biomarkers of carcinogenesis in ulcerative colitis. *Nat Rev Gastroenterol Hepatol*. 2011;8(7):395-404.

12. Nagib MM, Tadros MG, ElSayed MI, Khalifa AE. Anti-inflammatory and antioxidant activities of olmesartan medoxomil ameliorate experimental colitis in rats. *Toxicol Appl Pharmacol*. 2013;271(1):106-113.

13. Tian T, Wang Z, Zhang J. Pathomechanisms of oxidative stress in inflammatory bowel disease and potential antioxidant therapies. *Oxid Med Cell Longev*. 2017;4535194. doi:10.1155/2017/4535194

14. Jena G, Trivedi PP, Sandala B. Oxidative stress in ulcerative colitis: An old concept but a new concern. *Free Radic Res*. 2012;46(11):1339-1345.

15. Kang L, Fang X, Song YH, et al. Neutrophil-epithelial crosstalk

during intestinal inflammation. *Cell Mol Gastroenterol Hepatol.* 2022;14(6):1257-1267.

16. Loğoğlu E, Arslan S, Oktemer A, Sakōyan I. Biological activities of some natural compounds from *Sideritis sipylea* Boiss. *Phytother Res.* 2006;20(4):294-297.

17. Krgović N, Jovanović M, Aradski AA, et al. Bioassay-guided skin-beneficial effects of fractionated *Sideritis raeseri* subsp. *raeseri* Extract. *Plants (Basel).* 2022;11(20):2677-2692.

18. Bizim Bitkiler. Website. https://bizimbitkiler.org.tr/v2/hiyerarsi.php?c=Sideritis. Accessed October 09, 2024.

19. González-Burgos E, Carretero ME, Gómez-Serranillos MP. *Sideritis* spp.: Uses, chemical composition and pharmacological activities-A review. *J Ethnopharmacol.* 2011;135(2):209-225.

20. Charami MT, Lazari D, Karioti A, et al. Antioxidant and anti-inflammatory activities of *Sideritis perfoliata* subsp. *perfoliata* (Lamiaceae). *Phytother Res.* 2008;22(4):450-454.

21. Todorova M, Trendafilova A. *Sideritis scardica* Griseb., an endemic species of Balkan peninsula: Traditional uses, cultivation, chemical composition, biological activity. *J Ethnopharmacol.* 2014;152(2):256-265.

22. Aneva I, Zhelev P, Kozuharova E, et al. Genus *Sideritis*, section Empedoclia in southeastern Europe and Turkey-studies in ethnopharmacology and recent progress of biological activities. *Daru.* 2019;27(1):407-421.

23. Lall N, Chrysargyris A, Lambrechts I, et al. *Sideritis perfoliata* (Subsp. *Perfoliata*) nutritive value and its potential medicinal properties. *Antioxidants (Basel).* 2019;8(11):521-538.

24. Sahin T, Kılıç Ö, Taşkın T. Ethnobotanical and bioactive characteristics of some *Sideritis* L. Taxa and major essential oil compounds. *Russ J Biol Res.* 2023;10(1):17-29.

25. Koleva II, van Beek TA, Linssen JP, de Groot A, Evstatieva LN. Screening of plant extracts for antioxidant activity: A comparative study on three testing methods. *Phytochem Anal.* 2002;13(1):8-17.

26. Sezik E, Ezer N, Huesorodriguez JA, Rodriguez B. Ent-2-alpha-hydroxy-13-epi-manoyl oxide from *Sideritis perfoliata. Phytochem.* 1985;24:2739–2740.

27. Ezer N, Sakar MK, Rodriguez B, De La Torre MC. Flavonoid glycosides and a phenylpropanoid glycoside from *Sideritis perfoliata. Int J Pharmacogn.* 1992;30:61–65.

28. Zou Y, Chang SK, Gu Y, Qian SY. Antioxidant activity and phenolic compositions of lentil (*Lens culinaris* var. Morton) extract and its fractions. *J Agric Food Chem.* 2011;59(6):2268-2276.

29. Phosrithong N, Nuchtavorn N. Antioxidant and anti-inflammatory activites of *Clerodendrum* leaf extracts collected in Thailand. *Eur J Integr Med.* 2016;8(3):281-285.

30. Gao X, Ohlander M, Jeppsson N, Björk L, Trajkovski V. Changes in antioxidant effects and their relationship to phytonutrients in fruits of sea buckthorn (*Hippophae rhamnoides* L.) during maturation. *J Agric Food Chem.* 2020;48:1485-1490.

31. Yıldırım A, Şen A, Doğan A, Bitiş L. Antioxidant and anti-inflammatory activity of capitula, leaf and stem extracts of *Tanacetum cilicicum* (Boiss.) Grierson. *Int J Second Metab.* 2019;6:211-222.

32. Zhang R, Zeng Q, Deng Y, et al. Phenolic profiles and antioxidant activity of litchi pulp of different cultivars cultivated in Southern China. *Food Chem.* 2013;136(3-4):1169–1176.

33. Chang CL, Lin CS, Lai GH. Phytochemical characteristics, free radical scavenging activities, and neuroprotection of five medicinal plant extracts. *Evid Based Complement Alternat Med.* 2012;2012:984295. doi:10.1155/2012/984295

34. Balkan A, Balkan M. Legal requirements involving ethics in animal research, laboratory standardisation, and animal care. *Thorac Res Pract.* 2013;14(Supplement 2):6-9.

35. Jaafar FR, Abu-Raghif A. Comparative treatment of Sulfasalazine+Ezetimibe combination and Sulfasalazine in a rat model with induced colitis. *J Med Life.* 2023;16(8):1165-1169.

36. Tadić VM, Jeremic I, Dobric S, et al. Anti-inflammatory, gastroprotective, and cytotoxic effects of *Sideritis scardica* extracts. *Planta Med.* 2012;78(5):415-427.

37. MacPherson BR, Pfeiffer CJ. Experimental production of diffuse colitis in rats. *Digestion.* 1978;17(2):135–150.

38. Karakoyun B, Ertaş B, Yüksel M, et al. Ameliorative effects of riboflavin on acetic acid-induced colonic injury in rats. *Clin Exp Pharmacol Physiol.* 2018;45:563-572.

39. Özbeyli D, Şen A, Aykaç A, et al. Therapeutic effects of *Momordica charantia* L. ethanolic extract on acetic acid-induced ulcerative colitis in rats. *Eur J Biol.* 2021;80(2):119-128.

40. Haklar G, Ulukaya-Durakbaşa C, Yüksel M, Dağli T, Yalçin AS. Oxygen radicals and nitric oxide in rat mesenteric ischaemia-reperfusion: modulation by L-arginine and NG-nitro- L-arginine methyl ester. *Clin Exp Pharmacol Physiol.* 1998;25(11):908-912.

41. Iseri SO, Ersoy Y, Ercan F, et al. The effect of sildenafil, a phosphodiesterase-5 inhibitor, on acetic acid-induced colonic inflammation in the rat. *J Gastroenterol Hepatol.* 2009;24(6):1142–1148.

42. Arabacı Tamer S, Akbulut S, Erdoğan Ö, et al. Neuropeptide W exhibits preventive and therapeutic effects on acetic acid-induced colitis via modulation of the cyclooxygenase enzyme system. *Dig Dis Sci.* 2023;68(6):2441-2453.

43. Moga DK, Adipo N, Matu EN, Kirira PG. Antioxidant and antiproliferative activity of *Azadirachta indica* A. Juss extracts against cancer cell lines: An experimental study. *Afr J Health Sci.* 2012;34(5):650-656.

44. Sarikurkcu C, Locatelli M, Mocan A, Zengin G, Kirkan B. Phenolic profile and bioactivities of *Sideritis perfoliata* L.: The plant, its most active extract, and its broad biological properties. *Front Pharmacol.* 2020;10:1642. doi:10.3389/fphar.2019.01642

45. Lu Y, Han X. Therapeutic implications of phenolic acids for ameliorating inflammatory bowel disease. *Nutrients.* 2024;16(9):1347. doi:10.3390/nu16091347

46. Vezza T, Rodríguez-Nogales A, Algieri F, et al. Flavonoids in inflammatory bowel disease: A review. *Nutrients.* 2016;8(4):211-232.

47. Biasi F, Leonarduzzi G, Oteiza PI, Poli G. Inflammatory bowel disease: Mechanisms, redox considerations, and therapeutic targets. *Antioxid Redox Signal.* 2013;19(14):1711-1747.

48. Roda G, Marocchi M, Sartini A, Roda E. Cytokine networks in ulcerative colitis. *Ulcers.* 2011; 2011(1):1-5

49. Xue JC, Yuan S, Hou XT, et al. Natural products modulate NLRP3 in ulcerative colitis. *Front Pharmacol.* 2023;14:1265825. doi:10.3389/fphar.2023.1265825

50. Badr G, Elsawy H, Amalki MA, et al. Protective effects of myristicin against ulcerative colitis induced by acetic acid in male mice. *Food Agr Immunol.* 2020;31(1):435–446.

51. Yamamoto T, Saniabadi AR, Umegae S, Matsumoto K. Impact of selective leukocytapheresis on mucosal inflammation and ulcerative colitis: Cytokine profiles and endoscopic findings. *Inflamm Bowel Dis.* 2006;12(8):719-726.

52. Buran T, Batır MB, Çam FS, et al. Molecular analyses of

ADAMTS-1, -4, -5, and IL-17 a cytokine relationship in patients with ulcerative colitis. *BMC Gastroenterol*. 2023;23(1):345. doi:10.1186/s12876-023-02985-z

53. Fujino S, Andoh A, Bamba S, et al. Increased expression of interleukin 17 in inflammatory bowel disease. *Gut*. 2003;52(1):65-70.

54. Niu Z, Li X, Yang X, Sun Z. Protective effects of sinomenine against dextran sulfate sodium-induced ulcerative colitis in rats via alteration of HO-1/Nrf2 and inflammatory pathway. *Inflammopharmacology*. 2024;32(3):2007-2022.

55. Han Y, Ma TM, Lu ML, et al. Role of moxibustion in inflammatory responses during treatment of rat ulcerative colitis. *World J Gastroenterol*. 2014;20(32):11297-11304.

56. Sánchez-Muñoz F, Fonseca-Camarillo GC, Villeda-Ramirez MA, et al. TLR9 mRNA expression is upregulated in patients with active ulcerative colitis. *Inflamm Bowel Dis*. 2010;16(8):1267-1268.

57. Sánchez-Muñoz F, Fonseca-Camarillo G, Villeda-Ramírez MA, et al. Transcript levels of Toll-Like Receptors 5, 8 and 9 correlate with inflammatory activity in ulcerative colitis. *BMC Gastroenterol*. 2011;11:138. doi:10.1186/1471-230X-11-138

58. Atreya R, Bloom S, Scaldaferri F, et al. Clinical effects of a topically applied toll-like receptor 9 agonist in active moderate-to-severe ulcerative colitis. *J Crohns Colitis*. 2016;10(11):1294-1302.

59. Atreya R, Reinisch W, Peyrin-Biroulet L, et al. Clinical efficacy of the Toll-like receptor 9 agonist cobitolimod using patient-reported-outcomes defined clinical endpoints in patients with ulcerative colitis. *Dig Liver Dis*. 2018;50(10):1019-1029.

60. Ren MT, Gu ML, Zhou XX, et al. Sirtuin 1 alleviates endoplasmic reticulum stress-mediated apoptosis of intestinal epithelial cells in ulcerative colitis. *World J Gastroenterol*. 2019;25(38):5800-5813.

61. Sun J, Zhang H, Guan L, Zhou H, Sun M. Alpha-lipoic acid attenuates trinitrobenzene sulfonic acid-induced ulcerative colitis in mice. *Int J Clin Exp Med*. 2015;8(1):358-367.

62. Zhu L, Dai LM, Shen H, et al. Qing Chang Hua Shi granule ameliorate inflammation in experimental rats and cell model of ulcerative colitis through MEK/ERK signaling pathway [published correction appears in *Biomed Pharmacother*. 2023 Jul;163:114854. doi: 10.1016/j.biopha.2023.114854]. *Biomed Pharmacother*. 2019;116:108967. doi:10.1016/j.biopha.2019.108967

63. Khajah MA, Orabi KY, Hawai S, Sary HG, El-Hashim AZ. Onion bulb extract reduces colitis severity in mice via modulation of colonic inflammatory pathways and the apoptotic machinery. *J Ethnopharmacol*. 2019;241:31-40.

64. Kobayashi K, Arimura Y, Goto A, et al. Therapeutic implications of the specific inhibition of causative matrix metalloproteinases in experimental colitis induced by dextran sulphate sodium. *J Pathol*. 2006;209(3):376-383.

65. Marônek M, Marafini I, Gardlík R, et al. Metalloproteinases in inflammatory bowel diseases. *J Inflamm Res*. 2021;14:1029-1041.

How to cite this article

İSTANBUL UNIVERSITY PRESS
— P R E S S —

The Molecular Landscape of Glioblastoma: Implications for Diagnosis and Therapy

Ozlem Yildirim[1] (iD), Evren Onay-Ucar[2] (iD)

[1]Istanbul University, Institute of Science, Department of Molecular Biyology and Genetics, Istanbul, Türkiye
[2]Istanbul University, Faculty of Science, Department of Molecular Biyology and Genetics , Istanbul, Türkiye

ABSTRACT

Glioblastoma, classified as grade IV astrocytoma by the World Health Organisation, is the most common and malignant primary brain tumour in adults, with a high mortality rate. It accounts for 14.5% of central nervous system tumours and 45.6% of primary malignant brain tumours, with an annual incidence of 3.19 per 100,000 people. Despite advances in our understanding of its molecular biology, patient outcomes remain poor, with a median survival of approximately 1 year. Glioblastoma is categorised into four subtypes: IDH wild-type, IDH mutant, not otherwise specified (NOS), and not elsewhere classified (NEC), each affecting prognosis and treatment. Key molecular alterations include *IDH1/2, ATRX, TERT, TP53, B-RAF, EGFR, MGMT*, and *PTEN* mutations, which contribute to tumour behaviour and therapeutic targets. Current diagnostic methods, including magnetic resonance imaging and advanced molecular imaging, aid in accurate diagnosis and treatment planning. Although existing therapies offer limited survival benefits, novel treatments like immunotherapy, oncolytic viral therapy, and targeted molecular therapies, are currently being investigated. These emerging therapies overcome challenges such as the blood-brain barrier and tumour heterogeneity, providing hope for improved outcomes. Future perspectives emphasise the importance of integrating molecular biomarkers, optimising treatment strategies, and enhancing clinical trial designs to develop more effective therapies for patients with glioblastoma.This review aims to delve into the intricate facets of glioblastoma, including its classification, histopathology, interactions with the microenvironment, molecular pathogenesis, diagnostic imaging techniques, clinical progression, current therapeutic approaches, challenges in treatment, identifiable risk factors, and exploration of emerging therapies and prospects in glioblastoma management.

Keywords: Glioblastoma, Temozolomide, IDH mutations, Diagnostic imaging, Blood-brain barrier

INTRODUCTION

Glioblastoma, classified as grade IV astrocytoma by the World Health Organisation (WHO), is the most prevalent and aggressive primary brain tumour in the adult population. It is the leading cause of death among patients with primary brain tumours. This disease accounts for 14.5% of central nervous system (CNS) tumors and 45.6% of primary malignant brain neoplasms.[1,2] Its annual incidence is 3.19 per 100,000 people, with the age-specific annual incidence reaching 0.15 per 100,000 in children and reaching a peak incidence of 15 per 100,000 among patients aged 75-84 years.[3] Newly diagnosed patients with glioblastoma typically have a median survival of approximately 1 year and often exhibit poor responses to all therapeutic modalities. Survival rates also decline with increasing age. Only 5% of all patients diagnosed with glioblastoma

survive for five years, and this rate drops to 2% among patients aged 65 years and older.[4]

This review comprehensively explores the multifaceted aspects of glioblastoma, including its classification, histopathology, interactions within the microenvironment, molecular pathogenesis, diagnostic imaging modalities, clinical progression, existing therapeutic strategies, treatment challenges, and identifiable risk factors, as well as exploring emerging therapies and prospects in glioblastoma management.

CLASSIFICATION OF GLIOBLASTOMA

The WHO classification is the international standard for glioma nomenclature. According to this classification, glioblastoma is classified as a grade IV malignant tumor. The 2016 fourth edition of the WHO glioma classification predicts the degree of

malignancy based on histopathological criteria. Histopathological features of glioblastoma include necrosis and endothelial proliferation, and four subtypes are defined in this classification[5]:

1. Isocitrate Dehydrogenase (IDH) Wild-Type Glioblastoma: This type typically develops *de novo* around the age of 60. The subgroup lacking IDH mutation has a worse prognosis and comprises approximately 90% of glioblastomas.[6]

2. IDH-Mutant Glioblastoma: This type generally develops in younger patients with more highly differentiated gliomas, known as "secondary glioblastoma," evolving from prior WHO grade II or III glioma diagnoses. Instead, for such tumours, it proposes the term "astrocytoma", IDH-mutant, WHO grade IV. These conditions account for approximately 10% of the cases. Tumours carrying specific point mutations in *IDH 1* or *2* genes are associated with younger age and better prognosis.[7] However, the Consortium to Inform Molecular and Practical Approaches to central nervous system Tumour Taxonomy (cIMPACT-NOW), which focuses on IDH mutant grade IV gliomas, emphasises that IDH mutant gliomas have distinct biology and clinical behaviours from IDHwt glioblastomas. Consequently, the authors recommend that the term "glioblastoma" should no longer be applied to IDH-mutant tumours. cIMPACT-NOW was established to inform molecular and practical approaches to the classification of CNS tumours. Although not officially recognised by the WHO, this consortium provides significant updates and recommendations for the classification and diagnosis of CNS tumours.

3. Not Otherwise Specified Glioblastoma: This subtype describes tumours for which the presence of an IDH mutation cannot be determined owing to the absence of requisite histological or molecular material for testing.

4. Not-Elsewhere-Classified Glioblastoma: This category refers to tumours that have undergone the necessary examinations for classification but cannot be matched with any of the categories in the 2016 WHO classification based on the results. This can occur due to inconsistencies between the clinical, histological, immunohistochemical, and genetic characteristics. Additionally, there is a possibility of the existence of glioblastoma subtypes exhibiting an unidentified combination of characteristics that have not yet been incorporated into the WHO classification.

HISTOPATHOLOGY

The pathological features of glioblastoma include a diffusely infiltrative tumour with an astrocytic morphology, high mitotic rates, microvascular proliferation, and/or pseudopalisading necrosis.[8] Additionally, immunohistochemical markers commonly used to diagnose glioblastoma include the expression of glial fibrillary acidic protein. The MIB-1/Ki-67 index is also examined to help determine the extent of proliferation.[9] Some-

times, a tumour sample may not exhibit the typical histopathological characteristics of glioblastoma. Before the integration of molecular classification with histopathology, these tumours would have been categorised with a lower WHO grades. Nevertheless, if a tumour is shown to carry the molecular profile of glioblastoma, it is anticipated to behave like a glioblastoma, and a treatment plan is recommended accordingly. For these types of tumours, cIMPACT-NOW has proposed the diagnostic criteria of "diffuse astrocytic gliomas, IDH-wild type, with molecular features of glioblastoma, WHO grade IV".[10] The recently defined CNS Tumour Methylation Classifier identifies specific glioblastoma subclasses, representing a significant advancement in the diagnostic accuracy of brain tumors.[11] Although the clinical significance of these glioblastoma variants has not been demonstrated, using a classifier to verify glioblastoma diagnosis can be advantageous in unusual clinical scenarios, such as patients with a long patient survival history or atypical tumour histopathology.

INTERACTION OF GLIOBLASTOMA WITH MICROENVIRONMENTS

The close interaction of glioblastoma with its microenvironment in the central nervous system is crucial for tumour development, particularly given the specificity of brain cell populations and the extracellular space.[12] Glioblastoma exhibits significant cellular heterogeneity and includes the tumour perivascular niche, which is the primary site of glioblastoma stem cell-like (GSC) populations.[13] This niche consists of stromal cells, such as microglia, astrocytes, pericytes, fibroblasts, and endothelial cells, which support tumour progression.[14] Interaction with the extracellular matrix of the brain is critical for glioblastoma cell survival and invasion.[15] Glioblastoma growth is associated with neo-angiogenesis, and it secretes proangiogenic factors like VEGF-A.[16] Antiangiogenic therapies offer limited benefits.[17] Moreover, endothelial cells and microglia secrete mediators that promote GSC renewal and activate MMP2 and MMP9, which support tumour invasion.[18,19] The impact of astrocytes on GBM is not fully understood, but research in this area is increasing.[20,21]

MOLECULAR PATHOGENESIS

Comprehensive large-scale analyses of genetic, epigenetic, and expression data significantly contribute to understanding the biological mechanisms of glioblastoma. These insights facilitate the continuous development of subclassification of glioblastomas beyond traditional histological grading. In a study conducted in 2006, three gene expression subtypes (proneural, mesenchymal, and proliferative) were identified, each characterised by specific somatic alterations among 35 genes strongly associated with survival.[22] Among these subtypes, the proneural subtype did not exhibit changes in the phosphatase and

tensin homologue (PTEN) or epidermal growth factor receptor (EGFR) expression profiles and was associated with younger age, longer survival, and anaplastic histology. The proliferative subtype was associated with genes related to proliferation. The mesenchymal subtype expressed genes associated with angiogenesis. Both proliferative and mesenchymal subtypes were linked to poor survival. These analyses were later conducted using broader datasets and mutation analyses for comprehensive evaluation. In 2008, The Cancer Genome Atlas Research (2008) identified three major signalling pathways: Receptor tyrosine kinase (RTK)/rat sarcoma (RAS)/phosphoinositide 3-kinase (PI3K), p53, and retinoblastoma protein (RB). In the same year, *IDH-1/2* mutations were identified as molecular markers closely linked to secondary glioblastoma, younger age, and improved survival. In 2010, the initially proposed gene expression-based glioblastoma subclassification was updated to four subtypes (proneural, neural, classical, and mesenchymal) based on similar gene expression profiles.[23] In 2012, the epigenetic profiling results were also evaluated, leading to the classification of six subtypes. These six subtypes were correlated with different prognoses, tumour locations, and age distributions.[24] In addition to the data obtained from these genetic, epigenetic, and expression studies, next-generation sequencing technologies currently provide an additional layer of detail for understanding intra-tumour diversity and tumour progression in glioblastoma. Table 1 summarises the principal molecular changes identified in glioblastoma.

IDH1/2 Mutations

In adults, *IDH1/2* mutations in widespread diffuse gliomas predict long-term patient outcomes. IDH mutations are found in approximately 5-10% of all glioblastomas and are associated with younger age and more favourable prognosis.[25] They are rarely observed in patients aged 65 years and older. Mutant IDH generates the oncometabolite 2-hydroxyglutarate[26], which is associated with a unique epigenetic pattern called the glioma CpG island methylator phenotype (G-CIMP).[27] In the first stage of screening for IDH mutations, the main focus is on IDH1-R132H, which accounts for 90% of IDH mutations found in glioblastoma.[28,29] This analysis was performed using IDH1-R132H-specific immunohistochemistry, which is a rapid and cost-effective method. Targeted sequencing was performed for *IDH2* (codon 172) and *IDH1* R132C and R132S mutations. These can now be sequenced simultaneously as part of a larger next-generation sequencing (NGS) panel. Generally, IDH mutations are very rarely observed in older patients (>55 years).[30] On the other hand, IDH wild-type glioblastoma is typically observed in older patients and is associated with a poorer prognosis; the *TERT* promoter mutation, in particular, indicates a poor outcome in these patients.[31]

ATRX (a-thalassaemia/mental-retardation X-linked Gene) Mutations

A protein encoded by *ATRX* is responsible for chromatin remodelling and the incorporation of histone H3.3 into heterochromatin.[32] Mutations in *ATRX* are found in approximately 57% of secondary glioblastomas. Within glioblastoma cells, *ATRX* mutations are more common in IDH-mutant tumours than in wild-type tumors.[5] *ATRX* mutations are associated with better prognosis.[33]

TERT (Telomerase Reverse Transcriptase Gene) Promoter Mutations

Mutations in the *TERT* gene promoter, which encodes telomerase, elongates telomeres by adding the missing 3' end during DNA replication, result in increased telomerase activity.[34,35] The most prevalent mutations in the *TERT* promoter are C228T and C250T[36], which cause a substantial increase in TERT expression, almost quadrupling it.[34,37] These mutations are present in nearly 80% of glioblastoma cases.[34,38,39] *TERT* promoter mutations are more common in IDH wild-type glioblastoma than in IDH mutant glioblastoma.[5] However, the prognostic role of *TERT* promoter mutations has not been definitively established due to the presence of several confounding factors. To independently evaluate the prognostic influence of *TERT* promoter mutations, further prospective studies on large homogeneous patient populations are needed.[40]

TP53 (Tumour Protein P53 Gene) Mutations

The p53 protein is critical for regulating proliferation, survival, genomic integrity, and other cellular functions. *TP53* mutations contribute to the advancement of glioblastoma.[41] These mutations are more frequent in IDH-mutant glioblastoma than in IDH-wild type glioblastoma.[5] Gain-of-function (GOF) *TP53* mutations endow the protein with a new function or alter its expression, leading to increased cellular malignancy.[41,42] GOF mutations increase *MGMT* expression, thereby reducing the sensitivity of glioblastoma to temozolomide and decreasing overall survival.[43]

BRAF (B-Rapidly Accelerated Fibrosarcoma Gene) V600E Mutations

As part of the RAS-RAF-MEK-ERK MAP kinase pathway governing cell growth, *B-RAF* can exhibit constitutive kinase activity due to mutations in its gene, fostering unregulated cell proliferation and tumour genesis. The V600E mutation, one of the most common *B-RAF* mutations, produces a constitutively active serine/threonine kinase *B-RAF*. This mutation activates ERK1/2 and MAP kinases, disrupting the tightly regulated control of this crucial pathway. The frequency of all *B-RAF* mutations in glioblastoma is estimated to be around 2-5%.[44] This mutation is considered suitable for personalised cancer therapy with kinase inhibitors.[45]

Table 1. Key molecular alterations in glioblastoma.

Gene	Mutation/Alteration	Impact on Glioblastoma	Prognostic Value
IDH1/2	R132H, R132C, R132S, and	Associated with younger age and better prognosis	Positive
ATRX	Mutations	Involvement in chromatin remodelling	Positive
TERT	C228T, C250T	Increased telomerase activity	Variable requires further study
TP53	Gain of Function (GOF)	Increased proliferation and drug resistance	Negative
B-RAF	V600E	Constitutive kinase activity and cell proliferation	Suitable for targeted therapy
EGFR	Amplification, EGFRvIII	Promotes cell proliferation	Mixed, not definitively established

EGFR Mutations

EGFR functions as a receptor with tyrosine kinase activity, promoting cell proliferation via the activation of the mitogen-activated protein kinase (MAPK) and PI3K-Akt pathways.[46] Approximately 40% of glioblastoma cases exhibit *EGFR* amplification.[47] While some studies have reported an association between *EGFR* amplification and poor prognosis, this relationship has not been definitively established.[48,49] *EGFR* amplification is more common in IDH-wild-type glioblastomas than in IDH-mutant glioblastoma.[5] The most common *EGFR* mutation is a large deletion spanning exons 2 to 7, known as EGFRvIII.[50]

MGMT (O6-methylguanine DNA Methyltransferase Gene) Mutations

The protein encoded by the *MGMT* gene is responsible for repairing DNA by removing an alkyl group located at the O6 position of guanine, a critical site for DNA alkylation. *MGMT* promoter methylation predicts the efficacy of temozolomide chemotherapy in both newly diagnosed and potentially recurrent glioblastomas.[51,52] The role of *MGMT* in resistance to alkylating chemotherapy was idehas beenfied, leadingand it has the most impactful biomarker in clinical decision-making, particularly for older patients glioblastoma patients.[53]

PTEN Mutations

The loss of heterozygosity or methylation mutations in *PTEN* results in the loss of functional *PTEN*, which disrupts the PI3K/Akt pathway and affects cell survival, growth, and proliferation regulation.[54] This disruption affects pathways involved in PI3K. *PTEN* mutations are found in at least 60% of glioblastoma cases.[55] The loss of *PTEN* function is associated with poor prognosis in glioblastoma.[56]

DIAGNOSIS AND IMAGING

Most glioblastomas are diagnosed symptomatically because of their rapid growth, which leads to the development of seizures or neurological deficits. Symptoms can include new-onset epilepsy, headache, altered mental status, and signs of increased intracranial pressure. Contrast-enhanced magnetic resonance imaging (MRI) is the diagnostic method of choice for glioblastoma diagnosis. These tumours typically appear as contrast-enhancing necrotic mass with surrounding oedema and infiltrative tumour tissue. Contrast-enhanced computed tomography is less sensitive in detecting the typical features of glioblastoma and is reserved for acute situations, such as suspected haemorrhage or when MRI is not possible because of the presence of a pacemaker or other metallic implants. Amino acid positron emission tomography (PET) is increasingly performed before biopsy to direct the biopsy site to metabolic hot spots that might represent higher tumour grades.[57] However, PET imaging is excluded from the conventional treatment regimen for individuals with glioblastoma. MRI offers crucial anatomical information about the tumour and surrounding brain structures, thereby aiding in surgical planning. Functional MRI is particularly valuable for tumours near critical areas, helping to plan the best surgical approach and ensuring the safe maximal resection of contrast-enhancing tumours to enhance patient survival. Additionally, MRI facilitates the differentiation of glioblastomas from other contrast-enhancing lesions like abscesses, primary central nervous system lymphomas, and metastases from non-primary brain tumors.[58,59] Despite this, the imaging characteristics of glioblastoma can vary greatly, necessitating a tissue-based diagnosis.[53] The tissue required to confirm the diagnosis of glioblastoma can be acquired through stereotactic or open biopsy or microsurgical resection of the tumour.

CLINICAL COURSE

Glioblastoma clinical progression is dictated by the tumour's location and spread dynamics within the brain. Tissue destruction, oedema, and epilepsy exacerbate clinical symptoms, resulting in rapid deterioration in some patients. Although the prognosis for glioblastoma is inevitably fatal, standard treatments can temporarily stabilise or improve quality of life and cognitive functions, even in older and severely affected populations.[60-62] Approximately 20% of glioblastoma patients initially show sensorimotor deficits, whereas around 5% experience aphasia due to tumours in the speech-dominant hemisphere, usually the left side.[63] Epilepsy occurs initially in 24-68% of patients and develops in 19-38% as the disease progresses.[64,65] Early epilepsy symptoms are linked to longer survival, likely due to younger age, cortical tumour location, and smaller tumour size, indicating better surgical outcomes and earlier detection.[63,64] Less than one-third of patients report headache as the initial symptom.[63] Other symptoms like increased intracranial pressure, nausea, vomiting, dizziness, fatigue, and cognitive decline, may appear at diagnosis and may worsen over time. A few patients may have stable disease and remain largely neurologically asymptomatic for years. However, most patients experience a significant decline in quality of life after failure of first-line treatments.[60-62] In summary, glioblastoma lacks a typical clinical presentation. Compared with other gliomas, glioblastoma is characterised by faster dynamics and a slightly lower incidence of epilepsy.

CURRENT TREATMENTS

Despite recent advances in the understanding of the biology of glioblastoma, patient prognosis remains poor. Current treatment methods rely on a combination of surgery, radiotherapy, and chemotherapy. Even with this standard treatment, the median overall survival is approximately 15-18 months, and the 5-year survival rate is below 10%.[65,66]

Temozolomide, an alkylating agent used in chemotherapy, is a key component of treatment. The methylation status of the *MGMT* promoter predicts the benefit of alkylating chemotherapy with temozolomide and guides treatment choices. Phase III trials have consistently shown that glioblastoma patients with *MGMT* promoter methylation experience approximately 50% longer median survival when treated with Temozolomide. In glioblastomas without *MGMT* promoter methylation, temozolomide has little to no benefit.[51] The use of temozolomide in these patients, particularly within the context of clinical trials, is debated, but an increasing number of studies are exploring this approach. Currently, detecting specific gene mutations in the tumour provides valuable information about the clinical course of the disease and enables the development of targeted therapies. However, there are still many hurdles to overcome for treating this invariably fatal cancer.

Challenges in the treatment of glioblastomas

Due to their aggressive behaviour and resistance to treatment, glioblastomas have high mortality rates. This is partly attributed to the tumours' location within the central nervous system and the neurological toxicities associated with treatment.[67] Another critical issue is the blood-brain barrier. Glioblastomas utilise the blood-brain barrier, a natural defence mechanism of the brain against toxins. This barrier restricts the diffusion of compounds to small, uncharged, lipid-soluble molecules. Since most drugs do not possess these characteristics, they cannot significantly penetrate the blood-brain barrier.[68] Given that several recent clinical trials have failed to improve survival due to the inability to achieve therapeutic concentrations in the target area, brain penetration remains a major challenge in glioblastoma treatment. Approaches to tackle this challenge involve developing a greater number of substances that can effectively penetrate the blood-brain barrier, utilising endogenous entry transporters, and employing focused ultrasound to temporarily disrupt the blood–brain barrier.[69]

Another critical challenge in treating glioblastoma is the high degree of heterogeneity. Glioblastomas exhibit multiple genetic factors throughout tumour progression.[70] Intratumoral heterogeneity at both the molecular and functional levels heightens the complexity of glioblastomas. For example, various regions within the same tumour may possess distinct genetic compositions, transcriptional subtypes, or cells with varying proliferation kinetics.[71-75] This heterogeneity can impact treatment outcomes, as functionally diverse glioma cells within the tumour may respond differently to temozolomide or ionising radiation.[75,76]

RISK FACTORS

The vast majority of glioblastoma patients have no prior history of cancer, with approximately 5% of all gliomas being familial. However, there are multiple rare Mendelian inherited syndromes associated with adult glioma and glioblastoma. Less than 1% of glioblastomas are related to hereditary cancer syndromes, such as Li-Fraumeni Syndrome, Turcot Syndrome, Neurofibromatosis Types 1 and 2, tubrous Sclerosis Complex, and Cowden Syndrome. These glioblastomas are often diagnosed as secondary to WHO grade II or III gliomas.[77] Given family history data, the frequency of germline variants was higher than expected. Data indicate that 13% of patients with gliomas have at least one pathogenic or likely pathogenic variant.[78] Genome-wide association studies have identified 25 single-nucleotide polymorphisms (SNPs) associated with an increased risk of glioma, with 11 of these specifically linked to glioblastoma.[79] These studies have also identified loci involving critical glioma genes, such as *EGFR, TERT*, cyclin-dependent kinase inhibitor 2B (*CDKN2B*), and regulator of telomere elongation helicase 1 (*RTEL1*).[79]

Among long-term survivors who received high-dose radiation for primary brain tumours in childhood, an increased risk of glioblastomas has been demonstrated.[80] The findings indicate that patients who received high-dose radiation therapy were significantly more likely to develop glioblastoma than those who did not receive such treatment. These findings suggest that high-dose radiation can cause DNA damage and malignant transformation, thereby increasing the risk of glioblastoma. However, radiation doses during diagnostic imaging are not considered a risk factor.[81,82]

The potential risk factor for cell phone use (non-ionising radiation exposure) for brain tumours has been extensively studied, but no definitive link has been established.[4,83] No association with smoking or other carcinogens. The expression of cytomegalovirus genes and their interaction with key pathways that drive the malignant phenotype of glioblastoma suggest a potential oncomodulatory role for cytomegalovirus, although its role as an initiating agent for glioma has not been definitively confirmed.[84,85]

Ionising radiation to the brain is the only external risk factor for the development of glioblastoma.[86-88]

There is no strong link between specific ethnic groups and glioblastoma risk although one study found higher incidence rates among Caucasians than among Asians and African Americans.[2] Another study showed high molecular similarity in glioblastoma between Japanese and Swiss patients despite their different genetic backgrounds.[89,90]

Conducting more extensive epidemiological studies, genome-wide association studies (GWAS), and molecular and biomarker studies will contribute significantly to the better identification of potential risk factors. These efforts will be crucial in future research into the risk factors associated with glioblastoma.

NOVEL THERAPIES AND FUTURE PERSPECTIVES OF GLIOBLASTOMA TREATMENT

Advancements in the molecular characterisation of glioblastoma have paved the way for the development of new therapeutic strategies. The traditional WHO classification based on histology is complemented by evaluating molecular markers. A more personalised approach to glioblastoma treatment is necessary. However, the molecular profile of glioblastoma exhibits both intratumoral and temporal heterogeneity, thereby complicating treatment strategies.[71,74] Despite these challenges, emerging technologies and increased knowledge continue to facilitate the discovery and clinical testing of promising novel treatment concepts. Completed and ongoing clinical trials related to glioblastoma are shown in Table 2.[91-94]

Immunotherapy

The application of immunotherapy in glioblastoma treatment has been investigated for many years, with limited success so far.[95] However, the discovery of promising targets, technological advancements, and success in early-stage clinical trials have reignited interest in this approach. Recurrence of glioblastoma is a common issue that limits patient recovery, with approximately 50% of patients unable to access second-line treatments.[96,97] Research has shown that glioblastoma tumour cells create an immunosuppressive microenvironment by increasing factors such as FASL, PD-1, indoleamine 2,3-dioxygenase (IDO), and STAT3.[98] Microglial cells promote systemic immunosuppression by producing IL-1 and TGF-β.[99] Immunosuppressive markers like PD-1 increase, altering CTL phenotypes. Vaccination and anti-PD-1/CTLA-4 treatment targets glioblastoma-associated antigens (e.g., EGFRvIII). Oncolytic viral therapy uses viruses to trigger an immune response against the tumour, exploiting viral defence weaknesses to infect tumour cells.[100] U.S Food and Drug Administration (FDA) has approved monoclonal antibodies targeting PD-1, CTLA-4, and PD-L1 for cancer treatment.[101,102]

In recent years, the therapeutic successes achieved with immune checkpoint blockade and CAR-T cells in immunotherapy aimed at utilising the immune system to treat cancer have laid the foundation for the clinical development of immunotherapy, significantly improving treatment outcomes for many cancer patients.[103-105] Using this method, T cells are genetically engineered to express Chimeric Antigen Receptors (CAR) that are specifically directed against antigens on tumour cells.[106] The clinical potential of CAR-T cell therapy has been best demonstrated in haematologic malignancies.[107,108] Various clinical studies have tested CAR-T cell therapies targeting epidermal growth factor receptor variant III (EGFRvIII), interleukin (IL)13Rα2 (IL-13Ra2), and ephrin-A2 (Her2) for glioblastoma, showing clinical benefits in progressive glioblastoma patients.[109-111] However, antigen escape mechanisms can negatively impact the durability of responses to CAR-T cell therapy.[104]

Oncolytic Viral Therapy

For treating glioblastoma, oncolytic viruses are used as vectors for somatic gene therapy by targeting the molecular pathways that drive malignant tumour. These viruses exert their effects by either provoking an inflammatory host response or directly destroying glioma cells through extensive replication (Figure 1).[112] Oncolytic virotherapy, a promising immunotherapy for glioblastoma, includes replication-competent viruses that destroy cancer cells and replication-deficient viral vectors that deliver therapeutic genes.[113,114] The first group of oncolytic viruses includes Newcastle disease viruses, reoviruses, and parvoviruses. The second group consists of adenoviruses, herpes simplex viruses, vaccinia viruses, vesicular stomatitis viruses,

Table 2. Clinical trials for glioblastoma.

Therapeutic Approach	Trial Name	Status	Outcome	Participants	Start Date	NCT Number
Oncolytic Viral Therapy	Phase II DNX-2401 for Recurrent Glioblastoma	Active, not recruiting	Median survival improvement	25	2017	NCT03152318
	DNX-2401 plus pembrolizumab	Active	Improved survival and safety rates	48	2018	NCT02798406
	Toca 511 and Toca FC	Completed	Increased overall survival	403	2015	NCT02414165
	PVSRIPO for Recurrent GBM	Active	Enhanced survival and safety	61	2017	NCT01491893
	Oncolytic DNX-2401 adenovirus	Recruiting	Tumour response and safety	170	2017	NCT03178032
	Adenoviral gene therapy vector carrying IL-12 (NCT03636477)	Recruiting	Safety and efficacy evaluation	35	2024	NCT03636477
	Oncolytic herpes simplex virus (oHSV) with IL-12 (NCT02062827)	Completed	Increased immune cell infiltration	25	2023	NCT02062827
	Adenovirus DNX-2401 with mesenchymal stem cells (NCT03896568)	Recruiting	Reduction in tumour size	50	2024	NCT03896568
Immunotherapy	PD-1 Blockade in Recurrent Glioblastoma	Active	Increased survival in some patients	30	2015	NCT02337686
	Nivolumab + Bevacizumab	Completed	Optimal dosing and safety	75	2017	NCT03452579
	Ipilimumab and Nivolumab	Active	Tumour response and survival	153	2016	NCT02311920
	Dual-target CAR T-cell therapy (NCT05168423)	Ongoing	Tumour size reduction	6	2024	NCT05168423
	CAR-TEAM cells (NCT02986178)	Ongoing	Tumour regression	3	2023	NCT02986178
	mRNA Vaccine Boost (NCT05101212)	Ongoing	Immune response boosting	4	2024	NCT05101212
Molecular Therapeutic Targets	BRAF V600E Mutation in Paediatric Glioblastoma	Completed	Tumour response to targeted therapy	30	2013	NCT01677741
	Targeting EGFRvIII with Rindopepimut	Completed	No significant benefit	745	2015	NCT01480479
	BRAF Inhibitor Vemurafenib for Recurrent GBM	Active	Efficacy and safety	25	2019	NCT03973918

Table 2. Continued

|						
	CDK4/6 inhibitor abemaciclib/EGFR/HER2 inhibitor ceratinia (INSIGhT trial)	Ongoing	No improvement in overall survival	150	2023	NCT02977780
Anti-Angiogenic Therapy	Bevacizumab Plus Radiotherapy for Newly Diagnosed Glioblastoma	Completed	Progression-free survival	120	2011	NCT01390948
	Bevacizumab + Radiation + Temozolomide	Completed	No improvement in overall survival	978	2008	NCT00884741
	Blood-brain barrier opening using ultrasound for chemotherapy	Recruiting	Increased drug concentrations in the brain	20	2024	NCT04121455
Targeting DNA Damage Response	PARP Inhibitor along with Temozolomide for Glioblastoma	Completed	Enhanced DNA damage in tumour cells	40	2012	NCT01477489
	PARP Inhibitor Olaparib + Temozolomide	Recruiting	Safety and efficacy	60	2018	NCT03212742
	PARP inhibitor velitaris combined with temozolomide	Ongoing	Enhanced sensitivity to chemotherapy	38	2023	NCT03581292
	Veliparib and Radiation for MGMT-unmethylated GBM	Active	Increased survival and safety	150	2017	NCT02152982
Targeting Tumour Metabolism	Targeting Tumour Metabolism in Glioblastoma Cells using Ketoconazole	Terminated	No significant benefit was observed	15	2016	NCT02873416
	Metformin with Temozolomide and Radiation Therapy	Active	Tumour response and progression-free survival	30	2016	NCT02338516
	PTEN pathway inhibition with posaconazole	Recruiting	Tumour size reduction	40	2024	NCT03757805
	Ketogenic Diet for Recurrent Glioblastoma	Active	Feasibility and safety	18	2019	NCT05110918
Others	Mesenchymal Stem Cells in Recurrent GBM	Recruiting	Safety and preliminary efficacy	15	2017	NCT03072134
	Dose-escalated Photon Irradiation or Proton Beam Radiation Therapy	Active	Tumour response and safety	110	2017	NCT02179086
	Temozolomide vs. Radiotherapy for Elderly Patients	Completed	Survival benefit for specific patient populations	373	2011	NCT00786682
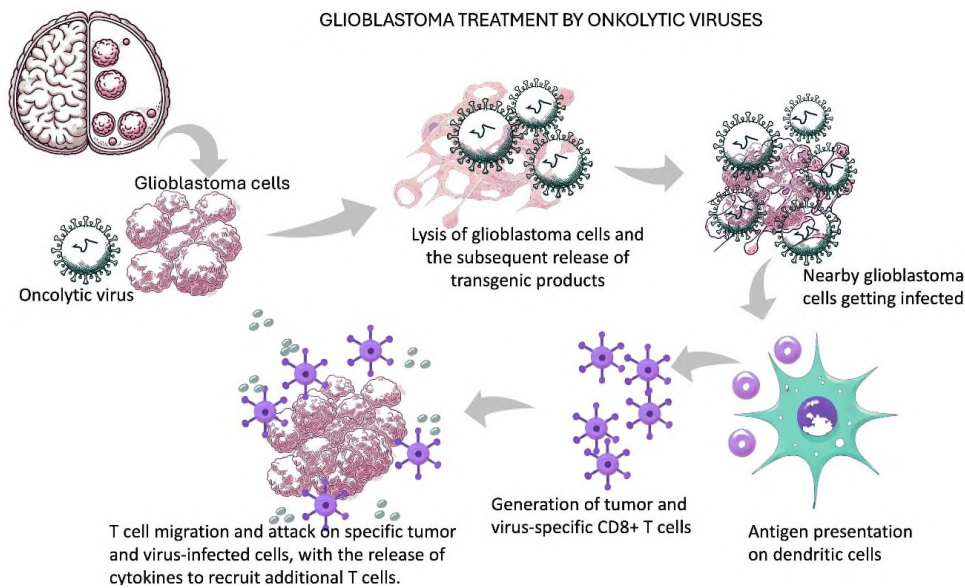
Figure 1. Mechanism of oncolytic virus-induced glioblastoma treatment.

polioviruses, and measles viruses. These viruses are genetically modified to improve their ability to target tumours specifically and to reduce their pathogenic effects.[113-115] To date, over 20 oncolytic virus candidates have been tested in clinical trials for the treatment of glioblastoma.[116-119] Oncolytic viruses are effective in glioblastoma treatment because they replicate rapidly in fast-growing cells and adapt well to the brain environment, where distant metastases are absent.[120,121] They initiate an anti-cancer immune response by transforming "cold tumours" into "hot tumours," making them susceptible to immune attacks.[122,123] This process, called immunogenic cell death, involves the release of DAMPs, PAMPs, TAAs, and cytokines.[124-126] Oncolytic viruses also enhance antigen-presenting cell function, leading to the recruitment of cytotoxic CD8$^+$ T lymphocytes to the tumour site, resulting in tumour cell destruction.[127,128]

Numerous oncolytic viral therapies for glioblastoma recurrence are either in Phase I clinical trials or have completed this phase. Clinical research studies for the treatment of recurrent glioblastoma using an adenoviral gene therapy vector carrying IL-12 cDNA, which is activated by an orally administered agent (NCT03636477), are still ongoing. Recent updates indicate that the trial is actively recruiting patients and is in the phase of evaluating the results. This study aimed to investigate the efficacy and safety of the combination of adenoviral gene therapy and valacyclovir, particularly in patients who do not respond to immune checkpoint inhibitors. In this study (NCT03576612), participants taking the oral drug valacyclovir were administered an adenoviral vector carrying thymidine kinase cDNA, which causes cytotoxicity. This trial is investigating the safety and efficacy of adenoviral vectors combined with valacyclovir and chemoradiation in patients newly diagnosed with glioblastoma. The treatment involving the stereotactic in-

jection of oncolytic herpes simplex virus type 1 carrying IL-12 cDNA (NCT02062827) aims to evaluate the safety and efficacy of a genetically engineered herpes simplex virus type 1 in patients with recurrent or progressive glioblastoma, anaplastic astrocytoma, or gliosarcoma.[100,118] The treatment involving the stereotactic injection of an oncolytic herpes simplex virus engineered to better replicate in glioblastoma cells and in cells expressing the stem cell marker nestin (NCT03152318) uses an oncolytic herpes simplex virus designed to replicate more efficiently in cells expressing nestin.[112] Another clinical trial (NCT03896568) is evaluating the intra-arterial delivery of the oncolytic adenovirus DNX-2401 loaded with allogeneic bone marrow-derived human mesenchymal stem cells.[124,128] The study (NCT03072134) involving the injection of neural stem cells carrying oncolytic adenovirus into newly diagnosed glioblastoma patients is being conducted to gather safety and efficacy data.[124,128] Based on the results, both oncolytic viral and gene therapy treatments have been observed to be well tolerated. Posttreatment tissue analysis revealed increased immune cell infiltration and changes in immune response, including the presence of cytotoxic T cells.

Advanced stage trials (Phase II and beyond), such as the recombinant nonpathogenic polio-rhinovirus chimaera PVSRIPO trial (NCT02986178) for patients with recurrent glioblastoma, also show promise. To overcome the limitations posed by the BBB, Desjardins et al. reported a new technique for convection-enhanced delivery of PVSRIPO.[129] convection-enhanced delivery is an innovative method that uses a pressure gradient in a catheter to deliver therapeutic agents to the CNS's interstitial areas.[130] For successful virotherapy, oncolytic viruses need safe and effective delivery. Given the challenges of transporting viruses to the central nervous system and the immune system's ability to neutralise them, intratumoral delivery has become

the primary method. This treatment is typically administered via injection during surgical procedures. PVSRIPO is a live attenuated poliovirus type 1 vaccine modified with the internal ribosome entry site of human rhinovirus type 2 to reduce neurovirulence. Targeting glioblastoma via CD155, which is commonly upregulated in malignant cells, PVSRIPO showed no neurovirulent potential in a Phase I trial (NCT01491893) using intratumoral convection-enhanced delivery in patients with recurrent glioblastoma. Additionally, preliminary data indicated that patients receiving PVSRIPO immunotherapy had higher 24- and 36-month survival rates compared with the control groups.[129] Based on the findings from Phase I, a Phase II randomised trial (NCT02986178) is ongoing, investigating PVSRIPO alone or in combination with lomustine in patients with recurrent glioblastoma. The FDA has granted PVSRIPO both breakthrough therapy designation and an orphan drug status, highlighting its potential for significant therapeutic advancement for patients with glioblastoma. The therapeutic efficacy of this novel treatment modality is eagerly anticipated in patients with glioblastoma.

Another viral therapy, foraneen obadenovec (VB-111), was evaluated in a phase III trial that revealed that the combination of VB-111 with bevacizumab did not offer a survival advantage compared with bevacizumab alone.[131] This failure suggests that the simultaneous administration of bevacizumab may have inhibited the viral therapy's effects. Despite this, optimism remains for developing new treatment strategies. This optimism is further supported by ongoing research efforts to identify molecular and immunological variables and targets.

Molecular Therapeutic Targets

The discovery of small molecules that interfere with the molecular mechanisms of glioblastoma treatment is promising. However, significant challenges remain, such as the scarcity of agents capable of crossing the blood-brain barrier, recurrent signalling pathways, and tumour heterogeneity. The 2016 WHO classification includes molecular parameters for some brain tumours (e.g., *BRAF* V600E, *IDH1*-R132H). Biomarkers like EGFR amplification and EGFRvIII mutation are prominent in glioblastoma treatment.[132,133]

IDH mutations are observed in approximately 10% of glioblastomas and serve as significant therapeutic targets.[23] Mutant IDH inhibitors have shown promising preclinical findings, but they need to be validated through clinical trials.[133] EGFR amplification is mutually exclusive to IDH mutations and is present in approximately 50% of IDH wild-type glioblastomas.[134]

Receptor tyrosine kinase inhibitors like erlotinib and sorafenib are among the molecular targets used in glioblastoma treatment. It is crucial to verify the presence of molecular targets in tumours to evaluate the efficacy of these inhibitors. Accordingly, clinical trials on selected patients possessing spe-

cific molecular characteristics are ongoing. The NCT01975701 trial investigated the efficacy of targeted therapy in newly diagnosed patients with glioblastoma, focusing on fibroblast growth factor (FGF) fusion proteins and activation mutations.[135,136]

The NCT01349660 trial evaluated the use of a PI3K inhibitor in patients with recurrent glioblastoma. The completed NCT01339052 trial assessed the efficacy of PI3K inhibitors, alone or in combination with other anti-angiogenic agents, in patients with recurrent glioblastoma. The results indicated that while PI3K inhibitors were effective, they did not significantly improve overall survival. Similarly, the NCT01870726 trial also examined the impact of PI3K inhibitors in patients with recurrent glioblastoma.[137] The findings revealed that although PI3K inhibitors were safe and well-tolerated, they did not provide substantial clinical benefits.

These findings highlight the importance of molecular-based patient selection for targeted therapies against glioblastoma. Future studies should focus on optimising treatment strategies by investigating novel therapeutic targets.

Anti-Angiogenic Therapy

Angiogenesis is a hallmark of glioblastoma, and the anti-VEGF antibody bevacizumab is the most extensively studied drug targeting this process. While bevacizumab extends progression-free survival, it has not demonstrated a clear benefit in overall survival.[131,137] Ongoing research is focused on identifying molecular markers that could predict which patients would benefit from antiangiogenic therapies.[138]

Targeting DNA Damage Response Pathways

Among the most effective nonsurgical treatments for gliomas are radiotherapy and cytotoxic chemotherapy, both of which induce DNA damage.[65] Enhancing the effects of these agents on tumours while protecting normal tissue is particularly crucial for the treatment of glioblastoma. DNA damage response (DDR) inhibitors, when used with these therapies, can increase unrepaired double-strand breaks and single-strand breaks, thereby enhancing sensitivity to chemotherapy and radiotherapy.[139] However, DDR inhibitors can cause myelosuppression, limiting their combination with temozolomide.[140] The combination of DDR inhibitors with temozolomide could be an important biomarker.[140,141] Loss of MGMT protein expression predicts sensitivity to temozolomide, and PARP inhibitors, a type of DDR inhibitor, have proven to be effective biomarkers in combination with temozolomide.[140,141] Therefore, identifying molecular biomarkers associated with glioblastoma is critical for developing effective and safe drug combinations.

Targeting Tumour Metabolism

Targeting tumour metabolism is a significant strategy for glioblastoma treatment. The inhibition of metabolic regulators,

such as PTEN, HK2, and PINK1, has shown therapeutic benefits in glioblastoma.[142,143] Additionally, cholesterol metabolism presents a potential therapeutic target in some glioblastomas.[144]

Tumour-Treating Fields Therapy

Tumour-treating field therapy is an innovative approach for treating glioblastoma that employs low-intensity alternating electric fields to disrupt tumour cell division. This non-invasive therapy has been integrated into standard treatments for glioblastoma, recurrent glioblastoma, and mesothelioma, demonstrating significant survival benefits by exerting biophysical forces on charged molecules, thereby inhibiting cancer cell proliferation and affecting processes such as DNA repair and immunological responses.[145,146] Current research underscores tumour-treating fields therapy's efficacy when combined with conventional treatments like chemotherapy and radiation, leading to promising advancements in patient survival outcomes. Ongoing studies refine treatment protocols, elucidate their mechanistic impact on glioblastoma progression, and explore innovative applications to enhance therapeutic effectiveness. Future directions include investigating personalised approaches and integrating tumour-treating fields therapy into comprehensive treatment strategies to improve patient outcomes.

CONCLUSION

Despite substantial advancements in our understanding of the molecular pathogenesis and biology of glioblastoma, patient outcomes have not significantly improved. Glioblastoma remains a highly aggressive and lethal cancer with limited effective treatment options. The prognosis for patients with glioblastoma is generally poor, with standard treatments offering only temporary stabilisation and modest improvements in quality of life. To address these challenges, several promising therapeutic strategies are being explored and translated into clinical practise. The development of novel therapies grounded in robust scientific rationale is crucial. Moreover, enhancing the efficiency of clinical trial evaluations is essential for accelerating the discovery of effective treatments. Increasing the participation of patients with glioblastoma in phase I oncology trials can help identify potential new therapies earlier in the treatment pipeline. Conducting "window-of-opportunity" phase 0 surgical studies to assess blood-brain barrier penetration and pharmacodynamic effects can provide early insights into the potential efficacy of new treatments. Incorporating molecular imaging techniques and using blood and cerebrospinal fluid biomarkers more extensively can help monitor treatment responses and better understand the disease. Including a broad range of molecular biomarkers in clinical trial designs can help tailor treatments to individual patients and improve outcomes. Streamlining the design of clinical trials and increasing patient enrolment can accelerate the development of new therapies. By implementing these changes, the goal is to identify more

effective treatments for patients with glioblastoma, ultimately improving survival and quality of life.

Peer Review: Externally peer-reviewed.

Author Contributions: Conception/Design of Study- O.Y., E.O.U.; Data Acquisition- O.Y.; Data Analysis/Interpretation-O.Y., E.O.U.; Drafting Manuscript- O.Y.; Critical Revision of Manuscript- E.O.U. ; Final Approval and Accountability- O.Y., E.O.U.

Conflict of Interest: Authors declared no conflict of interest.

ORCID IDs of the authors

Ozlem Yildirim   0000-0003-2674-4828
Evren Onay-Ucar   0000-0003-1152-4881

REFERENCES

1. Koshy M, Villano JL, Dolecek TA, et al. Improved survival time trends for glioblastoma using the SEER 17 population-based registries. *J Neurooncol*. 2012;107:207–212.

2. Ostrom QT, Gittleman H, Farah P, et al. CBTRUS statistical report: Primary brain and central nervous system tumors diagnosed in the United States in 2006–2010. *Neuro-Oncology*. 2013;15–ii56.

3. Batash R, Asna N, Schaffer P, et al. Glioblastoma multiforme, diagnosis and treatment; Recent literature review. *Curr Med Chem*. 2017;24:3002–3009.

4. Ostrom QT, Bauchet L, Davis FG, et al. The epidemiology of glioma in adults: A "state of the science" review. *Neuro Oncol*. 2014;16:896–913.

5. Louis DN, Perry A, Reifenberger G, et al. The 2016 World Health Organization classification of tumors of the central nervous system: A summary. *Acta Neuropathol*. 2016;131:803–820.

6. Yan H, Parsons DW, Jin G, et al. *IDH1* and *IDH2* mutations in gliomas. *N Engl J Med*. 2009;360(8):765–773.

7. Ohgaki H, Kleihues P. The definition of primary and secondary glioblastoma. *Clin Cancer Res*. 2013;19:764-772.

8. Louis DN, Ohgaki H, Wiestler OD, et al. The 2007 WHO classification of tumours of the central nervous system. *Acta Neuropathol*. 2007;114(1):97-109.

9. Capper D, Zentgraf H, Balss J, et al. Monoclonal antibody specific for *IDH1* R132H mutation. *Acta Neuropathol*. 2009; 118(1):599-601.

10. Brat DJ, Aldape K, Colman H, et al. cIMPACT-NOW update 3: Recommended diagnostic criteria for "Diffuse astrocytic glioma, IDH-wildtype, with molecular features of glioblastoma, WHO grade IV". *Acta Neuropathol*. 2018;136(5):805–810.

11. Capper D, Jones DTW, Sill M, et al. DNA methylation-based classification of central nervous system tumours. *Nature*. 2018;555(7697):469–474.

12. Ferrer VP, Moura Neto V, Mentlein R. Glioma infiltration and extracellular matrix: Key players and modulators. *Glia*.

2018;66:1542–1565.

13. Chen JT, Mao SF, Li HF, et al. The pathological structure of the perivascular niche in different microvascular patterns of glioblastoma. *PLoS One*. 2017;12(8):12. doi: 10.1371/journal.pone.018283.

14. Zhao X, Chen RJ, Liu M, Feng JF, Chen J, Hu KL. Remodeling the blood-brain barrier microenvironment by natural products for brain tumor therapy. *Acta Pharm Sin B*. 2017;7(5):541–553.

15. Nakod PS, Kim Y, Rao SS. Biomimetic models to examine microenvironmental regulation of glioblastoma stem cells. *Cancer Lett*. 2018;429:41–53.

16. Dey M, Ulasov IV, Lesniak MS. Virotherapy against malignant glioma stem cells. *Cancer Lett*. 2010;289(1):1–10.

17. Simon T, Gagliano T, Giamas G. Direct effects of anti-angiogenic therapies on tumor cells: VEGF signaling. *Trends Mol Med*. 2017;23(3):282–292.

18. Fessler E, Borovski T, Medema JP. Endothelial cells induce cancer stem cell features in differentiated glioblastoma cells via bFGF. *Mol Cancer*. 2015;14:157.

19. Hu F, Ku MC, Markovic D, et al. Glioma associated microglial MMP9 expression is upregulated by TLR2 signalling and sensitive to minocycline. *Int J Cancer*. 2014;135(11):2569–2578.

20. Jakel S, Dimou L. Glial cells and their function in the adult brain: A journey through the history of their ablation. *Front Cell Neurosci*. 2017;11. doi: 10.3339/fncel.2017.00024

21. Quail DF, Joyce JA. The microenvironmental landscape of brain tumors. *Cancer Cell*. 2017;31(3):326–341.

22. Phillips HS, Kharbanda S, Chen R, et al. Molecular subclasses of high-grade glioma predict prognosis, delineate a pattern of disease progression, and resemble stages in neurogenesis. *Cancer Cell*. 2006;9(1):157-173.

23. Verhaak RG, Hoadley KA, Purdom E, et al. Integrated genomic analysis identifies clinically relevant subtypes of glioblastoma characterized by abnormalities in *PDGFRA, IDH1, EGFR*, and *NF1*. *Cancer Cell*. 2010;17(1):98-110.

24. Sturm D, Witt H, Hovestadt V, et al. Hotspot mutations in *H3F3A* and *IDH1* define distinct epigenetic and biological subgroups of glioblastoma. *Cancer Cell*. 2012;22(1):425-437.

25. Parsons DW, Jones S, Zhang X, et al. An integrated genomic analysis of human glioblastoma multiforme. *Science*. 2008;321(5897):1807–1812.

26. Turcan S, Rohle D, Goenka A, et al. *IDH1* mutation is sufficient to establish the glioma hypermethylator phenotype. *Nature*. 2012;483(1):479-483.

27. Noushmehr H, Weisenberger DJ, Diefes K, et al. Identification of a CpG island methylator phenotype that defines a distinct subgroup of glioma. *Cancer Cell*. 2010;17(1):510-522.

28. Horbinski C. What do we know about *IDH1/2* mutations so far, and how do we use it? *Acta Neuropathol*. 2013;125(5):621–636.

29. Capper D, Weissert S, Balss J, et al. Characterization of R132H mutation-specific IDH1 antibody binding in brain tumors. *Brain Pathol*. 2010;20(1):245–254.

30. DeWitt JC, Jordan JT, Frosch MP, et al. Cost-effectiveness of IDH testing in diffuse gliomas according to the 2016 WHO classification of tumors of the central nervous system recommendations. *Neuro Oncol*. 2017;19(12):1640–1650.

31. Labussiere M, Di Stefano AL, Gleize V, et al. *TERT* promoter mutations in gliomas, genetic associations and clinicopathological correlations. *Br J Cancer*. 2014;111(1):2024-2032.

32. Schwartzentruber J, Korshunov A, Liu XY, et al. Driver mutations in histone H3.3 and chromatin remodelling genes in paediatric glioblastoma. *Nature*. 2012;482:226–231.

33. Chaurasia A, Park SH, Seo JW, et al. Immunohistochemical analysis of ATRX, IDH1 and p53 in glioblastoma and their correlations with patient survival. *J Korean Med Sci*. 2016;31:1208–1214.

34. Killela PJ, Reitman ZJ, Jiao Y, et al. *TERT* promoter mutations occur frequently in gliomas and a subset of tumors derived from cells with low rates of self-renewal. *Proc Natl Acad Sci USA*. 2013;110(1):6021-6026.

35. Vinagre J, Pinto V, Celestino R, et al. Telomerase promoter mutations in cancer: An emerging molecular biomarker? *Virchows Arch*. 2014;465:119–133.

36. Nakahara Y, Okamoto H, Mineta T, et al. Expression of the Wilms' tumor gene product WT1 in glioblastomas and medulloblastomas. *Brain Tumor Pathol*. 2004;21:113–116.

37. Fredriksson NJ, Ny L, Nilsson JA, et al. Systematic analysis of noncoding somatic mutations and gene expression alterations across 14 tumor types. *Nat Genet*. 2014;46:1258–1263.

38. Eckel-Passow JE, Lachance DH, Molinaro AM, et al. Glioma groups based on *1p/19q, IDH*, and *TERT* promoter mutations in tumors. *N Engl J Med*. 2015;372:2499–2508.

39. Spiegl-Kreinecker S, Lötsch D, Ghanim B, et al. Prognostic quality of activating *TERT* promoter mutations in glioblastoma: Interaction with the rs2853669 polymorphism and patient age at diagnosis. *Neuro-Oncology*. 2015;17:1231–1240.

40. Olympios N, Gilard V, Marguet F, et al. *TERT* promoter alterations in glioblastoma: A systematic review. *Cancers*. 2021;13:1147.

41. Wang TJ, Huang MS, Hong CY, et al. Comparisons of tumor suppressor *p53, p21*, and *p16* gene therapy effects on glioblastoma tumorigenicity *in situ*. *Biochem Biophys Res Commun*. 2001;287:173–180.

42. Oren M, Rotter V. Mutant *p53* gain-of-function in cancer. *Cold Spring Harb Perspect Biol*. 2010;2(2):a001107. doi: 10.1101/cshperspect.a001107

43. Adorno M, Cordenonsi M, Montagner M, et al. A Mutant-p53/Smad Complex Opposes p63 to Empower TGFβ-Induced Metastasis. *Cell*. 2009;137:87–98.

44. Behling F, Barrantes-Freer A, Skardelly M, et al. Frequency of *BRAF* V600E mutations in 969 central nervous system neoplasms. *Diagn Pathol*. 2016;11:55. doi: 10.1186/s13000-016-0506-2.

45. Bautista F, Paci A, Minard-Colin V, et al. Vemurafenib in pediatric patients with *BRAFV*600E mutated high-grade gliomas. *Pediatr Blood Cancer*. 2014;61(1):1101-1103.

46. Patel R, Leung HY. Targeting the EGFR-family for therapy: Biological challenges and clinical perspective. *Curr Pharm Des*. 2012;18:2672–2679.

47. Ekstrand AJ, Sugawa N, James CD, Collins VP. Amplified and rearranged epidermal growth factor receptor genes in human glioblastomas reveal deletions of sequences encoding portions of the N- and/or C-terminal tails. *Proc Natl Acad Sci USA*. 1992;89(1):4309-4313.

48. Cowppli-Bony A, Bouvier G, Rué M, et al. Brain tumors and hormonal factors: Review of the epidemiological literature. *Cancer Causes Control*. 2011;22:697–714.

49. Smith JS, Tachibana I, Passe SM, et al. *PTEN* mutation, *EGFR* amplification, and outcome in patients with anaplastic astrocytoma and glioblastoma multiforme. *J Natl Cancer Inst*. 2001;93:1246–1256.

50. Heimberger AB, Sampson JH. The PEPvIII-KLH (CDX-110) vac-

cine in glioblastoma multiforme patients. *Expert Opin Biol Ther.* 2009;9:1087–1098.

51. Hegi ME, Diserens AC, Gorlia T, et al. *MGMT* gene silencing and benefit from temozolomide in glioblastoma. *N Engl J Med.* 2005;352(10):997–1003.

52. Malmström A, Grønberg BH, Marosi C, et al. Temozolomide versus standard 6-week radiotherapy versus hypofractionated radiotherapy in patients older than 60 years with glioblastoma: The Nordic randomised, phase 3 trial. *Lancet Oncol.* 2012;13(1):916-926.

53. Weller M, van den Bent M, Hopkins K, et al. EANO guideline for the diagnosis and treatment of anaplastic gliomas and glioblastoma. *Lancet Oncol.* 2014;15(9):e395-403. doi: 10.1016/S1470-2045(14)70011-7

54. Hopkins BD, Hodakoski C, Barrows D, Mense SM, Parsons RE. PTEN function: The long and the short of it. *Trends Biochem Sci.* 2014;39:183–190.

55. Koul D. PTEN signaling pathways in glioblastoma. *Cancer Biol Ther.* 2008;7:1321–1325.

56. Knobbe CB, Merlo A, Reifenberger G. PTEN signalling in gliomas. *Neuro-Oncology.* 2002;4:196–210.

57. La Fougere C, Suchorska B, Bartenstein P, et al. Molecular imaging of gliomas with PET: Opportunities and limitations. *Neuro Oncol.* 2011;13(1):806-819.

58. Kono K, Inoue Y, Nakayama K, et al. The role of diffusion-weighted imaging in patients with brain tumors. *AJNR Am J Neuroradiol.* 2001;22(1):1081-1088.

59. Law M, Yang S, Wang H, et al. Glioma grading: Sensitivity, specificity, and predictive values of perfusion MR imaging and proton MR spectroscopic imaging compared with conventional MR imaging. *AJNR Am J Neuroradiol.* 2003;24(1):1989-1998.

60. Roa W, Brasher PM, Bauman G, et al. Abbreviated course of radiation therapy in older patients with glioblastoma multiforme: A prospective randomized clinical trial. *J Clin Oncol.* 2004;22(1):1583-1588.

61. Taphoorn MJ, Stupp R, Coens C, et al. Health-related quality of life in patients with glioblastoma: A randomised controlled trial. *Lancet Oncol.* 2005;6(1):937-944.

62. Keime-Guibert F, Chinot O, Taillandier L, et al. Radiotherapy for glioblastoma in the elderly. *N Engl J Med.* 2007;356(1):1527-1535.

63. Wick W, Menn O, Meisner C, et al. Pharmacotherapy of epileptic seizures in glioma patients: Who, when, why and how long? *Onkologie.* 2005;28(1):391-396.

64. Chaichana KL, Parker SL, Olivi A, et al. Long-term seizure outcomes in adult patients undergoing primary resection of malignant brain astrocytomas. *J Neurosurg.* 2009;111(1):282-292.

65. Stupp R, Mason WP, van den Bent MJ, et al. Radiotherapy plus concomitant and adjuvant temozolomide for glioblastoma. *N Engl J Med.* 2005;352(1):987-996.

66. Gilbert MR, Wang M, Aldape KD, et al. Dose-dense temozolomide for newly diagnosed glioblastoma: A randomized phase III clinical trial. *J Clin Oncol.* 2013;31(1):4085-4091.

67. Murphy ES, Xie H, Merchant TE, Yu JS, Chao ST, Suh JH. Review of cranial radiotherapy-induced vasculopathy. *J Neurooncol.* 2015;122(3):421–429.

68. Heffron TP. Challenges of developing small-molecule kinase inhibitors for brain tumors and the need for emphasis on free drug levels. *Neuro Oncol.* 2018;20(3):307–312.

69. Idbaih A, Canney M, Belin L, et al. Safety and feasibility of repeated and transient blood-brain barrier disruption by pulsed ultrasound in patients with recurrent glioblastoma. *Clin Cancer Res.* 2019;25(13):3793–3801.

70. Brennan CW, Verhaak RG, McKenna A, et al. TCGA Research Network. The somatic genomic landscape of glioblastoma. *Cell.* 2013;155(2):462–477.

71. Sottoriva A, Spiteri I, Piccirillo SG, et al. Intratumor heterogeneity in human glioblastoma reflects cancer evolutionary dynamics. *Proc Natl Acad Sci USA.* 2013;110(10):4009–4014.

72. Francis JM, Zhang CZ, Maire CL, et al. *EGFR* variant heterogeneity in glioblastoma resolved through single-nucleus sequencing. *Cancer Discov.* 2014;4(8):956–971.

73. Neftel C, Laffy J, Filbin MG, et al. An integrative model of cellular states, plasticity, and genetics for glioblastoma. *Cell.* 2019;178(4):835–849.

74. Patel AP, Tirosh I, Trombetta JJ, et al. Single-cell RNA-seq highlights intratumoral heterogeneity in primary glioblastoma. *Science.* 2014;344(6190):1396–1401.

75. Lan X, Jörg DJ, Cavalli FMG, et al. Fate mapping of human glioblastoma reveals an invariant stem cell hierarchy. *Nature.* 2017;549(7671):227–232.

76. Chen J, Li Y, Yu TS, et al. A restricted cell population propagates glioblastoma growth after chemotherapy. *Nature.* 2012;488(7412):522–526.

77. Ohgaki H, Kim YH, Steinbach JP. Nervous system tumors associated with familial tumor syndromes. *Curr Opin Neurol.* 2010;23(1):583-591.

78. Jonsson P, Lin AL, Young RJ, et al. Genomic correlates of disease progression and treatment response in prospectively characterized gliomas. *Clin Cancer Res.* 2019;25(18):5537–5547.

79. Melin BS, Barnholtz-Sloan JS, Wrensch MR, et al. GliomaScan Consortium. Genome-wide association study of glioma subtypes identifies specific differences in genetic susceptibility to glioblastoma and non-glioblastoma tumors. *Nat Genet.* 2017;49(5):789–794.

80. Neglia JP, Robison LL, Stovall M, et al. New primary neoplasms of the central nervous system in survivors of childhood cancer: A report from the Childhood Cancer Survivor Study. *J Natl Cancer Inst.* 2006;98(1):1528-1537.

81. Minniti G, Traish D, Ashley S, et al. Risk of second brain tumor after conservative surgery and radiotherapy for pituitary adenoma: Update after an additional 10 years. *J Clin Endocrinol Metab.* 2005;90(1):800-804.

82. Brada M, Ford D, Ashley S, et al. Risk of second brain tumour after conservative surgery and radiotherapy for pituitary adenoma. *Br Med J.* 1992;304(1):1343-1346.

83. Interphone Study Group. Brain tumour risk in relation to mobile telephone use: results of the INTERPHONE international case-control study. *Int J Epidemiol.* 2010;39(1):675-694.

84. Dziurzynski K, Chang SM, Heimberger AB, et al. Consensus on the role of human cytomegalovirus in glioblastoma. *Neuro Oncol.* 2012;14(1):246-255.

85. Wick W, Platten M. CMV infection and glioma, a highly controversial concept struggling in the clinical arena. *Neuro Oncol.* 2014;16(1):332-333.

86. Connelly JM, Malkin MG. Environmental risk factors for brain tumors. *Curr Neurol Neurosci Rep.* 2007;7(1):208-214.

87. Bondy ML, Scheurer ME, Malmer B, et al. Brain tumor epidemiology: Consensus from the Brain Tumor Epidemiology Consortium. *Cancer.* 2008;113(1):1953-1968.

88. Ostrom QT, Barnholtz-Sloan JS. Current state of our knowledge on brain tumor epidemiology. *Curr Neurol Neurosci Rep.* 2011;11(1):329-335.

89. Ohgaki H, Dessen P, Jourde B, et al. Genetic pathways to glioblastoma: A population-based study. *Cancer Res.* 2004;64:6892–6899.

90. Fukushima T, Favereaux A, Huang H, et al. Genetic alterations in primary glioblastomas in Japan. *J Neuropathol Exp Neurol.* 2006;65:12–18.

91. UC Clinical Trials.http://www.ucclinicaltrials.com. Accessed on July 10, 2024.

92. Mayo Clinic. http://www.mayoclinic.org. Accessed on July 10, 2024.

93. Clinical Trials at UCSF. http://www.ucsfclinicaltrials.org. Accessed on July 10, 2024.

94. Memorial Sloan Kettering Cancer Centre. http://www.mskcc.org. Accessed on July 10, 2024.

95. Wilson CB. Current concepts in cancer: Brain tumors. *N Engl J Med.* 1979;300:1469-1471.

96. Weller M, Cloughesy T, Perry JR, Wick W. Standards of care for treatment of recurrent glioblastoma – Are we there yet? *Neuro Oncol.* 2013;15(1):4-27.

97. Gramatzki D, Dehler S, Rushing EJ, et al. Glioblastoma in the canton of Zurich, Switzerland revisited, 2005 to 2009. *Cancer.* 2016;122(16):2206-2215.

98. Jackson CM, Kochel CM, Nirschl CJ, et al. Systemic tolerance mediated by melanoma brain tumors is reversible by radiotherapy and vaccination. *Clin Cancer Res.* 2016;22(5):1161-1172.

99. Topalian SL, Taube JM, Anders RA, Pardoll DM. Mechanism-driven biomarkers to guide immune checkpoint blockade in cancer therapy. *Nat Rev Cancer.* 2016;16:275-287.

100. Aurelian L. Oncolytic viruses as immunotherapy, progress and remaining challenges. *OncoTargets Ther.* 2016;9:2627-2637.

101. Mellman I, Coukos G, Dranoff G. Cancer immunotherapy comes of age. *Nature.* 2011;480:480-489.

102. Topalian SL, Drake CG, Pardoll DM. Immune checkpoint blockade: A common denominator approach to cancer therapy. *Cancer Cell.* 2015;27:450-461.

103. Brown CE, Alizadeh D, Starr R, et al. Regression of glioblastoma after chimeric antigen receptor T-cell therapy. *N Engl J Med.* 2016;375(26):2561-2569.

104. O'Rourke DM, Nasrallah MP, Desai A, et al. A single dose of peripherally infused EGFRvIII-directed CAR T cells mediates antigen loss and induces adaptive resistance in patients with recurrent glioblastoma. *Sci Transl Med.* 2017;9(399):eaaa0984 doi: 10.1126/scitranslmed.aaa0984

105. Bagley SJ, Desai AS, Linette GP, June CH, O'Rourke DM. CAR T-cell therapy for glioblastoma: Recent clinical advances and future challenges. *Neuro Oncol.* 2018;20(11):1429-1438.

106. Sadelain M, Riviere I, Riddell S. Therapeutic T cell engineering. *Nature.* 2017;545:423-431.

107. Beyar-Katz O, Gill S. Advances in chimeric antigen receptor T cells. *Curr Opin Hematol.* 2020;27:368-377.

108. Batlevi CL, Matsuki E, Brentjens RJ, Younes A. Novel immunotherapies in lymphoid malignancies. *Nat Rev Clin Onco.* 2016;13:25-40.

109. Brown MP, Ebert LM, Gargett T. Clinical chimeric antigen receptor-T cell therapy: A new and promising treatment modality for glioblastoma. *Clin Transl Immuno*l. 2019;8(5):e1050. doi: 10.1002/cti2.1050

110. Brown CE, Badie B, Barish ME, et al. Bioactivity and safety of IL13Ralpha2-redirected chimeric antigen receptor CD8+ T cells in patients with recurrent glioblastoma. *Clin Cancer Res.* 2015;21:4062-4072.

111. Ahmed N, Brawley V, Hegde M, et al. HER2-specific chimeric antigen receptor-modified virus-specific T cells for progressive glioblastoma: A phase 1 dose-escalation trial. *JAMA Oncol.* 2017;3:1094-1101.

112. Kaufmann JK, Chiocca EA. Glioma virus therapies between bench and bedside. *Neuro Oncol.* 2014;16(3):334-351.

113. Blitz SE, Kappel AD, Gessler FA, et al. Tumor-associated macrophages/microglia in glioblastoma oncolytic virotherapy: A double-edged sword. *Int J Mol Sci.* 2022;23(3):1808. doi: 10.3390/ijms23031808

114. Zhou C, Chen Q, Chen Y, Qin CF. Oncolytic Zika virus: New option for glioblastoma treatment. *DNA Cell Biol.* 2023;42:267-273.

115. Chen Q, Wu J, Ye Q, Ma F, Zhu Q, Wu Y, et al. Treatment of human glioblastoma with a live attenuated Zika virus vaccine candidate. *mBio.* 2018;9(5):e01683-18. doi: 10.1128/mBio.01683-18

116. Chiocca EA, Abbed KM, Tatter S, et al. A phase I open-label, dose-escalation, multi-institutional trial of injection with an E1B-attenuated adenovirus, ONYX-015, into the peritumoral region of recurrent malignant gliomas, in the adjuvant setting. *Mol Ther.* 2004;10:958-966.

117. Markert JM, Razdan SN, Kuo HC, et al. A phase 1 trial of oncolytic HSV-1, G207, given in combination with radiation for recurrent GBM demonstrates safety and radiographic responses. *Mol Ther.* 2014;22:1048-1055.

118. Marelli G, Howells A, Lemoine NR, Wang Y. Oncolytic viral therapy and the immune system: A double-edged sword against cancer. *Front Immunol.* 2018;9:866. doi: 10.3389/fimmu.2018.00866

119. Kicielinski KP, Chiocca EA, Yu JS, et al. Phase 1 clinical trial of intratumoral reovirus infusion for the treatment of recurrent malignant gliomas in adults. *Mol Ther.* 2014;22:1056-1062.

120. Gujar S, Bell J, Diallo JS. SnapShot: Cancer immunotherapy with oncolytic viruses. *Cell.* 2019;176:1240-1240.e1. doi: 10.1016/j.cell.2019.01.051

121. Angom RS, Nakka NMR, Bhattacharya S. Advances in glioblastoma therapy: An update on current approaches. *Brain Sci.* 2023;13:1536. doi: 10.3390/brainsci13111536

122. Asija S, Chatterjee A, Yadav S, et al. Combinatorial approaches to effective therapy in glioblastoma (GBM): Current status and what the future holds. *Int Rev Immunol.* 2022;41:582-605.

123. Huang B, Li X, Li Y, Zhang J, Zong Z, Zhang H. Current immunotherapies for glioblastoma multiforme. *Front Immunol.* 2021;11:603911. doi: 10.3389/fimmu.2020.603911

124. Shoaf ML, Desjardins A. Oncolytic viral therapy for malignant glioma and their application in clinical practice. *Neurotherapeutics.* 2022;19:1818–1831.

125. Qi Z, Long X, Liu J, Cheng P. Glioblastoma microenvironment and its reprogramming by oncolytic virotherapy. *Front Cell Neurosci.* 2022;16:819363. doi: 10.3389/fncel.2022.819363.

126. Kamynina M, Tskhovrebova S, Fares J, et al. Oncolytic virus-induced autophagy in glioblastoma. *Cancers.* 2021;13:3482. doi: 10.3390/cancers13143482

127. Haddad AF, Young JS, Mummaneni NV, Kasahara N, Aghi MK.

Immunologic aspects of viral therapy for glioblastoma and implications for interactions with immunotherapies. *J Neuro-Oncol*. 2021;152:1–13.

128. Ali S, Xia Q, Muhammad T, et al. Glioblastoma therapy: Rationale for a mesenchymal stem cell-based vehicle to carry recombinant viruses. *Stem Cell Rev Rep*. 2022;18:523–543.

129. Desjardins A, Gromeier M, Herndon JE 2nd, et al. Recurrent glioblastoma treated with recombinant poliovirus. *N Engl J Med*. 2018;379:150–161.

130. Gromeier M, Lachmann S, Rosenfeld MR, Gutin PH, Wimmer E. Intergeneric poliovirus recombinants for the treatment of malignant glioma. *Proc Natl Acad Sci USA*. 2000;97:6803–6808.,

131. Gilbert MR, Dignam JJ, Armstrong TS, et al. A randomized trial of bevacizumab for newly diagnosed glioblastoma. *N Engl J Med*. 2014;370:699–708.

132. Hegi ME, Rajakannu P, Weller M. Epidermal growth factor receptor: A re-emerging target in glioblastoma. *Curr Opin Neurol*. 2012;25:774-779.

133. Rohle D, Popovici-Muller J, Palaskas N, et al. An inhibitor of mutant *IDH1* delays growth and promotes differentiation of glioma cells. *Science*. 2013;340:626-630.

134. Cancer Genome Atlas Research. Comprehensive genomic characterization defines human glioblastoma genes and core pathways. *Nature*. 2008;455:1061-1068.

135. Lee EQ, Kuhn J, Lamborn KR, et al. Phase I/II study of sorafenib in combination with temsirolimus for recurrent glioblastoma or gliosarcoma: North American Brain Tumor Consortium study 05-02. *Neuro Oncol*. 2012;14:1511–1518.

136. Wen PY, Chang SM, Lamborn KR, et al. Phase I/II study of erlotinib and temsirolimus for patients with recurrent malignant gliomas: North American Brain Tumor Consortium trial 04-02. *Neuro Oncol*. 2014;16:567–578.

137. Chinot OL, Wick W, Mason M, et al. Bevacizumab plus radiotherapy-temozolomide for newly diagnosed glioblastoma. *N Engl J Med*. 2014;370:709–722.

138. Sandmann T, Bourgon R, Garcia J, et al. Patients with proneural glioblastoma may derive overall survival benefit from the addition of bevacizumab to first-line radiotherapy and temozolomide: retrospective analysis of the AVAglio trial. *J Clin Oncol*. 2015;33:2735–2744.

139. Pilié PG, Tang C, Mills GB, Yap TA. State-of-the-art strategies for targeting the DNA damage response in cancer. *Nat Rev Clin Oncol*. 2019;16(2):81–104.

140. Gupta SK, Mladek AC, Carlson BL, et al. Discordant in vitro and in vivo chemopotentiating effects of the PARP inhibitor veliparib in temozolomide-sensitive versus -resistant glioblastoma multiforme xenografts. *Clin Cancer Res*. 2014;20(14):3730–3741.

141. Venneti S, Thompson CB. Metabolic reprogramming in brain tumors. *Annu Rev Pathol*. 2017;12:515–545.

142. Agnihotri S, Golbourn B, Huang X, et al. PINK1 is a negative regulator of growth and the Warburg effect in glioblastoma. *Cancer Res*. 2016;76(16):4708–4719.

143. Agnihotri S, Mansouri S, Burrell K, et al. Ketoconazole and posaconazole selectively target HK2-expressing glioblastoma cells. *Clin Cancer Res*. 2019;25(2):844–855.

144. Villa GR, Hulce JJ, Zanca C, et al. An LXR-cholesterol axis creates a metabolic co-dependency for brain cancers. *Cancer Cell*. 2016;30(5):683–693.

145. Rominiyi O, Vanderlinden A, Clenton SJ, et al. Tumour treating fields therapy for glioblastoma: current advances and future directions. *Br J Cancer*. 2021; 124:697–709.

146. Olatunji G, Aderinto N, Adefusi T, et al. Efficacy of tumour-treating fields therapy in recurrent glioblastoma: A narrative review of current evidence. Medicine (Baltimore). 2023 102(48):e36421. doi: 10.1097/MD.0000000000036421

How to cite this article

Overexpression of Pepper Capsaicinoid Pathway Genes in Tomato (*Solanum lycopersicum* L.)

Chudamani Sharma Prakash[1] (iD), Yi-Hong Wang[1] (iD)

[1]Department of Biology, University of Louisiana at Lafayette, Lafayette, LA 70503, USA

ABSTRACT

Objective: The Solanaceae family includes many unique and popular fruits and vegetables such as potato, tomato, and pepper. Peppers are a group of plants that produce pungent fruits favoured by many in various parts of the world. This spiciness is due to a class of compounds called capsaicinoid which are synthesized in peppers but not in tomatoes. Both pepper and tomato genomes have been sequenced, and genes involved in the capsaicinoid biosynthesis pathway have been identified in both genomes. Along with expression profiling, there were only three genes in the tomato pathway that were not expressed. In this study, we attempted to overexpress the three pepper genes in tomato to produce spicy fruits.

Materials and Methods: The three genes, *BCAT* (branched-chain amino acid aminotransferase), *Kas* (ketoacyl-ACP synthase), and *CS/AT* (capsaicin synthase/acyltransferase), were separated using P2Am and T2Am sequences in a tricistronic cassette driven by the 35S promoter. Transgenic tomato plants containing the gene construct were generated via *Agrobacterium*-mediated transformation.

Results: RT-PCR indicated that the genes were expressed in all transgenic tomato plants. Some transgenic fruits resembled hot peppers with elongated shapes and wrinkled surfaces, but tomato fruits were not spicy based on two-person tasting evaluations.

Conclusion: P2Am and T2Am sequences can be used for the overexpression of multiple genes in tomatoes. Further studies with tissue-specific promoters and metabolic profiling are necessary.

Keywords: Capsaicinoid pathway genes, Overexpression, Pepper, Tomato

INTRODUCTION

The pungency of hot peppers (*Capsicum ssp.*) is the accumulation of a group of alkaloids called capsaicinoid, such as capsaicin and dihydrocapsaicin.[1] Capsaicinoids are synthesised in pepper fruit placenta through two biochemical pathways. In the phenylpropanoid pathway, phenylalanine is converted to vanillylamine, and in the branched chain fatty acid pathway, valine is converted to 8-methyl nonenoic acid.[2] Capsaicin synthase (CS) then combines both compounds to produce capsaicin and other capsaicinoids.[3]

Pepper is a common spice used in varieties of cuisine all over the world and is an excellent source of vitamins C, A, B-complex, and E.[4] As a medicine, it is a counter irritant in lumbago, neuralgia, rheumatic disorder, and non-allergic rhinitis and as a folk remedy for dropsy, colic, diarrhoea, asthma, arthritis, muscle cramps, and toothache.[5,6] These findings suggest that a diet with capsaicinoid is beneficial for health and thus hot peppers should be considered a functional food.[7] Peppers are often cultivated in open fields and are vulnerable to environmental conditions that are detrimental to fruit yield.[2] For example, high temperature, high CO_2 level, and excess rain can all reduce plant growth and fruit yield and increase disease incidence in the plants.[8] Seed germination rate highly depends on fruit maturity, species, cultivar, and post-harvest handling.[9] In addition, environmental factors heavily influence capsaicinoid biosynthesis and consequently pungency levels.[10]

Plant breeding has significantly contributed to the development of new varieties.[11] Other genetic manipulations such as *Agrobacterium*-mediated genetic transformation are not trivial for peppers. Currently available pepper transformation protocols have low efficiency, poor reproducibility, and high genotype-dependence.[12,13] Engineering tomatoes to produce capsaicinoid represents an alternative.[14]

Tomato (*Solanum lycopersicum*) is the most important horticultural crop.[15] Despite their divergence 19 million years ago[16], the genomes of pepper and tomato are significantly conserved,

with a basic chromosome number of x = 12 in both species and major conserved syntenic segments between them.[17] Tomatoes are more amenable to genetic transformation, are highly productive with a short cropping cycle, and can be used to produce capsaicinoids.[18,19] Phylogenetic analysis of gene families involved in capsaicinoid biosynthesis in pepper and their orthologs in tomato, potato, and *Arabidopsis* identified 51 gene families, of which 13 had independent pepper-specific duplication (such as *ACLd, AT3, b-CT, C3H, CAD, CCR, Kas I* and *PAL* genes).[17] Comparative transcriptome analysis identified several genes in the capsaicin biosynthesis pathway with different expressions between pepper and tomato fruits. At the fruiting stage *BCAT* (branched-chain amino acid aminotransferase), *Kas* (ketoacyl-ACP synthase), and *CS/AT* (capsaicin synthase/acyltransferase) are highly expressed in pepper fruit placenta but not in the tomatoes.[3] Comparative expression studies in non-pungent peppers vs pungent pepper also showed large deletions in the *CS* gene, which cause no or very low expression in non-pungent pepper.[20] These results indicate that changes in the expression of *BCAT, Kas*, and *CS/AT* enabled capsaicinoid synthesis in hot pepper fruits.[3,20] Therefore, pungency in pepper is under transcriptional control, and higher expression of capsaicinoid biosynthesis genes in the placental septum increases pungent levels.[21,22] Compared with peppers, some genes in tomatoes have lower levels of expression (*PAL, C4H, ACL* and *AMT*), others have lower levels of expression with temporally restricted expression (*COMT* and *FaTA*), and some are not expressed at all (*Kas, BCAT* and *CS*).[3]

Based on the genetic information on both pepper and tomato, it is theoretically possible to activate the capsaicinoid pathway in tomato. Three genome engineering strategies can be employed for this purpose. One is to use transcriptional activators like effectors (TALEs)[23] or CRISPR/Cas9[24] for multiplex activation of genes in pepper. The second strategy is the use of targeted promoter replacement through genome engineering for the activation of inactive genes in tomatoes.[25,26] The third involves the overexpression of the pepper genes (*Kas, BCAT* and *CS*) in tomato through *Agrobacterium*-mediated transformation. This study has used *Agrobacterium*-mediated tomato transformation to insert and overexpress three pepper genes involved in capsaicin biosynthesis: *BCAT, Kas*, and *CS/AT*. Two different vectors were prepared: one with the 35s promoter and the other with the fruit-specific E8 promoter. All three genes were included in a single tricistronic vector for transformation. All three genes are involved in capsaicin biosynthesis through the branched chain fatty acid pathway. *BCAT* condenses valine to alpha ketoisovalerate. *Kas* along with *ACL* (acyl carrier protein) is involved in fatty acid synthesis through isobutyryl-CoA to 8-methyl-6-nonenoic acid. CS/AT/PUN1 condenses vanillylamine from the phenylpropanoid pathway with 8-methyl-6-noneoyl-CoA from the branched chain fatty acid pathway to synthesize capsaicin.[3]

MATERIALS AND METHODS

Preparation of the Overexpression Gene Construct

The pCAMBIA1301 vector was used to prepare the overexpression gene construct. The tricistronic cassette with the three pepper genes was arranged as shown in Figure 1A. The three genes were separated using P2Ap and T2Ap peptides (Figure 1B) from Osborn et al. [27]. The peptides were reverse translated to DNA sequences (P2A and T2A in Figure 1B) and optimized for plants (*Arabidopsis*) using JCat [28] to produce the P2Am and T2Am (Figure 1B) used in Figure 1A. The cassette (Figure 1C) was synthesized by BioBasic (Amherst, NY, USA) and ligated into pCAMBIA1301 after digestion with *Nco*I and *Bst*EII. The construct was used to transform *Agrobacterium tumefaciens* strain LBA4404, and positive clones were used for tomato transformation (see Transformation of tomato below).

Agrobacterium Preparation

Competent *Agrobacterium tumefaciens* strain LBA4404 cells with an OD_{600} of 0.1 were transformed with the construct described above using electroporation. A single colony from transformed *Agrobacterium* cells was inoculated into 10 mL LB broth with 50 mg l^{-1} kanamycin and grown for 24 h at 28 °C. An aliquot of the cultured cells was subsequently inoculated into 50-mL LB with 50 µg l^{-1} kanamycin and grown for another 24 h. This culture was harvested and used for the transformation described below.

Transformation of Tomato

The tomato transformation was modified from Wang and Campbell.[29] Tomato seeds (*Solanum lycopersicum*) cv Micro-Tom and Micro-Tina from Tomato Growers Supply Company, Fort Meyers, FL were surface sterilized in 40 mL of 25% bleach with 2 drops of tween 20 for 15 min and rinsed 5-7 times with distilled water before plating in seed germination medium (MS salt 4.3 g l^{-1}, Nitsch vitamin 1 mL l^{-1}, sucrose 30 g l^{-1} and agar 6 g l^{-1}, pH 5.8). Hypocotyls and cotyledon leaves of 7-10 days old seedlings were used for transformation. Three days before transformation, *Agrobacterium* culture was started in 20 mL LB medium supplemented with 50 mg l^{-1} kanamycin. A day before transformation, hypocotyl and cotyledon leaves were cut from seedlings at the petioles and the tip using a sterile razor on the co-cultivation media (MS salt 4.3 g l^{-1}, thiamine-HCL 0.4 mg l^{-1}, Myo-inositol 100 mg l^{-1}, sucrose 30 g l^{-1}, 2,4-D 0.2 mg l^{-1}, agar 6 g l^{-1} and kinetin 0.1 mg l^{-1}) with sterile filter paper laid on the surface. The bacteria from the LB broth were harvested by centrifugation and resuspended in co-cultivation media (without agar). Leaves from overnight incubation were scraped, mixed with bacteria, and incubated at room temperature for 30 min with occasional mixing. The bacterial suspension was then drained, and the leaves were dried on sterile paper
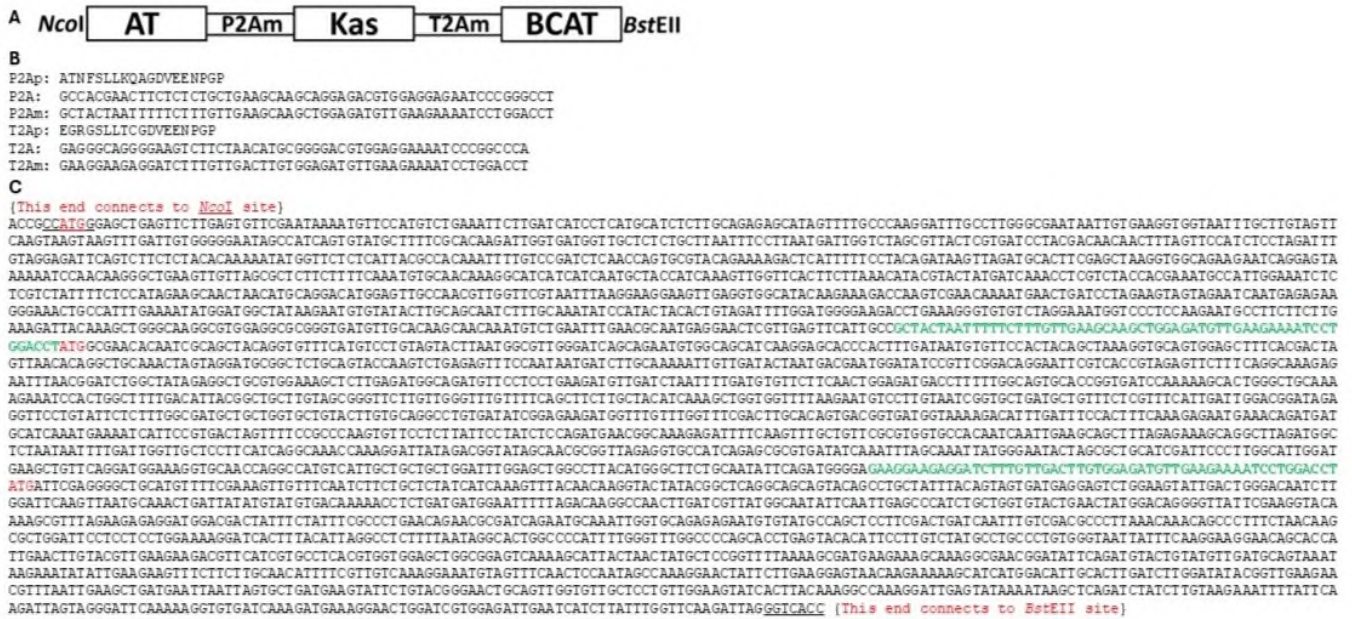
Figure 1. Tricistronic overexpression cassette. (A) Schematic of the tricistronic cassette. (B) P2Am and T2Am sequences used to facilitate cleavage of the three proteins. (C) DNA sequence of the cassette (P2Am and T2Am are in bold/green). BCAT:branched-chain amino acid aminotransferase; Kas:ketoacyl-ACP synthase; CS/AT/*PUN1:capsaicin* synthase/acyltransferase.

towels and returned to co-cultivation media with filter paper on the surface. These plates were sealed with micropore tape and incubated in the dark at room temperature for 3 days. After 3 days of co-cultivation, leaves were placed on regeneration medium (MS salts 4.3 g l^{-1}, Nitsch vitamin mL l^{-1}, sucrose 30 g l^{-1}, zeatin 1.5 mg l^{-1}, IAA 0.2 mg l^{-1}, carbenicillin 400 mg l^{-1}, hygromycin 30 mg l^{-1}, agar 6 g l^{-1} and pH 5.8) and incubated under natural day/light cycle for 3-8 weeks with media change every 3 weeks. Shoots will regenerate during this period. Regenerated shoots were transferred to rooting medium (MS salts 4.3 g l^{-1}, Nitsch vitamin 1mL l^{-1}, sucrose 30 g l^{-1}, IBA 0.5 mg l^{-1}, carbenicillin 400 mg l^{-1}, hygromycin 30 mg l-1, agar 6 g l^{-1} and pH 5.8) for further growth and rooting and then transferred to soil after acclimatization for few days.

Transformation Confirmation

Transformation and insertion of the transgene were confirmed by plant regeneration on hygromycin-containing regeneration media and then by PCR using hygromycin primers (forward: GATGTTGGCGACCTCGTATT and reverse: GATGTAGGAGGGCGTGGATA) on DNA from transgenic plants.

RNA Extraction

Total RNA was extracted using TRIzol®.[30] From T_0 transgenic plants, RNA was extracted for RT-PCR. Leaf samples from young transgenic plants were bulked to isolate RNA. Fresh 50-100 mg of leaf tissue was frozen in liquid N_2 and ground to powder using a mortar and pestle. One millilitre of TRIzol®

reagent was used to homogenise 50-100 mg of tissue. After 5 min of incubation, 0.2 mL of chloroform was added to the sample and further incubated for 3 min. The mixture was centrifuged at 4 °C for 15 min. The supernatant was transferred to a new tube mixed with 0.5 mL of isopropanol and incubated for 10 min. After centrifuging at 4°C for 5 min, the supernatant was discarded, and the RNA pellet was mixed with 1 mL of 75% ethanol and centrifuged for 5 min at 4°C. The supernatant was discarded, and the pellet was dried by inverting tubes on clean filter paper for 10 min. Around 25-30 µL of DNase/RNase-free water was used to dissolve the RNA. An aliquot of this RNA were treated with DNase I at 37 °C for 10 min. This followed phenol:chloroform extraction with isopropanol precipitation and two 75% ethanol washes. The purity of the RNA was treated with DNase I and quantified using Nanodrop. Samples with 260/280 values between 1.9 and 2.1 were used for further analysis.

RT-PCR

Semiquantitative RT-PCR was performed to confirm transgene expression using qScript® XLT One-Step RT-PCR kit from QuantaBio in Applied Biosynthesis 2720 Thermocycler. Manufacturer's guidelines were followed for reaction setup and thermocycler procedures. In short, RT-PCR was performed for RNA of both transgenic and control plants in 10 µL volume. All reagents, RNA, and primers were thawed on ice for 15 min, and the reaction was set up on ice. For each 10 µL reaction, 5 µL one-step ToughMix (20X), 0.2 µL each of forward and reverse

primers, 0.4 µL of qScript® XLT One-Step reverse transcriptase (25X), 2.2 µL of nuclease free water and 2 µL of RNA were added and mixed. The PCR plate was then spun briefly to remove any bubbles and collect the contents at the bottom of the well. In the thermocycler, RT-PCR was programmed as follows: cDNA synthesis at 48°C for 20 min, initial denaturation at 94°C for 3 min, 35 cycles of denaturation at 94°C for 20 sec, annealing at 56°C for 30 sec, and extension at 72°C for 1 min. This was followed by 72°C for 5 min and 4°C for forever. The PCR product was run on 1% agarose gel along with loading dye to visualize the presence of the transgene in RNA.

Phenotypic Observations

Transgenic tomatoes were regularly checked for any visual phenotypic changes in their fruit shape and surface texture from early fruit stages to late maturity stages. Two people tasted the spiciness of ripened tomato fruits in the laboratory.

RESULTS AND DISCUSSION

Transformation of Tomato

Two tomato lines (Micro-Tina and Micro-Tom) were used in the transformation studies. The construct with the 35S promoter was used to transform Micro-Tina, and the construct with the E8 promoter was used to transform Micro-Tom. Although the number of infected leaves was not counted, regeneration of callus from leaves was variable for both Micro-Tina and Micro-Tom lines. Micro-Tom showed an early advantage with better germination and faster growth than Micro-Tina (data not collected). During callus regeneration, the adaxial side of cotyledon leaves increased the chance of regeneration. Once calli started to produce shoots, they were transferred to a Magenta box to have more room to grow. In total, 30 transgenic plants from the 35S vector and 35 transgenic lines from the E8 vector were generated.

Confirmation of Transgene Insertion

Genomic DNA was extracted from the leaves of transgenic and control tomato plants for PCR. Hygromycin primers were used to confirm the presence of the transgene in the T_0 generation of transgenic plants (Figure 2). Hygromycin bands were observed in both Micro-Tina and Micro-Tom transgenic lines but were absent from control plants, confirming the insertion of the transgene into the tomato genome.

Gene Expression

Expression of the transgene was confirmed by semiquantitative RT-PCR using pepper gene-specific primers. For each primer set, once the primers were designed, they were BLASTed against the tomato sequence to confirm their absence from
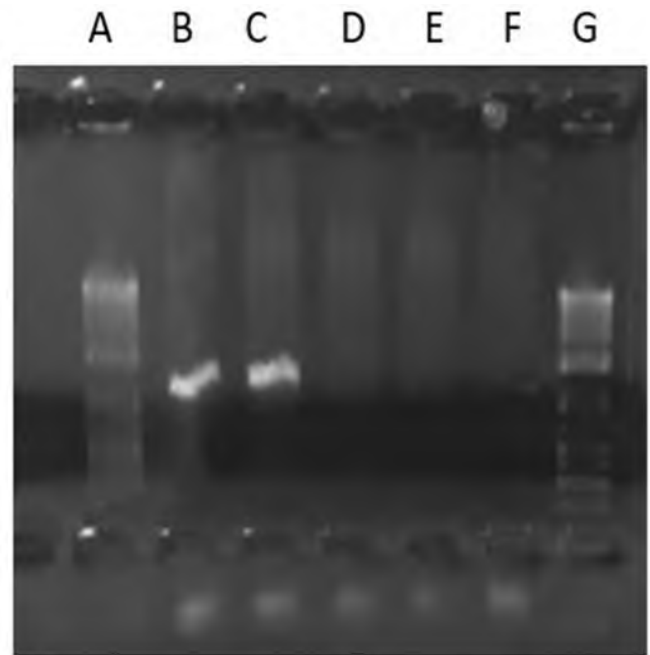

Figure 2. PCR confirmation of transgene. Lanes A and G-1 kb ladder; B, transgenic line 1; C, transgenic line 2; D, Micro-Tina control; E, Micro-Tom control and F-PCR negative control.

tomato. For each of the three genes, one specific primer set was designed. RT-PCR was performed using these primers on RNA derived from control and transgenic plants. Gel electrophoresis of the RT-PCR product showed gene bands for all three target genes (*AT, BCAT*, and *Kas*) in both transgenic lines tested, whereas the control plant did not have any transgene expression (Figure 3). This shows that all three pepper genes were integrated with the tomato genome and were being expressed.
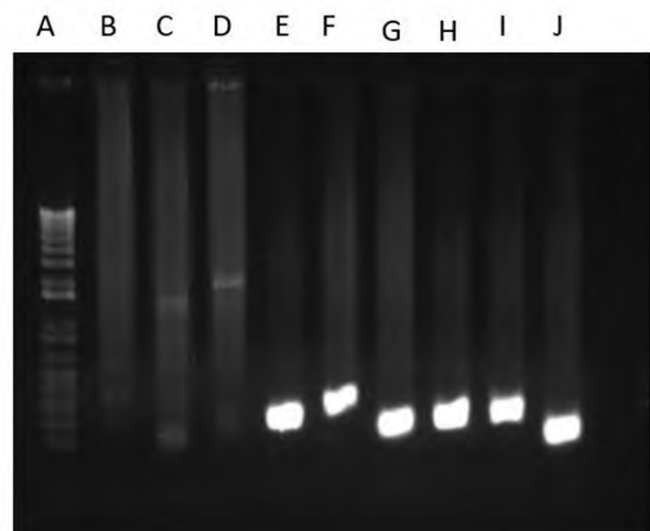

Figure 3. Gene expression in transgenic plants. Lanes A: ladder; B, C, D: control for *AT, BCAT*, and *Kas* genes; E, F, G: transgenic line 1 for *AT, BCAT*, and *Kas*; H, I, J: transgenic line 2 for *AT, BCAT*, and *Kas*.

Phenotypic Changes

Transgenic plants were observed for any phenotypic structural changes in plants and fruits. There were no overwhelming changes that were consistent throughout all transgenic lines. However, some transgenic tomato plants did produce fruits with pepper-like rough skin (Figure 4).

Figure 4. Some transgenic tomato fruits showed rough skins at the T_0 generation before turning red.

Spiciness

Ripened transgenic tomato fruits were tasted for a hint of heat. Two people independently tasted the juice from the same fruit to determine whether it was hot. There was consensus that none of the transgenic tomato fruits carried any spiciness. Although our results from RT-PCR suggested the expression of all three genes in transgenic plants, the lack of heat in fruit suggests either that there is no detectable increase in capsaicin production or that the biosynthetic pathway requires more than three genes to be overexpressed.

Tomato as a biofactor for the production of secondary metabolites is not a new concept. Butelli et al.[31] could use tomato to produce betalain (food colour). Other studies have used tomatoes to increase the production of various flavonoids[32] and phenylpropanoid compounds like resveratrol and genistin[33]. Tomato fruits are rich in primary metabolites such as citrate, malate, and ascorbic acids and secondary metabolites such as carotenoids, phenylpropanoid and terpenoids.[34] This suggests the presence of a basic biosynthetic pathway for each in tomatoes, which has led many to believe that tomatoes can be used as a chassis to produce various economically as well as pharmacologically important metabolites such as retinol (Vitamin A) through B-carotene biosynthesis and dioscin through steroidal glycoalkaloid production.[35,36]

The presence of the defunct capsaicinoid biosynthesis pathway in tomatoes offers an opportunity to produce capsaicin in this plant. This will alleviate the problems associated with pepper farming, such as varying levels of pungency, environmental distress, slow seed germination and long life cycle, as well as high levels of soil-borne diseases and nematode infection.[2] Both pepper and tomato, being members of the same nightshade family (Solanaceae), have major conserved synteny with a basic chromosome number of x=12 in both species and share many traits between them.[17] Comparative genomics revealed the presence of all necessary capsaicinoid genes in tomato with varying expression.[3] Overexpression of those less expressed genes in tomatoes should, in theory, make tomato fruit spicy, but other regulatory factors cannot be excluded.

By inserting three capsaicinoid genes (*BCAT, Kas* and *AT*), we aimed to activate the capsaicinoid pathway in tomato. The *Agrobacterium*-mediated transformation method was successful in the delivery of all three genes, as evidenced by the regeneration of hygromycin-resistant transgenic plants and the expression of three pepper genes, as seen in RT-PCR. This, however, did not result in any increase in capsaicin synthesis or accumulation in tomato fruits. The generation of transgenic tomato plants expressing pepper gene, however, is a significant step towards the generation of spicy tomato. There could be many reasons why our plants did not produce spicy fruits. It could be that there is too little capsaicin to be detected by tasting, or the three genes might not be enough to activate the whole capsaicin biosynthesis pathway as it comprises more than 51 gene families.[17] Gene duplication during capsicum evolution meant that the biosynthesis pathway has up to 13 pepper-specific duplication compared to tomato[17], also tissue specific and developmental expression of genes involved in capsaicinoid biosynthesis[3] could play a role in making tomato spicy.

To the best of our knowledge, the only species other than peppers metabolically engineered to produce capsaicin, the main capsaicinoid in peppers[37], is the baker's yeast *Saccharomyces cerevisiae*. Zhao et al. [38] overexpressed in yeast all the genes for the enzymes catalysing seven steps that produce vanillylamine from phenylalanine[17], *Kas*, *thioesterase* (*Fat*), and *ACL* to reconstruct the fatty acid pathway, as well as *CS/AT*. Culturing the engineered yeast for 120 h in a 1 L fermenter containing 20 g/L glucose, they were able to produce 80.23 µg/L capsaicin in *S. cerevisiae*.[38]

CONCLUSION

To conclude, in this study, we showed that P2Am and T2Am sequences can be used in the overexpression of multiple genes in tomatoes. Future work in tomatoes may include metabolic profiling to examine the changes in metabolites in transgenic plants.

ORCID IDs of the authors

Chudamani Sharma Prakash   0000-0002-2923-8448
Yi-Hong Wang   0000-0001-6414-3308

REFERENCES

1. Aza-González C, Nunez-Palenius HG and Ochoa-Alejo N. Molecular biology of capsaicinoid biosynthesis in chili pepper (*Capsicum* spp.). *Plant Cell Rep*. 2011;30:695–706.

2. Naves ER, Silva L De A, Sulpice R, et al. Capsaicinoids: Pungency beyond *Capsicum. Trends Plant Sci*. 2019;24:109-120.

3. Kim S, Park M, Yeom SI, et al. Genome sequence of the hot pepper provides insights into the evolution of pungency in *Capsicum* species. *Nat Genet*. 2014;46:270-278.

4. Simonne AH, Simonne EH, Eitenmiller RR, Mill HA, Green NR. Ascorbic acid and pro-vitamin A contents in unusually colored bell peppers (*Capsicum annuum* L.). *J Food Comp Anal*. 1997;10:299-311.

5. Kothari SL, Joshi A, Kachhwaha S, Ochoa-Alejo N. Chilli pepper- A review on tissue culture and transgenesis. *Biotech Adv*. 2010;28:35-48.

6. Ravishankar GA, Suresh B, Giridhar P, Rao SR, Johnson TS. Biotechnological studies on *Capsicum* metabolite production and plant improvements. In: De AK (ed.), *Capsicum*: the genus *Capsicum*. London: CRC Press. 2003.

7. Hardy G. Nutraceuticals and functional foods: Introduction and meaning. *Nutrition* 2000;16:688-689.

8. Lee SG, Kim SK, Lee HJ, Lee HS, Lee JH. Impact of moderate and extreme climate change scenarios of growth, morphological features, photosynthesis, and fruit production of hot pepper. *Ecol Evol*. 2018;8:197-206.

9. Demir I and Ellis RH. Development of pepper (*Capsicum annuum*) seed quality. *Ann Appl Biol*. 1992;121:385-399.

10. Zewdie Y and Bosland PW. Evaluation of genotype, environment, and the genotype-by-environment interaction for capsaicinoids in *Capsicum annuum L. Euphytica*. 2000;111:185-190.

11. Onus AN, and Pickersgill B. Unilateral incompatibility in *Capsicum* (Solanaceae): Occurrence and taxonomic distribution. *Ann Bot*. 2004;94:289-295.

12. Heidmann I and Boutilier K. Pepper, sweet (*Capsicum annuum*). *Methods Mol Biol*. 2015;1223:321-334.

13. Min J, Shin SH, Jeon EM, Park JM, Hyun JY and Harn CH. Pepper, chilli (*Capsicum annuum*). *Method Mol Biol*. 2015;1223:311-320.

14. Li Y, Wang H, Zhang Y and Martin C. Can the world's favorite fruit, tomato, provide an effective biosynthetic chassis for high-value metabolites? *Plant Cell Rep*. 2018;37:1443-1450.

15. Peixoto JV, Neto CM, Campos LF, Dourado WS, Nogueira AP, Nascimento AD. Industrial tomato lines: Morphological properties and productivity. *Genet Mol Res*. 2017;16:1-15.

16. Sarkinen T. Bohs L, Olmstead RG and Knapp S. A phylogenetic framework for evolutionary study of the nightshades (Solanaceae): A dated 1000-tip tree. *BMC Evol Biol*. 2013;13:214. doi:10.1186/1471-2148-13-214

17. Qin C, Yu C, Shen Y, et al. Whole-genome sequencing of cultivated and wild peppers provides insights into *Capsicum* domestication and specialization. *Proc Natl Acad Sci USA*. 2014;111:5135-5140.

18. Food and Agriculture Organization of the United Nations. FAO Statistical Yearbook 2015: World Food and Agriculture, FAO.

19. Jenkins T. Bovi A and Edwards R. Plants: Biofactories for a sustainable future? *Philos Trans A Math Phys Eng Sci*. 2011;369:1826-1839.

20. Stewart C, Kang BC, Liu K, et al. Pun1 gene for pungency in pepper encodes a putative acyltransferase. *Plant J*. 2005;42:675-688.

21. Kim M, Kim S, Kim S and Kim BD. Isolation of cDNA clones differentially accumulated in the placenta of pungent pepper by suppression subtractive hybridization. *Mol Cells*. 2001;11:213-219.

22. Tanaka Y, Nakashima F, Kirii E, Goto T, Yoshida Y, Yasuba KI. Difference in capsaicinoid biosynthesis gene expression in the pericarp reveals elevation of capsaicinoid contents in chilli peppers *(Capsicum chinense). Plant Cell Rep*. 2017;36:267-279.

23. Sanjana NE, Cong L, Zhou Y, Cunniff M, Feng G and Zhang F. A transcriptional activator-like effector toolbox for genome engineering. *Nat Protoc*. 2012;7:171-192.

24. Songstad DD, Petolino JF, Voytas DF and Reichert NA. Genome editing in plants. *Crit Rev Plant Sci*. 2017;36:1-23.

25. Schouten HJ and Jacobsen E. Cisgenesis and intragenesis, sisters in innovative plant breeding. *Trends Plant Sci*. 2008;13:260-261.

26. Hou H, Atlihan N and Lu ZX. New biotechnology enhances the application of cisgenesis in plant breeding. *Front Plant Sci*. 2014;5:389. doi:10.3389/fpls.2014.00389

27. Osborn MJ, Panoskaltsis-Mortari A, McElmurry RT, et al. A picornaviral 2A-like sequence-based tricistronic vector allowing for high-level therapeutic gene expression coupled to a dual-reporter system. *Molecular Ther*. 2008;12:569-574.

28. Grote A, Hiller K, Scheer M, et al. JCat: A novel tool to adapt codon usage of a target gene to its potential expression host. *Nucleic Acids Res*. 2005;33:W526-531.

29. Wang Y-H, Campbell MA. *Agrobacterium*-mediated transformation of tomato elicits unexpected flower phenotypes with similar gene expression profiles. *PLoS ONE* 2008;3: e2974. doi:10.1371/journal.pone.0002974

30. Bleeker PM, Spyropoulou EA, Diergaarde PJ, et al. RNA-seq discovery, functional characterization, and comparison of sesquiterpene synthases from *Solanum lycopersicum* and *Solanum habrochaites trichomes. Plant Mol Biol*. 2011;77:323-336.

31. Butelli E, Titta L. Giorgio M, et al. Enrichment of tomato fruit with health-promoting anthocyanins by expression of select transcription factors. *Nat Biotech*. 2008;26:1301-1308.

32. Tzin V, Rogachev I, Meir S, et al. Tomato fruits expressing bacterial feedback insensitive 3-deoxy-d-arabino-heptuloconate 7-phosphate synthase of shikimate pathway possess enhanced levels of multiple specialized metabolites and upgraded aroma. *J Exp Bot*. 2013;64: 4441-4452.

33. Zhang Y, Butelli E, Alseekh S, et al. Multi-level engineering facilitates the production of phenylpropanoid compounds in tomato. *Nat Commun*. 2015;6:8635-8655.

34. Siddiqui MW, Ayalazavala JF, Dhua RS. Genotypic variation in tomatoes affecting processing and antioxidant attributes. *Crit Rev Food Scie Nutr.* 2015;55:1819-1835.

35. Ru M, Wang K, Bai Z, et al. Molecular cloning and characterization of two enzymes involved in the rosmarinic acid biosynthesis pathway of *Prunella vulgaris* L. *Plant Cell Tissue Organ Cult.* 2016;128:381-390.

36. Sonawane PD, Pollier J, Panda S, et al. Plant cholesterol biosynthetic pathways overlaps with phytosterol metabolism. *Nat Plants*. 2016;3:16205-16218.

37. Davis CB, Markey CE, Busch MA, Busch KW. Determination of capsaicinoids in habanero peppers by chemometric analysis of UV spectral data. *J Agric Food Chem.* 2007;55:5925-5933.

38. Zhao J, Li Y, Yi L, Zhang G, Ye B. Yeast-based whole-cell factory for the ecofriendly synthesis of vanillylamine as a critical step toward capsaicin production. *ACS Sustain. Chem Eng.* 2023;11:7683-7691.

How to cite this article

Effect of Dose-Dependent Application of Fungicides Propineb and Mancozeb on H_2O_2, Lipid Peroxidation, and Photosynthetic Pigment in Tomato Leaves

Elif Yuzbasioglu[1] , Eda Dalyan[1] , Ilgın Akpinar[2]

[1]Department of Botany, Faculty of Science, Istanbul University, Beyazıt, Istanbul, Türkiye
[2]General Directore of Nature Conservation and National Park Ministry of Agriculture and Forestry, Ankara, Türkiye

ABSTRACT

Objective: The study investigated the growth, photosynthetic pigment, hydrogen peroxide (H_2O_2), and malondialdehyde (MDA) contents of tomato leaves under different concentrations of two modern fungicides, mancozeb and propineb.

Materials and Methods: Tomato plants were cultivated for 45 days and irrigated with ¼ Hoagland solution. Three different concentrations of propineb and mancozeb; half of the recommended dose (1.5 g/L and 1 g/L), recommended dose (3 g/L and 2 g/L), and two times higher (6 g/L and 4 g/L) sprayed on tomato leaves, respectively. After the fungicide treatment, tomato leaves were harvested at 1, 3, and 7 days after the treatment (DAT).

Results: The highest doses of propineb and mancozeb inhibited shoot growth compared with the control at 7 DAT. The chlorophyll a, b and carotenoid contents were significantly reduced with all mancozeb and propineb treatment doses at 3 and 7 DAT. The phytotoxic effects of fungicides were determined by H_2O_2 and MDA content 1, 3, and 7 days after treatment in leaves. The foliar application of propineb and mancozeb altered the production of H_2O_2 and MDA, depending on the time and concentration. The analysis of the data revealed that the application of propineb and mancozeb at higher concentrations significantly increased H_2O_2 and MDA levels, which caused toxicity in tomato leaves.

Conclusion: The findings revealed that higher doses of mancozeb and propineb fungicides exert phytotoxic effects by inhibiting growth and photosynthetic pigment production and increasing oxidative stress in tomato leaves.

Keywords: Fungicides, Tomato, Cholorophyll, Oxidative stress, Malondialdehyde

INTRODUCTION

Fungal infections cause diseases in grain, fruit, and vegetables, reducing yields by 20% of food production worldwide.[1] Fungicides, which are low cost, easy to use, and have a broad spectrum range, have become an effective solution to control fungal disease in recent decades in agriculture. In addition to the protective role of fungicides against fungal disease, fungicide application is commonly used in postharvest packaging plants, parks in urban areas, and protected forest areas.[2] Global fungicide application is four hundred thousand tonnes, indicating 17.5% of global pesticide usage worldwide.[2] According to the FAO report[3], global pesticide use increased by 53 percent for herbicides, 111% for fungicides and bactericides, and 44 percent for insecticides compared with the most recent decade with the 1990s. However, the most used pesticide ratio report fungicides (38.4%), herbicides (27.4%), and insecticides (23.0%) in Turkey in 2022.[4]

A member of the Solanaceae family, tomato (*Lycopersicon esculentum* Mill.) is a popular vegetable. The tomato is consumed fresh and processed, so it has great economic value worldwide. According to an agricultural production statistics report by the FAO[3], tomatoes were the most produced vegetable, with 189 million tonnes in 2021. Moreover, annual tomato production exceeds 13 million mT in Türkiye which is the third largest tomato producer in the world.[5] Tomato is commonly grown in fields and greenhouses in the Aegean, Mediterranean, and Marmara regions of Türkiye. Greenhouse cultivation of tomatoes occurs in two seasons and is monoculture. This continued plantation causes an increase in fungal diseases that cause notable yield loss in greenhouse and

field tomato cultivation.[5] In particular, fungal diseases, such as fusarium wilt, grey mould, early blight etc., reduce the yield of tomatoes, and tomato cultivation is dependent on fungicide use for the control of fungal disease. In the data of table tomato production in Turkiye, the insecticides, fungicides, and herbicides applied per hectare on average per hectare were nearly 1.3 g and 1.4 g, 1.8 g and 2.0 g, 1.5 g and 1.7 g respectively.[6] The results indicate that fungicides are the most used pesticide in tomato cultivation in Turkiye. In addition, Engindeniz and Öztürk Çoşar revealed that mancozeb (Manzep, Tri-miltox), copper oxychloride (Hektas), propineb (Antrocol), metalaxyl + mancozeb (Ridomil), and copper salts of fatty and rosin acids (Tenn-Cop) are commonly used fungicides in tomato production.[6] They suggested that common and high levels of pesticide use relate to farmer opinion. The farmers believed that if they did not use pesticides to control pests, productivity would lose more than half of the yield. Engindeniz and Öztürk Çoşar also showed that farmers use an excess amount of pesticides in tomato cultivation.[6] Excessive use of pesticides induces environmental contamination, exposure to side effects on non-target organisms, and pesticide residues accumulate at unacceptable levels in foods.

Fungicides are classified into a broad range of compounds by their mode of action and chemical composition. Contact fungicides prevent the growth and development of fungi by killing their spore germination in plant tissue. Among the contact fungicides, dithiocarbamates were developed in the 1940s for fungal diseases, leading to improved anti-fungal formulations. After the first dithiocarbamate fungicide, thiram, ferbam and ziram, was commercialised, mancozeb (manganese ethylene bisdithiocarbamate) and propineb (zinc propylene bisdithiocarbamate) have become widely used fungicides in plant protection since 1962.[7] The mode of action of these fungicides inactivates the thiol group of enzymes and metabolites in fungus cells.[1] For a long time, the use of mancozeb and propineb on a variety of vegetable, fruit, and grain crops has caused environmental problems. In addition, these fungicides have deleterious effects on humans, fish, birds, and plants. Contact fungicides remain on the plant surface to prevent the germination of fungal spores and the penetration of spore germ tubes into the host epidermis.[7] Contact fungicides affect CO_2 assimilation and stomatal activity due to leaf surface action. Thus, fungicide treatments primarily have a deleterious effect on the photosynthesis. Many physiological studies have revealed that fungicide treatment decreases chlorophyll a fluorescence[8], CO_2 assimilation[9], intercellular CO_2 concentration[10], Rubisco content, ribulose 1.5 bisphosphate regeneration[1], and pigment content in plants.[11] Dias et al.[12] reported that the commercially recommended dose of mancozeb in *Lactuca sativa L.* leaves reduced the efficiency of photosystem II, decreased photosynthetic pigments, and induced lipid peroxidation. Different concentrations of benzimidazole (Carbendazim) and dithiocarbamate (Mancozeb) fungicides decrease root/shoot length

and germination, and they affect chlorophyll (Chla, Chlb, total chlorophyll) content in chickpea seedlings.[13]

Reactive oxygen species (ROS) are rapidly produced due to breakdown of the cellular balance in plants. Fungicide-induced toxicity triggers the accumulation of ROS species such as hydrogen peroxide (H_2O_2), superoxide (O_2^-), and hydroxyl radicals (OH•). ROS, highly reactive molecules, induce oxidative stress that damages the fatty acids of the cell membrane. This phenomenon is known as lipid peroxidation and is a marker of disturbed redox status in plants.[14] Lipid peroxidation determined by the product of polyunsaturated precursors that include small hydrocarbon fragments and MDA (malondialdehyde). Many studies have shown that fungicide-induced toxicity triggered accumulation MDA in lettuce[12], wheat[15], and pea[16].

Recently, the over-application of pesticides has become a potential risk due to their biomagnification and long life span in the environment. Moreover, excessive pesticide use results in ecosystem pollution that causes serious problems for non-target organisms such as humans, fish, bees, and plants. The present study investigated the effects of different doses of a broad range of fungicides (propineb and mancozeb) on the growth, photosynthetic pigment, H_2O_2 and MDA contents in tomato leaves. The findings of this study revealed the effects of the dose-dependent phytotoxicity of propineb and mancozeb in non-target plants. Also, the results can provide a new perspective on the formulation and concentration of fungicides for minimising the adverse effects on non-target plants.

MATERIALS AND METHODS

Experimental Design

The tomato (*Lycopersicon esculentum* Mill. Narcan-8) seeds were purchased from Seed Corporation (Balıkesir Küçükçiftlik) in Turkey. Before the imbibition, the seeds were sterilised in a 5% NaOCl solution for 10 min. Three seeds were planted in plastic pots containing perlite irrigated by ¼ Hoagland solution (Caisson Labs, USA). The tomato seedlings were grown for 45 days in a plant growth chamber. The chamber conditions were as follows: 16–8 h photoperiod, 25°C/20°C, and 60% relative humidity. Fungicides were purchased commercially as mancozeb (MAYCEB M-45) and propineb (Antracol® WP 70). MAYCEB M-45 included 80% mancozeb, which was recommended at a dose of 2 g/L (3 mM). Antracol® WP 70 included %70 propineb, which was recommended at a dose of 3 g/l (7,25 mM).

45-day-old tomato seedlings were sprayed with mancozeb at 1 g/L (half of the recommended dose), 2 g/L (recommended dose), and 4 g/L (two times higher) in tomato laves. Propineb was sprayed at 1.5 g/L (half of the recommended dose), 3 g/L (recommended dose), and 6 g/L (two times higher) in tomato laves. The control tomato plants were sprayed the deionised water. Fungicide treatment was performed in 18 pots, and 3

pots were used for each fungicide treatment. Each pots were consisted the three plants. The control group also had three replicated pots. The tomato leaves were harvested from three independent plants and randomly pooled at 1, 3, and 7 days after treatment.

Growth Parameter

The shoot lengths of the plants were recorded in cm for all experimental groups.

Photosynthetic Pigment Content

Photosynthetic pigment contents were determined using the method of Lichtenthaler and Buschmann.[17] Fresh weights of leaf samples were collected and extracted in 100% acetone. After the samples were kept at 4 °C for 24 h and centrifuged at 3.000 x g for 15 min, the absorption values of the supernatants were measured using a spectrophotometer (Epoch 2 Microplate Spectrophotometer) at 661.6, 644.8, and 470 nm.

Hydrogen Peroxide Content

The amount of H_2O_2 was determined according to the method of Velikova et al.[18] The fresh leaf samples (0.5 g) were extracted in 5 mL of 0.1% trichloroacetic acid in an ice bath. After the extract was centrifuged at 12.000 x g for 15 min at 4 ºC, 0.5 mL of 10 mM potassium phosphate buffer (pH: 7.0) and 1 mL of 1 M potassium iodide were added to 0.5 mL of the supernatant. The absorbance of the mixture was determined using a spectrophotometer (Epoch 2 Microplate Spectrophotometer) at 390 nm. The amount of H_2O_2 was calculated in µmol/mL from the standard curve.

MDA Content

Lipid peroxidation was analysed for MDA content using the method of Jiang and Zhang.[19] Fresh leaf samples (0.5 g) were extracted using 10 mL of 0.25% thiobarbituric acid in 10% trichloroacetic acid in a cold mortar. The mixture was boiled at 95 °C for 30 min and quickly cooled in an ice bath. The absorbance of the supernatants obtained from the samples centrifuged at 5.000 x g for 10 min was measured using a spectrophotometer (Epoch 2 Microplate Spectrophotometer) at 532 nm and 600 nm. The MDA level was calculated in µmol/g fresh weight using an extinction coefficient (EC) value of 155 $mM^{-1}cm^{-1}$.

Statistical Analysis

The standard error values (±) were calculated for at least five replicates. All data sets statistically evaluated by GraphPad Prism version 10.1.2 software (GraphPad Software, San Diego, CA, USA). A one-way analysis of variance (ANOVA) followed by Dunnett's multiple comparison test was performed to compare the significance between the results.

RESULTS AND DISCUSSION

Successful tomato production requires fungicides and insecticides to prevent diseases, minimise production loss and meet quality standards. However, the widespread use of fungicides causes numerous environmental concerns, including soil and water contamination, and side effects on non-target organisms. The mode of action of pesticides affects both pests and non-target organisms such as humans and plants because of similar targeting systems or enzymes. The beneficial effects of pesticides have become a risk due to their phytotoxicity when applied at higher concentrations in plants. A small percentage of the pesticides reach the sites of action for pest control (approximately <0.1%), and larger amounts are degraded via light and heat and non-target accumulation in the environment. Pesticide toxicity is related to many factors, such as environmental conditions (temperature, moisture, pH), application dose, and technique. Pesticide toxicity shows several morphological symptoms, such as necrosis, chlorosis, stunting, burns twisting of leaves, and it also negatively affects plant growth and development.[20] Pesticides inhibit biological processes such as reactive oxygen balance, synthesis of photosynthetic pigments, cell division, enzyme function, and photosynthesis.[21]

One of the most essential reasons for non-target pesticide toxicity is the use of doses higher than the recommended dose by farmers. Although higher doses help temporarily the pest struggle, they can cause stress to non-target plants, resistance to pesticides, and pesticide residue in soil and water, and finally, it results in environmental pollution in the long term.[2] For this reason, it is important to understand how the dose-dependent application of pesticides affects non-target plants. This study aimed to investigate the effects of different doses of the fungicides mancozeb and propineb on the growth, oxidative stress, and photosynthetic pigments of tomato leaves.

Plant growth is an indicator of changes in plant performance and monitoring responses to environmental stress factors. Three different concentrations of propineb and mancozeb; a half of the recommended dose (1,5 g/L and 1 g/L), recommended dose (3 g/L and 2 g/L), and two times higher (6 g/L and 4 g/L) were sprayed on 45-day-old tomato plants. Plant growth was recorded 3 and 7 days after treatment with propineb and mancozeb (Figure 1). Shoot growth was affected by different doses of propineb and mancozeb application. At 3 and 7 days after treatment, shoot growth did not differ significantly between the recommended and half-dose fungicide application and control. However, the highest dose of mancozeb and propineb (two times higher dose) inhibited shoot growth compared with the control. Shoot growth was negatively affected at 7 days after fungicide application (Figure 1). All concentrations of mancozeb inhibited shoot growth in 45-day-old tomato plants. Pereira et al.[22] determined showed that amino acid metabolism was disturbed in the later growth stages of lettuce under mancozeb treatment, as well as decreased levels of Ala, Asn, GABA, Ile,

Leu, and Val. They also reported that the expanded growth stage of lettuce leaves was negatively affected by exposure to mancozeb. Based on the results of this study, mancozeb inhibited the growth of lettuce leaves because of decreased amino acid metabolism. In contrast, Shakir et al.[23] reported that four commonly used pesticides (emamectin benzoate, alpha-cypermethrin, lambda-cyhalothrin and imidacloprid) reduced tomato growth at higher concentrations. Growth inhibition can be associated with oxidative stress in tomato leaves following pesticide application.
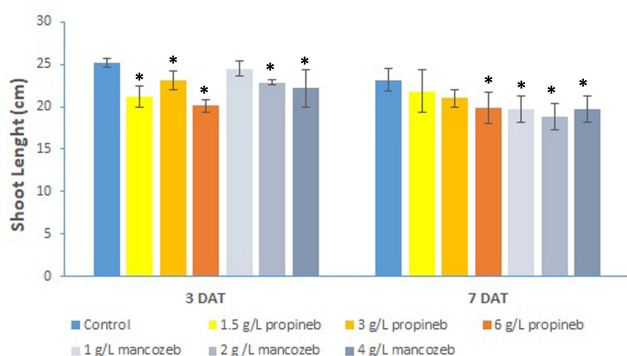

Figure 1. Effect of half of the recommended dose (1.5 g/L and 1 g/L), recommended dose (3 g/L and 2 g/L), and double of the recommended dose (6 g/L and 4 g/L) of propineb and mancozeb on shoot growth in 45-day-old tomato seedlings. Astericks showed adjusted p <0.05 for statistically significant differences from the control as determined by one-way analysis of ANOVA followed by Dunnett's Multiple Comparison Test. Bars represent standard deviations (SD). DAT: Days after treatment.

ROS production is the balance between the antioxidative defence system under optimal growth conditions in plants.[14] The balance between ROS production and scavenging may be disrupted in plants exposed to abiotic and biotic stress factors. This imbalance of the ROS system causes an increase in ROS levels, which causes injury to nucleic acid and oxidising proteins and membrane lipids in plant cells.[14] H_2O_2 is produced from the univalent reduction of O_2 by superoxide dismutase H_2O_2 is the most stable ROS because of its long half-life, but it can inactive enzymes by oxidating their thiol groups.[14] Excessive accumulation of H_2O_2 triggers oxidative stress, and it has become an important indicator of toxicity against different stress factors in plant cells.[24] Fungicide spraying (propineb and mancozeb) remarkably induced the H_2O_2 level, proving the occurrence of oxidative stress in tomato leaves (Figure 2). Different concentrations of propineb and mancozeb changed the H_2O_2 levels 1, 3 and 7 days after treatment. Propineb at 1.5 and 3 mg/L significantly decreased the H_2O_2 level 1 day after treatment, whereas it remarkably increased the H_2O_2 level 7 days after treatment. However, 6 mg/L propineb caused the highest increase in H_2O_2 level 1 day after treatment. In the following days (3 and 7 days after treatment), the H_2O_2 level decreased according to 1 days after treatment, even if it was higher in the control groups. In propineb administration, half (1.5 g/L) of the

recommended dose and recommended dose (3 g/L) showed a significant increase in the H_2O_2 level at 7 day after treatment, yet two doses (6 mg/L) suddenly increased in the H_2O_2 level at 1 day after treatment (Figure 2). The results of the H_2O_2 level indicated that a low dose of propineb slowly caused oxidative stress, whereas a high dose of propineb quickly triggered oxidative stress after treatment in tomato leaves. The application of 1, 2, and 4 g/L of mancozeb gave rise increment of the H_2O_2 level 1, 3, and 7 days after treatment compared with the control. Moreover, the highest level of H_2O_2 was observed in 4 mg/L mancozeb spraying (two times higher doses) 3 days after treatment in tomato leaves.
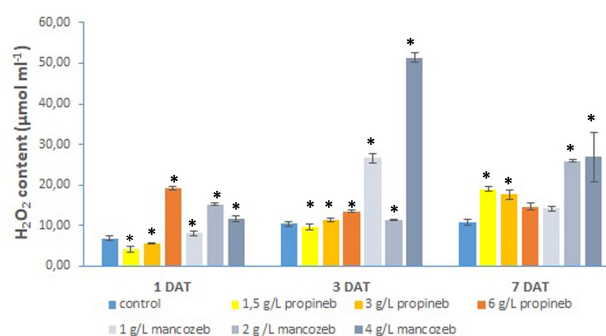

Figure 2. Effect of half of the recommended dose (1.5 g/L and 1 g/L), recommended dose (3 g/L and 2 g/L), and double of the recommended dose (6 g/L and 4 g/L) of propineb and mancozeb on H_2O_2 content in 45-day-old tomato seedlings. Astericks showed adjusted p<0.05 for statistically significant differences from the control as determined by one-way analysis of ANOVA followed by Dunnett's Multiple Comparison Test. Bars represent standard deviations (SD). DAT: days after treatment.

Excessive ROS accumulation can damage many cellular functions by disrupting nucleic acids, proteins, carbohydrates, and lipids in plants. Lipid peroxidation is an indicator of oxidative injury caused by ROS in cells. The harmful effects of lipid peroxidation are associated with fluidity, specific ion channels, proteins, receptors, and enzymes in membranes.[14] Lipid peroxidation determined by MDA, a polyunsaturated precursor that includes small hydrocarbon fragments. The analysis of MDA content proved that the application of the two fungicides significantly induced membrane damage in the leaves of tomatoes compared with the control plants (Figure 3). The half of recommended (1.5 g/L) and recommended dose (3 g/L) of propineb showed trends similar to control or decreased MDA content at 1 and 3 days after treatment, yet these two concentrations of propineb triggered the MDA content at 7 days after treatment. In addition, two-fold higher doses of propineb (6 g/L) remarkably increased MDA content compared with the control in tomato leaves at 1, 3, and 7 days after treatment. On the first day after treatment, there were similar trends in MDA content at all concentrations of mancozeb. Besides, two times higher doses of mancozeb (4 g/L) significantly increased MDA content compared with the control at 3 and 7 days after treatment (Figure 3). The experimental results revealed that different doses

Table 1. Effect of half of the recommended dose (1.5 g/L and 1 g/L), recommended dose (3 g/L and 2 g/L), and double of the recommended dose (6 g/L and 4 g/L) of propineb and mancozeb on chlorophyll a, chlorophyll b, carotenoid, and total chlorophyll content in 45-day-old tomato seedlings. Astericks showed adjusted p values<0.05 for statistically significant differences from the control as determined by one-way analysis of ANOVA followed by Dunnett's Multiple Comparison Test. Bars represent standard deviations (SD). DAT: days after treatment.

Time	Treatment	Chl a (µg/mL)	Chl b (µg/mL)	Carotenoid (µg/mL)	Total Chlorophyll
1 DAT	Control	380.38 ± 5.41	147.30 ± 5.44	179.68 ± 3.01	527.67 ± 8.86
	1.5 g/L propineb	380.76 ± 17.42	156.84 ± 8.46	196.28 ± 10.31*	537.60 ± 25.75
	3 g/L propineb	313.28 ± 6.02*	126.30 ± 9.01*	154.93 ± 5.44*	439.59 ± 15.00*
	6 g/L propineb	227.26 ±3.69*	97.36 ± 5.11*	114.67 ± 2.78*	324.62 ± 7.20*
	1 g/L mancozeb	364.46 ±10.70	141.61 ± 15.35	174.88 ± 9.61	506.07 ± 26.03
	2 g/L mancozeb	284.41 ±2.20*	112.37 ± 5.22*	139.86 ± 3.65*	396.78 ± 6.85*
	4 g/L mancozeb	280.73 ±2.76*	111.32 ± 3.77*	138.41 ± 3.15*	392.05 ± 6.15*
3 DAT	control	356.11 ± 1.94	151.98 ± 8.47	178.01 ± 4.62	508.09 ± 6.53
	1.5 g/L propineb	316.63 ± 2.66*	122.63 ± 5.39*	148.91 ± 3.44*	439.26 ± 7.66*
	3 g/L propineb	255.42 ± 2.68*	102.36 ± 1.92*	121.86 ± 2.26*	357.77 ± 3.42*
	6 g/L propineb	242.90 ± 7.38*	97.82 ± 5.99*	124.84 ± 5.70*	340.72 ± 12.01*
	1 g/L mancozeb	300.54 ± 2.25*	121.37 ±5.98*	148.80 ± 3.86*	421.91 ± 8.20*
	2 g/L mancozeb	280.78 ± 3.70*	105.49 ± 1.47*	129.68 ± 1.63*	386.27 ± 3.88*
	4 g/L mancozeb	298.01 ± 9.20*	116.99 ± 3.04*	144.37 ± 2.22*	414.99 ± 6.84*
7 DAT	control	303.27 ± 1.41	107.76 ± 1.56	136.70 ± 0.68	411.03 ± 1.96
	1.5 g/L propineb	257.76 ± 1.36*	95.19 ± 1.81*	121.82 ± 1.09*	352.95 ± 2.20*
	3 g/L propineb	258.89 ± 5.90*	100.09 ± 9.08	122.68 ± 3.85*	358.98 ± 14.90*
	6 g/L propineb	284.03 ± 1.93*	108.15 ± 1.26	133.36 ± 1.56	392.18 ± 3.12*
	1 g/L mancozeb	201.51 ± 0.92*	90.01 ± 4.52*	105.96 ± 2.70*	291.52 ± 5.39*
	2 g/ mancozeb	196.19 ± 1.94*	83.76 ± 8.47*	100.07 ± 4.62*	279.95 ± 6.53*
	4 g/L mancozeb	243.84 ± 0.60*	96.50 ± 0.89*	120.58 ± 0.93*	340.34 ± 1.19*

of mancozeb and propineb enhanced the H_2O_2 and MDA levels within 7 days of treatment in tomato leaves. The increase in H_2O_2 and MDA content indicates oxidative stress caused by the application of propineb and mancozeb in tomato leaves. Shahid et al.[16] reported that three different fungicides enhanced the accumulation of H_2O_2 and MDA content with increasing dosages of the fungicides.

The photosynthesis apparatus is strongly influenced by environmental conditions that change the function and structure of the photosynthesis machinery in plants.[25] Physiological studies have revealed that fungicide toxicity primarily affects the photosynthetic process in plants.[1] Fungicide treatments have been shown to decrease photosynthetic activity and chlorophyll fluorescence, reduction of net CO_2 assimilation, transpiration rate, stomatal conductance, and intercellular CO_2 concentration. Pigment biosynthesis, chlorophyll a, chlorophyll b, and carotenoids are inhibited by fungicide application in grapevine[9], maize[26], and chickpea[13]. Petit et al.[9] reported that all concentrations of the fungicide fludioxonil (fdx) inhibited photosynthesis in non-target grapevines. In addition, lower fdx concentrations decreased photosynthesis from the first day after treatment, whereas higher concentrations decreased pho-
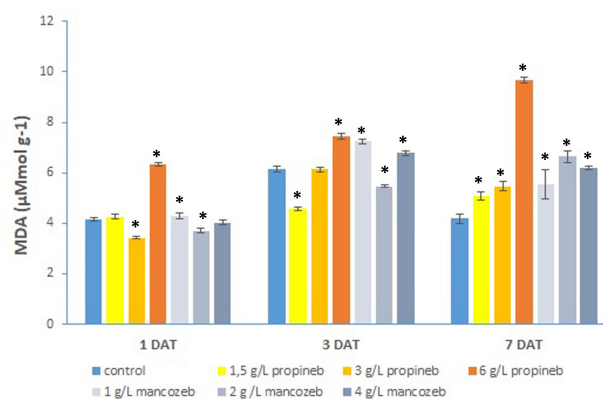

Figure 3. Effect of half of the recommended dose (1.5 g/L and 1 g/L), recommended dose (3 g/L and 2 g/L), and double of the recommended dose (6 g/L and 4 g/L) of propineb and mancozeb on malondialdehyde (MDA) content in 45-day-old tomato seedlings. Astericks showed adjusted p<0.05 for statistically significant differences from the control as determined by one-way analysis of ANOVA followed by Dunnett's Multiple Comparison Test. Bars represent standard deviations (SD).

tosynthesis after 7 days. Dias et al.[12] the effect of a commercial dose of mancozeb on the photosynthetic pigment in *Lactuca sativa* leaves. They found that mancozeb had a neg-

ative effect on chlorophyll and carotenoids due to sensitivity of pigment-protein complex of the photosynthesis apparatus. Similarly, commonly used pesticides (emamectin, benzoate, alpha-cypermethrin, lambda-cyhalothrin and imidacloprid) decreased pigment content at higher doses in 21-day-old tomato leaves.[23] In this study, the effects of propineb and mancozeb on the pigment content of tomato leaves (Table 1). On the first day after treatment, chlorophyll a, b, and carotenoid content exhibited similar trends as the control at half the recommended dose of propineb (1.5 g/L) and mancozeb (1 g/L). However, recommended and twice-dosed propineb and mancozeb significantly decreased pigment content in tomato leaves. At 3 and 7 days after treatment, chlorophyll and carotenoid pigment degradation was remarkably induced by all concentrations of propineb and mancozeb. Interestingly, the highest pigment increment was observed in 6 g/L propineb and 4 g/L mancozeb on the first day of treatment compared with the control. Morover, after treatment (3 and 7) the pigment degradation rate slowed down as compared with the control (Table 1). The results show that propineb and mancozeb have acute harmful effects on photosynthetic pigments at two doses in tomato leaves.

CONCLUSION

The results of this study show that the dose-dependent application of propineb and mancozeb fungicides negatively affects the growth and photosynthetic pigments of tomato leaves by triggering oxidative stress. The overdose of fungicides can be harmful and reduce the vegetative growth of tomato seedlings. These findings can help understand the toxicity of fungicides in non-target plants. The results of the study indicate the risk of excessive fungicide use in plant growth, development, and yield.

ORCID IDs of the Authors

Elif Yuzbasioglu   0000-0003-3691-6283
Eda Dalyan   0000-0001-8637-2275
Ilgın Akpinar   0000-0002-9198-2307

REFERENCES

1. Dias, MC. Phytotoxicity: An overview of the physiological responses of plants exposed to fungicides. *J Bot*. 2012;135479. doi.org/10.1155/2012/135479.

2. Gikas GD, Parlakidis P, Mavropoulos T, Vryzas Z. Particularities of fungicides and factors affecting their fate and removal efficacy: A Review. *Sustainability*. 2022;14:4056. doi.org/10.3390/su14074056

3. FAO. Pesticides use and trade, 1990–2021. FAOSTAT Analytical Briefs Series No. 70. Rome, 2023: doi.org/10.4060/cc6958en

4. Özercan B, Taşçı R. Investigation of pesticide use in Türkiye in terms of provinces, regions and pesticide groups. *Ziraat Mühendisliği*. 2022;375:75-88.

5. Yücel S, Can C, Yurtmen M, Cetinkaya-Yildiz R, Aysan Y. Tomato pathology in Turkey. *Eur J Plant Sci Biotechnol*. 2008;2(1):38-47.

6. Engindeniz S, Öztürk Coşar G. An economic comparison of pesticide applications for processing and table tomatoes: A case study for Turkey. *J Plant Prot Res*. 2013;53(3):230-237.

7. Thind TS, Hollomon DW. Thiocarbamate fungicides: Reliable tools in resistance management and future outlook. *Pest Manag Sci*. 2018;74:1547-1551.

8. Dewez D, Geoffroy L, Vernet G, Popovic R. Determination of photosynthetic and enzymatic biomarkers sensitivity used to evaluate toxic effects of copper and fludioxonil in alga *Scenedesmus obliquus*. *Aquat Toxicol*. 2005;74:150–159.

9. Petit AN, Fontaine F, Clément C, Vaillant-Gaveau N. Photosynthesis limitations of grapevine after treatment with the fungicide fludioxonil. *J Agric Food Chem*. 2008;13(15):6761-6767.

10. Xia XJ, Huang YY, Wang L, et al. Pesticides-induced depression photosynthesis was alleviated by 24-epibrassinolide pretreatment in *Cucumis sativus*. *Pestic Biochem and Physiol*. 2006;86:42–48.

11. Marques LN, Balardin RS, Stefanello MT, et al. Physiological, biochemical, and nutritional parameters of wheat exposed to fungicide and foliar fertilizer. *Semin-Ciencias Agrar*. 2016;37(3):1243-1254.

12. Dias MC, Figueiredo P, Duarte IF, Gil AM, Santos C. Different responses of young and expanded lettuce leaves to fungicide Mancozeb: Chlorophyll fluorescence, lipid peroxidation, pigments and proline content. *Photosynthetica*. 2014;52:148–151.

13. Singh G, Sahota HK. Impact of benzimidazole and dithiocarbamate fungicides on the photosynthetic machinery, sugar content and various antioxidative enzymes in chickpea. *Plant Physiol Biochem*. 2018;132:166-173.

14. Gill SS, Tuteja N. Reactive oxygen species and antioxidant machinery in abiotic stress tolerance in crop plants. *Plant Physiol Biochem*. 2010;48(12):909-930.

15. Liu R, Li J, Zhang L, Feng T, Zhang Z, Zhang B. Fungicide difenoconazole induced biochemical and developmental toxicity in wheat (*Triticum aestivum* L.). *Plants*. 2021;10(11):2304. doi.org/10.3390/plants10112304.

16. Shahid M, Ahmed B, Zaidi A, Khan M S. Toxicity of fungicides to *Pisum sativum*: A study of oxidative damage, growth suppression, cellular death and morpho-anatomical changes. *RSC Adv*. 2018;8:38483-38498.

17. Lichtenthaler HK, Buschmann C. Chlorophylls and carotenoids: Measurement and characterization by UV-VIS spectroscopy. *Curr Protoc Chem Biol*. 2001; 1:F4.3.1-F4.3.8.

18. Velikova V, Yordanov I, Edreva A. Oxidative stress and some antioxidant systems in acid rain-treated bean plants: Protective role of exogenous polyamines. *Plant Sci*. 2000;151:59–66.

19. Jiang M, Zhang J. Effect of abscisic acid on active oxygen species, antioxidative defense system and oxidative damage in leaves of maize seedlings. *Plant Cell Physiol*. 2001;42:1265-1273.

20. Parween T, Jan S, Mahmooduzzafar S, Fatma T, Siddiqui Z H.

Selective effect of pesticides on plant—A Review. *Crit Rev Food Sci Nutr.* 2016;56(1):160-179.

21. Yüzbaşıoğlu E, Dalyan E. Salicylic acid alleviates thiram toxicity by modulating antioxidant enzyme capacity and pesticide detoxification systems in the tomato (*Solanum lycopersicum* Mill.). *Plant Physiol Biochem.* 2019;135:322-330.

22. Pereira SI, Figueiredo PI, Barros AS, et al. Changes in the metabolome of lettuce leaves due to exposure to mancozeb pesticide. *Food Chem.* 2014;1(154):291-298.

23. Shakir SK, Kanwal M, Murad W, et al. Effect of some commonly used pesticides on seed germination, biomass production and photosynthetic pigments in tomato (*Lycopersicon esculentum*). *Ecotoxicol*. 2016;25:329–341.

24. Akter S, Khan MS, Smith EN, Flashman E. Measuring ROS and redox markers in plant cells. *RSC Chem Biol.* 2021;2:1384-1401.

25. Sherin G, Aswathi KPR, Puthur JT. Photosynthetic functions in plants subjected to stresses are positively influenced by priming. *Plant Stress.* 2022;4:100079. doi 10.1016/j.stress.2022.100079.

26. Kılıç S, Duran RE, Coskun Y. Morphological and physiological responses of maize (*Zea mays* L.) seeds grown under increasing concentrations of chlorantraniliprole insecticide. *Pol J Environ Stud*. 2015;24(3):1069-1075.

How to cite this article